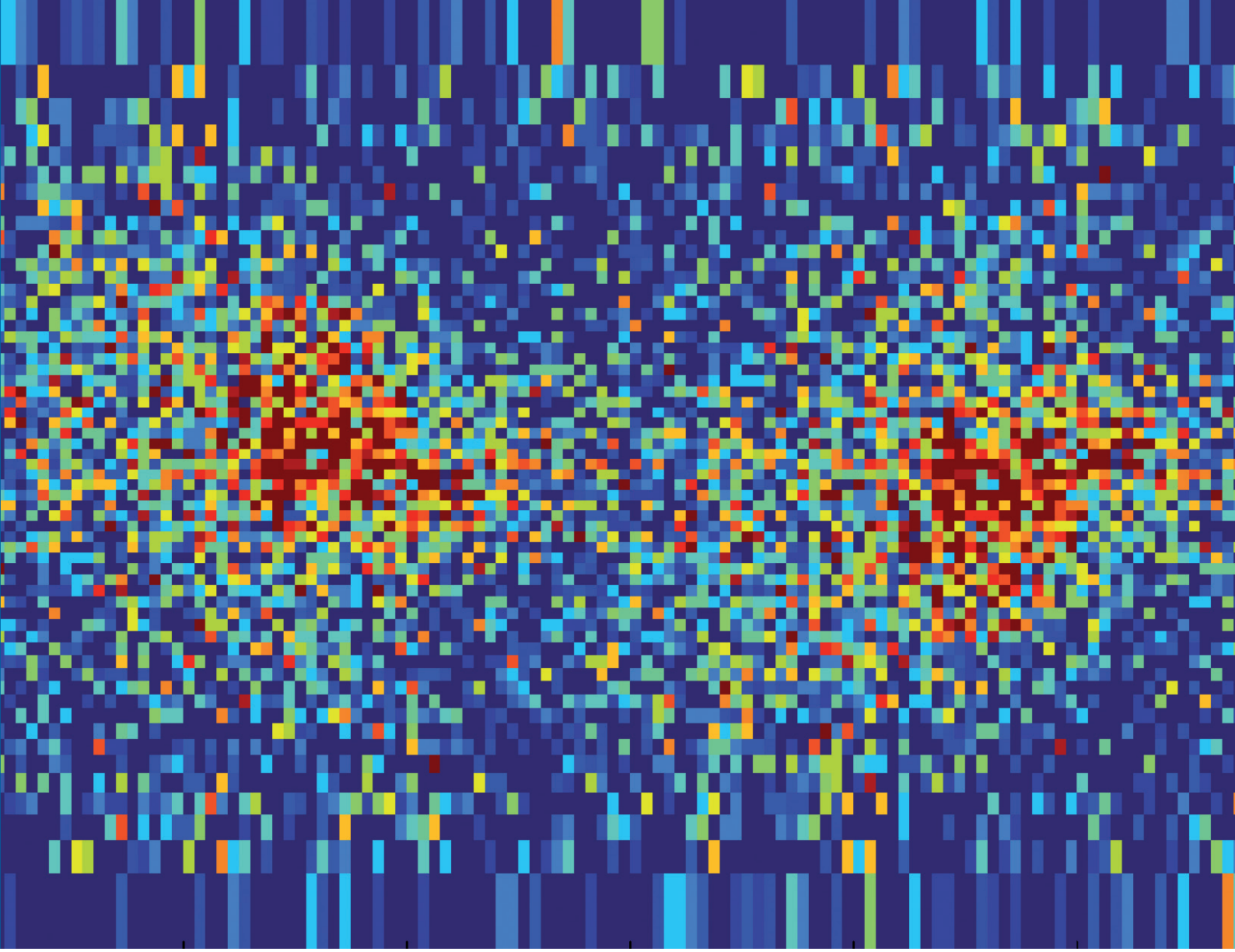


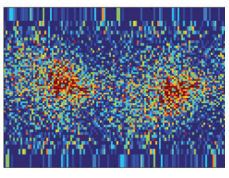
PHOTON SCIENCE 2018.

Highlights and Annual Report

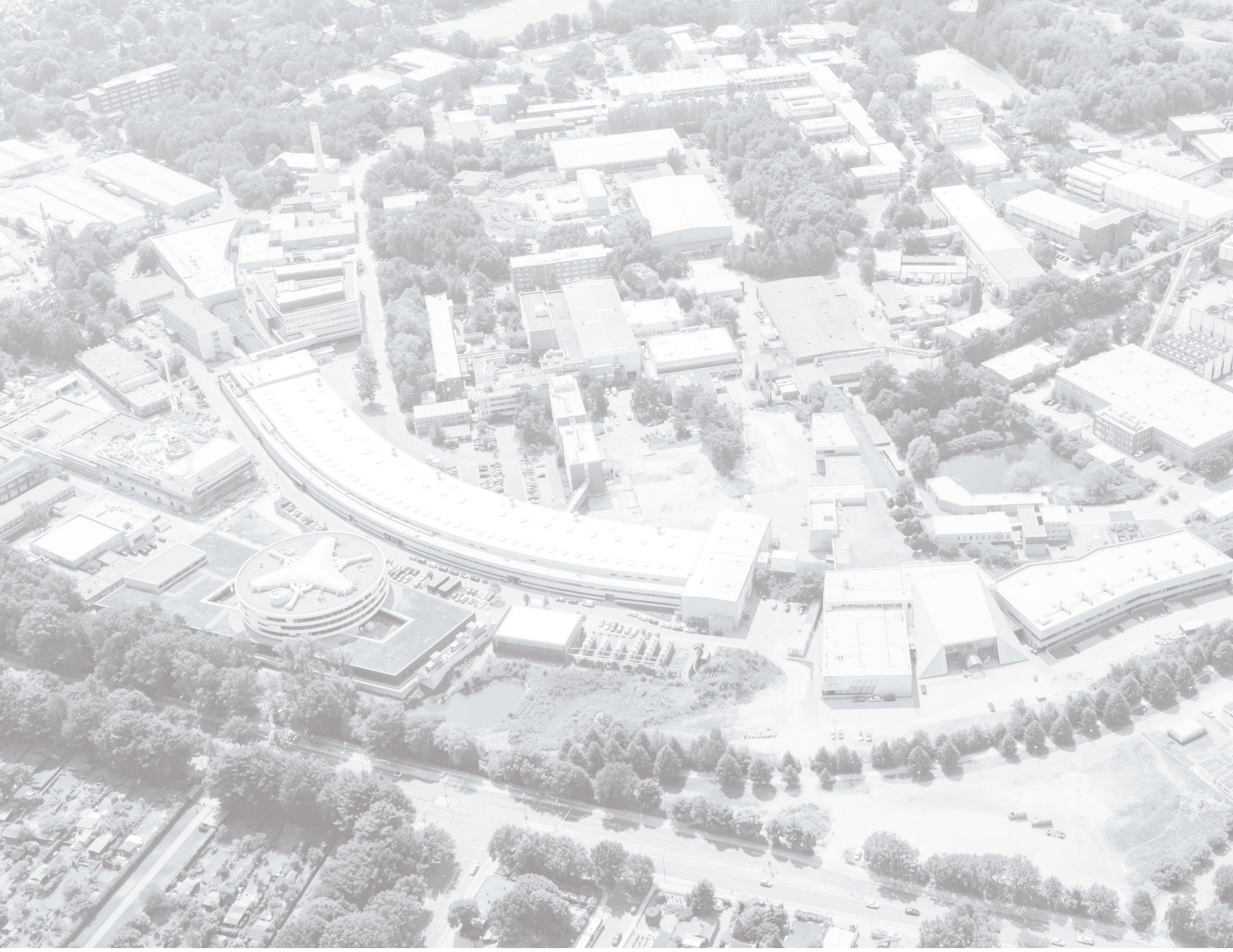
Deutsches Elektronen-Synchrotron
A Research Centre of the Helmholtz Association

DESY.

Cover

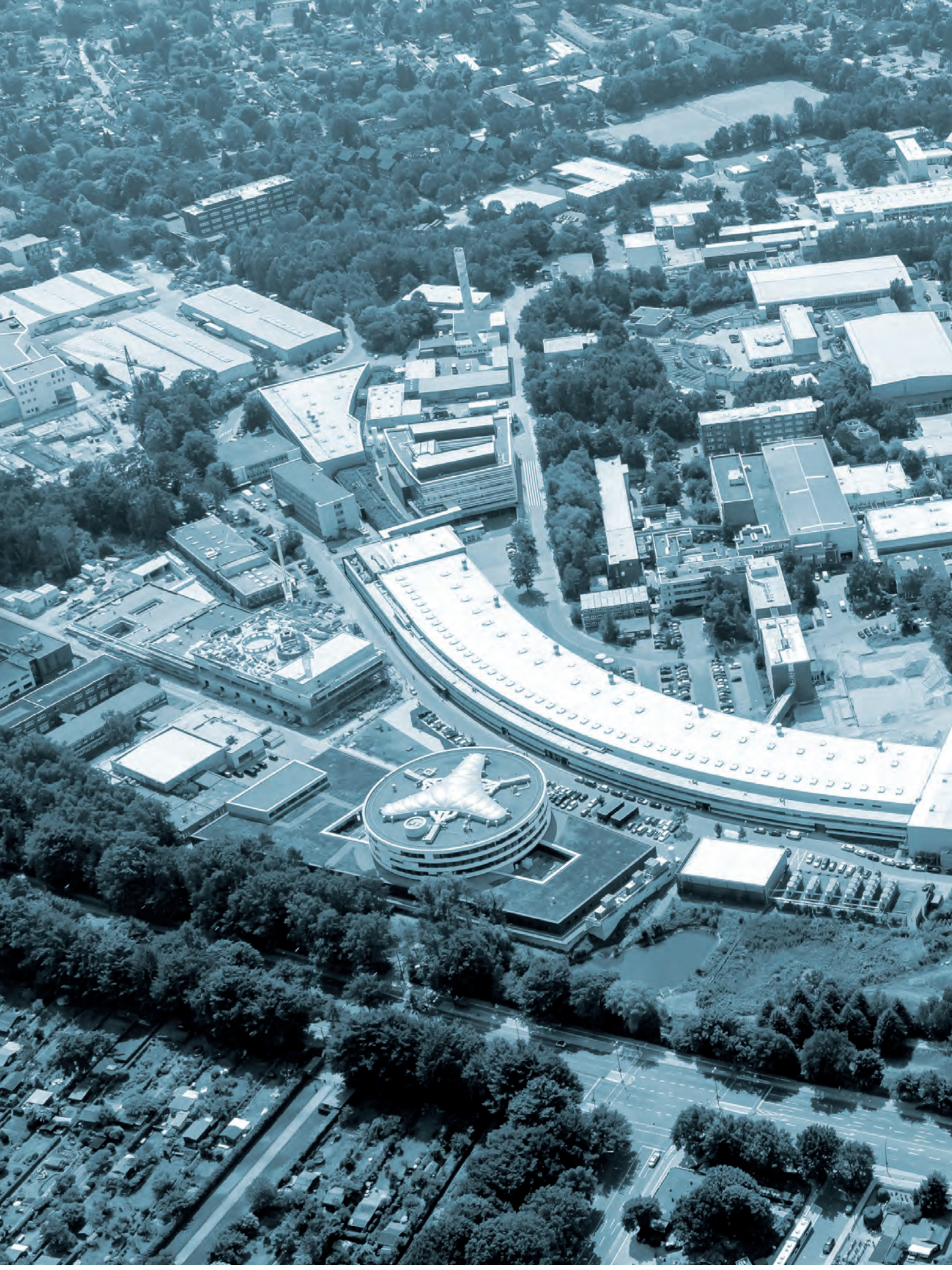


Non-invasive virtual histology of brain tissue: with the combination of data recorded by propagation-based phase-contrast tomography at PETRA III beamline P10 and at a laboratory X-ray source it was possible to visualise about 1.8 million nerve cells in the human cerebellum. The image shows the angular distribution of neighbouring cells in the granular layer of the cerebellar cortex. A strong anisotropy can be observed, showing that the majority of these cells is aligned in parallel to the dendritic tree of the Purkinje cell layer which defines a natural coordinate system in the cerebellum due to its almost two-dimensional shape. Only by mapping the cerebellum in three dimensions and in a non-destructive manner Mareike Töpperwien, Tim Salditt and coworkers from the Universität Göttingen were able to observe these previously unknown spatial relations in the human brain (details see page 52-53).



PHOTON SCIENCE 2018.

Highlights and Annual Report





Contents

> **Introduction** 4

> **News and Events** 8

> **Science Highlights** 20

- Nanomaterials 22
- Electronic and magnetic structure 34
- Structure and structural dynamics 42
- Life Sciences 52
- Quantum optics, atomic and molecular dynamics 62
- Science of laser and X-ray sources - methods and developments 74

> **Light Sources** 88

> **Campus and Collaborations** 100

> **Facts and Numbers** 118

Publications

The list of publications based on work done at DESY Photon Science is accessible online:
http://photon-science.desy.de/research/publications/list_of_publications/index_eng.html

DESY tries to keep this list as complete and as updated as possible, and relies on the support by all users, who are kindly requested to register their publications via DOOR (door.desy.de).

The year 2018 at DESY

Chairman's foreword

Dear Colleagues and Friends of DESY,

an eventful and very successful DESY year is drawing to a close.

After the comprehensive strategy process 'DESY 2030' and the very successful evaluation of the scientific clout of the research centre by a high-ranking international commission of experts, DESY is well prepared for the coming Helmholtz funding period 2021-2027. The outstanding results achieved in the Federal Excellence Initiative give the research campus an additional boost: In both physics clusters of excellence, the photon and nanosciences (AIM: Advanced Imaging of Matter) and particle and astroparticle physics (QU: Quantum Universe) DESY is a key partner of the Universität Hamburg, as well as involved in a third cluster of excellence 'Understanding Written Artefacts'.

All in all, the message is clear: the Bahrenfeld research campus in Hamburg is an international leader in the research of matter. There is no laboratory in the world with a comparable scientific thrust that can match the Bahrenfeld research campus in terms of its future-oriented interdisciplinary research orientation, its ultra-modern research infrastructures and the carat number of its scientists.

The work on the Conceptual Design Report (CDR) for DESY's future project, the upgrade of the synchrotron source PETRA III into a high-resolution 3D X-ray microscope ('PETRA IV'), is progressing very well. Over the next two years, we will enter a preparatory test phase at DESY. Here we will significantly strengthen the project group in terms of personnel and allocate funds for prototype development in order to prepare a solid Technical Design Report (TDR) by the end of 2020. The preparation phase 2019-2021 is a critical milestone and indispensable for a later smooth construction phase. Here we are planning considerable own funds, but need additional financial support from the Federal Ministry.

Almost routine, but still a triumph: the operation of the European XFEL. In the second half of the year, the superconducting linear accelerator was brought up to its nominal power. The DESY operating team, led by Winnie Decking, is mastering every physical and technical detail of the complex machine, which is of great benefit to the experiments on the campus in Schenefeld. Only one year after the start of the operation for users, the first successful results were published in Nature Communications.

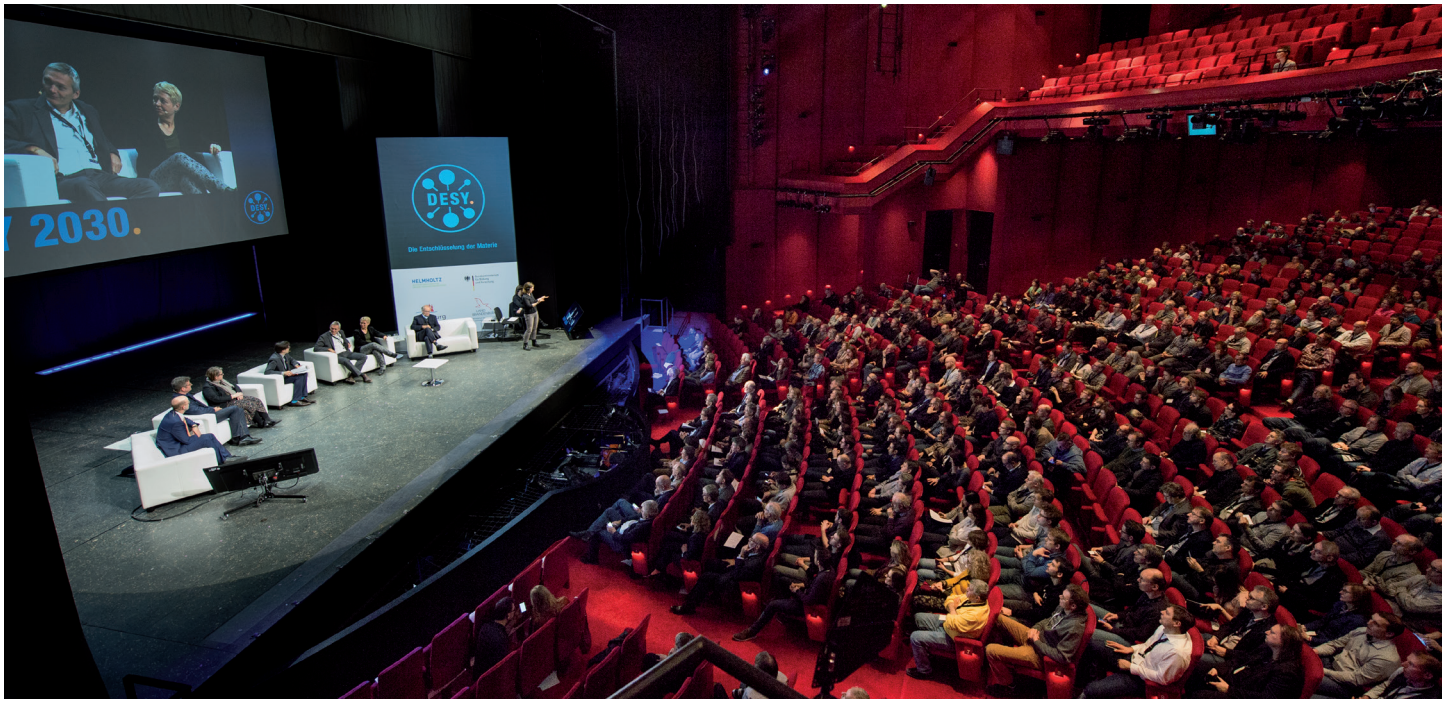
DESY continues to drive innovation forward. The 'Innovation Village' is currently being built on the DESY site, which will provide spin-offs with the necessary office space and infrastructure. Whereas the construction of the 'Innovation Centre' building, which unfortunately has been delayed, can now finally begin, after a suitable provider has been found. I very much welcome that our ambitious plans to expand the Bahrenfeld research campus into a modern ecosystem in which research, education and innovation intelligently stimulate each other, are strongly supported by the German Bundestag, the German Federal Ministry of Education and Research (BMBF) and the Behörde für Wissenschaft, Forschung und Gleichstellung (BWFG) in Hamburg.

With the special funding by the budget committee of the German Bundestag, necessary renovation and important construction measures can be initiated in the coming years, including the construction of the new DESY visitor centre 'DESYUM', the redesign of the main entrance and the urgently needed new construction of the DESY accelerator control centre.

DESY is currently planning new interdisciplinary research buildings, which will re-bundle existing expertise and focus on future new research potentials, among them the 'Centre for Data and Computing Science' (CDCS) and the 'Centre for Molecular Water Science' (CMWS).



Federal Minister Anja Karliczek visits DESY. Here with DESY Director Helmut Dosch (right) and Hamburg's Research Senator Katharina Fegebank (in the background).



'DESY 2030 - Our Strategy for the Future' event in a theatre in Hamburg on 20 March 2018 for all DESY staff and invited guests.

The CDCS is currently designed in close cooperation with all Hamburg universities. It is one of several projects that the BWFG is currently considering as part of the 'HamburgX project'. Fortunately, DESY was able to raise substantial Helmholtz funding for the Data Science in Hamburg – Helmholtz Graduate School for the Structure of Matter (DASHH). DASHH is supported by all CDCS partners.

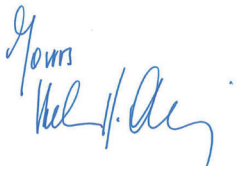
PETRA IV, a 3D X-ray microscope with the world's highest resolution, will be built in Hamburg. This is DESY's most visible entry into the century of complexity, in which novel multifunctional materials will ideally be built atom by atom. PETRA IV will provide the necessary analytical conditions for these challenges. This also creates a revolutionary new analytical approach to urgent questions related to the microscopic structures and processes in water and at its interfaces which extend into many fields of application and technologies. DESY has founded a European initiative 'Centre for Molecular Water Science' which brings together all leading experts and laboratories. In the meantime, a consortium of more than 30 laboratories from all over Europe has come together to design the pillars of the CMWS. One of these pillars is to become a new interdisciplinary centre at DESY, which will make targeted use of the research potential on the campus for water research.

In the end, it will be important to attract the leading experts and highly talented young scientists. DESY recruits talents on the international level, and it is committed to diversity and the promotion of women and to mutual respect regardless of nationality, skin colour, religion and personal life plans.

This year the focus was on a key appointment, the successor of our Director of the Accelerator Division, Reinhard Brinkmann, who will pass the baton on to his successor at the end of the year. We are proud and pleased to announce that the world's leading accelerator physicist in the field of plasma acceleration, Wim Leemans, could have been enticed away from the Lawrence Berkeley National Lab (LBNL) in the U.S. This is a great success, which will decisively strengthen the research centre and in particular the accelerator development in Hamburg. This appointment was not easy. I would like to express my gratitude to the BMBF, in particular to our Chairman of the Foundation Council, Dr. Dietz, for the great cooperation.

Last but not least, LEAPS, the 'League of European Accelerator-based Photon Sources' has made great progress since its foundation a year ago. On 12-13 November, more than 150 scientists from the 16 accelerator-based light sources in Europe, all members of LEAPS, met at DESY for its first plenary meeting, including representatives of eight national science ministries and research funding agencies as well as Philippe Froissard, the Deputy Head of the Research Infrastructure Unit of the Directorate on Open Innovation & Open Science of the European Commission.

I thank the DESY staff and all our users and partners, national and international, who have contributed to the success of the Bahrenfeld research campus.



Helmut Dosch
Chairman of the DESY Board of Directors

Photon Science at DESY

Introduction



The DESY site in Hamburg with the new CSSB building and the construction sites for the Max Planck Institute for the Structure and Dynamics of Matter (MPSD) and the Centre for X-ray and Nano Science (CXNS) on the left and right side of the curved PETRA III experimental hall 'Max von Laue' in May 2018.

Dear Colleagues and Friends,

Another very successful year for DESY Photon Science comes to an end. The year 2018 started with the traditional users' meeting that was organised in cooperation with European XFEL. With more than 1200 participants, which is a new record attendance, it demonstrates the great interest of the user community in our facilities. In frame of this meeting also 10 DESY workshops were organised providing many opportunities for discussions among experts in and across all fields of photon science. However, scientific discussions and exchange are not only limited to the time of the users' meeting. 21 workshops and 2 conferences with all together about 1000 participants were organised during the year at DESY Photon Science underpinning the vibrant scientific development of the Bahrenfeld research campus in Hamburg.

With a record number of more than 2900 users from all fields of science relevant to research at synchrotron and FEL radiation sources, the user operation at PETRA III and FLASH was again very successful over the past year. In 2018 at PETRA III two additional beamlines have started regular user operation in addition to the 18 beamlines already in operation. Two more beamlines are in commissioning and three are under construction. For the last two free undulator beamline slots, several ideas for new experimental techniques are discussed with various user communities, our advisory bodies and funding agencies.

Significant progress has been made at FLASH as well: with the new pump-probe laser at FLASH2, more accurate synchronisation and diagnostics capabilities, a time-delay compensating monochromator at FLASH2 and further experimental stations. For the first time, more users requested beamtime at FLASH2 as compared to FLASH1 in order to exploit the capabilities for fast changes of the photon energy by using the tuneable FEL undulator.

Meanwhile, the first publications from experiments at European XFEL have been published. Significant progress has

been made in the performance of the accelerator. During 2018, the full pulse repetition rate of 27000 pulses per second has been achieved as well as the design electron energy of 17.5 GeV. Furthermore, splitting of one bunch train such that the three SASE FEL-lasers did lase in parallel was demonstrated. This is a prerequisite for parallel user operation of more than one FEL. In addition to the instruments at SASE1 also at SASE3 first user experiments have been carried out successfully.

The strategy process 'DESY2030' that had started in 2017 was completed this year and the implementation of various measures is already in progress. Research at DESY Photon Science is now organised in the three competence fields 'Matter – Dynamics, Mechanisms and Control' (Mat-DMC), 'Nano and Materials Science' (Nano-Mat), and 'Biological and Soft Matter' (Bio-Soft). These fields are thematically well aligned with the corresponding research topics of the Helmholtz programme 'From Matter to Materials and Life' (MML). The research activities are carried out in various centres on-site that continue to develop dynamically. Scientists from the Center for Free-Electron Laser Science (CFEL) were among the first to carry out experiments at European XFEL. CFEL continues to grow and the civil construction for a new building to house further Max Planck CFEL groups is close to completion.

Meanwhile, the Centre for Structural Systems Biology (CSSB) is fully operational and groups from almost all partner institutions have moved into the new building on the DESY site. The new CSSB cryo-electron microscopy facility is now operational and adding to the spectrum of analytical capabilities on our campus for structural biology studies. Finally, the civil construction work for the Centre for X-ray and Nano Science (CXNS) has started with the first concrete poured in November. The CXNS will be realised in collaboration with Helmholtz-Zentrum Geesthacht (HZG) and Christian-Albrechts-Universität zu Kiel (CAU). It will also house the DESY NanoLab that provides sample preparation and handling capabilities as well as analytics for nanoscale samples complementary to our photon sources that are available to all researchers on campus and to the users of our facilities.

Last year DESY started an initiative for the establishment of what is now called the Centre for Molecular Water Science (CMWS). This idea has been developed further during the course of this year. With more than 30 Letters of Intent from scientific groups of German and European universities and research centres there is an overwhelming interest for this activity. At present the scope of this centre is further refined with a White Paper to be expected by mid 2019.

Since the past decade we are observing not only a revolution in light source performance but also in detectors. Nowadays we can take data faster, more accurately and more completely. However, these huge amounts of data are often difficult to handle. At present rapid feedback during the course of an experiment is hardly possible and thus severely limiting our ability to steer or control an experiment in real time. Within the 'DESY2030' strategy process these limitations were identified as one of the main future bottlenecks. In order to cope with this challenge DESY together with several partner universities plans to establish a Centre for Data and Computing Science (CDCS). As a first step into this direction we have been able to acquire funding for a new graduate school 'Data Science in Hamburg – Helmholtz Graduate School for the Structure of Matter' (DASHH) to educate the next generation of scientists in this particular topic.

The further development of our photon science facilities PETRA III and FLASH are a central part of the 'DESY2030' strategy. Within this context it is planned to upgrade PETRA III into an almost diffraction limited source in the harder X-ray regime, called PETRA IV. For the development of the scientific case 13 science workshops have been organised with more than 700 participants. A Conceptional Design Report (CDR) for this project is expected for mid 2019 and a complete Technical Design Report (TDR) by the end of 2021. If all schedules and funding issues turn out well, then the reconstruction work could start in 2025 and first beam could be offered in 2027. FLASH2020+, the project to upgrade and modernise our FLASH facility, aims for a number of long-awaited features like gap-tuneable undulators as well as external seeding schemes at FLASH1 and capabilities for new FEL schemes at FLASH2. As a next step a CDR will be presented by spring 2019.

Scientists from DESY Photon Science and users of our facilities received a number of prestigious awards this year. I would like to congratulate all the awardees on their successes. During the last round of the federal excellence initiative the University of Hamburg was extremely successful with four clusters approved. Scientists from DESY Photon Science contribute significantly to the clusters on Advanced Imaging of Matter (AIM) and Understanding Written Artefacts.

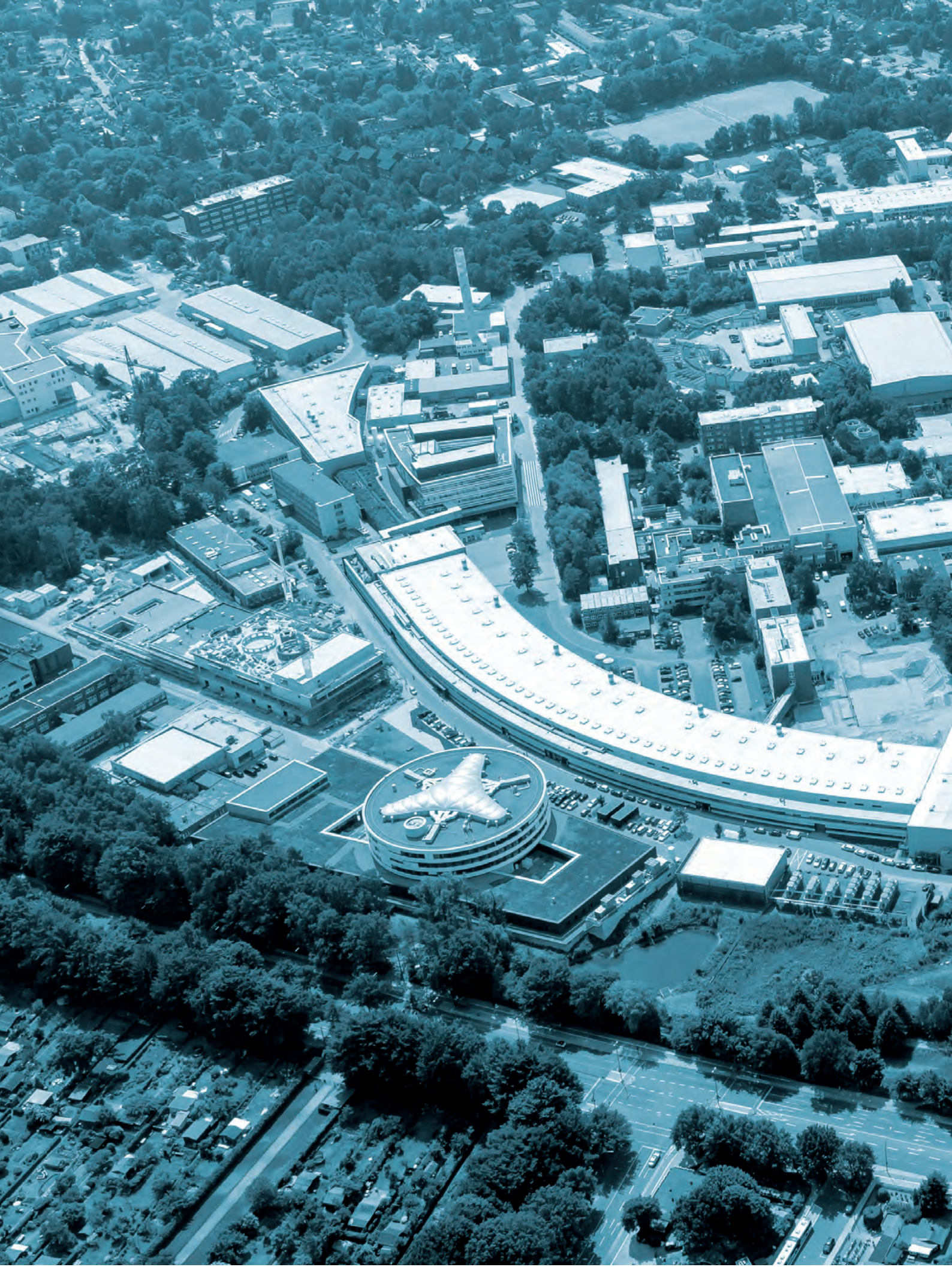
DESY is making great efforts to translate the knowledge it has acquired into innovations. Meanwhile, five start-up companies resulted from the work at DESY Photon Science with at least one of them being already in a scale-up phase. We wish them success and good luck in a competitive market!

Last but not least, many exciting science highlights have been obtained at our facilities but also within our own research groups. Please enjoy reading the examples in this brochure.

I am very grateful to all DESY staff, our advisory and review bodies, as well as to our users and collaboration partners for the continued support which is the key for our success.



Edgar Weckert
Director DESY Photon Science



News and Events



News and Events

A busy year 2018

January

24 – 26 January:
DESY Photon Science and European XFEL could welcome 1200 participants at the joint annual users' meeting

The users' meeting of DESY's research light sources and of the European XFEL once again drew a record number of attendees to Hamburg. About 1200 participants from nearly 100 institutions in around 30 countries registered for the three-day event held at DESY, more than ever before. A particular highlight during this year's meeting was the beginning of scientific user operation at European XFEL, from which first results were presented. In addition to these new exciting experimental possibilities, the further development of the currently most brilliant storage ring PETRA III into an even more brilliant diffraction limited X-ray source PETRA IV was discussed. Also, the rapidly growing activities of DESY and its partners on the Bahrenfeld research campus in Hamburg as well as scientific results were presented. Researchers reported on their work and discussed new experimental techniques with a total number of 375 posters, as well as in 30 lectures and 17 satellite workshops. In the frame of an accompanying trade fair, 65 companies displayed their products related to X-ray science.



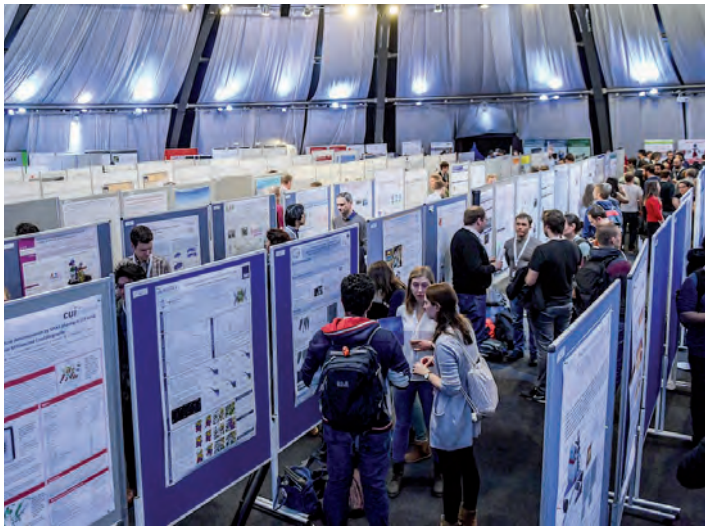
Full house in the DESY Auditorium at the users' meeting.

February

5 – 9 February:
In-depth scientific evaluation of all DESY activities

At the beginning of February, DESY underwent a scientific evaluation on behalf of the Helmholtz Association. The evaluation is part of the programme-oriented funding (POF), which provides funding to the 18 Helmholtz centres within the framework of cross-centre research programmes. The current third funding period started in 2015 and runs until 2019. The Helmholtz Association will use the completed evaluation to prepare the upcoming fourth funding period (POF IV).

During a five-day on-site visit DESY's research and user facilities were evaluated by an external panel of 26 international experts, chaired by Hugh E. Montgomery, the former director of the US accelerator centre Jefferson Lab.
In 70 talks, 126 posters and numerous personal encounters, about 400 DESY colleagues presented the scientific achievements and gave an outlook on DESY's strategy for the upcoming funding period. The staff members and in particular the high proportion of young researchers especially convinced the evaluators. 'You are part of a remarkable lab,' said Montgomery in the final presentation.



The poster session of the joint users' meeting took place in a huge tent.

March

26 February – 1 March:
XVII DESY Research Course and Symposium:
Trends in Water Research

More than 140 participants attended the 17th DESY Research Course and the international DESY symposium on water research. The symposium took place for the first time. Water is unambiguously the most important liquid on Earth and is therefore in the focus of physics, chemistry, geosciences, and biology. Its physical behaviour shows a remarkable variety of anomalies which are essential for our daily life and the development of life in general. Examples of these features are the density anomalies and the high surface tension of liquid water, which are caused by a complex network of hydrogen bonds. Even today by far not all details of this liquid are understood. Therefore, a common effort is needed to gain a comprehensive insight in the complex interaction of water molecules. This was the topic of this year's DESY Research Course which addresses master and PhD students, young research fellows and interested scientists. In the frame of the course also 40 posters on 'Trends in Water Research' were presented and four posters were awarded a poster prize.

The subsequent DESY Symposium on Water Research focused on possibilities and strategies to bring together scientists from different disciplines in this field, in order to establish a new Centre for Molecular Water Science (CMWS) at DESY. Future interdisciplinary research on water at the CMWS, and accompanying measurements at DESY's light sources PETRA III, FLASH and European XFEL, aim at deepening the insights in this unique substance.



Trends in Water Research: Group photo of the attendees.

5 March:
Elena Bykova receives the Max von Laue Prize

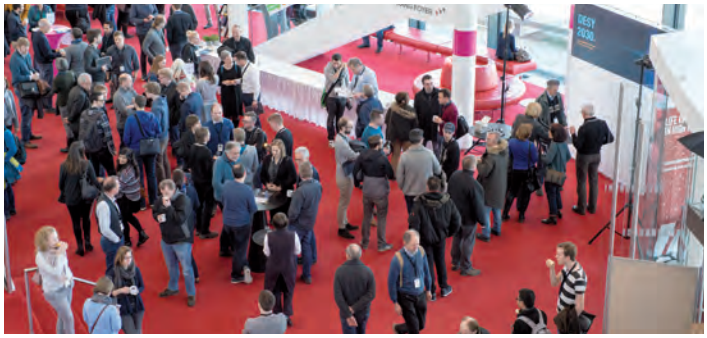


Elena Bykova.

Elena Bykova who received her PhD from the University of Bayreuth before joining DESY has been awarded the Max von Laue Prize 2018 by the German Crystallographic Society. The prize was presented at the society's annual conference in Essen. It recognises the outstanding achievements of the 29-year-old scientist in the field of ultra-high-pressure crystallography and the resulting unique scientific insights into novel high-pressure materials. The prize also explicitly recognises Bykova's contribution to establishing new research methods, for instance at the Extreme Conditions Beamline P02.2 at PETRA III. Bykova helped to develop high-pressure and high-temperature experiments on single crystals, which offer completely new insights into nature: far from the narrow range of temperatures and pressures that we describe as being normal, they reveal more general properties of matter and chemical compounds. For example, Bykova discovered nine new iron oxides with unusual crystal structures and unexpected compositions that can exist at high pressures and temperatures like those found deep in the Earth's interior. The Max von Laue Prize has been awarded annually since 1996 when Edgar Weckert was receiving the first one. It is conferred on promising young scientists for outstanding scientific achievements in the field of crystallography.

March

20 March:
Strategy event ‘DESY 2030’



Hall of the Hamburg Stage Theatre during a panel discussion at the ‘DESY 2030 - Our strategy for the future’ event

After a comprehensive strategy-finding process the future strategy ‘DESY 2030’ was officially presented at a large kick-off event, which took place at the Hamburg Stage Theatre. About 1000 DESY employees and external guests convened in this whole-day event. With its strategy, DESY is setting priorities in science and innovation as well as in the future development of its large-scale research facilities to address the upcoming scientific and societal challenges and demands. In panel discussions, at information booths, and in many personal discussions, representatives of the more than 400 colleagues, who had contributed to the strategy process, presented the key points of the DESY strategy.

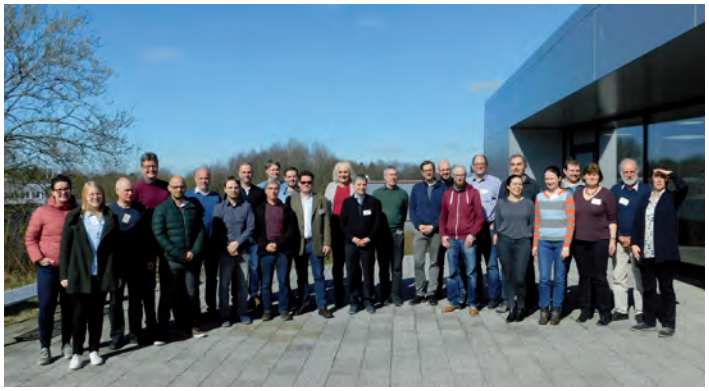
From the Photon Science perspective the key elements of DESY’s strategy cover the transformation of PETRA III into the diffraction limited 3D X-ray microscope PETRA IV which will operate at the physical limits of accelerator technology and will offer two orders of magnitude better resolution compared to the present source. DESY is planning an ambitious development programme called ‘FLASH2020+’ to ensure a high-level research programme at FLASH and the smooth transition to a joint strategy with European XFEL. Together with the European XFEL, DESY is planning to expand the European X-ray Free-Electron Laser and is continuing to further develop the technology, e.g. to increase the number of X-ray pulses from 27,000 to up to one million per second.

On the DESY campus in Hamburg, several interdisciplinary research buildings are foreseen to be established: the Centre for Data and Computing Science (CDCS) to meet the increasing demands made by data-intensive applications in research, the Wolfgang Pauli Centre (WPC) for theoretical physics, and the Centre for Molecular Water Science (CMWS), which will be established in collaboration with national and European partners. DESY will also further develop and test new concepts for building future compact particle accelerators as well as for realising new generations of high-resolution detector systems that will enable unparalleled insights into the structure of matter.

April

5 - 6 April:
First workshop on the planned small angle X-ray scattering beamline P62 at PETRA III

The aim of the workshop was to discuss the science case and suitable design parameters of a small angle X-ray scattering (SAXS) beamline P62 currently designed to be realised in the ‘Paul P. Ewald’ Experimental Hall of PETRA III. P62 is intended to be a versatile instrument, complementary to the existing instruments capable of performing SAXS experiments at PETRA III, which all feature a micro- or even nanometre sized primary beam. The workshop was attended by 37 experts from various research areas. In addition to the talks given by the potential users of the new instrument, users’ demands and ideas have been collected and discussed. Topics like optics specification, energy range, SAXS resolution as well as specialised sample environments, secondary techniques, and required infra-structure were discussed. The potential research topics can roughly be divided into hard and soft condensed matter research. The soft condensed matter research includes bio-based hierarchical materials like bones, teeth, etc. as well as health research related to cancer, drug carriers, etc. The hard condensed matter research includes *in situ* synthesis of nanoparticles and *in operando* studies of these particles during catalysis. It also involves the investigation of energy storage and conversion materials (fuel cells, batteries, etc.) in which structures at different length scales play an essential role for efficiency and lifetime. Several user groups are interested in confined systems such as water in nanoporous materials. The results of the workshop were integrated into the technical design report for P62 which was successfully reviewed later this year, on 24 September.



Participants of the first workshop for the planned new PETRA III SAXS beamline P62.

May

3 May:
The third light source SASE2 at European XFEL generates first light

European XFEL has successfully started operation of its third light source SASE2, exactly one year after the very first X-ray light was generated in the tunnels of European XFEL. SASE2 will provide light for the Materials Imaging and Dynamics (MID) and High Energy Density science (HED) instruments scheduled to start user operation in 2019. All three light sources will eventually provide X-rays for at least six instruments. Three of these six instruments can simultaneously receive X-ray beam for experiments. The MID instrument will be used, for example, to understand how glass forms on the atomic level, and to investigate cells and viruses with a range of imaging techniques. The HED instrument will enable the investigation of matter under extreme conditions such as inside planets, and will be used to investigate how solids react in high magnetic fields.



Aerial photo of the European XFEL site in Schenefeld on 31 May 2018.

17 May:
DESY start-up 'Class 5 Photonics' wins two prestigious awards

With its product 'Supernova OPCPA' DESY's start-up 'Class 5 Photonics' is the proud Gold Winner of the prestigious 'Laser Focus World Innovators Award 2018' in the laser category. This award recognises companies which have made major contributions to advancing the field of optics and photonics by means of recently launched products or services and is awarded yearly during the CLEO conference and tradeshow in San Jose (U.S.).

Back in February 2018 the company already received another prestigious industry prize. The PRISM awards gala is the premier worldwide event in photonics industry and takes place every year during the 'SPIE Photonics West' conference and tradeshow in San Francisco (U.S.). More than 150 applicants entered the competition in ten categories this year. With its high-performance laser 'SuperNova OPCPA' Class 5 Photonics convinced the jury.

Class 5 Photonics was founded in 2014 in Hamburg. The scientists from DESY and Helmholtz Institute Jena develop high power lasers with pulses in the femtosecond range. With industry-leading parameters (pulse energy 1 mJ, pulse rate 100 kHz and power 100 W at pulse lengths less than 10 fs), experiments with the Supernova OPCPA are up to ten times faster compared to conventional Ti:Sapphire lasers. Furthermore, shorter laser pulses for instance allow more precise treatment of materials.



Class 5 Photonics' Klaus Schmidt, Robert Riedel, Michael Schulz and Ivanka Grguras (from left to right) at the PRISM Awards ceremony in San Francisco.

June

15 June:
DESY and European XFEL will host SRI2021 Conference

At the 13th International Conference on Synchrotron Radiation Instrumentation SRI2018 in Taipei, Taiwan, it was announced that DESY and European XFEL have won the bid to host the 14th International Conference on Synchrotron Radiation Instrumentation. After nearly 40 years, the SRI will return to Hamburg, where the first meeting was held in 1982. At that time DORIS was the operating synchrotron source at DESY. Now scientists from the light source facilities around the world are looking forward to meet again in Hamburg in 2021. The SRI conference is the most significant and largest international conference in the synchrotron radiation and free-electron laser community. Alternating between Europe, America and the Asia-Pacific region, SRI conferences are hosted by countries with the most advanced light source facilities. SRI2021 will take place from 31 August to 3 September 2021 and is expected to attract more than 1000 participants.



DESY and European XFEL prepared a document to present Hamburg as an attractive place to host the SRI2021.



During the first SRI conference in 1982: Volker Soergel (right), the Chair of the DESY Board of Directors (1981-1993), talked to the participants in the DESY auditorium.

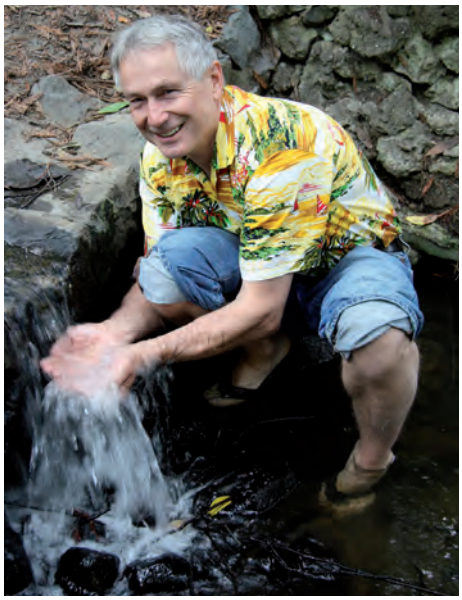
July

6 July:
International Helmholtz Fellow Award for Richard Saykally

Since 2012 the International Fellow Award of the Helmholtz Association is presented twice per year to scientists selected from candidates nominated by the Helmholtz centres. This year the physical chemist Richard Saykally – who had been proposed by DESY – was among the winners. Saykally is researcher at the University of California, Berkeley, where he studies for instance quantum effects at smallest molecular units of water and catalytic processes. Saykally investigates the disordered structure of water and how the characteristic structures of water in the gas phase are reflected in the liquid phase. His studies can help to better understand complex chemical processes in which water is involved and can lead to a better understanding of chemical quantities like the pH-value. Another topic in Saykally's water research is high resolution terahertz spectroscopy on extremely small water droplets. Furthermore, he plans to study catalysis at graphite surfaces and the chemistry of graphene by means of new methods of ultrafast X-ray diffraction and spectroscopy available at DESY.

All these are highly current topics within Photon Science at DESY. Some of Saykally's experiments can only be performed using the radiation of free-electron lasers like FLASH or European XFEL, while others demand for highly brilliant synchrotron radiation sources like PETRA III.

The International Helmholtz Fellow Award includes 20,000 Euro price money and an invitation for a research stay at one or more Helmholtz Centres. Saykally will realise his stay at DESY as guest of leading scientists Simone Techert and Jochen Küpper and their research groups.



Richard Saykally with his favorite research target.

15 – 20 July:
XXI International Conference on Ultrafast Phenomena UP2018



Participants of the UP2018. Credit: Michael Duncan/The Optical Society.

Nearly 500 participants from almost 30 countries attended the 21st International Conference on Ultrafast Phenomena in Hamburg. Supported by DESY, the University of Hamburg and European XFEL, the UP2018 conference was organised by the European Physical Society EPS. Every two years the Ultrafast Phenomena Conferences are held and are widely recognised as the premier and main international forum for the community of scientists and engineers working in research and development of generation, manipulation and use of ultrashort pulses. In the last years, this field has evolved rapidly, partly thanks to the development of new laser- and accelerator-based sources of ultrashort and ultrafast pulses of electrons and light, such as high harmonic generation or few-cycle optical pulses. Ultrafast phenomena typically cover time scales ranging from picoseconds ($1\ ps = 10^{-12}\ s$) to hundreds of attoseconds ($1\ as = 10^{-18}\ s$). Moreover, the spectral range of ultrashort pulses of radiation could be extended towards terahertz radiation and towards soft and hard X-rays. The UP2018 conference offered the ideal platform for stimulating talks, posters and discussions on all latest developments in this growing field. The conference was accompanied by a table top exhibit featuring the products of leading companies in lasers, optics, optoelectronics and instrumentation.

20 July:
DESY Summer Student Programme 2018

This year more than 860 students from all around the world applied for the Summer Student Programme. It started on 20 July with a record number of 100 selected participants from 35 countries. 36 students worked in the Photon Science part of the programme. The programme ended on 6 September with the usual big closing session, at which selected students presented their work done during the almost eight weeks of the programme. Working on a small project in the environment of a specific DESY or European XFEL research team was the essential part of the stay. In addition, the students were given a series of lectures on DESY activities which after a common part separated in specific lectures for the High Energy Physics and Photon Science students, respectively. A couple of social events completed the programme. The students again appreciated the open minded international atmosphere at DESY which made the stay an unforgettable experience.



The DESY Photon Science summer students of 2018.



All students attending the 2018 summer student programme at the DESY site in Hamburg and at European XFEL.

August

6 August:
Microscopy Today Innovation Award for Saša Bajt

For a novel X-ray lens with unprecedented properties, a team of researchers headed by DESY group leader Saša Bajt has been awarded the 'Microscopy Today Innovation Award' by the Microscopy Society of America. The team's 'High numerical aperture, high efficiency X-ray lenses' were judged as one of the ten best microscopy innovations in this year's competition. The prize was awarded during the Microscopy & Microanalysis 2018 meeting in Baltimore (U.S.).

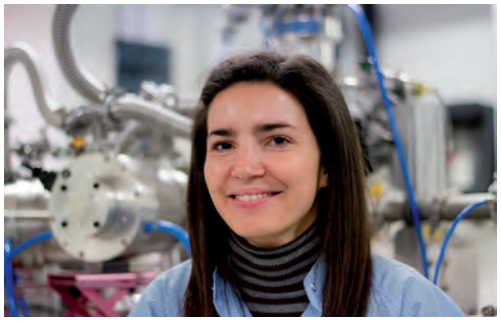
Later, in October 2018 a paper describing the innovative X-ray lens also won the Polish Synchrotron Radiation Society Award 2018 for the best peer-reviewed publication in the field of synchrotron radiation and free-electron laser research. Also in October, Saša Bajt was elected a Fellow of the Optical Society (OSA) for her major contributions to EUV and X-ray optics.



DESY scientist Saša Bajt.

31 August:
Zdenek Herman MOLEC Young Scientist Prize for Francesca Calegari

Francesca Calegari, who leads the DESY Attosecond Science division at CFEL, was awarded the Zdenek Herman MOLEC Young Scientist Prize for her promising work on femtosecond and attosecond laser spectroscopy. The prize was presented at the 22nd European Conference on the Dynamics of Molecular Systems (MOLEC2018) which took place in Dinard, France. The winner of the prize is selected by the international scientific committee of the conference.



DESY leading scientist Francesca Calegari.

September

17 – 19 September:
Workshop on FEL Photon Diagnostics, Instrumentation, and Beamline Design

FELs OF EUROPE is a collaboration of all free-electron laser (FEL) facilities in Europe, with the goal to meet the technological and scientific challenges of the novel and rapidly developing FEL technologies. About 100 participants mainly from China, Japan, Korea, U.S., Italy, Sweden, UK, and Germany joined the fourth workshop on FEL Photon Diagnostics, Instrumentation, and Beamline Design at DESY. The participants represented all existing and upcoming FELs worldwide and discussed how to measure key properties of FEL photon and electron beams, how to characterise the temporal behaviour of electron, FEL, and laser beams, and how to preserve the special properties of ultra-short and intense FEL pulses during beam transport and through optics. Further topics involved the challenges related to detectors and scientific computing for FEL experiments. The workshop comprised more than 40 high-quality oral presentations and 28 posters reflecting the forefront of current research in the corresponding fields.

A highlight was the presentation of the 'FELs of Europe Award on Photon Transport and Diagnostics 2018' to Jaromír Chalupský, deputy head of the Department of Radiation and Chemical Physics (Institute of Physics of the Czech Academy of Sciences in Prague). With the award his outstanding contribution to the development of novel techniques for the diagnostics of non-Gaussian pulses of XUV and X-ray light and his contributions to the study of related ablation and desorption processes are recognised.



Participants of the Workshop on FEL Photon Diagnostics, Instrumentation, and Beamline Design.

27 September:
Three accepted excellence clusters for Hamburg University with DESY participation

In the frame of the 'Excellence Initiative' the German Federal Government together with the federal states realises a strategic promotion of excellent science and cutting-edge research at German universities. End of September the 'Deutsche Forschungsgemeinschaft DFG' (German Research Association)

and the ‘Deutsche Wissenschaftsrat’ (German Research Council) announced, which clusters of excellence were selected by a committee supported by international top scientists. Finally 57 out of 88 submitted proposals were selected to receive a total of 385 million Euro funding for a period of seven years. The Universität Hamburg was very successful with four accepted proposals. Three of them involve collaboration with DESY; two with participation of DESY Photon Science. In the excellence cluster ‘Advanced Imaging of Matter (AIM)’ scientists aim to understand how superconductivity, drugs, and energy production function on the molecular level and how this functioning can be improved by manipulating the involved materials and systems on this molecular level. The second cluster with DESY Photon Science participation is entitled ‘Understanding Written Artefacts’ and aims to uncover old writings in archaeological finds. In the third cluster named ‘Quantum Universe’ scientists of Universität Hamburg and DESY want to bring the various disciplines and topics of particle physics into a common picture.

29 September:
Kick-off for new Data Science in Hamburg – Helmholtz Graduate School for the Structure of Matter

Hamburg gets a new graduate school. The ‘Data Science in Hamburg – Helmholtz Graduate School for the Structure of Matter, DASHH’ will offer young scientist an interdisciplinary and application oriented training for processing and analysis of large data volumes produced in the frame of structure of matter research. The initiative of DESY, University of Hamburg (UHH), Technical University Hamburg-Harburg (TUHH), and five other research institutes in northern Germany will be supported by the Helmholtz Association with around six million Euro for the next six years.

Data science has been identified as a key technology for present and future natural sciences. DESY’s research facilities produce huge amounts of data. The intelligent and efficient use of these data is the central topic of the new graduate school. The aim is to establish scientific informatics at the Campus Bahrenfeld in close co-operation with the universities, offering excellent research conditions in the field of big data science to young PhD students. They will be offered the opportunity to further develop informatics systems and data analysis methods on the basis of highly interesting data from cutting-edge research. This informatics will tackle many new and exciting research problems and the corresponding solutions will not only push forward the scientific research in the field of the structure of matter but also lead to new methods in informatics and mathematics. Speakers of the DASHH team are Nina Rohringer (DESY), Matthias Rarey (UHH) and Sabine Le Borne (TUHH).

October

1 – 2 October:
Second workshop on research at the Large Volume Press at PETRA III

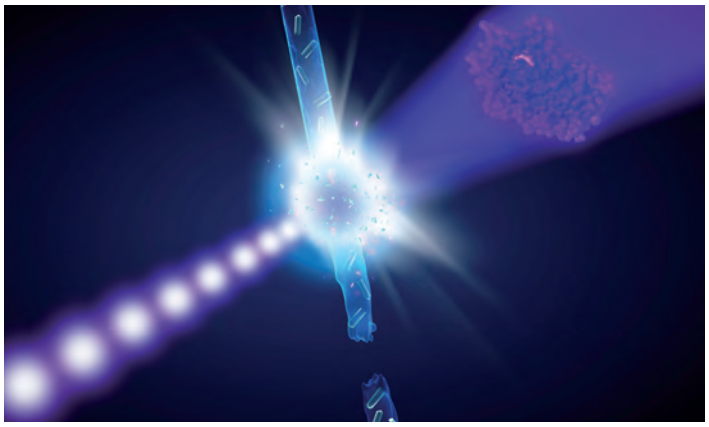
The construction of the Large Volume Press (LVP) – Extreme Conditions beamline P61B at PETRA III is approaching completion with first beam anticipated in spring 2019. The aim of the workshop was to prepare the German and international communities in Earth and Material Sciences for *in situ* studies under extreme conditions of high pressure and temperature using synchrotron radiation X-rays in a LVP. Science cases were presented, user requirements were discussed and a beamline tour was given. The workshop was also a platform to promote the necessity of a monochromator for high-resolution angle-dispersive X-ray diffraction, complementary to energy-dispersive X-ray diffraction. In addition, a number of smaller roll in – roll out LVP instruments were proposed. The workshop attracted about 40 participants. The 14 presentations given by leading experts in their respective fields highlighted a diverse range of research topics, which can be addressed by using diffraction and imaging techniques with a LVP at a synchrotron radiation beamline. Topics presented include: phase relations, solids, melts and fluids at elevated pressure and temperature, mechanical/seismic behaviour of deep-Earth materials, novel functional material synthesis, development of X-ray transparent sample assemblies, and 4D tomographic imaging of synthetic and natural ceramics and rocks.



About 40 participants registered for the second workshop on research at the upcoming Large Volume Press at PETRA III.

2 October:
First publication on results of measurements performed at European XFEL

An international collaboration led by DESY and consisting of over 120 researchers has reported on the results of the first scientific experiment at the new X-ray laser European XFEL. The pioneering work utilising a new method called Serial Femtosecond Crystallography (SFX) not only demonstrates that the new research facility can speed up experiments of this kind by more than an order of magnitude, but also reveals a previously unknown structure of an enzyme responsible for antibiotics resistance. Better understanding of the processes behind the formation of antibiotics resistance might help to design antibiotics that avoid this problem. The scientists published their results, including the first new protein structure solved at European XFEL, in the journal Nature Communications.



Artist's impression of the SFX experiment at the European XFEL: When the ultra-bright X-ray flashes (violet) hit the enzyme crystals in the water jet (blue), the recorded diffraction data allow to reconstruct the spatial structure of the enzyme (right).

21 – 26 October:
International Workshop on Radiative Properties of Hot Dense Matter

95 participants joined this workshop, which takes place every two years with the aim to bring together an international group of leading researchers who investigate radiation processes in hot dense matter. The RPHDM 2018 meeting was organised at DESY and therefore especially emphasised the prospects for future applications of the radiation sources FLASH and European XFEL in plasma research. The research involves topics like dense plasma absorption and emission spectroscopy, radiation heating, non-equilibrium atomic kinetics and radiation transfer, detailed X-ray spectra simulations and much more. The workshop was intended to identify current problems in these fields and to define directions for future research. A special session was held to thank R.W. Lee (UC Berkeley, U.S.) who initiated this conference series.

November

6 November:
Helmholtz Doctoral Prize for Oleg Gorobtsov

Every year, the Helmholtz Association awards one young scientist from each of its six research areas for an outstanding thesis. This year Oleg Gorobtsov from the DESY Photon Science research division was awarded the Helmholtz Doctoral Prize for his outstanding doctoral thesis on coherent X-ray scattering methods. In his thesis, Gorobtsov developed new concepts for utilising the coherence of hard X-ray radiation. His pioneering work will further establish this new research field at modern X-ray light sources. Gorobtsov successfully realised his ideas at the synchrotron radiation source PETRA III and at the free-electron lasers LCLS in the U.S. and FERMI in Italy.



Awardee of the Helmholtz Doctoral Prize: Oleg Gorobtsov.

12 – 13 November:
First LEAPS plenary meeting at DESY

The League of European Accelerator-based Photon Sources (LEAPS) is the association of European research light sources that was founded about one year ago. More than 150 scientists from the 16 involved light sources met at DESY for the first plenary meeting. The participants list also included the directors of all 16 institutions, representatives of eight national science ministries and research funding agencies, as well as a representative of the European Commission. The LEAPS consortium which is chaired by Helmut Dosch (DESY), Caterina Biscari being the Vice-Chairperson, represents the interest of more than 25000 users of the accelerator based research light sources in Europe.



Attendees of the first LEAPS plenary meeting in front of the DESY auditorium.

The LEAPS members have organised themselves into several working and strategy groups dealing with topics like new technological and scientific developments as well as with academic and industrial services and public relations. In addition, the LEAPS consortium also aims to contribute to solving major scientific and societal challenges in the fields of health, energy, food security, engineering and manufacturing, cultural and basic research – everything which can be addressed with the help of the modern research light sources. In the plenary meeting, 13 pilot research projects were presented by the spokespersons of the various collaborations. Representatives of the national funding agencies and the European Commission discussed how the LEAPS programme in future could be supported within the European research funding landscape.

19 November:
PhD thesis prize for Stefan Zeller for photon science at FLASH



At the prize ceremony for the PHD thesis award. From left: DESY Director Helmut Dosch, awardees Alexander Knetsch and Stefan Zeller, Friedrich-Wilhelm Büßer, Chairman of the 'Association of the Friends and Sponsors of DESY'.

Stefan Zeller was awarded the 2018 PhD thesis prize of the Association of the Friends and Sponsors of DESY. The prize was shared between him and Alexander Knetsch and was presented as part of DESY's Science Day in recognition of their excellent doctoral theses. Stefan Zeller started studying physics in 2005 at the Goethe University in Frankfurt. In 2012, he received his master's degree for research work in the field of nuclear, molecular and ion physics. He got a doctoral scholarship from the Helmholtz Centre FAIR (Facility for Antiproton and Ion Research) and took part in the programme of the Helmholtz Graduate School for Hadron and Ion Research. His awarded PhD thesis entitled 'The Helium Dimer' Zeller prepared at Goethe University in Frankfurt.

Although it was known that two helium atoms at ultra-low temperatures can form extremely large molecules, the structure of these helium dimer molecules was never observed before. The group of scientists working with Stefan Zeller used the extreme brightness of FLASH at DESY to remove electrons from the helium molecule in a controlled way, while measuring its shape with extreme precision. Alexander Knetsch (DESY and University of Hamburg) got his PhD in the field of accelerator physics with a work entitled: 'Acceleration of laser-injected electron beams in an electron-beam driven plasma wakefield accelerator'.

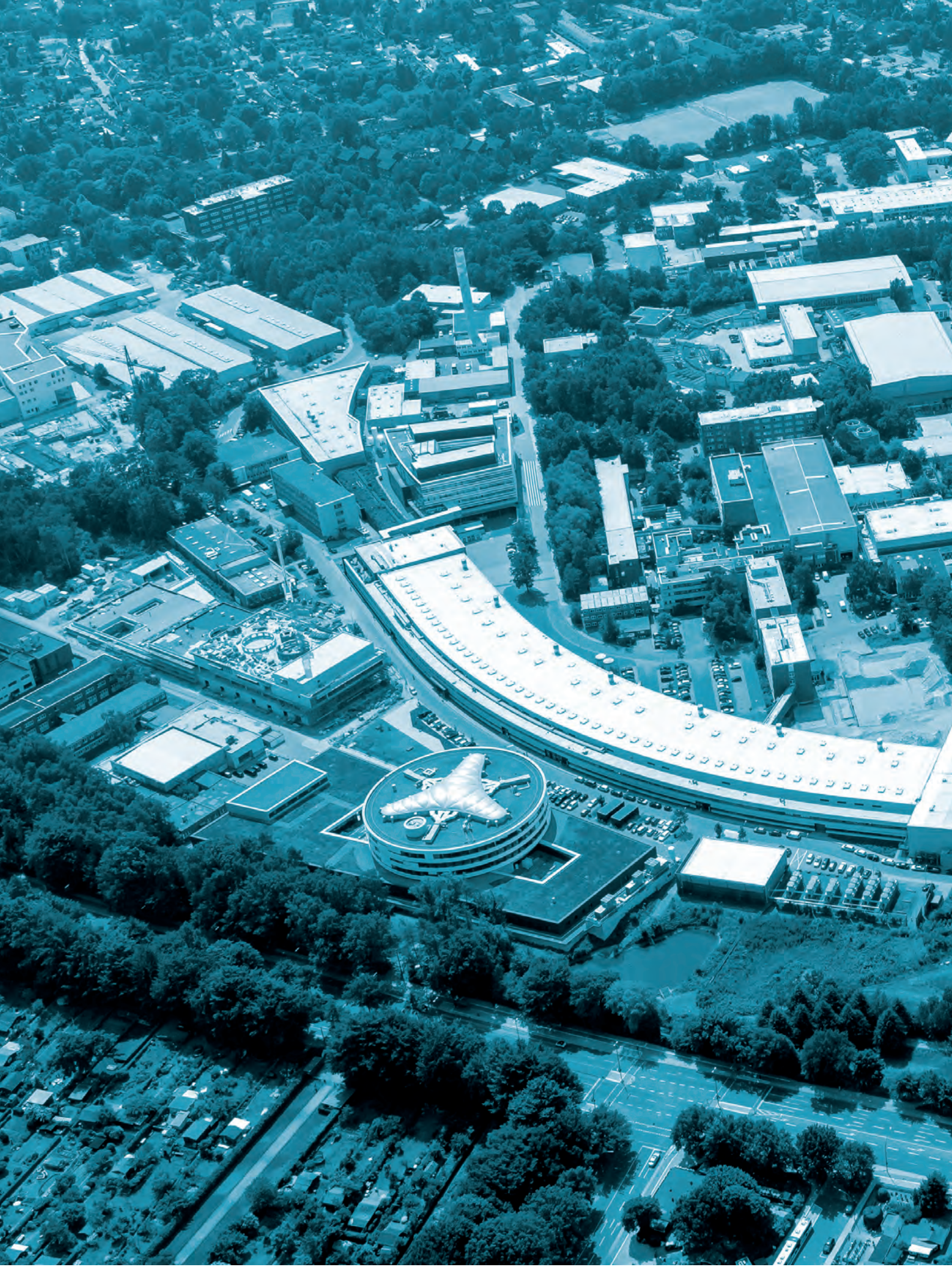
4 – 5 December:
2nd workshop for a new 'Centre for Molecular Water Science (CMWS)'

This workshop was related to the 2018 DESY Research Course and to the International Symposium on 'Trends in Water Research' which was held at DESY end of February and at which a group of local and external experts met to initiate steps towards the foundation of a 'Centre for Molecular Water Science' (CMWS). More than 100 participants registered for the workshop which was intended to bring together the potential partners to identify, discuss and further elaborate the questions driving the science of the CMWS and to summarise the outcome in a revised 'White Paper' defining the scope of activities at the CMWS.

This scope will range from studies of the fundamental properties of water to its role in real-time chemical dynamics, and biochemical- and biological reactions and will also cover water in geo- and astrophysical processes and in nanoscience and technology. The research programme will build on the suite of methods like coherent ultrafast imaging and scattering techniques and novel sample manipulation technologies available at DESY's light sources PETRA III, FLASH and at European XFEL, as well as on the substantial expertise in simulation and theory.



Participants of the 2nd workshop for the new 'Centre for Molecular Water Science'.





Science Highlights

Nanomaterials

- Nanoscale assembly gives the strongest bio-based material 22
- Discrete supermolecular ring assembly 24
- A growing business 26
- Zoom in on surface structures of catalyst particles at work 28
- Semiconductor nanowire under operation conditions 30
- Structure elucidation of large metallo-supramolecular catenanes and rotaxanes 32

Electronic and magnetic structure

- Crystal-field state of the topological Kondo insulator SmB_6 34
- Skyrmions on demand 36
- Magnetic composites with enhanced performance 38
- Rare-earth metals as a superior co-catalyst 40

Structure and structural dynamics

- Unravelling the oxidation state of iron in the deep Earth 42
- Clay mineral waters Earth's mantle from the inside 44
- Engineering alloys for 3D printing 46
- Catching the entatic state in photochemistry 48
- *In situ* coherent X-ray imaging reveals origin of voltage fade in batteries 50

Life Science

- Non-invasive virtual histology of the brain 52
- Coherent diffraction imaging of amyloid fibres 54
- Cells in a new light 56
- A new regulator of photosynthesis in cyanobacteria 58
- From water to plasma in femtoseconds 60

Quantum optics, atomic and molecular dynamics

- Superradiance of an ensemble of nuclei excited by a free-electron laser 62
- Cool chemistry with spatially separated molecular species 64
- Visualizing electron correlation 66
- Molecule formation in the universe 68
- Quantum boiling and relativity 70
- A new window to probe electron-electron interactions 72

Science of laser and X-rays sources - methods and developments

- How to keep up with X-ray FEL pulse trains 74
- Megahertz serial crystallography 76
- Generation of nanoscale liquid sheets 80
- STEAM - Segmented terahertz electron accelerator and manipulator 82
- Novel X-ray lenses for nanometre imaging 84
- Splitting hard X-ray FEL pulses enables measuring ultrafast dynamics 86

Nanoscale assembly gives the strongest bio-based material

Continuous fibres from nanocellulose

Nature provides a wide range of materials that have been subject to evolutionary development for millions of years. These materials, such as wood and spider silk often have a hierarchical material structure meaning that their structure is organised on all scales, from the nanoscale to the macroscopic material. By extracting nanocellulose from wood pulp, which is the high-performance nanoscale building-block giving the mechanical integrity of trees, and processing it in a microfluidic device under carefully chosen conditions, we were able to fabricate macroscopic fibres that outperform all other bio-based materials, natural as well as synthetic, including spider silk, which is considered to be the strongest natural bio-based material.

Nanocellulose is the most abundant biopolymer on earth, and it is the main structural building block of all plants including trees. It is a rod-like particle constituted of the biopolymer cellulose arranged in a predominantly crystalline structure. The length of these so-called nanocellulose fibrils typically ranges from 100 nm to 1000 nm, with a lateral dimension of 3-10 nm. Mechanical performance of individual nanocellulose fibrils is on par with Kevlar, a high-performance synthetic polyamide fibre. To provide necessary structural integrity biosynthesis not only produces fibrils but also organises them in a highly aligned structure that transfers their high performance from nanoscale to macroscopic properties [1].

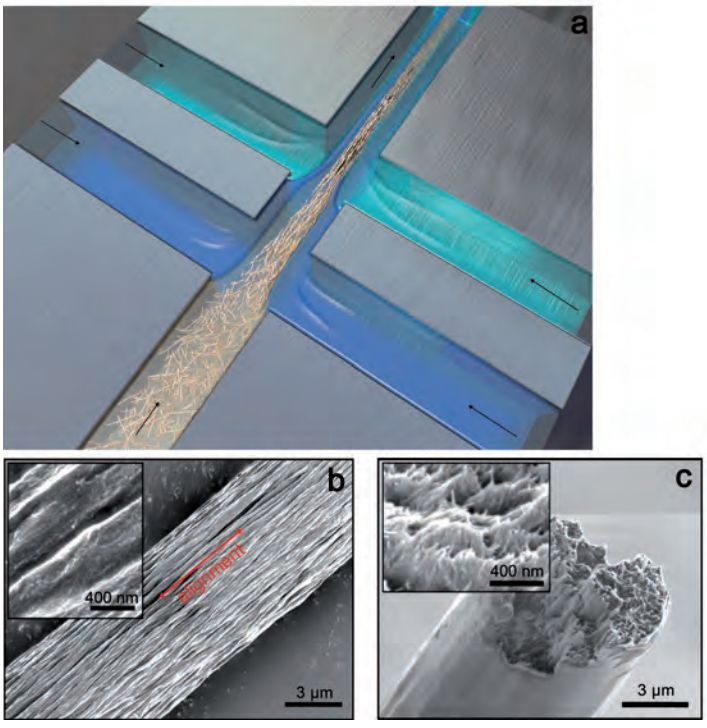


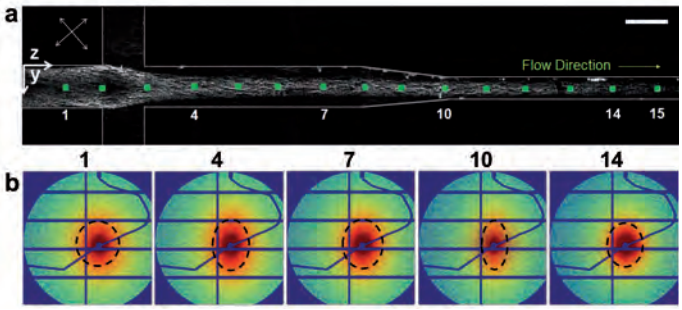
Figure 1

(a) Illustration of the flow assisted nanoscale assembly: nanocellulose fibrils (isotropic particles) in the core flow (light brown colour) are poorly aligned. The first sheath flow (blue colour) contains only water and initiates an alignment of the nanocellulose in the direction of the flow due to the acceleration caused by the sheath flow. The second sheath (light green colour) has low pH resulting in a strong gel thread that can be further processed into the final continuous filament. (b) Scanning electron microscopy (SEM) image of the fibre surface. (c) SEM image of the cross-section of the fibre.
Copyright © 2018 American Chemical Society.

During the last two decades, a wide range of processes have been developed, that today allow industrial extraction of nanocellulose from trees and plants, and several varieties are commercially available in large quantities (tonnes). In parallel there is a rapidly growing research field aiming at developing new and advanced materials based on nanocellulose in the form of aerogels, foams, films, fibres, etc., also including functionalisation, e.g. bioactivity, catalysis, filtering, energy storage and energy generation [1].

A key challenge for the development of any new material concept is thus to make optimal use of the potential provided by its nanoscale building blocks. In the case of man-made nanocellulose materials, as for other man-made materials nanocomponents, the macroscopic mechanical performance is typically significantly lower than that of the nanocomponent.

In 2014 a new concept for fabricating continuous filaments (fibres) from nanocellulose in water was developed based on the widely used microfluidic concept of flow-focusing [2]. An evolved, more robust, process is depicted in Fig. 1. It illustrates a flow-focusing geometry with a central core flow containing a suspension of nanocellulose in water, followed by two sheath flows that accelerate and gel the core-flow in two steps. Both sheath flows are set up by two opposing perpendicular channels that push fluid into the core-flow causing it to form a thread-like cylindrical structure at the centre of the channel. The properties and mechanical performance of the final



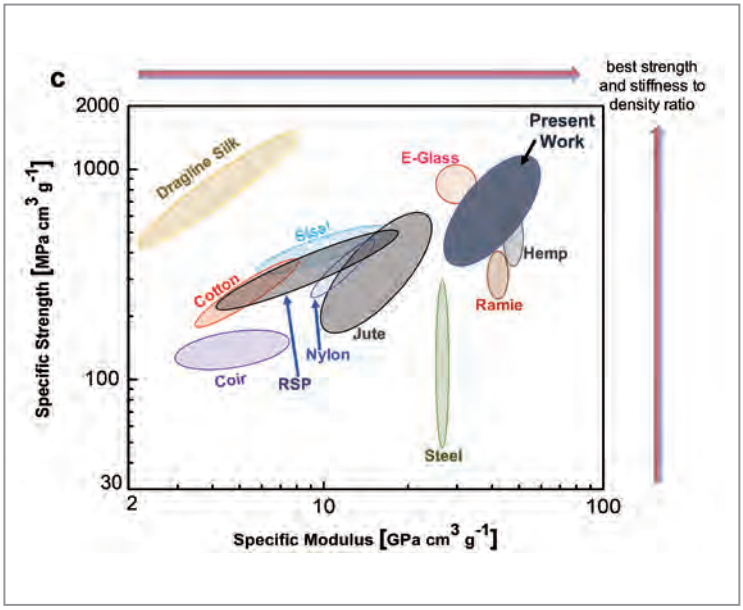


Figure 2

In situ study of the alignment, de-alignment and rotary diffusion of fibrils. (a) Polarised optical microscopy image of the channel used for μSAXS measurements. Lighter areas are caused by the birefringence signal obtained for the nanocellulose suspension. Numbers represent the positions where *in situ* μSAXS measurements (b) are performed. The deformation into an ellipse in the μSAXS diffractograms reflects fibril alignment downstream. (c) Tensile mechanical properties of selected bio-based and synthetic fibre materials. Copyright © 2018 American Chemical Society.

filament are highly dependent on the arrangement of the nanocellulose fibrils during processing and in the final fibres. Alignment of the nanocellulose fibrils in the direction of the final fibre results in a stiffer and stronger fibre.

Although the sheath flows readily aligns the nanocellulose fibrils, the dynamics of the fibrils are affected by e.g. of Brownian dynamics and fibril–fibril interactions. By combining microbeam small angle X-ray scattering (μSAXS) measurements at PETRA III beamline P03 at DESY with polarised optical microscopy, it is possible to elucidate the nanoscale behaviour and understand the controlling mechanisms (Fig. 2a-b). This knowledge not only applies to the case of highly anisotropic nanocellulose fibrils but is in principle applicable to other similar nanoparticles such as carbon nanotubes.

The key to the successful fabrication of filaments with a high degree of alignment resides in careful tuning of the concentration of fibrils in a suspension given their aspect ratio. In the dilute regime (no fibril–fibril interaction), any alignment imposed on the nanofibrils will be competing with dealignment caused by Brownian dynamics. For the case of nanocellulose fibrils in water, the time-scale for Brownian dealignment (~10^{-5} s) is much shorter than the hydrodynamic alignment process in our flow-focusing device (10^{-3}-10^{-2} s). On the other hand, at elevated concentrations, fibrils are highly entangled forming a percolated network that prevents Brownian rotation but at the same time opposes alignment by the accelerating flow. The high aspect ratio of the nanocellulose fibrils and their semi-flexible nature cause entanglement already at 0.03 % mass concentration [3].

The results allowed us to identify an intermediate regime where fibril–fibril interaction is sufficient to reduce rotation due to Brownian dynamics but weak enough to admit flow-induced alignment. This knowledge allows us to define process parameters (concentration, flow-speed, etc.) based on the characteristics of the nanofibrils and to fabricate for the first time continuous filaments from nanocellulose having mechanical properties which surpass other bio-based materials such as spider silk (Fig. 2c).

Author contact: Daniel Söderberg, dansod@kth.se

References

1. D. Klemm et al., 'Nanocelluloses: A New Family of Nature-Based Materials', Angew. Chem. Int. Ed., 50, 5438–5466 (2011).
2. K. M. O. Håkansson et al., 'Hydrodynamic alignment and assembly of nanofibrils resulting in strong cellulose filaments', Nature Communications, 5, 4018 (2014).
3. L. Geng et al., 'Understanding the Mechanistic Behavior of Highly Charged Cellulose Nanofibers in Aqueous Systems', Macromolecules, 51 (4), 1498–1506 (2018).

Original publication

'Multiscale Control of Nanocellulose Assembly: Transferring Remarkable Nanoscale Fibril Mechanics to Macroscale Fibers', ACS Nano 12 (7), 6378–6388 (2018).
DOI: 10.1021/acsnano.8b01084

Nitesh Mittal[1,2], Farhan Ansari[2,3], Krishne Gowda.V[1], Christophe Brouzet[1], Pan Chen[2], P. Tomas Larsson[2,5], Stephan V. Roth[4,6], Fredrik Lundell[1,2], Lars Wågberg[2,4], Nicholas A. Kotov[7] and L. Daniel Söderberg[1,2]

1. Linné FLOW Centre, KTH Mechanics, Stockholm, Sweden
2. Wallenberg Wood Science Centre, Stockholm, Sweden
3. Department of Materials Science and Engineering, Stanford University, United States
4. KTH Department of Fibre and Polymer Technology, Stockholm, Sweden
5. RISE Bioeconomy, Stockholm, Sweden
6. Deutsches Elektronen-Synchrotron DESY, Hamburg, Germany
7. Department of Chemical Engineering, University of Michigan, Ann Arbor, Michigan, United States

Discrete supermolecular ring assembly

From nanoscale physics to metamaterials science

Filling liquid crystals into nanopores results in properties that do not naturally occur in these materials. We show by optical birefringence, X-ray diffraction and Monte Carlo simulations that using disc-shaped molecules in nanopores leads to a temperature-tuneable nanoscale ring formation in combination with 1D charge carrier pathways. The peculiar optical properties and mechanical stability of the macroscopic confining porous matrix renders our system particularly interesting as an electronic and photonic metamaterial. Metamaterials derive their mechanical and functional properties not from the properties of the base materials, but from their newly designed, often multi-scale structures, in terms of precise shape, geometry, size, orientation, and elastic properties.

In general, liquid crystal molecules have the tendency to align along one direction called the director n. This characteristic behaviour gives rise to temperature dependent anisotropic properties, most prominently to optical birefringence [1, 2]. Discotic (disc-shaped) liquid crystals consisting of aromatic hydrocarbons substituted by alkyl side chains tend to stack up into 1D columns, which then arrange in a 2D hexagonal lattice. The liquid character along the columnar axis results from the melting of the alkyl chains, while the π-π-bonding of the conjugated hydrocarbons promotes crystalline properties. Due to the unique combination of these two states, discotic liquid crystals exhibit long-range self-assembly and self-healing mechanisms in combination with high one-dimensional charge mobility along the columnar axes [3].

To study spatial confinement effects on a discotic liquid crystal a macroscopic transparent monolithic silica membrane is synthesized by thermal oxidation of black nanoporous silicon, see inset in Fig.1 [4]. Embedding a discotic liquid crystal by capillary action into such a membrane results in interesting features of the optical properties, see Fig. 1a. At high temperature in the isotropic phase, i.e. the disordered state, the optical retardation vanishes. Upon decreasing temperature the molecules closest to the pore wall start to orient edge-on and with the in-disc direction parallel to the long pore axis due to specific surface conditions, see Fig. 1b. Resulting from the cylindrical confinement they form a bent columnar concentric ring [5]. Surprisingly, upon further cooling, the collective molecular order does not evolve in a continuous manner. Subsequently five pronounced changes in the optical retardation occur resulting from the formation of five concentric columnar rings as seen in the snapshots extracted from Monte Carlo simulations in Fig. 1b-c. Their curvature and geometric frustration is highest in the centre of the pores. Due to this fact, the disordered high-temperature phase is nucleated in the pore centre resulting in a pronounced temperature hysteresis between cooling and heating.

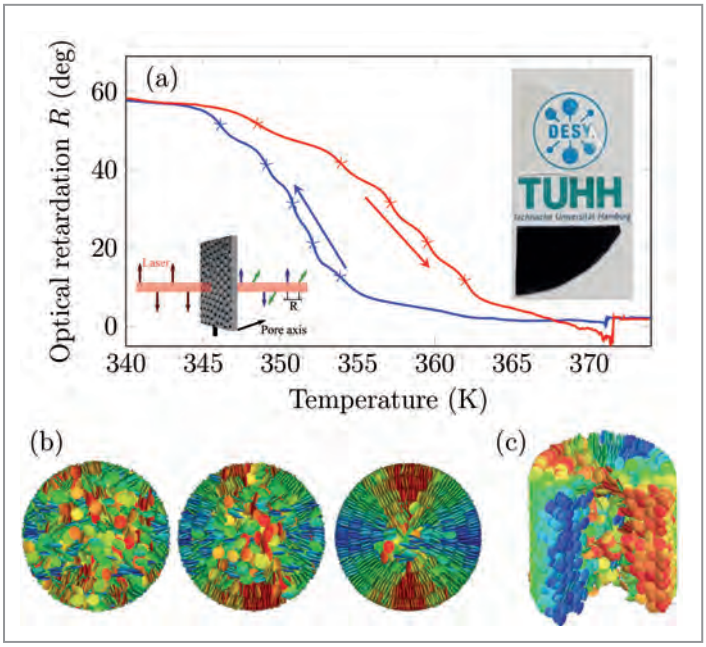


Figure 1

(a) Temperature evolution of the optical retardation R of the discotic liquid crystals in the confined state. Insets: (Left) Schematic of the optical retardation setup and (right) photographs of a black monolithic silicon (bottom) and an optical transparent nanoporous silica membrane (top) through which the DESY logo is visible. (b,c) Snapshots extracted from Monte-Carlo simulation illustrating the formation of concentric columnar rings.

By analysing the thermodynamics of the confined system, we found that the dominant mechanism contributing to the free energy is given by the strong bend of the columns. Extracting

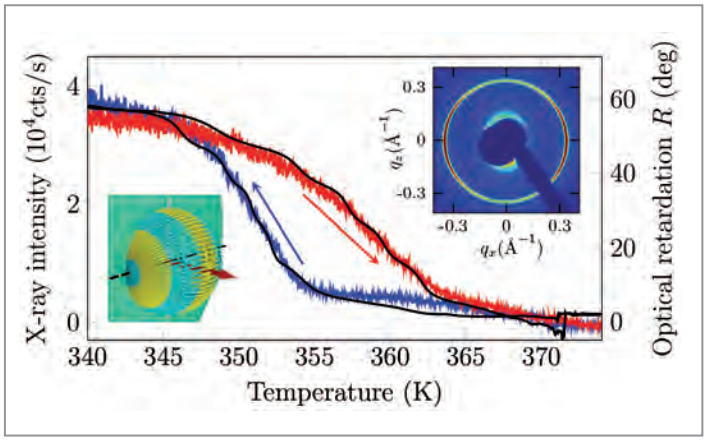


Figure 2

Temperature dependence of the (10) Bragg ring for a cooling/heating cycle. The optical retardation from Fig. 1 serves as a guide to the eye. Insets: (Right) X-ray diffraction pattern of the liquid crystals confined in nanopores focusing on the (10) Bragg ring. (Left) Enlarged reciprocal space assuming a randomization of the (10) reflections with regard to the mean pore axis direction. The red arrow indicates the beam direction, the black dashed line the pore axis and the large green section a part of the Ewald sphere.

the supercooling temperature differences between subsequent rings provides the otherwise hard to determine bend elastic constant K_3 of 2.7 pN. This material constant is a measure for the stiffness of the columns, i.e. how easy they bend. It is in reasonable agreement with values reported for chemically closely related discotic liquid crystals.

The optical measurements are only sensitive to the orientational order. Important complementary insights into the translational order are achieved by temperature-dependent X-ray diffraction experiments in transmission geometry at beamline P08 at PETRA III (see Fig. 2). The scattering geometry is chosen to be sensitive to the molecules' translational order in cross-sections aligned parallel to the long nanopore axes. Resulting from the hexagonal columnar arrangement, and in agreement with the molecules dimensions, an intensity ring at a wave vector transfer $q_{(10)}$ = 0.3445 Å^{-1}, typical of the leading (10) Bragg reflection, is detected. The temperature evolution of the (10) ring follows remarkably well the optical retardation, both in the onset and in the hysteresis width. However, the staircase behaviour is only marginally detectable. This results from defect healing and reorientation mechanisms during the phase transition as shown in parallel-tempering Monte Carlo simulations. The optical experiment is not sensitive to these processes that smear out the phase transition in the X-ray diffraction experiment.

In summary, we have found a near-room-temperature phase transition discretization in a discotic liquid crystal confined in cylindrical nanopores. Our study shows in a remarkable manner how geometrical confinement can alter the physics of liquid crystals. It also highlights how versatile soft matter can adapt to extreme spatial constraints. From a materials science point of view we provide a fine example that solids traversed by pores smaller than the wavelength of visible light can be fine-tuned with regard to their effective optical properties by infiltration of soft, liquid-crystalline fillings. Here, the resulting soft-hard metamaterial exhibits an optical birefringence that can be adapted step-wise by external temperature control.

Author contact: Kathrin Sentker, kathrin.sentker@tuhh.de; Patrick Huber, patrick.huber@tuhh.de

References

1. A. V. Kityk et al., 'Thermotropic orientational order of discotic liquid crystals in nanochannels: an optical polarimetry study', Soft Matter 10, 4522 (2014).
2. A. V. Kityk et al., 'Continuous paranematic-to-nematic ordering transitions of liquid crystals in tubular silica nanochannels', Phys. Rev. Lett. 101, 187801 (2008).
3. S. Chandrasekhar and G. S. Ranganath, 'Discotic liquid crystals', Rep. Prog. Phys. 53, 57 (1990).
4. P. Huber, 'Soft matter in hard confinement: phase transition thermodynamics, structure, texture, diffusion and flow in nanoporous media', J. Phys.: Cond. Matt. 27, 103102 (2015).
5. R. Zhang et al., 'Columnar liquid crystals in cylindrical nanoconfinement', ACS Nano 9, 1759 (2015).

Original publication

'Quantized Self-Assembly of Discotic Rings in a Liquid Crystal Confined in Nanopores', Physical Review Letters 120, 067801 (2018) DOI: 10.1103/PhysRevLett.120.067801

Kathrin Sentker[1], Arne W. Zantop[2], Milena Lippmann[3], Tommy Hofmann[4], Oliver H. Seeck[3], Andriy V. Kityk[5], Arda Yildirim[6], Andreas Schönhals[6], Marco G. Mazza[2] and Patrick Huber[1]

1. Institut für Materialphysik und -technologie, Technische Universität Hamburg, Germany
2. Max-Planck-Institut für Dynamik und Selbstorganisation, Göttingen, Germany
3. Deutsches Elektronen-Synchrotron DESY, Hamburg, Germany
4. Helmholtz-Zentrum für Materialien und Energie, Berlin, Germany
5. Faculty of Electrical Engineering, Czestochowa University of Technology, Poland
6. Bundesanstalt für Materialforschung und -prüfung, Berlin, Germany

A growing business

Growth processes in GaAs nanowires revealed by *in situ* X-ray diffraction

Compound semiconductor nanowires could be the fundamental building blocks of our future high-speed and high-efficiency electronics, but their fabrication includes crystal-growth processes based on self-organization which require a high degree of control. We have studied gallium arsenide nanowires on silicon while they grow and revealed novel details on the evolution of their crystal structure and shape using time-resolved *in situ* X-ray diffraction.

The rapid increase of the clock frequency of micro-processors in our computers and mobile phones, also known as Moore's law, may ultimately come to end, as miniaturization approaches fundamental physical limits. However, transistors based on compound semiconductors such as gallium arsenide (GaAs) or indium arsenide have properties far superior to that of their silicon-based counterparts, promising a tremendous boost of clock frequency of future processor chips.

Since the costs for their fabrication presently surpass those of silicon based devices, current research aims to integrate compound semiconductors into the cost-efficient silicon platform. However, the high lattice-mismatch between GaAs and silicon so far prevents conventional approaches relying on planar semiconductor heterostructures. Vertical semiconductor nanowires, in contrast, provide an elegant solution to this problem, since their small footprint allows accommodation of any lattice mismatch by elastic strain relaxation. Such utilization of the nanowire geometry for an epitaxial integration of GaAs into the well-established silicon platform represents a major step towards large scale application of semiconductor nanowires in electronics [1].

Using X-rays, we have monitored the structural evolution of GaAs nanowires live during their growth. Our observations reveal precise details of the growth process responsible for the evolving shape and crystal structure of the crystalline nanowires. Our findings also provide new approaches to tailor nanowires with desired properties for specific applications. To fabricate the nanowires, we employ the so-called self-catalyzed Vapor-Liquid-Solid (VLS) method, in which tiny droplets of liquid gallium are first deposited on a silicon crystal at a temperature of around 600 °C. Beams of gallium atoms and arsenic molecules are then directed at the silicon wafer, where they adsorb and dissolve in the gallium droplets. After some time, the crystalline nanowires begin to form below the droplets, whereby the droplets are gradually pushed upwards. In this process, the gallium droplets act as catalysts for the longitudinal growth of the nanowires. Although this process is already quite well established, it has not been possible until now to control the crystal structure of the nanowires mainly due to a lack of understanding of how the nanowires grow, which motivates our investigations.

For the experiment, we installed a mobile experimental setup for crystal growth at the resonant scattering beamline P09 at PETRA III. The setup used has been specifically developed by KIT for such X-ray experiments with funding support from the Federal Ministry of Education and Research (BMBF). Our installations at P09 allowed collecting X-ray data to simultaneously determine both the internal structure and the diameter of the growing nanowires. In addition, we

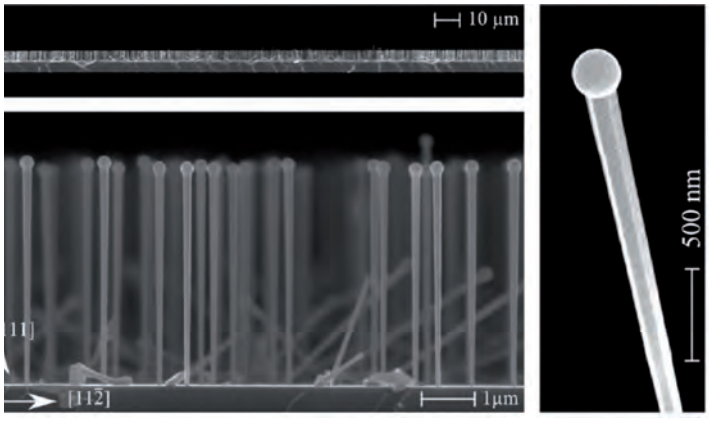


Figure 1

Side-view electron micrographs of self-catalyzed GaAs nanowires grown on silicon at different magnifications. On the right, a single nanowire with the gallium droplet on top and the side-facets is visible. Reprinted with permission from Nano Letters. Copyright (2018) American Chemical Society.

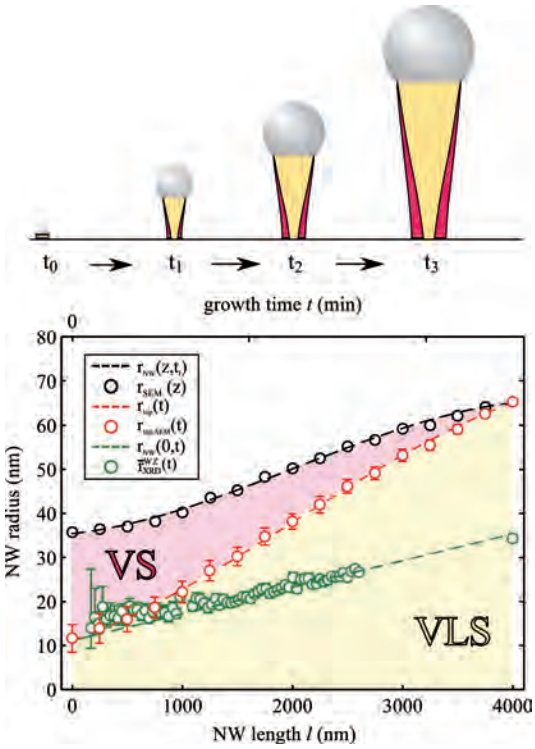


Figure 2

Growth model for radial growth due to increasing size of the gallium droplet (yellow shaded area, both in schematic and graph) and sidewall growth (red shaded area, both in schematic and graph). The final shape of the nanowires as seen by SEM is given by the black circles. The base radius of the nanowires during the growth, as revealed by X-ray diffraction, is shown by the green symbols. The red circles indicate the top radius of the nanowire during growth calculated based on SEM and XRD data. Reprinted with permission from Nano Letters. Copyright (2018) American Chemical Society.

characterized the fully-grown nanowires using the scanning electron microscope (SEM) at the DESY NanoLab.
Over a period of about four hours, the nanowires grew to a length of around 4000 nm. However, we also noticed that the nanowires did not only become longer during this time, but also thicker: their diameter increased from an initial 20 nm to up to 140 nm at the top of the nanowire (see Fig. 1).

We concluded that the growth of the nanowires is not only due to the VLS mechanism but that a second component also contributes, which we were able to observe and quantify for the first time in this experiment. This additional sidewall growth (illustrated in Fig. 2) lets the nanowires gain width. Independently of VLS growth, the vapor deposited material also attaches itself directly to the side walls, particularly in the lower region of the nanowire. This additional contribution can be determined by comparing the X-ray measurements taken during the growth of the nanowire and the *ex situ* SEM post growth analysis.

Furthermore, the gallium droplets are constantly becoming larger as further gallium is added in the course of the growth. This is of particular importance for the growth process, since the size of the droplet not only defines the actual diameter of the nanowire, but also its microstructure via the size-dependent shape of the droplet, and especially by the wetting conditions at the vapor-liquid-solid interface. Certain wetting conditions facilitate the nucleation of different GaAs crystal phases whose coexistence is called polytypism. The hexagonal wurtzite phase of GaAs (usually metastable in the bulk) grows at moderate wetting angles (90°), and the cubic zincblende phase generally at larger wetting angles (130°). The transition between the two phases is usually associated with faulted regions connected to the transient behavior of the liquid Ga-droplet [2].

Using and extending existing growth models [3], we were able to deduce the shape of the droplets, which had also been affected by the increasing droplet size. The effect of this is far-reaching: as the droplet changes in size, the angle of contact between the droplet and the surface of the nanowires also changes. Under certain circumstances, the nanowire then suddenly continues growing with a different crystal structure. Whereas the nanowires initially crystallise in wurtzite structure, this behavior changes after some time and the nanowires adopt a zincblende structure as they continue to grow. This change is important when it comes to applications, since the structure and shape of the nanowires have consequences for the properties of the resulting material.

Such detailed findings not only lead to a better understanding of the growth process; they also provide approaches for tailoring future nanowires to have special properties for specific applications – for example to improve the efficiency of solar panels for deployment in spacecraft.

Author contact: Philipp Schroth, philipp.schroth@kit.edu
Tilo Baumbach, tilo.baumbach@kit.edu
Ullrich Pietsch, pietsch@physik.uni-siegen.de

References

1. C. M. Lieber, 'Semiconductor nanowires: A platform for nanoscience and nanotechnology'. 3rd International Nanoelectronics Conference (INEC), 5–6 (2010).
2. D. Jacobsson, F. Panciera, J. Tersoff, M. C. Reuter, S. Lehmann, S. Hofmann, K. A. Dick, F. M. Ross, 'Interface dynamics and crystal phase switching in GaAs nanowires', Nature 531, 317–322 (2016).
3. J. Tersoff, 'Stable Self-Catalyzed Growth of III–V Nanowires', Nano Letters 15, 6609 6613 (2015).

Original publication

'Radial Growth of Self-Catalyzed GaAs Nanowires and the Evolution of the Liquid Ga-Droplet Studied by Time-Resolved *in situ* X-ray Diffraction', Nano Letters 18, 1, 101–108 (2018). DOI: 10.1021/acs.nanolett.7b03486

Philipp Schroth[1,2,3], Julian Jakob[2], Ludwig Feigl[3], Seyed Mohammad Mostafavi Kashani[1], Jonas Vogel[4,5], Jörg Strempfer[4], Thomas F. Keller[4,5], Ullrich Pietsch[1], and Tilo Baumbach[2,3]

1. Solid State Physics, Department of Physics, University of Siegen, Siegen, Germany
2. Laboratory for Applications of Synchrotron Radiation, Karlsruhe Institute of Technology, Karlsruhe, Germany
3. Institute for Photon Science and Synchrotron Radiation, Karlsruhe Institute of Technology, Eggenstein-Leopoldshafen, Germany
4. Deutsches Elektronen-Synchrotron DESY, Hamburg, Germany
5. Fachbereich Physik, Universität Hamburg, Hamburg, Germany

Zoom in on surface structures of catalyst particles at work

X-rays track ultra-thin oxides on individual nanoparticle facets and identify edges and corners as active sites

Catalysts accelerate desired chemical reactions in chemical industry, fuel cells and car exhausts. To improve their performance, an atomic-scale understanding of the interplay between gas phase and dynamic changes in the catalyst structure is required. This is hampered by the catalyst morphology's complexity, featuring faceted metal alloy nanoparticles on branched oxide supports. Here we combined surface X-ray diffraction and *in situ* mass spectrometry to study well-defined model catalysts, which allowed for tracking thin oxides on individual Pt-Rh nanoparticle facets under realistic reaction conditions, and for correlating them to the monitored catalytic activity. The data indicate that particle edges and corners play a vital role in the activity enhancement.

Our modern everyday life would not exist without the aid of catalysts: they produce more than 90 % of all fine chemicals, facilitate the production of fertilizers that guarantee our vegetable food, and it is the catalysts in fuel cells and car exhaust treatment that provide the world's energy supply and protection of the environment [1, 2].

Due to their wide application, it is of highest economic interest to increase catalyst efficiency. To tailor the underlying catalyst accordingly, an understanding of the correlation between the catalyst particle surface structure and the gas phase under realistic reaction conditions at elevated temperatures and pressures is vital [3]. However, for most characterization methods the dynamic nanoparticle surface structures are not accessible under such conditions, in particular since the catalyst nanoparticles feature a random orientation with concentrations of only a few weight percent [4, 5].

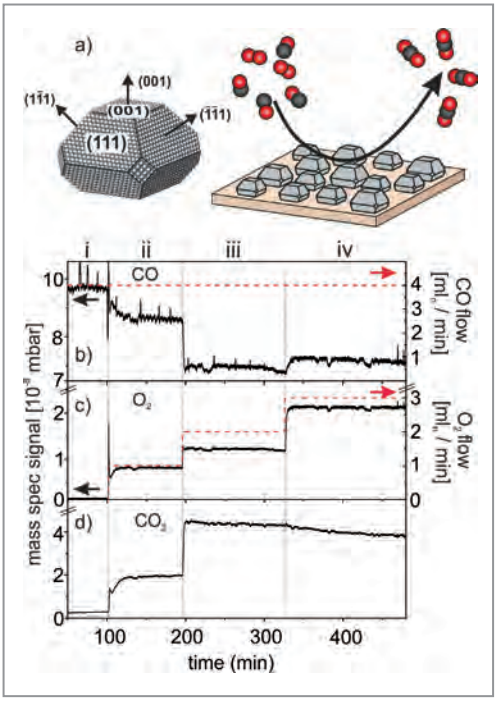


Figure 1
a) Sketch of the sample studied during CO oxidation containing Pt-Rh alloy particles oriented along the same direction and featuring truncated octahedral shapes with (100) and (111) facets. b)-d) Set gas flows of CO and O_2 (right y axis, red) and measured partial gas pressures of CO, O_2 and CO_2 as monitored by *in situ* mass spectrometry (left y axis, black) for conditions (i)-(iv).

In our experiment at beamline P09 at PETRA III, we combined surface X-ray diffraction and *in situ* mass spectrometry to investigate $MgAl_2O_4$(001)-supported Pt-Rh alloy nanoparticles during CO oxidation, an essential reaction in vehicle exhaust gas cleaning. The particles were of truncated octahedral shape featuring (100) and (111) facets, with all particles aligned along the same direction, see Fig. 1 a). This facilitated a summing up and hence an amplification of the diffraction signals of distinct facet surface structures. Thus, we reduced the heterogenic complexity of a real catalyst, and gained, with unprecedented spatial resolution, insight into the structural changes of individual nanoparticle facets under industrially relevant conditions.

The total reactor pressure and temperature were held constant at 50 mbar and 650 K, respectively, while the partial gas pressures of O_2 and CO were systematically varied to probe conditions (i) 4 ml/min CO, no O_2, (ii) 4 ml/min CO, 1 ml/min O_2, (iii) 4 ml/min CO, 2 ml/min O_2, and (iv) 4 ml/min CO, 3 ml/min O_2, with Ar flow adjusted to maintain a total gas flow of 50 ml/min.

Figures 1 b)-d) show the set gas flows and the measured partial pressures of CO, O_2, and the reaction product CO_2 as a function of the stepwise O_2 increase. When O_2 was introduced to the CO/Ar mixture (ii), the sample became catalytically active, evidenced by the sudden CO_2 production increase. The highest CO_2 production and catalytic activity were achieved under O_2/CO stoichiometry (iii). This is also underlined by the CO and O_2 partial pressures, which were reduced compared to their set values, indicating an immediate

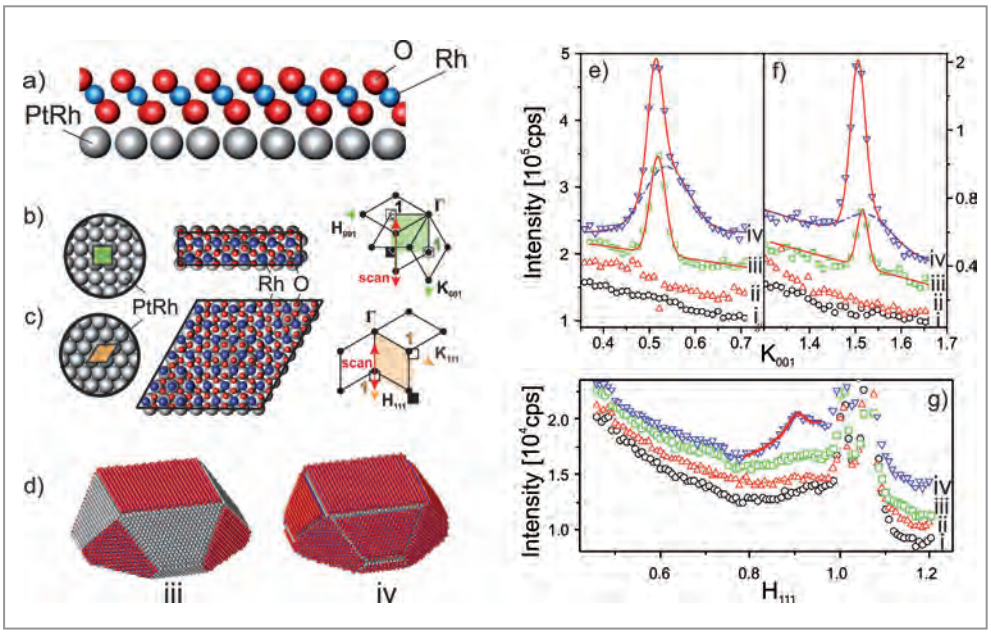


Figure 2

a) Side view of the trilayer Rh-O-Rh surface oxide that forms a Rh c(2x8) surface oxide on the (100) facets and a Rh p(9x9) surface oxide on the (111) facets. b) (100) metallic facet with the surface unit cell indicated in green, top view of the Rh c(2x8) surface oxide and reciprocal space in surface coordinates of the (100) facet. c) (111) metallic facet with the surface unit cell indicated in orange, top view of the Rh p(9x9) surface oxide and reciprocal space coordinates of the (111) facet. d) Determined averaged particle shapes with surface oxides for conditions (iii) and (iv). Reference scans for the e), f) Rh c(2x8) surface oxide on the (100) facets (H_{001} = 0.875) and the g) Rh p(9x9) surface oxide on the (111) facets (K_{111} = 0) for conditions (i)-(iv); solid (red) lines represent fits to the data.

consumption of CO and O_2. When switching to overstoichiometry (iv), the CO_2 production slightly decreased and less CO and O_2 were being consumed, indicating a partial catalyst poisoning.

To correlate the particle surface structures to the catalytic activity, we performed so called reference scans, in which the appearance/presence of distinctive peaks act as a fingerprint for the presence of the trilayer Rh-O-Rh surface oxide. As shown in Fig. 2 a) the trilayer surface oxide grows on the particle (100) facets as a Rh c(2x8) and on the (111) facets as a Rh p(9x9) structure [6]. Figs. 2 b) and c) display atomic models of the clean and the oxidized (100) and (111) facets, respectively, along with the reference scans' reciprocal space positions in the surface coordinates of the corresponding facets.

The experimentally retrieved particle shapes and their oxide coverages deduced from the reference scans for conditions (iii) and (iv) are shown in Fig. 2 d). The reference scans are summarized in Figs. 2 e), f) and g) for the (100) and the (111) facets, respectively. They reveal that under condition (ii) all particle facets featured a metallic surface. Under the highly active stoichiometric condition (iii) clear peaks evidencing the Rh c(2x8) surface oxide on the (100) facets were discernible while the (111) facets stayed metallic. Only under overstoichiometric conditions (iv) the Rh p(9x9) surface oxide was evidenced on the (111) facets, resulting in completely oxide-covered particles. Shoulders to the Rh c(2x8) surface oxide peaks under this condition indicate its coexistence with 3D bulk oxides, explaining the slight activity decrease due to bulk oxide poisoning.

As the catalytic activity increased tremendously in the transition to condition (iii) but decreased only slightly in the transition to condition (iv) we could assign the enhanced CO_2 production at the sites available at the metal-oxide-gas triple phase boundary of the nanoparticle edges and corners, at which the oxides cannot grow together.

Our approach employing well-defined model catalysts allows for yielding an atomic-scale insight into the dynamic changes of nanoparticle surface structures under realistic reaction conditions and contributes to the knowledge-based tailoring of improved catalysts.

Author contact: Uta Hejral, uta.hejral@sljus.lu.se
Andreas Stierle, andreas.stierle@desy.de

References

1. G. Ertl, H. Knözinger, F. Schüth and J. Weitkamp, 'Handbook of heterogeneous catalysis', Wiley-VHC, Weinheim, Germany (2008).
2. R. Schlögl, 'Heterogeneous Catalysis', Angew. Chem., Int. Ed. Engl. 54, 3465-3520 (2015).
3. K. F. Kalz, R. Kraehnert, M. Dvoyashkin, R. Dittmeyer, R. Glaser, U. Krewer, K. Reuter and J. D. Grunwaldt, 'Future challenges in heterogeneous catalysis: understanding catalysts under dynamic reaction conditions', ChemCatChem 9, 17-29 (2017).
4. M. A. Newton, 'Dynamic adsorbate/reaction induced structural change of supported metal nanoparticles: heterogeneous catalysis and beyond', Chem. Soc. Rev. 37, 2644-2657 (2008).
5. A. Frenkel, 'Solving the 3D structure of metal nanoparticles', Z. Kristallogr. 222, 605-611 (2007).
6. P. Nolte, A. Stierle, N. Y. Jin-Phillipp, N. Kasper, T. U. Schulli and H. Dosch, 'Shape changes of supported Rh nanoparticles during oxidation and reduction cycles', Science 321, 1654-1658 (2008).

Original publication

'Identification of a Catalytically Highly Active Surface Phase for CO Oxidation over PtRh Nanoparticles under Operando Reaction Conditions', Physical Review Letters 120, 126101-1–126101-6 (2018). DOI: 10.1103/PhysRevLett.120.126101

Uta Hejral[1,2,3], Dirk Franz[1,2], Sergey Volkov[1,2], Sonia Francoual[1], Jörg Strempfer[1] and Andreas Stierle[1,2]

1. Deutsches Elektronen-Synchrotron DESY, Hamburg, Germany
2. Fachbereich Physik, Universität Hamburg, Hamburg, Germany
3. Division of Synchrotron Radiation Research, Lund University, Lund, Sweden

Semiconductor nanowire under operation conditions

Nanowire in action

GaN nanowires are promising building blocks for future optoelectronic devices and nanoelectronics. They exhibit stronger piezoelectric properties than bulk GaN. This phenomenon may be crucial for applications of nanowires and makes their study highly important. We report on an investigation of the structure evolution of a single GaN nanowire under an applied voltage bias till its mechanical break. From the coherent X-ray Bragg diffraction of a single nanowire and a finite element method model, we determined its piezoelectric constant to be ~ 7.7 pm/V and the ultimate tensile strength ~ 1.22 GPa. Our work demonstrates the power of *in operando* X-ray structural studies of single nanowires for their effective design and implementation with desired functional properties.

Semiconductor nanowires (NWs) based on gallium nitride (GaN) have promising applications for light-emitting diodes (LEDs), low-cost solar cells, transistors, single photon sources, and other devices [1]. The hexagonal wurtzite (WZ) crystal structure of GaN NWs has an internal electric field along the [0001] crystallographic direction. Nitride-based LEDs grown on a c-plane GaN substrate usually exhibit the blue shift with increased injected current. Integration of the nanowires into an electric circuit by metallic contacts may induce strain and, therefore, may lead to additional piezoelectric effect in the structure. This may dramatically influence electron-hole pair recombination and alter the efficiency of optoelectronic devices based on GaN NWs. Therefore, the investigation of the influence of applied voltages on the structure of a single GaN NW is of significant importance.

In this work, we applied the newly developed coherent X-ray Bragg diffraction technique [2] to investigate the influence of an applied voltage bias on the structure of a single GaN NW. This technique allows non-destructive investigation of nanostructures *in situ* and *in operando* and provides information in three dimensions (3D) about strain and deformation of single nanostructures with the spatial resolution reaching 10 nm [3, 4]. The experiment was performed at the coherence beamline P10 at PETRA III. The geometry of the experiment is presented in Fig. 1. The X-ray beam with photon energy of 9.6 keV was focused at the sample down to one micrometre in size. The samples were provided by the NanoLund Laboratory at Lund University, Sweden. The GaN NWs with a diameter of 350 nm and a length of 3.5 µm were deposited on a Si (111) chip with a 100 nm thermally grown SiO_2 insulating layer on top. Further, 220 nm thick gold (Au) contacts were deposited to connect the ends of the single NW to the electrical power supply.

The structural changes of the NW were investigated using coherent X-ray Bragg diffraction. The 3D scattered intensity

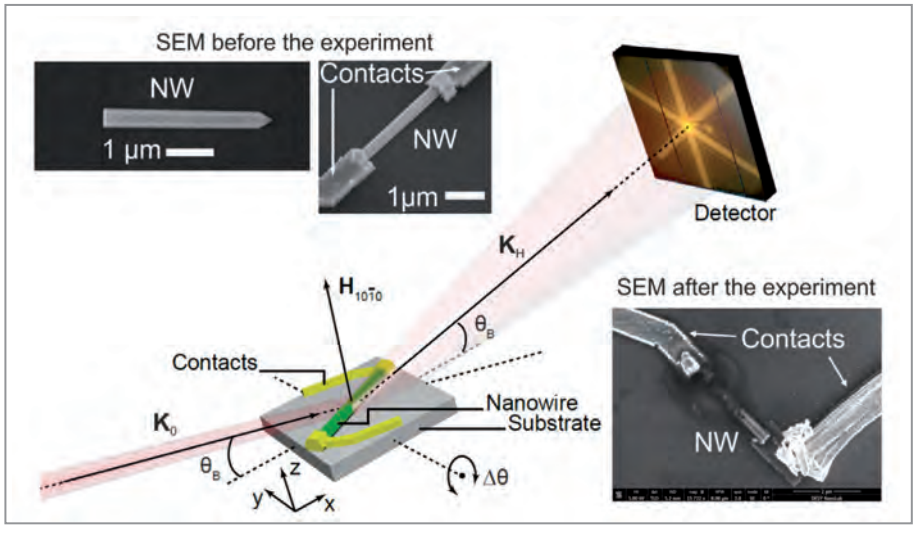


Figure 1

Scheme of the Bragg coherent scattering measurement geometry. The incoming X-ray beam $\boldsymbol{K}_0$ is scattered by a GaN NW at the Bragg angle θ_B and the resulting diffraction pattern is recorded by the 2D detector in the far-field. In the insets on the top, the SEM images of a free-lying NW and the NW with metal contacts (taken at NanoLund) are shown. The inset in the bottom (taken at DESY NanoLab) presents the SEM image of the broken NW after the voltage bias of 15 volts was applied.

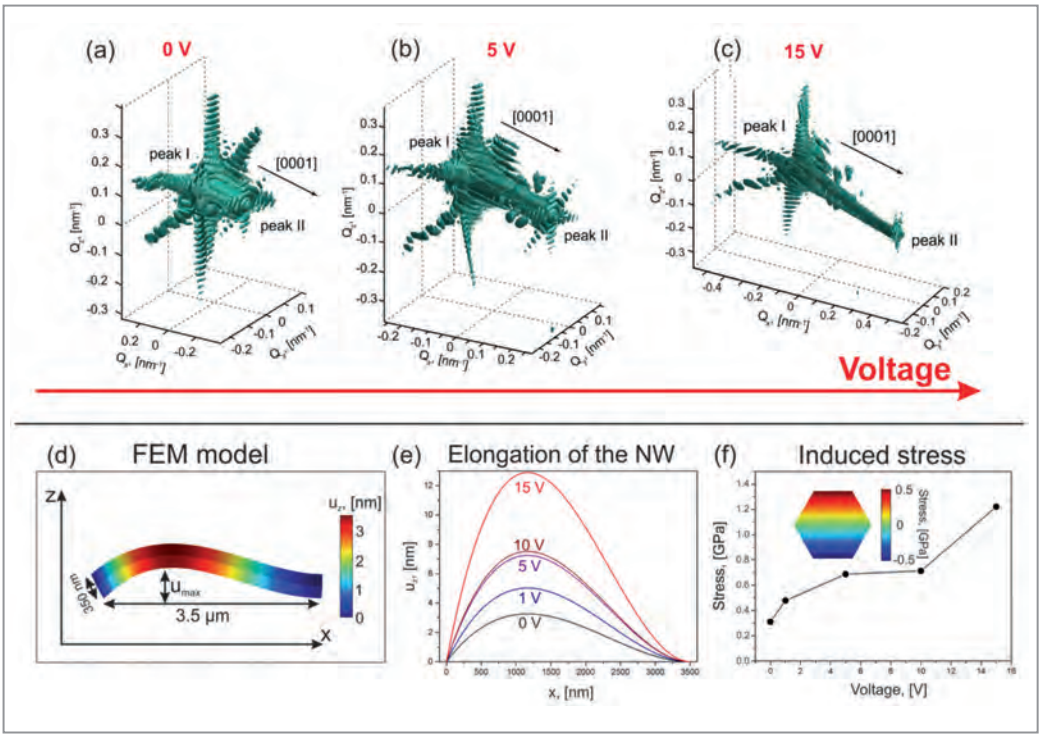


Figure 2

(a-c) Evolution of the 3D intensity distribution around the $10\bar{1}0$ Bragg reflection of a GaN NW under the given applied voltage bias. (d) Equilibrium shape of the NW determined from the model. (e) Displacement profile $u_z(x)$ of the NW along its length determined by the analytical solution and FEM model for different voltage values. (f) Dependence of the maximum value of the tensile stress as a function of the applied voltage bias. The ultimate tensile stress of the GaN NW of 1.22 GPa was reached at the maximum voltage of 15 V, after which the NW was broken.

distributions of the NWs without metal contacts, with contacts and under applied voltage bias were analysed. The SEM images of the NWs are shown as insets in Fig. 1. The experimental data revealed the presence of significant structural changes of the NWs already after the deposition of the metal contacts, which were increased at the applied voltage (see Figs. 2(a-c)).

Bending of the GaN NW under the applied voltage was the major effect observed in our experiment. We followed the evolution of the intensity distribution of the $10\bar{1}0$ GaN Bragg peak of the GaN NW as shown in Figs. 2(a-c), until its breakdown at 15 V (see SEM images in Fig. 1). Employing analytical simulations based on elasticity theory and a finite element method (FEM) approach, we developed a 3D model of the NW bending. The equilibrium shape of the NW in FEM simulations given by the analytical solution is shown in Fig. 2(d). We used our analytical solution to the elasticity equation for a thin rod to determine the elongation Δl of the NW as a function of the applied voltage bias (see Fig. 2(e)). In this way we found the average value of the piezoelectric constant d_{33} of the GaN NW in [0001] crystallographic direction to be $d_{33} = 7.7 \pm 2.2$ pm/V. The determined value of the piezoelectric constant is significantly higher than that of the bulk GaN value of 2 pm/V.

Bending of the NW induces tensile and compressive strain fields in the NW [5]. We expect that the failure of the GaN NW is likely to start at the mostly strained top facet of the NW (see Fig. 2(d)). We therefore determined the maximum tensile stress σ_{max} values on the top facet of the NW for different applied voltage values (see Fig. 2(f)). From the break of the GaN NW at 15 V we deduce the ultimate tensile strength to be ~ 1.22 GPa.

In summary, our measurements of the single GaN NW demonstrated a visible distortion of the $10\bar{1}0$ GaN Bragg peak intensity due to the bend of the NW under applied voltage bias. Our work demonstrates the power of *in operando* X-ray structural studies of single NWs for their effective design and implementation with desired properties.

Author contact: Sergey Lazarev, sergey.lazarev@desy.de
Ivan Vartaniants, ivan.vartaniants@desy.de

References

1. W. Lu, 'Semiconductor Nanowires: From Next-Generation Electronics to Sustainable Energy', The Royal Society of Chemistry, (2014).
2. I. A. Vartanyants, O. M. Yefanov, 'X-ray Diffraction. Modern Experimental Techniques. Coherent X-ray Diffraction Imaging of Nanostructures', Pan Stanford Publishing: Singapore, Chapter 12, pp 341–384, (2015).
3. D. Dzhigaev, A. Shabalin, T. Stankevič, U. Lorenz, R. P. Kurta, F. Seiboth, J. Wallentin, A. Singer, S. Lazarev, O. M. Yefanov, M. Borgström, M. N. Strikhanov, L. Samuelson, G. Falkenberg, C. G. Schroer, A. Mikkelsen, R. Feidenhans, I. A. Vartanyants, 'Bragg coherent x-ray diffractive imaging of a single indium phosphide nanowire', J. Opt., 18, 064007, (2016).
4. M. C. Newton, S. J. Leake, R. Harder, I. K. Robinson, 'Three-dimensional imaging of strain in a single ZnO nanorod', Nat. Mater., 9, 120–124 (2010).
5. L. D. Landau, E. M. Lifshitz, 'Theory of Elasticity': Vol. 7 (Course of Theoretical Physics), 3rd ed., Elsevier, (2012).

Original publication

'Structural Changes in a Single GaN Nanowire under Applied Voltage Bias', Nano Letters 18 (9), 5446–5452 (2018). DOI: 10.1021/acs.nanolett.8b01802

Sergey Lazarev[1,2], Dmitry Dzhigaev[1], Zhaoxia Bi[3], Ali Nowzari[3], Young Yong Kim[1], Max Rose[1], Ivan A. Zaluzhnyy[1,4], Oleg Yu. Gorobtsov[1], Alexey V. Zozulya[1], Filip Lenrick[3], Anders Gustafsson[3], Anders Mikkelsen[3], Michael Sprung[1], Lars Samuelson[3], and Ivan A. Vartanyants[1,4]

1. Deutsches Elektronen-Synchrotron DESY, Hamburg, Germany
2. National Research Tomsk Polytechnic University (TPU), Tomsk, Russia
3. NanoLund, Department of Physics, Lund University, Lund, Sweden
4. National Research Nuclear University MEPhI (Moscow Engineering Physics Institute), Moscow, Russia

Structure elucidation of large metallo-supramolecular catenanes and rotaxanes

Mechanical bonding in Pd(II)-mediated coordination architectures

Catenane and rotaxane nanostructures are raising considerable interest as components of artificial molecular machines, selective receptors, enzyme-mimicking catalysts and stimuli-responsive materials. Beyond multistep organic synthesis, self-assembly of organic building blocks with pre-programmed shape and connectivity, mediated by transition metal cations such as Pd(II), gives access to nano-sized architectures of increasing size and complexity. The structure elucidation of such assemblies, some of which reach the size of small proteins, poses tremendous challenges to modern analytical techniques. Besides multi-dimensional NMR techniques and high resolution mass spectrometry, single crystal structure determination by X-ray diffraction methods is an indispensable tool. PETRA III's highly brilliant synchrotron radiation and automated crystal handling implemented at beamline P11 allowed us to obtain structures of large assemblies from small, fragile and solvent-soaked crystals, not accessible by conventional diffractometers.

Supramolecular coordination chemistry describes the construction of complex nano-architectures by reacting tailor-made organic molecules with suitable metal cations, acting as some kind of glue [1]. Coordination bond reversibility, together with iterative reshuffling of components until reaching the thermodynamically most stable structure, are key characteristics of a process called 'self-assembly'. The latter phenomenon may be compared to a children's puzzle with only one solution that solves itself, just by shaking the box.

A popular combination of organic ligands and metal cations are bi-functional pyridine bridges L and palladium(II) cations, offering a robust, square-planar coordination environment.

Depending on ligand length and shape, ring- or cage-like Pd_nL_{2n} structures of different sizes and geometries are formed [2]. In certain cases, topologically more advanced structures result, for example interpenetrated double cages [3] or supramolecular knots [4].

NMR and mass spectrometry are usually the first methods of choice to get insight into the nature of such a self-assembly reaction product. While the former method gives information about the symmetry of the architecture, the latter technique reveals its stoichiometry. Precise spatial information, however, requires single-crystal diffraction data. As the trend is going to larger and larger assemblies, and crystals of ring- and cage-shaped compounds often contain substantial

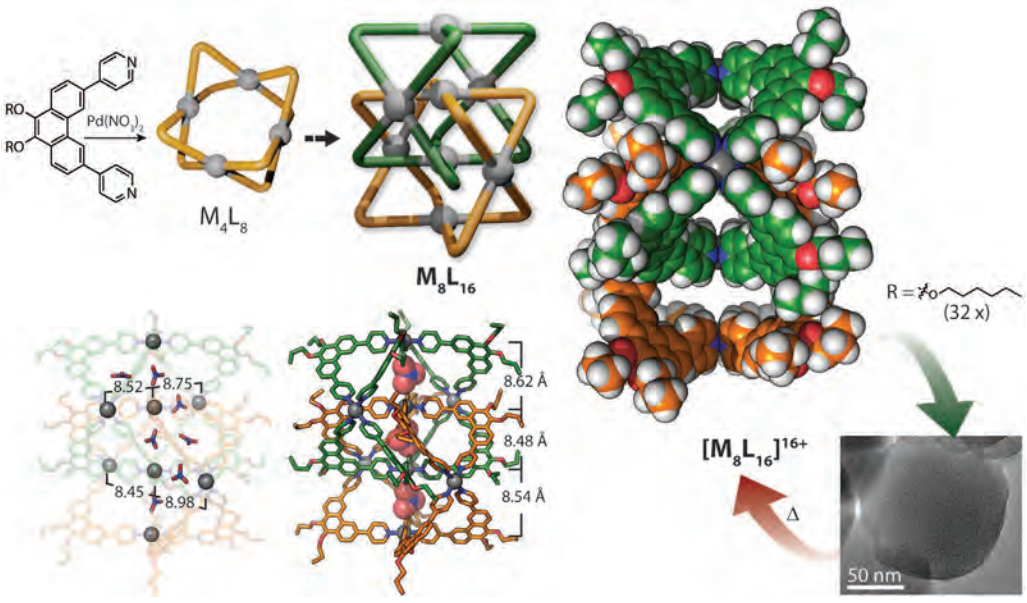


Figure 1

A simple bis-monodentate ligand self-assembles with Pd(II) cations to M_4L_8 ring structures that dimerize to an unprecedented M_8L_{16} catenane when nitrate anions are offered. Synchrotron single crystal X-ray analysis at beamline P11, PETRA III allowed for collecting diffraction data from tiny, fragile crystals, revealing details of the interlocked structure. Catenanes equipped with alkyl chain substituents were further shown to aggregate to vesicles in a solvent dependent process.

amounts of disordered solvent molecules, challenges for X-ray structure analysis are increasing.

We recently reported two unprecedented, mechanically interlocked compounds, one being a Pd_8L_{16} catenane, the other a Pd_6L_{12} rotaxane. Both systems allow comparing different aspects of state-of-the-art metallo-supramolecular self-assembly, showcased by their single-crystal synchrotron structures.

The first study describes the supramolecular assembly of phenanthrene-based ligands forming a Pd_8L_{16} metallo-supramolecular catenane of record-breaking size, composed of two entangled Pd_4L_8 rings (Fig. 1). It only forms in acetonitrile in the presence of nitrate anions, whereas in other solvents its formation is disfavoured. X-ray analysis revealed this self-assembled structure to be a very large 'Hopf link' catenane featuring channel-like cavities which are occupied by nitrate anions. The importance of the anions as catenation templates became particularly imminent when we observed the nitrate-triggered structural rearrangement of a mixture of M_3L_6 and M_4L_8 assemblies, formed in the presence of tetrafluoroborate anions, into the same interlocked molecule.

Our second report deals with the unique supramolecular morphology of a rotaxane-like Pd_6L_{12} cage-in-ring structure which self-assembled from 12 BODIPY dye-based ligands together with 6 palladium ions (Fig. 2). The overall structure is a result of the perfect geometrical complementarity of a cage-like Pd_2L_4 core and a surrounding Pd_4L_8 macrocycle, both composed of the same ligand and metal building blocks. Synchrotron X-ray structure analysis revealed extensive π-stacking as major stabilizing interaction.

In comparison, both studies show the large scope of possible architectures resulting from Pd(II)-mediated assembly of organic ligands. Elucidation of their 3-dimensional structures would not have been possible without the use of a powerful synchrotron radiation source. Understanding design principles and formation pathways of such intricate metallo-supramolecular assemblies is the key requirement for fostering the development of functional nano-devices, supramolecular catalysts and smart materials.

Author contact: Guido Clever, guido.clever@tu-dortmund.de
Arne Lützen, arne.luetzen@uni-bonn.de

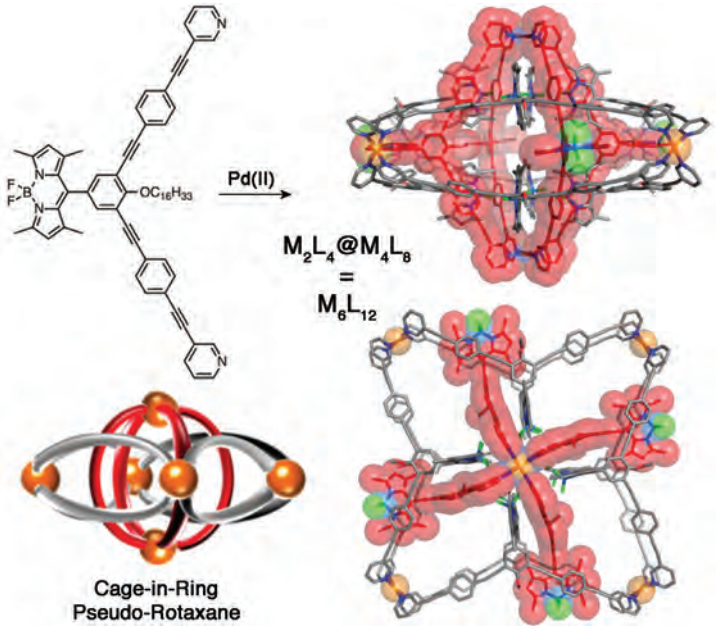


Figure 2

A longer bis-monodentate ligand carrying a BODIPY-dye as part of its backbone reacts with Pd(II) cations to a unique mechanically interlocked structure of M_6L_{12} stoichiometry in which a M_2L_4 cage is embedded inside a M_4L_8 ring. Synchrotron diffraction data shows that the structure is governed by a perfect size match and mutual π-stacking.

References

1. T. R. Cook, Y.-R. Zheng and P. J. Stang, 'Metal–Organic Frameworks and Self-Assembled Supramolecular Coordination Complexes: Comparing and Contrasting the Design, Synthesis, and Functionality of Metal–Organic Materials', Chem. Rev. 113, 734 (2013).
2. G. H. Clever and P. Punt, 'Cation-Anion Arrangement Patterns in Self-Assembled Pd_2L_4 and Pd_4L_8 Coordination Cages', Acc. Chem. Res. 50, 2233 (2017).
3. M. Frank, M. D. Johnstone and G. H. Clever, 'Interpenetrated Cage Structures', Chem. Eur. J. 22, 14104 (2016).
4. D. M. Engelhard, S. Freye, K. Grohe, M. John and G. H. Clever, 'NMR-Based Structure Determination of an Intertwined Coordination Cage Resembling a Double Trefoil Knot', Angew. Chem. Int. Ed. 51, 4747 (2012).

Original publications

'Hierarchical Assembly of an Interlocked M_8L_{16} Container', Angew. Chem. Int. Ed. 57, 5534 (2018). DOI: 10.1002/anie.201800490

Witold M. Bloch[1,2], Julian J. Holstein[1], Birger Dittrich[3], Wolf Hiller[1] and Guido H. Clever[1]

1. Technische Universität Dortmund, Fakultät für Chemie und Chemische Biologie, Dortmund, Germany
2. Department of Chemistry and Centre for Advanced Nanomaterials, School of Physical Sciences, The University of Adelaide, Adelaide, Australia
3. Institute for Inorganic Chemistry and Structural Chemistry, Heinrich-Heine University Düsseldorf, Düsseldorf, Germany

'A Rotaxane-like Cage-in-Ring Structural Motif for a Metallosupramolecular Pd_6L_{12} Aggregate', Angew. Chem. Int. Ed. 57, 12171 (2018). DOI: 10.1002/anie.201806814

Martin Käseborn[1], Julian J. Holstein[2], Guido H. Clever[2] and Arne Lützen[1]

1. Rheinische Friedrich Wilhelms-Universität Bonn, Kekulé-Institut für Organische Chemie und Biochemie, Bonn, Germany
2. Technische Universität Dortmund, Fakultät für Chemie und Chemische Biologie, Dortmund, Germany

Crystal-field state of the topological Kondo insulator SmB_6

A core-level non-resonant inelastic X-ray scattering study

Topological insulators (TIs) are receiving tremendous attention in recent years because they have promising applications in spintronic devices, and perhaps also enable the development of dissipation-less transistors for quantum computing. TIs are insulating or semiconducting in the bulk, but have symmetry protected metallic states on the surface. The most studied materials in this context are band insulators or semiconductors. Here, we focus our efforts on the search for strongly correlated materials that could also have non-trivial topological properties but with even more exotic properties. The Kondo insulator SmB_6 is very promising in this respect. In the present study we determined the ground state symmetry of the Sm bulk states in SmB_6 with non-resonant inelastic X-ray scattering (NIXS), also called X-ray Raman scattering (XRS).

SmB_6 has very recently been identified as the candidate to be the first topological insulator that is also strongly correlated [1-3]. It is a so-called Kondo insulator with an intermediate Sm 4f valence (2.6^+). Being a bad metal at room temperature, it opens up a gap at low temperatures due to correlation effects involving the Sm 4f orbitals which hybridize with the conduction band states [4, 5]. Strikingly, it always exhibits conducting properties at the surface no matter how the surface was prepared [6], so that it is tempting to take this observation as evidence for the topological nature of SmB_6, but a fierce debate is still going on about the identification of the topological surface states.

There is a need to establish the symmetries of the bulk Sm 4f states, since the existence and character of the topological surface states is essentially determined by the bulk. It is therefore surprising that the ground state wave function of the Sm^{3+} ions in the bulk is not even known so far, despite attempts with e.g. neutron scattering (Sm and B are strong neutron absorbers). In the present study we have carried out a core-level non-resonant inelastic X-ray scattering (NIXS) study to resolve this issue.

Figure 1 shows the total energy diagrams of the two Sm configurations involved. As shown there the Sm^{2+} ground state is not split by the cubic crystal-electric field so that its electron density remains spherical. The ground state multiplet of Sm^{3+}, however, is split into a Γ_8 quartet and a Γ_7 doublet. We want to know which of the two forms the ground state.

In our NIXS experiment, the core hole excitation 4d→4f (N-edge) probes directly the 4f states and the directional dependence of the scattering function $S(\vec{q},\omega)$ gives insight into the ground state symmetry in analogy to a linear polarized X-ray absorption experiment. However, in a NIXS experiment the core hole excitation is measured at such large

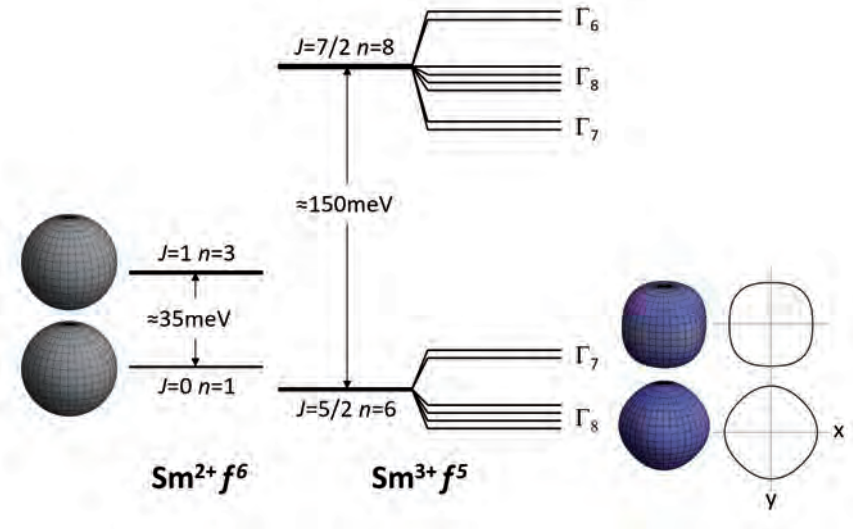


Figure 1

Sm^{2+} and Sm^{3+} total energy level diagram. The Sm^{2+} configuration is split into a J = 0 and J = 1, and the Sm^{3+} into a J = 5/2 and J = 7/2 multiplet. The label *n* indicates the degeneracy. The Sm^{3+} ground state multiplet is further split into a Γ_7 doublet and Γ_8 quartet by the cubic crystal-electric field. The insets show the corresponding charge densities for six and five electrons and their 2D projections, respectively.

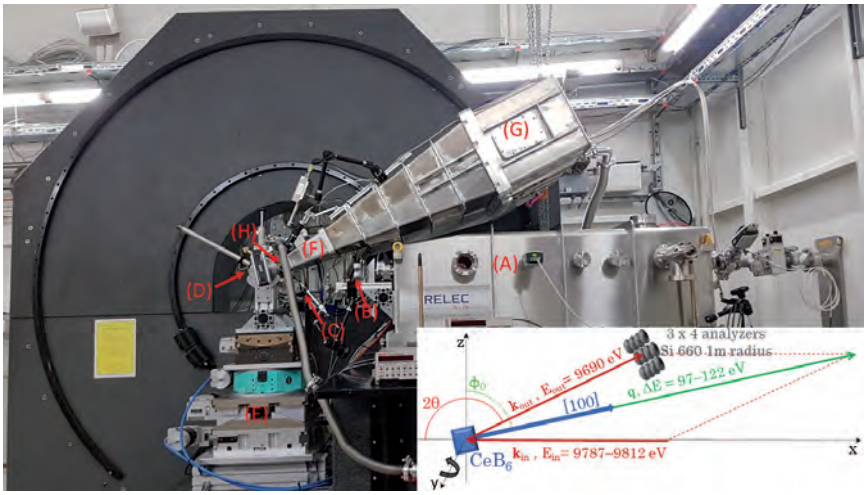


Figure 3

Image of the of the XRS end station at the Dynamics Beamline P01 at PETRA III in Hamburg. The monochromatized beam enters from the tube at the right hand side to the Kirkpatrick-Baez (KB) focusing mirror tank (A). It passes through a slit (B) behind the tank and is seen by a 300 μm thick pin diode (C) before it reaches the sample inside the He-flow cryostat (D) on top of the translation and rotation stage (E). The scattered light enters the vacuum tank (here in back-scattering geometry) through a collimator (F) and the 12 analyzers (G) project the sample spot onto the 2D-Medipix3 LAMBDA pixel detector (H). The inset shows a cartoon of the scattering triangle.

momentum transfers that higher multipoles contribute to $S(\vec{q},\omega)$. As a result, asymmetries can be detected even in a cubic environment.

Figure 2 shows the main result of the NIXS experiment: the experimental dichroic spectrum (black dots) and simulated dichroic spectra for the Γ_8 quartet (orange) and Γ_7 doublet (light blue) scaled with the factor of 0.6 to account for the Sm^{3+} component of the ground state; dashed lines with energy independent broadening, solid lines with extra broadening in the dipole region. We can clearly conclude from the good quantitative agreement that the ground state is the Γ_8 quartet. In fact, the opposite dichroism at 125 and 140 eV (see red arrows) reduces the experimental challenge to a simple yes-no experiment and makes the determination of the ground state wave function of the Sm^{3+} in SmB_6 straightforward. A great advantage is that the Sm^{2+} configuration does not contribute to the directional dependence of the scattering signal due to its spherical symmetry.

The finding that the ground state of Sm^{3+} is the Γ_8 quartet and not the Γ_7 doublet, contradicts all existing band structure calculations and illustrates in a sobering manner the difficulties in making reliable predictions for the properties of correlated systems. Our experimental results point out that future calculations of the low energy properties of SmB_6 should be performed within a reduced basis of only Γ_8 states.

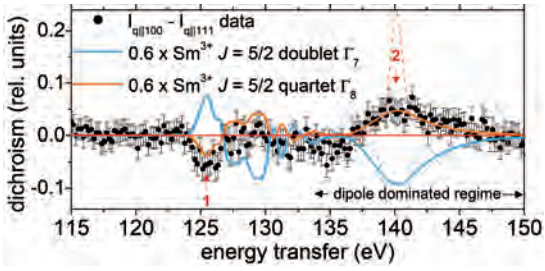


Figure 2

Experimental dichroic spectrum (black dots) and simulated dichroic spectra for the Γ_8 quartet (orange) and Γ_7 doublet (light blue) scaled with the factor of 0.6 to account for the Sm^{3+} component of the ground state; dashed lines with energy independent broadening, solid lines with extra broadening in the dipole region.

The NIXS experiment was possible thanks to the high brilliance of modern synchrotrons and major advances in X-ray instrumentation since the non-resonant scattering process is very photon hungry. The experiment was carried out at the P01 beamline at PETRA III in Hamburg, which is presently being upgraded with contributions from MPI-CPfS in Dresden and the MPI-FKP in Stuttgart. Figure 3 shows shows the XRS end station at P01 in its present form together with a cartoon of the scattering configuration.

Author contact: Liu Hao Tjeng, hao.tjeng@cpfs.mpg.de and Andrea Severing, severing@ph2.uni-koeln.de

References

1. M. Dzero, K. Sun, V. Galitsky, and P. Coleman, 'Topological Kondo Insulators', Phys. Rev. Lett. 104, 106408 (2010).
2. T. Takimoto, 'SmB_6: A Promising Candidate for Topological Insulator', J. Phys. Soc. Jpn. 80, 123710 (2011).
3. M. Dzero, J. Xia, V. Galizsky, P. Coleman, 'Topological Kondo Insulators', Annual Rev. Cond. Mat. Phys. 7, 249-280 (2016).
4. A. Menth, E. Buehler, and T. H. Geballe, 'Magnetic and semiconducting properties of SmB_6', Phys. Rev. Lett. 22, 295 (1996).
5. P. S. Riseborough, 'Heavy Fermion semiconductors', Adv. Phys. 49, 257 (2000).
6. S. Wolgast, C. Kurdak, K. Sun, J. W. Allen, D.-J. Kim, and Z. Fisk, 'Low-temperature surface conduction in the Kondo insulator SmB_6', Phys. Rev. B 88, 180405 (2013).

Original publication

'4f Crystal Field Ground State of the Strongly Correlated Topological Insulator SmB_6'
Physical Review Letters 120, 016402 (2018). DOI: 10.1103/PhysRevLett.120.016402

Martin Sundermann[1,2], Hasan Yavas[3], Kai Chen[1], D. J. Kim[4], Zachary Fisk[4], Deepa Kasinathan[2], Maurits W. Haverkort[5], Peter Thalmeier[2], Andrea Severing[1,2] and Liu Hao Tjeng[1]

1. Institute of Physics II, University of Cologne, Cologne, Germany
2. Max Planck Institute for Chemical Physics of Solids, Dresden, Germany
3. Deutsches Elektronen-Synchrotron DESY, Hamburg, Germany
4. Department of Physics and Astronomy, University of California, Irvine, USA
5. Institute for Theoretical Physics, Heidelberg University, Heidelberg, Germany

Skyrmions on demand

Deterministic nucleation of topological magnetic quasi-particles

Magnetic skyrmions are tiny vortex-like spin textures with a characteristic topological charge and quasi-particle behaviour. In systems with strong asymmetric (chiral) interactions, skyrmions are of fixed chirality. Chiral skyrmions can be driven by a current in an adjacent heavy metal with strong spin-orbit torques. However, no practical means to create individual skyrmions controllably and deterministically in an integrated device design has been reported yet. Here, we use X-ray holography to demonstrate that sub-nanosecond spin–orbit torque pulses can generate single skyrmions at custom-defined positions in a magnetic racetrack. This implementation exploits a defect, such as a constriction in the magnetic track, which can serve as a skyrmion generator.

Magnetic skyrmions are circular entities with diameters on the nanoscale, see Fig. 1. They can be stabilized in magnetic multilayers at room temperature by a combination of external magnetic fields, magnetic stray field, and local spin interactions, such as the Dzyaloshinski-Moriya interaction (DMI). The DMI leads to chiral skyrmions, i.e., to a globally fixed sense of rotation of the spins. The chirality originates from spin-orbit interactions at asymmetric interfaces, e.g., when a Pt layer is below a ferromagnetic layer and a different material is on top. Exploiting another quantum effect, the spin Hall effect, the Pt layer can furthermore generate so-called spin–orbit torques in the ferromagnet: An electric current through the Pt leads to a vertical spin current that is injected into the ferromagnet and exerts a spin-torque on the magnetic moments constituting the skyrmion. For chiral skyrmions, this leads to coherent transverse motion [1].

Based on this motion of nanoscale magnetic skyrmions, a magnetic solid state memory concept that has been proposed, the so-called skyrmion racetrack memory (Fig. 1). This memory consists of a nanoscale stripline with a longitudinal distribution of skyrmions and is operated as a shift register. Digital information is encoded by the presence or absence of a skyrmion. The bit pattern of skyrmions is driven along the track towards read and write elements placed at fixed positions on the track. However, the controlled generation and annihilation of skyrmions (i.e. writing or deleting of a bit in a racetrack) in a device-compatible fashion has remained an unsolved challenge.

In a recent study at beamline P04 at PETRA III, we have demonstrated that the same spin–orbit torques that move skyrmions can also be used to create skyrmions. The imaging technique to observe the skyrmions experimentally is based on Fourier-transform holography with soft X-rays at a wavelength of 1.6 nm [2]. This lensless imaging method is based on the interference of coherent X-rays scattered from the object and an additional reference beam emerging from a tiny pinhole next to the object (Fig. 2a). Magnetization contrast is achieved by tuning the wavelength of the radiation to particular electronic excitations of the magnetic element (here, Co) and by using circularly polarized X-rays. Due to the very large coherent photon flux delivered by the soft X-ray beamline at the synchrotron radiation facility PETRA III, we are able to image the spin textures with down to 15 nm spatial resolution.

In our experiments, we have patterned a $[Pt/CoFeB/MgO]_{15}$ multilayer into an electrically contacted nanotrack. We find that single unipolar current pulses deterministically nucleate skyrmions in the stripline (Fig. 2b). The critical current density for this process depends on the pulse length. Interestingly, in contrast to all previous spin–orbit torque switching experiments, a symmetry-breaking external in-plane magnetic field is not required. Nucleation predominantly takes place at

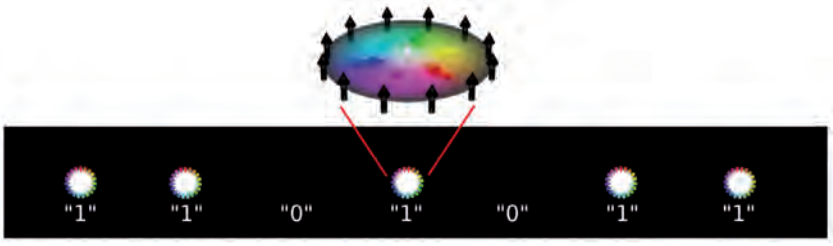
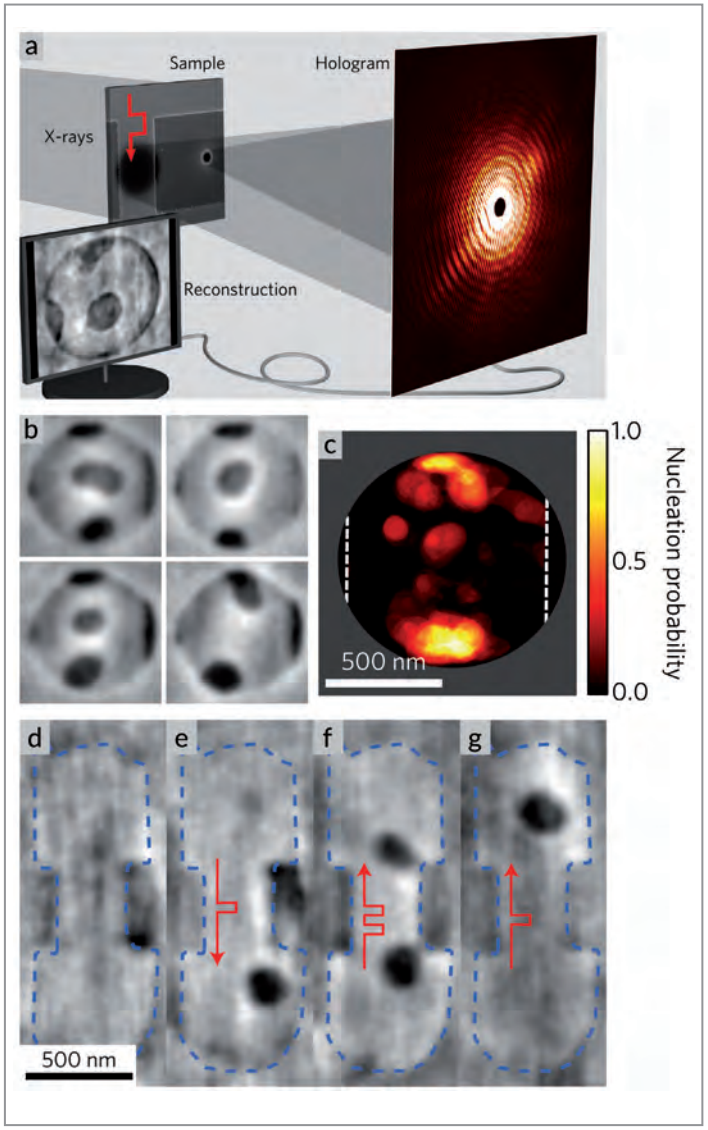


Figure 1

A skyrmion racetrack memory, encoding '0' and '1' by presence and absence of skyrmions. The call-out shows the spin structure of a single skyrmion.

Figure 2

Experimental demonstration of skyrmion nucleation. (a) Sketch of the holographic soft X-ray setup to image magnetic skyrmions in a stripline. The microscopic field of view is located on the stripline; a pinhole next to the object acts as source for a reference wave. An X-ray sensitive area detector records the interference pattern, i.e., the hologram. The real-space image, showing magnetization contrast only, is retrieved digitally. Prior to recording an image, a current pulse is sent through the magnetically saturated stripline to generate magnetic skyrmions. (b) Four examples of skyrmion configurations created by single current pulses at defects. The stripline is oriented vertically and covers almost the whole field of view with 1 µm diameter. (c) Spatial probability map for the nucleation of skyrmions in the field of view. (d)–(g) Images of skyrmion generation at a constriction. (d) Saturated state before pulse injection, (e) skyrmion generated after single pulse injection, (f) nucleation of another skyrmion at the opposite end of the constriction after applying two pulses with inverted polarity, (g) subsequent movement of the second skyrmion by a single pulse, the first skyrmion was annihilated at the same time. Adapted from the original publication.



particular hotspot positions (Fig. 2c). By reproducing the experiments with micromagnetic simulations, we understand that the usually required external fields are generated intrinsically by the chiral DMI near gradients of the magnetization. Such gradients are mediated by lateral symmetry breaking, e.g., due to pinning sites in the material. This mechanism is inspired by similar theoretical suggestions to nucleate skyrmions via spin-transfer torques [3-5].

In a second step, we could demonstrate that the position for skyrmion nucleation on the stripline can be perfectly controlled. Towards this end, we lithographically fabricated a constriction into the stripline, which acted as an integrated skyrmion generator due to the combination of increased current density and locally tilted magnetization at the boundary of the structure. We could show that reverse domains nucleate at the downstream corners of the constricted part of the stripline, detaching and forming a skyrmion at one corner only (Fig. 2e). This right-left asymmetry reflects the chiral nature of the skyrmion, which experiences a skyrmion Hall effect during the current pulse [1]. An additional, weaker current pulse can subsequently shift the skyrmion away from the edge (Fig. 2g). A change of the current pulse polarity results in a nucleation on the opposite side of the constriction (Fig. 2f). The nucleation characteristics observed were again reproduced by micromagnetic simulations to understand the mechanisms at play.

We could demonstrate a practical means for deterministic generation of skyrmions in racetrack memories, without having to resort to external magnetic fields, which would be unsuitable in integrated devices. The constriction can be freely positioned in a racetrack and the nucleation times and applied voltages already match today's computer architectures.

Author contact: Felix Büttner, felixbuettner@gmail.com

References

1. K. Litzius et al. 'Skyrmion Hall effect revealed by direct time-resolved X-ray microscopy', Nat. Phys. 13, 170–175 (2017).
2. S. Eisebitt et al. 'Lensless imaging of magnetic nanostructures by X-ray spectro-holography', Nature 432, 885–888 (2004).
3. J. Iwasaki, M. Mochizuki and N. Nagaosa, 'Current-induced skyrmion dynamics in constricted geometries', Nat. Nanotech. 8, 742–747 (2013).
4. M. Stier, W. Häusler, T. Posske, G. Gurski and M. Thorwart, 'Skyrmion–Anti-Skyrmion Pair Creation by in-Plane Currents', Phys. Rev. Lett. 118, 267203 (2017).
5. K. Everschor-Sitte, M. Sitte, T. Valet, A. Abanov and J. Sinova, 'Skyrmion production on demand by homogeneous DC currents', New J. Phys. 19, 092001 (2017).

Original publication

'Field-free deterministic ultrafast creation of magnetic skyrmions by spin–orbit torques', Nat. Nanotech. 12, 1040–1044 (2017). DOI: 10.1038/nnano.2017.178

Felix Büttner[1], Ivan Lemesh[1], Michael Schneider[2], Bastian Pfau[2], Christian Günther[2,3], Piet Hessing[2], Jan Geilhufe[2], Lucas Caretta[1], Dieter Engel[2], Benjamin Krüger[4], Jens Viefhaus[5], Stefan Eisebitt[2,3], Geoffrey S. D. Beach[1]

1. Massachusetts Institute of Technology, Cambridge, USA
2. Max-Born-Institut, Berlin, Germany
3. Technische Universität Berlin, Berlin, Germany
4. Institut für Lasertechnologien in der Medizin und Messtechnik an der Universität Ulm, Ulm, Germany
5. Deutsches Elektronen-Synchrotron DESY, Hamburg, Germany.

Magnetic composites with enhanced performance

Preparation of $CoFe_2O_4$/Co-Fe studied *in situ*

Combination of two dissimilar magnetic species into an exchange-coupled composite is expected to enhance the magnetic properties. Composites of magnetically hard cobalt spinel ($CoFe_2O_4$) and soft Co-Fe alloy are good candidates for exchange-coupled materials as they can be prepared in one step by partial reduction of $CoFe_2O_4$ nanoparticles. However, metallic monoxides, i.e. FeO or CoO, are often found as secondary phases which hamper an effective coupling between the magnetic species. It is not clear whether monoxides form during the reduction itself or at a later stage, which makes them hard to avoid. Here, the reduction of $CoFe_2O_4$ was investigated *in situ* and monoxide was found as an intermediate. It was concluded that eradicating the monoxide from the final product is only possible through an exhaustive control of the experimental conditions.

Magnetic materials are loosely divided into hard and soft. Hard phases are very resistant to demagnetisation, but they are generally limited in the maximum magnetic moment they can produce. Soft phases, on the other hand, can often reach very high magnetization values, but their magnetic moment is practically lost upon removal of the external magnetising field. In the early 90s, theory predicted that mixing a hard and a soft phase would yield a new material withholding the best of both worlds as long as the two phases were magnetically coupled [1]. This prediction heralded a big leap forward in the field of permanent magnets. However, realising an effective coupling across the interfaces of two distinct magnetic phases has proven rather challenging in practice [2, 3].

The $CoFe_2O_4$/Co-Fe alloy system has drawn special attention since it can be prepared in one step by partial reduction of $CoFe_2O_4$ nanoparticles. This method directly leads to coexistence of the two phases, increasing the likelihood of building an intimate contact between the interfaces of the two magnetic materials. However, the method often leads to formation of monoxides (i.e. FeO or CoO) as secondary phases, which should be avoided as they have a negative effect on the magnetic properties. Previous literature does not clarify whether the formation of monoxide occurs during the reduction itself or at a later stage, which complicates eradication of this impurity from the final product.

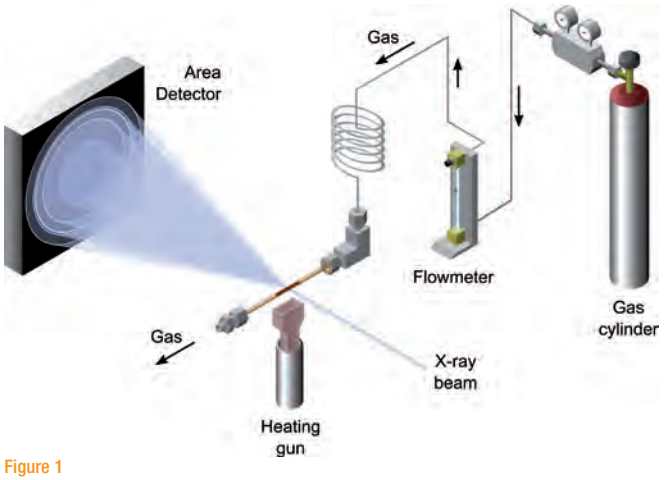


Figure 1

Custom-designed reactor optimized for *in situ* diffraction studies on solid-state reactions in a gas atmosphere of choice and at temperatures up to ≈1000 K. In the present work, $CoFe_2O_4$ nanoparticles were reduced in a 4% H_2/Ar gas mixture (flow rates = 5 – 30 mL/min) and at temperatures in the range 300 – 500 °C.

To address this issue, a novel experimental setup was specifically designed to follow the reduction of $CoFe_2O_4$ in real time. The setup sketched in Fig. 1 was mounted at beamline P02.1, PETRA III [4]. Synchrotron powder X-ray diffraction (PXRD) data were collected *in situ* during the reduction at 5 s intervals to monitor the phases appearing and disappearing in the process. A representative PXRD dataset is displayed in Fig. 2a. The starting from $CoFe_2O_4$, is fully transformed into a Co-Fe alloy after 30 min, going through an intermediate monoxide phase. The same was observed for all our experiments, albeit at different speeds depending on the specific temperature and flow rate of the reducing gas, thus confirming the monoxide as a reaction intermediate.

Figure 2b shows the Rietveld models fitted to the diffraction data collected at three selected reaction times: single-phase $CoFe_2O_4$ at the start, pure Co-Fe alloy at the end, and coexistence of the three phases at intermediate times. Sequential Rietveld analysis throughout the whole *in situ* dataset yielded time-resolved, quantitative information on the composition, structure and microstructure of the samples. The refined weight fractions for a reduction experiment performed at 400 °C and a gas flow rate of 10 mL/min are

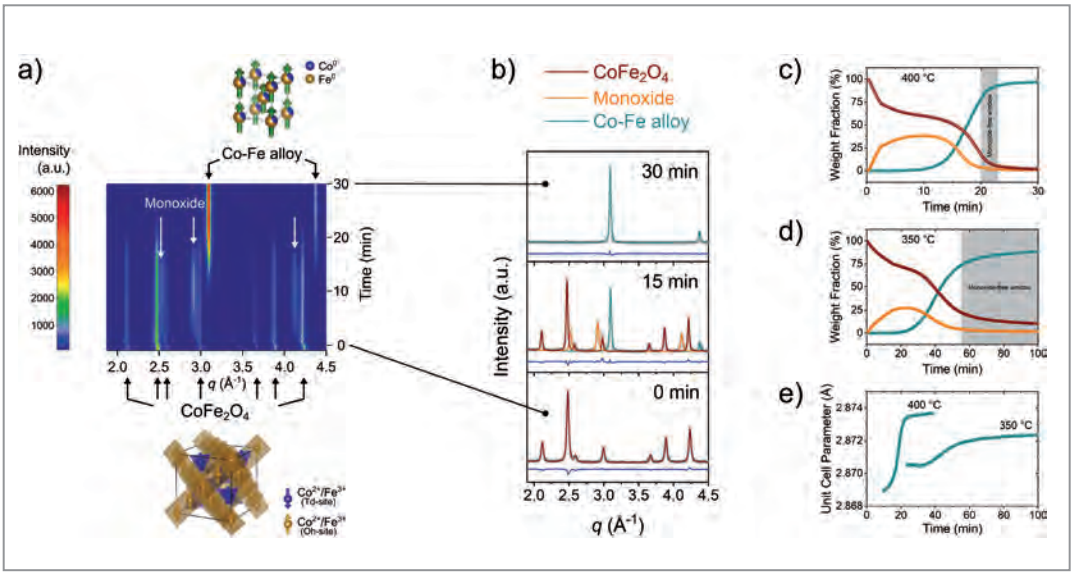


Figure 2

a) *In situ* PXRD data collected during the reduction of $CoFe_2O_4$ (time resolution is 5 s). The colour scale represents the diffracted intensity. b) PXRD patterns measured at selected reaction times (0, 15, 30 min) and corresponding Rietveld models of the phases present in the sample. The blue line represents the difference between the Rietveld model and the experimental data. c) Refined weight fractions corresponding to reduction experiments carried out at 400 °C and d) 350 °C, in a gas flow of 10 mL/min. Grey area shows the monoxide-free state. e) Refined unit cell parameter for the alloy in c) and d).

represented as a function of time in Fig. 2c. In these particular experimental conditions, monoxide-free composites are only obtained inside a very narrow time-window, and so, avoiding the impurity is hard. This window may be broadened by slowing down the process, which we were able to do by reducing the temperature (see Fig. 2d) and/or decreasing the gas flow (not shown here). We conclude that it is possible to avoid the monoxide in the final product by fine tuning of the experimental conditions of temperature, time, and gas flow.

Regardless of the temperature, the unit cell parameter of the alloy is seen to increase with time until it stabilises at a final value (see Fig. 2e). This suggests that there must be a change on the elemental composition of the alloy as the reduction progresses. Unfortunately, Co:Fe ratios could not be extracted from the refinements – Co and Fe being next-neighbours in the periodic table makes them practicably indistinguishable by X-rays at the wavelength used.

Using the knowledge retrieved from the *in situ* experiments, $CoFe_2O_4$/Co-Fe composites were prepared at a laboratory scale. Neutron powder diffraction data were collected on those samples at the HRPT instrument, Paul Scherrer Institute [5], revealing that the reduced phases tend to arise in a Co-rich form, to later incorporate Fe in the structure. This result is in agreement with the unit cell trends observed *in situ*. The late incorporation of Fe along with the crystallite sizes refined for the individual phases can explain the improvement or deterioration of the magnetic properties (not shown here).

Besides the findings relative to this specific system, the relevance of this study resides on the potential to apply the method to other case studies. The reactor we have designed is easy to use and quick to install at synchrotron beamlines and it allows for *in situ* diffraction studies on any solid-state reaction in a gas atmosphere of choice and at temperatures up to 1000 K. Regardless of the specific material or application, an *in situ* investigation on the preparation of a material is a great tool to correlate the material synthesis to its structure.

Author contact: Cecilia Granados-Miralles, c.granados.miralles@icv.csic.es

References

1. E. F. Kneller and R. Hawig, 'The Exchange-Spring Magnet: A New Material Principle for Permanent Magnets', IEEE Trans. Magn. 27, 3588 (1991).
2. H. Zeng, J. Li, J. P. Liu, Z. L. Wang and S. Sun, 'Exchange-Coupled Nanocomposite Magnets by Nanoparticle Self-Assembly', Nature 420, 395 (2002).
3. L. H. Lewis and F. Jimenez-Villacorta, 'Perspectives on Permanent Magnetic Materials for Energy Conversion and Power Generation', Metall. Mater. Trans. A-Physical Metall. Mater. Sci. 44A, 2 (2013).
4. A. C. Dippel, H. P. Liermann, J. T. Delitz, P. Walter, H. Schulte-Schrepping, O. H. Seeck and H. Franz, 'Beamline P02.1 at PETRA III for High-Resolution and High-Energy Powder Diffraction', J. Synchrotron Radiat. 22, 675 (2015).
5. P. Fischer, G. Frey, M. Koch, M. Könnecke, V. Pomjakushin, J. Schefer, R. Thut, N. Schlumpf, R. Bürge, U. Greuter, S. Bondt and E. Berruyer, 'High-Resolution Powder Diffractometer HRPT for Thermal Neutrons at SINQ', Phys. B Condens. Matter 276–278, 146 (2000).

Original publication

'Approaching Ferrite-Based Exchange-Coupled Nanocomposites as Permanent Magnets', ACS Applied Nano Materials 1, 3693–3704 (2018). DOI: 10.1021/acsanm.8b00808

Cecilia Granados-Miralles[1,2], Matilde Saura-Muzquiz[1], Henrik L. Andersen[1], Adrián Quesada[2], Jakob V. Ahlburg[1], Ann-Christin Dippel[3], Emmanuel Canevet[4,5] and Mogens Christensen[1]

1. Center for Materials Crystallography (CMC), Department of Chemistry and iNANO, Aarhus University (AU), Aarhus, Denmark
2. Electroceramic Department, Instituto de Ceramica y Vidrio, CSIC, Madrid, Spain
3. Deutsches Elektronen-Synchrotron DESY, Hamburg, Germany
4. Laboratory for Neutron Scattering and Imaging, Paul Scherrer Institute (PSI), Villigen, Switzerland
5. Department of Physics, Technical University of Denmark (DTU), Lyngby, Denmark

Rare-earth metals as a superior co-catalyst

Improving electrochemical activity

Transition metals are the foremost choice to improve electrocatalytic activity of active metals ever since the advent of catalysis, while rare-earths are ignored owing to their deceptive name 'Rare-Earth' and cost. In reality, most of the rare-earths are abundant and less expensive than the widely used transition metals. In order to explore, we tried to study the chemical effect of small amount of rare-earth elements (RE 10 %) substitution in palladium (Pd) lattice (*RE*Pd) and compared with transition metals (TM) substituted Pd (*TM*Pd) towards ethanol oxidation reaction.

Both ethanol and methanol are being used as fuel in direct ethanol fuel cells (DEFC) and direct methanol fuel cells (DMFC), respectively, and recognised as potential candidates to compete with advanced batteries and portable electronic devices owing to their uniquely high specific energy [1]. However, the use of ethanol fuel cells is favoured over methanol fuel cells due to several reasons such as less toxicity of ethanol, higher volumetric energy capacity of 6.3 kWh/L and easy availability through fermentation of biomass with high sugar content such as corn (glucose) and sugarcane (sucrose).

The electrochemical activity of *RE*Pd (*RE* = Eu, Yb) towards ethanol oxidation reaction was found to show several fold increase in both specific and mass activities compared to *TM*Pd (TM = Cr, Ni) and commercial Pd/C. DFT calculations support the experimental observations and attribute the unprecedented activity of *RE*Pd to the perfect synergy between the adsorption energy of –OH and $–COCH_3$ to the catalyst surface. Electrochemical studies, X-ray absorption near edge spectroscopy and DFT calculations explains the promotional effect of *RE* in enhancing the activity and stability of Pd towards an ethanol oxidation reaction.

Tweaking electronic structure of Pd with transition metal substitutes have always been preferred over any other group of metals due to their incompletely filled *d*-orbital, ability to form complexes and ability to change oxidation state, giving rise to unprecedented electrocatalytic activity. Rare-earth metals, because of its similar properties to transition metal, have the potential to show unique catalytic properties. They have a partially filled 4*f* orbital. In this context, it is worthwhile to highlight that the role of rare-earth metals in improving the catalytic activity of Pd or Pt has not been explored much instead of the fact that they are found to be more abundant and cheaper than transition metals.

This work explores the role of rare-earth metals in enhancing the catalytic activity of Pd towards ethanol electrooxidation. Pd nanoparticles were substituted with Yb and Eu and compared with Ni and Cr. The optimum activity for an ethanol oxidation reaction was observed at 10 % substitution and so the substitution percentage was fixed at 10 % for all the catalysts. However, rare-earth metals are found to enhance the activity of palladium to a much greater extent compared to that of the transition metals and its Pt counterparts, *RE*Pt. Theoretical investigations were carried out using DFT calculations to understand the role of Yb and Eu during the oxidation activity better.

Corresponding oxidation state of the elements is verified using X-ray absorption near edge structure (XANES) measurements at PETRA III beamline P65, shown in Fig. 1(i). Field emission electron microscopy (FESEM) images of YbPd and EuPd are shown in Fig. 1(ii). The specific activity of both YbPd and EuPd nanoparticles was approximately 5 and 3 times, respectively higher than the corresponding value for the commercial Pd/C (20 wt%) modified electrode which increased to 13.8 and 9.9, respectively after 1000 cycles. This can be attributed to the effective removal of poisonous carbonaceous species like 'CO' from the catalyst surface [2].

In order to get a 'mechanistic' insight of an ethanol oxidation reaction, oxygen scavenging capability of Yb and Pd were determined by XANES experiment in presence and absence of concentrated KOH, which provides a basic medium for the elements to scavenge –OH from the solution. As seen from Fig. 1(i), white line intensity of the Yb-L_{III} edge of YbPd increased, indicating the depopulation of *d*-bands and the attachment of an electronegative element i.e. 'O' to the Yb site [3]. However, no change in the white line intensity of Pd-*K* edge was detected in the presence of KOH. This confirms the much higher oxophilicity of Yb compared to Pd. Due to this effective interaction of –OH with oxophilic site like Yb, active sites of Pd are more available for the adsorption of ethanol [4, 5]. Although, a higher Yb content decreases the occupancy of the active Pd atom on the surface and consequently impairs the dissociation of ethanol molecule leading to lesser

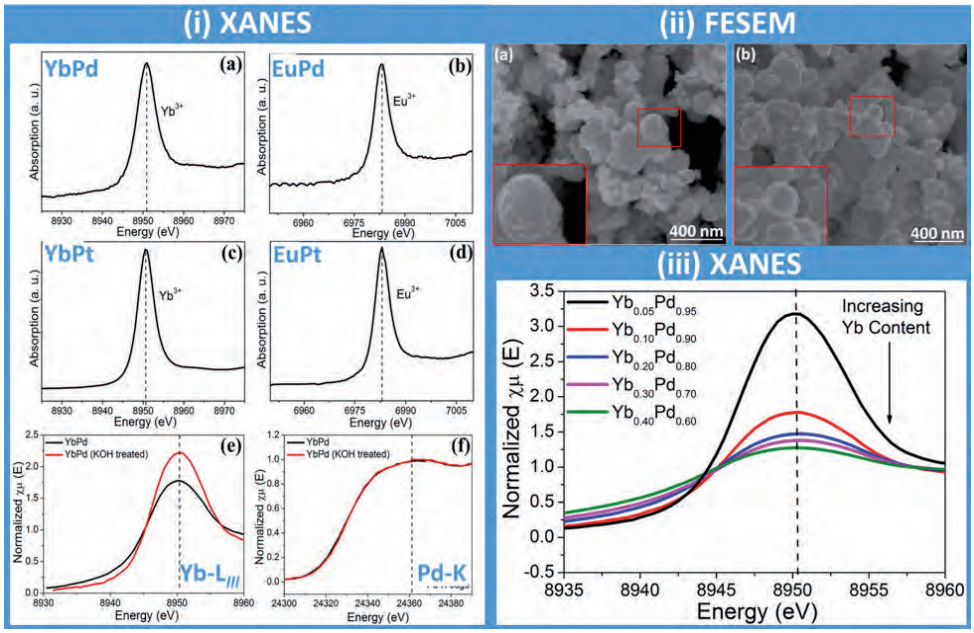


Figure 1

(i) X-ray absorption near edge spectroscopy of Yb-L_{III} edge of (a) YbPd and (c) YbPt and Eu-L_{III} edge of (b) EuPd and (d) EuPt catalyst. Comparison of change in white line intensity of (e) Yb-L_{III} edge and (f) Pd-*K* edge of YbPd and KOH-treated YbPd showing the most preferred adsoption site for –OH is Yb rather than Pd, (ii) FESEM images of (a) YbPd and (b) EuPd nanoparticles. Inset shows the zoomed in image of one of the particles and (iii) comparison of white line intensity of $Yb_{0.05}Pd_{0.95}$, $Yb_{0.10}Pd_{0.90}$, $Yb_{0.20}Pd_{0.80}$, $Yb_{0.30}Pd_{0.70}$ and $Yb_{0.40}Pd_{0.60}$ measured at Yb L_{III} edge.

activity. Therefore, an optimal percentage of Yb is necessary for the maximum activity. Another reason for lower ethanol oxidation reaction activity for higher Yb percentage may be due to weaker bonding energy for –OH, which is supported by Yb L_{III} edge XANES spectra of Yb_xPd_{1-x} (x = 0.05, 0.10, 0.20, 0.30 and 0.40) as shown in Fig. 1(iii). The white line intensity of the spectrum continuously decreases with increase in Yb content, which indicates the shift of the *d*-band centre of the catalyst away from the Fermi level [6]. Downward shift of the *d*-band signifies filled anti-bonding orbital and hence weaker bonding to –OH intermediate species, which decreases the oxidation activity. Hence, $Yb_{0.1}Pd_{0.9}$ shows the optimum activity for an ethanol oxidation reaction.

Thus, the main intermediate species formed during ethanol electro-oxidation are $–COCH_3$, –CO and –OH. The adsorption energies of –OH on Pd, YbPd, EuPd, CrPd and NiPd are -214.2, -334.3, -237, -328.3 and -353.2 kJ/mol, respectively, indicating that YbPd, CrPd, and NiPd compounds are good catalysts for –OH chemisorption. The $–COCH_3$ intermediate has a weaker adsorption energy of -190.7 and -186.9 kJ/mol on YbPd and EuPd, respectively. However, comparison of adsorption energy of –CO (-132.25 kJ/mol) and $–COCH_3$ (-190.72 kJ/mol) reveals that the poisoning-intermediate pathway (–CO adsorption) is uphill and hence least favored in the case of YbPd and other catalysts. A good catalyst for the ethanol oxidation reaction should bind strongly with –OH and weakly with $–COCH_3$; these two criteria are well satisfied by YbPd. In addition, the formation of CO_{ads} should also be minimized which is true for the catalyst under consideration. Hence, YbPd shows many fold better catalytic activity compared to EuPd, NiPd and CrPd.

In conclusion, the activities of the rare-earth metals have been compared with their transition metal counterparts (CrPd and NiPd) and they are found to be most favorable in enhancing the activity. On the other hand, Pt counterparts show less activity due to CO poisoning. The experimentally observed data was successfully interpreted in terms of the combined effect of both adsorption energies of reaction intermediates on the catalyst surfaces and *d*-band theory. YbPd stands out among all the catalyst as it has a perfect balance of adsorption energies among the reaction intermediates. This work highlights the importance of rare-earth metals as an electrocatalyst and can be used as a model catalyst for tuning the catalytic behavior of any active metal, intermetallics, alloys etc.

Author contact: Sebastian C. Peter, sebastiancp@jncasr.ac.in

References

1. S. Y. Shen, T. S. Zhao, J. B. Xu and Y. S. Li, 'Synthesis of PdNi catalysts for the oxidation of ethanol in alkaline direct ethanol fuel cells', J. Power Sources 195, 1001-1006, (2010).
2. M. V. F. Delmonde, L. F. Sallum, N. Perini, E. R. Gonzalez, R. Schlogl and H. Varela, 'Electrocatalytic Efficiency of the Oxidation of Small Organic Molecules under Oscillatory Regime', J. Phys. Chem. C 120, 22365-22374 (2016).
3. S. Stoupin, H. Rivera, Z. R. Li, C. U. Segre, C. Korzeniewski, D. J. Casadonte, H. Inoue and E. S. Smotkin, 'Structural analysis of sonochemically prepared PtRu versus Johnson Matthey PtRu in operating direct methanol fuel cells', Phys. Chem. Chem. Phys. 10, 6430-6437 (2008).
4. S. Sarkar, R. Jana, Suchitra, U. V. Waghmare, B. Kuppan, S. Sampath and S. C. Peter, 'Ordered Pd_2Ge Intermetallic Nanoparticles as Highly Efficient and Robust Catalyst for Ethanol Oxidation', Chem Mater 27, 7459-7467 (2015).
5. Z. Y. Zhang, L. Xin, K. Sun and W. Z. Li, 'Pd-Ni electrocatalysts for efficient ethanol oxidation reaction in alkaline electrolyte', Int. J. Hydrogen Energ. 36, 12686-12697 (2011).
6. W. Du, G. Yang, E. Wong, N. A. Deskins, A. I. Frenkel, D. Su and X. Teng, 'Platinum-Tin Oxide Core–Shell Catalysts for Efficient Electro-Oxidation of Ethanol', J. Am. Chem. Soc. 136, 10862-10865 (2014).

Original publication

'Are we underrating rare earths as an electrocatalyst? The effect of their substitution in palladium nanoparticles enhances the activity towards ethanol oxidation reaction', Journal of Materials Chemistry A 5, 23369–23381 (2017). DOI: 10.1039/C7TA07945A

Saurav Ch. Sarma[1,2], Udumula Subbarao[1,2], Yatish Khulbe[1,2], Rajkumar Jana[1,2], Sebastian C. Peter[1,2]

1. New Chemistry Unit, Jawaharlal Nehru Centre for Advanced Scientific Research, Jakkur, Bengaluru, India
2. School of Advanced Materials, Jawaharlal Nehru Centre for Advanced Scientific Research, Jakkur, Bengaluru, India

Unravelling the oxidation state of iron in the deep Earth

Garnet inclusions in diamonds reveal oxidised material at up to 550 km depth

After the first 30 million years of its evolution, the planet Earth had developed its metallic core (2900-6300 km), silicate mantle (50-2900 km) and crust (0-50 km). The deeper the layer, the harder it is to sample. There are no samples from the Earth's core, while the top part of the mantle, called the lithosphere (50-200 km) is sampled through xenoliths, pieces of rocks that are brought to the surface by volcanic eruptions. The only samples from the deeper levels of the Earth's mantle are inclusions in diamonds. We studied garnet inclusions in diamonds from the depths between 250-550 km to unravel the compositions and oxidation state in the lower parts of the upper mantle and the mantle transition zone.

The oxidation state of the Earth's mantle controls important parameters and processes such as magma generation, deep carbon cycle, formation and stability of diamonds, recycling of oceanic crust back into the mantle, speciation of mantle fluids and many others [1, 2]. The main three layers of the Earth – its crust, mantle and core, reveal profound changes in the oxidation state of iron from ferric (Fe^{3+}) at the surface to mostly ferrous (Fe^{2+}) in the silicate minerals in the upper mantle, transition zone and the lower mantle and ultimately, to metallic Fe in the core (Fig. 1).

A simple explanation for the changes would be that shortly after planet formation, Earth's silicate mantle was in equilibrium with the metallic core and contained little oxidised iron, but through subduction and recycling of surface material rich in oxidised carbon, sulphur and iron species, it systematically became more oxidised with time. This hypothesis was tested in multiple studies on minerals from mantle xenoliths, carried to the surface by volcanoes. These xenoliths, however, derive from the depths that do not exceed ~150-200 km below the surface, impeding our ability to directly estimate the oxidation state of the material from the deeper mantle by this method.

A way to address the lowermost upper mantle and the mantle transition zone depths (410-660 km) is through inclusions in diamonds. They provide a unique window in the deep mantle. One such inclusion is majoritic garnet, which can be described as a marker mineral for the mantle transition zone due to its formation under the pressures prevailing at these depths. It has a complex structure, complex history and a complex composition, that depend on the source lithology, pressure and oxidation state during its formation. Therefore, majoritic garnets provide a great opportunity to shed light onto the evolution of plate tectonics and transport of material from the surface into the deep Earth and vice versa.

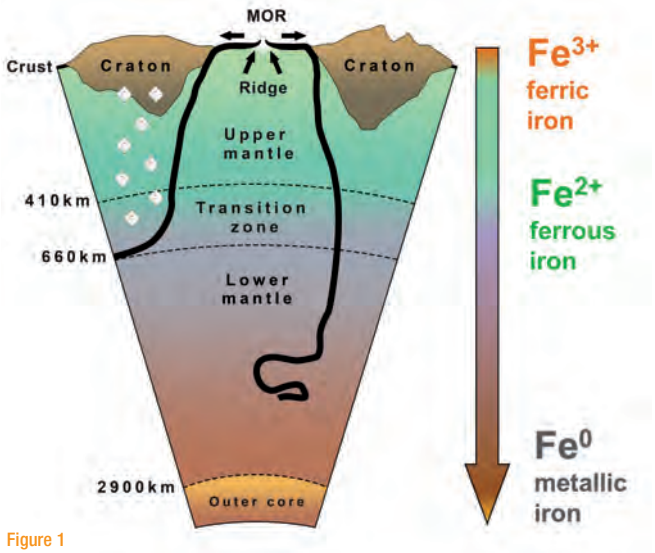


Figure 1

Schematic cartoon of the Earth showing the distribution of iron between the main geological reservoirs. Not to scale. Diamonds are shown to be present in the mantle transition zone, subcratonic upper mantle and in the lower parts of craton, at depths of about 150 km and deeper. MOR stands for mid-ocean ridge where new oceanic crust is formed pushing the plates and ultimately triggering subduction. In black are shown subducted slabs.

The compositions of the majoritic garnets reported in literature differ substantially. Surprisingly, the majority of the inclusions reported in literature, including the only ones clearly derived from the mantle transition zone, are neither pure peridotitic, nor pure eclogitic, but intermediate in composition between the two lithologies [3].

In this study we measured Fe^{3+}/Fe^{2+} in 13 majoritic inclusions in diamonds from lithologies of such intermediate composition from Jagersfontein kimberlite (South Africa). This unique set of majoritic garnets covers a substantial compositional and depth range, while the original source material is considered

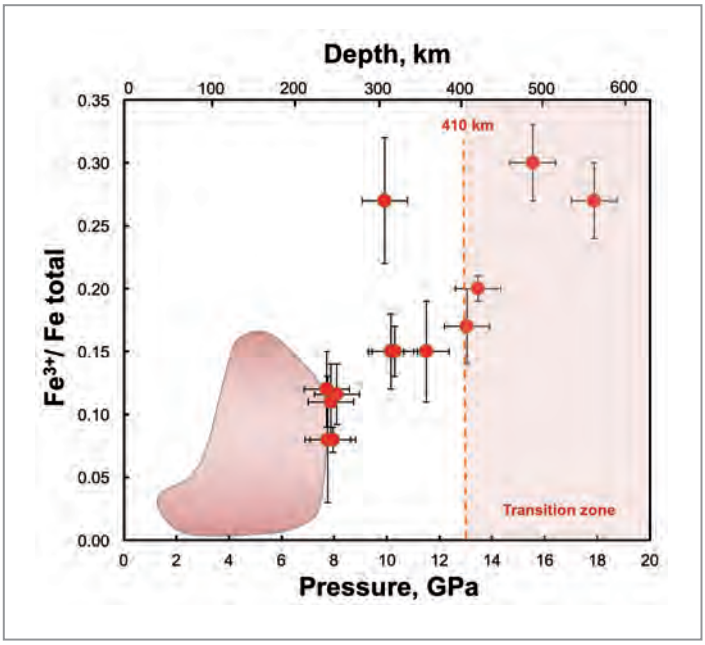


Figure 2

Fe^{3+}/Fe_{tot} ratios as a function of pressure and hence depth in the majoritic garnets examined in this study. Pink area shows the literature data for the upper mantle from mantle xenoliths (see [3] for references).

to have been carried into the transition zone with an early subduction process more than 2 billion years ago [4, 5].

Despite being one of the dominant phases in the deep mantle, majoritic garnets are extremely rarely found, with up to date, only about 150-200 crystals of them being reported in literature. Predominantly, this is because majoritic garnets break down during their ascent to the surface and can be found intact only in meteorites or rarely, as inclusions in diamonds. Even within the inclusions, majoritic garnets are prone to breaking down into low-pressure phases [6]. Therefore, in order to test the integrity of the grains and their crystal structure, we used a single-crystal X-ray diffraction at the Extreme Conditions Beamline P02.2 at PETRA III. This method has shown that all garnet inclusions were single crystals, mostly mono-domain (only two samples contained more than two domains, but all with the same lattice parameters within measurement uncertainty), confirming that no break down has occurred and these crystals are preserved with the same structure and composition they had in the mantle transition zone. The samples were then studied for their ferric iron content at Synchrotron Mössbauer Source (ESRF, France). Measuring Fe^{3+} concentrations in mantle minerals is the most common way of inferring the oxidation state of the mantle. The rationale behind this is relatively simple: the valence state of iron in a silicate phase depends on the activity of oxygen, thus, the relative abundances of Fe^{3+} and Fe^{2+} (and the Fe^{3+}/Fe_{tot} ratio) of a mineral or melt should be indicative of the activity of oxygen in the environment in which it formed.

The results were surprising (Fig. 2). The Fe^{3+}/Fe_{tot} ratios in the studied garnets were increasing from 0.08 at approximately 240 km depth to 0.30 at approximately 500 km depth. It is also important to note that the majoritic garnets are at least twice as rich in Fe^{3+} as any garnet from xenoliths of the upper mantle. This means that unlike rocks from the upper mantle, the rocks present in the mantle transition zone contain significant amounts of the trivalent iron, which is the most oxidised species of iron. These measurements of the ferric/ferrous ratios of majoritic garnets represent a significant advancement in our understanding of the oxidation state of the deep mantle.

We hypothesised that such elevated ferric iron contents were probably linked to the carbonate that was brought into the transition zone via subduction of altered and CO_2-rich oceanic crust (Fig. 1). A reaction between carbonate and ferrous iron present in the mantle, would lead to the reduction of carbonate into carbon (in the form of diamond) with simultaneous oxidation of the ferrous iron into the ferric iron. Such mechanism would provide explanation for the presence of highly oxidised garnets as inclusions in diamonds.

Author contact: Kate Kiseeva, kate.kiseeva@earth.ox.ac.uk

References

1. A. Woodland and M. Koch, 'Variation in oxygen fugacity with depth in the upper mantle beneath the Kaapvaal craton, Southern Africa', Earth Planet. Sci. Lett. 214, 295-310 (2003).
2. V. Stagno, D. Ojwang, C. McCammon and D. Frost, 'The oxidation state of the mantle and the extraction of carbon from Earth's interior', Nature 493, 84-88 (2013).
3. E. Kiseeva, D. Vasiukov, B. Wood, C. McCammon, T. Stachel, M. Bykov, E. Bykova, A. Chumakov, V. Cerantola, J. Harris and L. Dubrovinsky, 'Oxidized iron in garnets from the mantle transition zone', Nature Geoscience 11, 144-150 (2018).
4. R. Tappert, T. Stachel, K. Muehlenbachs, T. Ludwig and G. Brey, 'Diamonds from Jagersfontein (South Africa): messengers from the sublithospheric mantle', Contrib. Mineral. Petrol. 150, 505-522 (2005).
5. R. Ickert, T. Stachel, R. Stern and J. Harris, 'Extreme ^{18}O-enrichment in majorite constrains a crustal origin of transition zone diamonds', Geochem. Persp. Lett. 1, 65-74 (2015).
6. B. Harte and N. Cayzer, 'Decompression and unmixing of crystals included in diamonds from the mantle transition zone', Phys. Chem. Minerals 34, 647-656 (2007).

Original publication

'Oxidized iron in garnets from the mantle transition zone', Nature Geoscience 11, 144-150 (2018). DOI: 10.1038/s41561-017-0055-7

Ekaterina S. Kiseeva[1], Denis M. Vasiukov[2], Bernard J. Wood[1], Catherine McCammon[3], Thomas Stachel[4], Maxim Bykov[3,5], Elena Bykova[3,5], Alexander Chumakov[6], Valerio Cerantola[6], Jeff W. Harris[7] and Leonid Dubrovinsky[3]

1. Department of Earth Sciences, University of Oxford, Oxford, UK
2. Laboratory of Crystallography, University of Bayreuth, Bayreuth, Germany
3. Bayerisches Geoinstitut, Universität Bayreuth, Bayreuth, Germany
4. Department of Earth and Atmospheric Sciences, University of Alberta, Edmonton, Canada
5. Deutsches Elektronen-Synchrotron DESY, Hamburg, Germany
6. ESRF-The European Synchrotron, Grenoble, France
7. School of Geographical and Earth Sciences, University of Glasgow, Glasgow, UK

Clay mineral waters Earth's mantle from the inside

Super-hydrated kaolinite

Water, the most abundant volatile and pivotal molecule in biosphere on the surface of the Earth, is transported into the deep Earth via subduction zones and cycled via geodynamical processes. In a subduction zone, a heavy oceanic plate moves under a second, lighter continental plate and into the Earth's mantle. As water travels deeper into the Earth, it is exposed to an enormous increase of pressure and temperature. The related pressure-temperature induced interaction of rocks and minerals with water drives the Earth's internal processes and causes geological activities such as volcanism and earthquakes on the surface. In this work, we created such extreme pressure and temperature conditions in the laboratory, and discovered a new form of clay mineral, super-hydrated kaolinite, that marks the most hydrated silicate mineral and acts as a water sponge in the Earth's deep water cycle.

Water influences mantle dynamics by altering physical and chemical properties of mantle rocks and minerals. Kaolinite ($Al_2Si_2O_5(OH)_4$) is one of the naturally occurring hydrous clay minerals and makes up as much as <5 % to 60 % of oceanic sediments [1]. There are few high-pressure and high-temperature studies of clay minerals, although knowledge of their behaviour especially under subduction zone conditions is extremely important to understand and model water transport and recycling in the Earth's interior [2].

We have performed *in situ* high-pressure and high-temperature X-ray diffraction experiments on kaolinite at PETRA III beamline P02.2. Additional experiments have been conducted at the Stanford Synchrotron Radiation Light Source, the Advanced Photon Source, the Advanced Light Source (U.S.) and the Pohang Accelerator Laboratory (Korea).

We were able to establish that kaolinite becomes super-hydrated above 2.5 GPa and 200 ˚C which corresponds to a depth near 75 km in a cold subducting slab (Fig. 1). This is manifested by the appearance of the expanded (001) reflection with d-spacing ~10 Å concomitantly to the intensity decrease of the original (001) reflection with d-spacing ~7 Å. This expansion of the basal (001) reflection is caused by direct

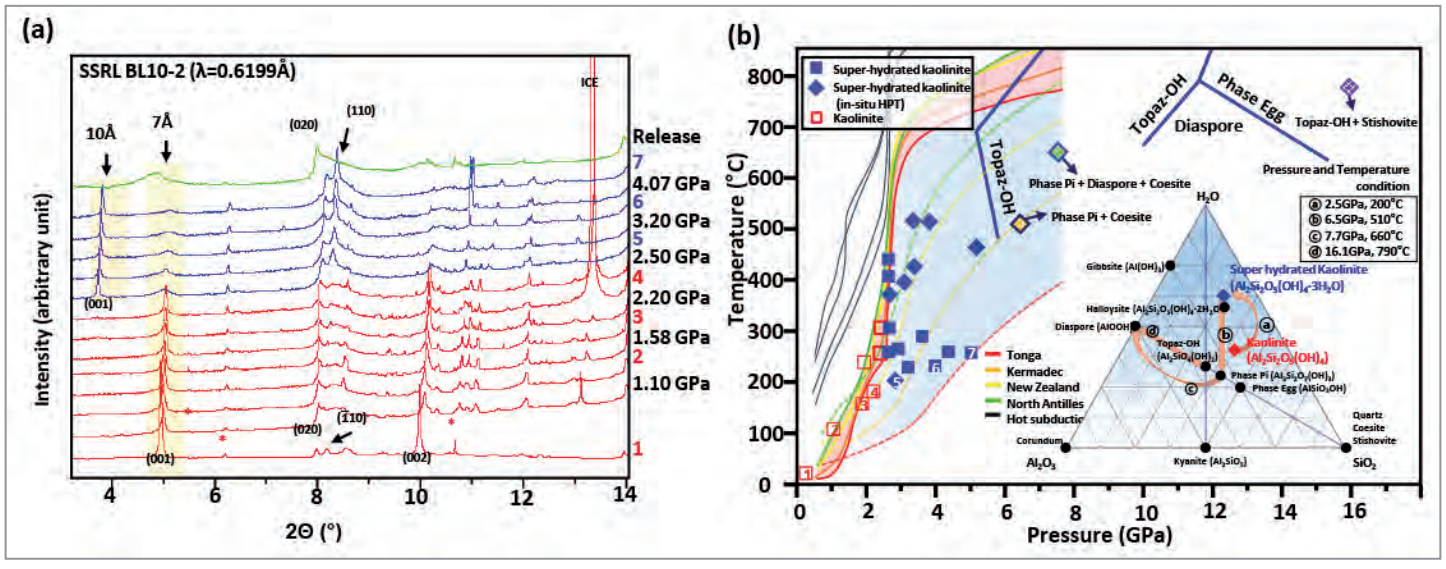


Figure 1

(a) Synchrotron XRD powder patterns of kaolinite at ambient and high-pressures, as well as annealed at different temperatures, in the presence of water. The appearance of a 10 Å peak marks the formation of super-hydrated kaolinite. (b) Results of high-pressure and temperature experiments on kaolinite. The coloured lines represent the P–T paths of the subducting slab surfaces from different subduction zones. The dotted lines in matching colours indicate the average P–T paths of the corresponding slab. Symbols with numbers correspond to XRD patterns in (a). Inset in (b): Ternary diagram for selected phases in the ASH system. The arrows indicate the super-hydration and breakdown sequence of kaolinite.

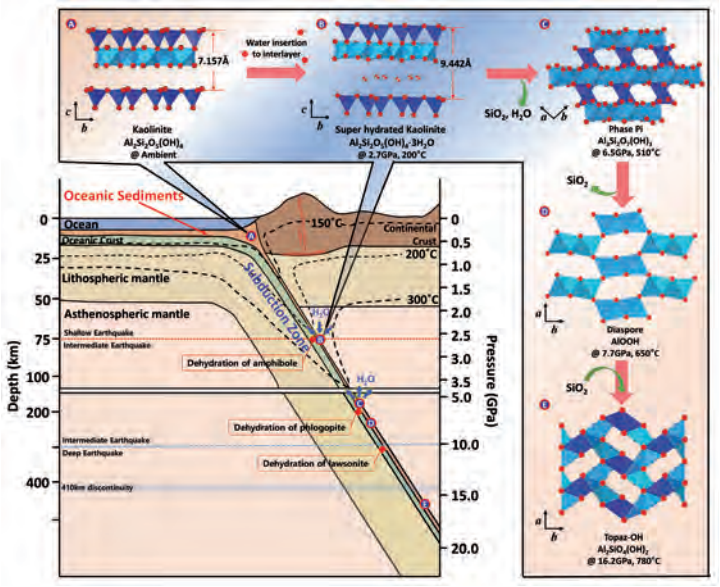


Figure 2

Illustration of a (cold) subduction zone showing the super-hydration and breakdown sequence of kaolinite.

water intercalation between the kaolinite layers. As a result, the unit cell volume expands by ca. 31 %. This new super-hydrated kaolinite appears to be less resistant to pressure showing a smaller bulk modulus of K_0 = 49.8 GPa compared to K_0 = 57.4 GPa for the original kaolinite before water intercalation, signalling further transitions and break downs at higher depths. The structural model of the super-hydrated kaolinite has been derived using Rietveld refinements of synchrotron XRD powder data taken at 4.1(1) GPa after heating at 200 °C (Fig. 1). The measured diffraction peaks are indexed in space group C1, the same as the original kaolinite [3]. Subsequent modelling and refinement of the electron densities by the oxygen atoms of the H_2O molecules at three distinct interlayer sites results in a chemical composition of $Al_2Si_2O_5(OH)_4 \cdot 2.97(2)\ H_2O$.

During an *in situ* high-pressure and high-temperature experiment using a graphite resistive heater in a diamond anvil cell at PETRA III beamline P02.2, we were able to show that with increasing pressure and temperature up to ca. 19 GPa and ca. 800 ˚C, sequential breakdown of super-hydrated kaolinite proceeds to phase-Pi ($Al_3Si_2O_7(OH)_3$), diaspore (α-AlOOH), and topaz-OH ($Al_2SiO_4(OH)_2$) along with the formation of coesite (SiO_2) and stishovite (SiO_2) (Fig. 2).

Super-hydrated kaolinite is the most hydrated aluminosilicate mineral and its formation and sequential breakdowns are important new results that explain the origins of other mantle minerals in the Al_2O_2–SiO_2–H_2O (ASH) system. During the breakdown of super-hydrated kaolinite to phase-Pi and coesite, water de-intercalates at pressures and temperatures that correspond to a depth near 200 km in a cold subducting slab. The hydroxyl group remains present throughout the breakdowns to phase-Pi, diaspore and the topaz-OH transition, which occur at depths between 200 km and 480 km.

Based on our structural model, the amount of water in super-hydrated kaolinite is ~17.3 wt%, and taking into account the original OH^- species, the total amount of water is ~28.9 wt%. This water content of super-hydrated kaolinite is the highest of any known aluminosilicate mantle mineral; for example, it is about two to three times the amount found in lawsonite (11.5 wt% of H_2O), serpentine (14 wt% of OH^-) and diaspore (15 wt% of OH^-) [4]. Our results bear important information for understanding deep water cycling and volcanism along the (cold) subduction zones as both super-hydration and dehydration occur at conditions that correspond to depths between about 75 km and 480 km (Fig. 2), where geophysicists suspect changes in earthquake formation mechanism.

We suggest that other (clay) minerals and/or multicomponent systems in the oceanic sediment and crust could undergo similar super-hydration during subduction. It is also possible that the subduction interface might not be homogeneous but is made up of patches of kaolinite, which will then serve as clear rupture points after super-hydration. The dehydration and breakdown sequence of super-hydrated kaolinite provides new insights into the geochemical and seismic processes occurring along subduction zones and needs to be incorporated in future modelling studies.

Author contact: Yongjae Lee, yongjaelee@yonsei.ac.kr

References

1. H. L. Windom, 'Lithogenous material in marine sediments', Chem. Oceanogr. 5, 103–135 (1976).
2. E. M. Syracus, P. E. van Keken and G. A. Abers, 'The global range of subduction zone thermal models', Phys. Earth Planet. Inter. 183, 73-90 (2010).
3. D. L. Bish and R. B. Vondreele, 'Rietveld refinement of non-hydrogen atomic positions in kaolinite', Clay Clay Min. 37, 289-296 (1989).
4. E. Ohtani, 'Water in the mantle', Elements 1, 25-30 (2005).

Original publication

'A role for subducted super-hydrated kaolinite in Earth's deep water cycle', Nature Geoscience 10, 947-953 (2017). DOI: 10.1038/s41561-017-0008-1

Huijeong Hwang[1], Donghoon Seoung[1,2], Yongjae Lee[1,3], Zhenxian Liu[4], Hanns-Peter Liermann[5], Hyunchae Cynn[6], Thomas Vogt[7], Chi-Chang Kao[2] and Ho-Kwang Mao[3,8]

1. Department of Earth System Sciences, Yonsei University, Seoul, Republic of Korea
2. Stanford Synchrotron Radiation Lightsource, SLAC National Accelerator Laboratory, Menlo Park, CA, USA
3. Center for High Pressure Science & Technology Advanced Research, Shanghai, China
4. Department of Civil and Environmental Engineering, George Washington University, Washington, DC, USA
5. Deutsches Elektronen-Synchrotron DESY, Hamburg, Germany
6. High-Pressure Physics Group, Physics and Life Sciences, Lawrence Livermore National Laboratory, Livermore, CA, USA
7. Nano Center & Department of Chemistry and Biochemistry, University of South Carolina, Columbia, SC, USA
8. Geophysical Laboratory, Carnegie Institution of Washington, Washington, DC, USA

Engineering alloys for 3D printing

A transformation path opens up novel alloy design

The alloys used nowadays for metal-based additive manufacturing – colloquially termed 3D printing – are mostly based on compositions inherited from conventional production techniques. The strong anisotropy exhibited by alloys that solidify with cubic lattices (e.g. conventional compositions of Ni- or Ti-based alloys) represents a deep-rooted drawback during AM. The reason is that thermo-mechanical processing as implemented in traditional manufacturing for breaking up anisotropy, as well as controlling grain size and texture, is not considered in AM owing to the attractiveness of near net-shape fabrication. In this work, a phase transformation path opens up an alternative to avoid the typical coarse anisotropic microstructures obtained upon AM of titanium alloys and provides new windows for alloy design of other metallic systems.

Metal-based additive manufacturing (AM) is resulting in a paradigm change across multiple industries such as the aerospace, biomedical and automotive sectors. One of its key strengths is the fabrication of near net-shape metallic components with complex geometries providing e.g. inner channels for cooling fluids, or bionic and load-optimised structures of minimal weight not achievable by conventional production methods like casting or machining. Layer-by-layer AM production from a 3D computer-aided design provides design freedom, increased product customization and shorter time to market. For Ti-based components, these advantages account for estimated production savings up to 50 %, by basically missing out exorbitant machining costs and material loss. In aerospace, AM is capable to reduce buy-to-fly ratios from 40:1 or 20:1 to 1:1 [1].

Nowadays, the strong anisotropy exhibited by alloys that solidify with fcc or bcc primary phases (e.g. conventional compositions of Ni- or Ti-based alloys) represents a critical issue for acceptance as well as certification of AM parts. This is a consequence of the steep, directional thermal gradient in the molten metal pool, which prevents nucleation ahead of the solidification front provoking epitaxial growth across solidified layers [2]. For instance, severe texture associated with anisotropic structural properties usually remains upon AM and even after post-processing. This effect is particularly relevant for powder-bed AM techniques such as selective laser melting (SLM, shown in Fig.1a), and well-known to occur in the popular Ti-6Al-4V alloy, which accounts for more than 50 % of the titanium market (Fig. 1b).

During AM of Ti-alloys, the strong texture of the bcc β-phase <100> oriented along the SLM building direction, is transmitted to the strengthening hcp α-phase by satisfying the Burgers orientation relationship (OR) $\{002\}\alpha \parallel \{110\}\beta$. Our approach aims at tackling anisotropy by exploring alternative paths of α formation altering the regular Burgers-related $\beta \rightarrow \alpha$ transformation. The solute α-stabiliser lanthanum (La) is added to commercially pure titanium (CP Ti) to exploit metastability around liquid-solid and solid-solid states during

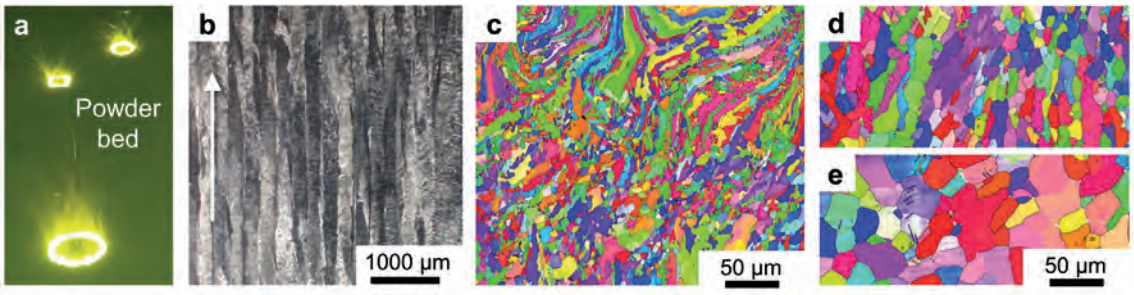


Figure 1

a) Selective laser melting (SLM) is a powder bed-based additive manufacturing process where alloys undergo series of sharp thermal cycles tracing fast heating (~10^6 – 10^7 K/s) and cooling rates (~10^3 – 10^8 K/s). b) Common microstructure obtained after SLM of Ti-6Al-4V showing epitaxially grown prior grains of β phase. c) SLM of Ti-2La leads to texture reductions along the SLM building direction pointed by the arrow in b), owing to the formation of small equiaxed grains of α phase with multiple orientations. Post thermal treatment of the SLM as-built condition in c) by cooling with d) 100 °C/min and e) 5 °C/min from 950 °C (L_1+β field) down to room temperature, results in the formation of new α grains of smaller size with increasing cooling rate and extensive globularization.

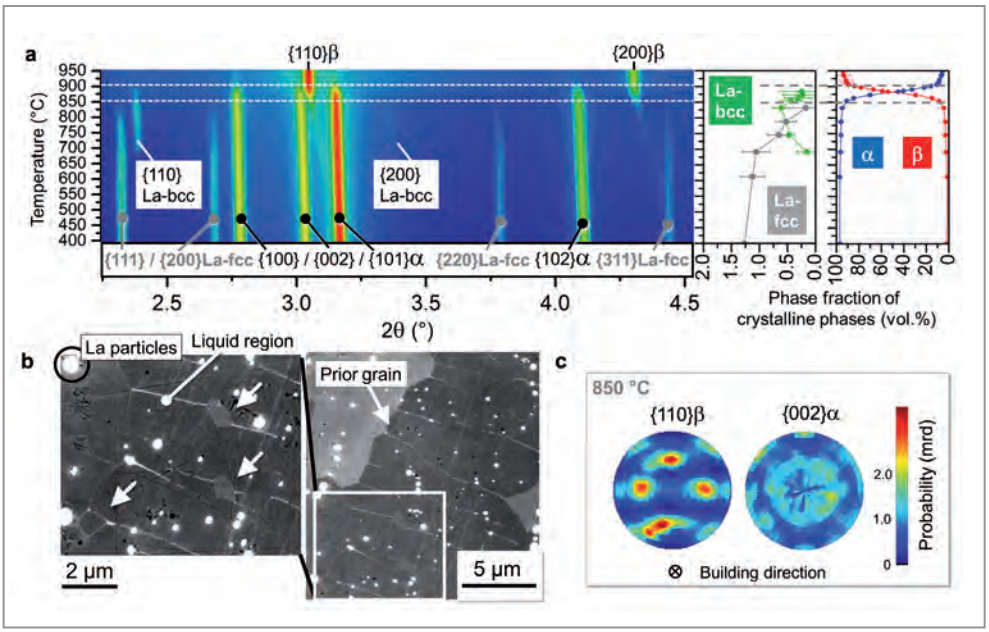


Figure 2

Phase transformation kinetics in the SLM Ti-2La alloy. a) Colour-coded 2D plot of the evolution of {hkl} reflections of α, β, La-bcc and La-fcc for a representative 2θ range of 2.25° – 4.55°, combined with the simultaneous evolution of volume fractions of phases during continuous cooling from 950 °C down to 400 °C with 20 °C/min. b) α particles (pointed by arrows) formed at prior β/L_1 interfaces in a microstructure quenched from 950 °C. c) Normalized pole figures of {110}β and {002}α at 850 °C indicating that the α phase does not fully inherit the texture of the parent β phase. The transformation β →α is reflected in the rapid increase in the volume fraction of α between 900 – 850 °C shown in a).

SLM. Besides tortuous grains, the microstructure obtained upon SLM of a Ti-2 wt.% La alloy ('Ti-2La') consists in extensive distributions of fine equiaxed α grains (Fig. 1c). These microstructural features are not characteristic of typical transformation mechanisms usually observed in CP Ti or α+β Ti-alloys, namely neither displacive nor diffusive nucleation and growth leading to parent β grains filled with α+β Widmanstätten structures [3].

Upon cooling of the Ti-2La SLM as-built state from 950 °C (L_1+β field) down to room temperature with 100 °C/min and 5 °C/min (i.e. thermal conditions closer to thermodynamic equilibrium than SLM, shown in Fig. 1d and 1e, respectively), formation of new α grains and extensive globularisation takes place resulting in recrystallised-like microstructures that do not inherit the usual SLM-induced texture of the parent β phase. Also, grain refinement of α grains is obtained with increasing cooling rate.

The phase transformation kinetics during post-thermal treatment of the SLM as-built state was investigated by *in situ* high energy synchrotron X-ray diffraction (HEXRD) at the P07-HEMS beamline of PETRA III. A rapid transformation β → α takes place between 900 °C and 850 °C (Fig. 2a). At the beginning of the transformation, L_1, β and α are present, while La reflections are absent. As was also directly confirmed by the raw diffraction images, this points to formation of α phase prior to the peritectic L_1+β →La-bcc reaction given by the Ti-La equilibrium phase diagram [4] starting after about 50 % completion of the diffusive β → α transformation (Fig. 2a). Metallographic analysis of the SLM Ti-2La alloy quenched from 950 °C (L_1+β) shows small α particles (pointed by arrows) at β/L_1interfaces (Fig. 2b). This, together with the results obtained from *in situ* HEXRD, suggests that nuclei of α form at β/L_1 interfaces via the peritectic path L_1+β → α, expanding during the subsequent β → α transformation.

The pole figures in Fig. 2c for {002}α and {110}β at 850 °C, i.e. at the end of the β → α transformation, clearly show that to a large extent α does not inherit the texture of β within this temperature range. Thus, the usual Burgers OR typical for a β → α transformation (and inheritance of texture by α) is partially avoided.

We have discovered a transformation path that offers significant texture reduction as well as equiaxed microstructures for a model Ti-2La alloy produced by SLM. This approach can be extended to Ti-alloys with α+β microstructures as proved for a Ti-1.4-Fe-1La alloy and represents a step-forward towards a next generation of titanium alloys for AM.

Moreover, the approach shown in our investigations to adapt alloys to AM using a peritectic reaction opens up windows for target oriented alloy design in other alloy systems.

Author contact: Pere Barriobero-Vila, pere.barrioberovila@dlr.de

References

1. B. Dutta and F. H. Froes, 'Additive Manufacturing (AM) of Titanium Alloys', Elsevier, Oxford, (2015).
2. P. C. Collins, D. A. Brice, P. Samimi, I. Ghamarian and H. L. Fraser, 'Microstructural control of additively manufactured metallic materials', Annu. Rev. Mater. Res. 46, 1 – 18 (2016).
3. G. Lütjering and J. C. Williams, 'Titanium', Springer, Berlin, (2007).
4. N. Mattern, Y. Yokohama, A. Mizuno, J. H. Han, O. Fabrichnaya, M. Richter and S. Kohara, 'Experimental and thermodynamic assessment of the La-Ti and La-Zr systems', Calphad 52, 8–20 (2016).

Original publications

'Peritectic titanium alloys for 3D printing', Nature Communications 9, 3426 (2018).
DOI: 10.1038/s41467-018-05819-9

Pere Barriobero-Vila[1], Joachim Gussone[1], Andreas Stark[2], Norbert Schell[2], Jan Haubrich[1] and Guillermo Requena[1,3]

1. Institute of Materials Research, German Aerospace Center (DLR), Cologne, Germany
2. Helmholtz-Zentrum Geesthacht, Geesthacht, Germany
3. Metallic Structures and Materials Systems for Aerospace Engineering, RWTH Aachen University, Aachen, Germany

Catching the entatic state in photochemistry

Copper complexes in pump-probe studies

What enables electrons to be transferred efficiently, for example during photosynthesis and other biochemical processes that are relevant for e.g. the tanning of skin, breathing, and immunological responses of plants and insects? An interdisciplinary team of researchers has worked out the details of how important bio-inorganic electron transfer systems operate. Entatic state model complexes are key for biochemical electron transfer since they optimise the energies of starting and final configuration to enable fast reaction rates, e.g. in biological and chemical electron transfer reactions. The team demonstrates with pre-organised biomimetic copper complexes that the entatic state principle can be used to tune the photochemistry of copper complexes.

The entatic state principle is normally applied to interpret thermally activated electron transfer processes at copper centres. Entasis denotes a structural pre-distortion of a transition metal complex towards a reaction transition state, thus, facilitating a chemical reaction and, in a narrower sense, enabling faster electron transfer (Fig. 1a). This pre-distortion is also discussed as energisation of reactive states and is crucial for efficient catalysis in chemistry and biology in copper or iron metalloproteins [1]. Depending on its oxidation state, the copper atom either prefers a planar configuration or a tetrahedral arrangement of the neighbouring ligands. However, the binding partner in the protein forces the copper atom to adopt a sort of intermediate structurally pre-distorted arrangement. This highly distorted tetrahedron allows a very rapid shift between the two oxidation states of the copper atom.

We examined a model system consisting of a copper complex with specially tailored ligands, so-called guanidinoquinoline ligands. Recently, we reported a series of bis(chelate) Cu(I) and Cu(II) complex cations $[Cu^{II}(TMGqu)_2]^+$ and $[Cu^{I}(TMGqu)_2]^{2+}$ (see Fig. 1b for an overlay of both cations) [2]. They display the astonishing feature that their structures are very similar with a coordination polyhedron in the centre between tetrahedral and square-planar environments. A resonance Raman study of these Cu(I/II) complexes in solution showed that they come into resonance at nearly the same energy around ~3.5 eV by metal-to-ligand charge-transfer (MLCT) and ligand-to-metal charge-transfer (LMCT) processes. We found a dominant Cu-N vibrational mode that couples the optical charge-transfer excitation with the distortion along the reaction coordinate leading from the more tetrahedral Cu(I) to a more flattened (towards square-planar coordination) Cu(II) geometry. The donor interplay between guanidine and quinoline units as well as the large steric encumbrance of guanidines were found to be crucial for this constrained coordination.

In this study, we report on the dynamics of the structural and electronic changes as induced by an MLCT photoexcitation process utilising a collection of complementary experimental transient techniques, which provide crucial information on time scales covering more than four orders of magnitude. With time-resolved optical absorption and emission spectroscopy in the visible and UV range we identify short-lived

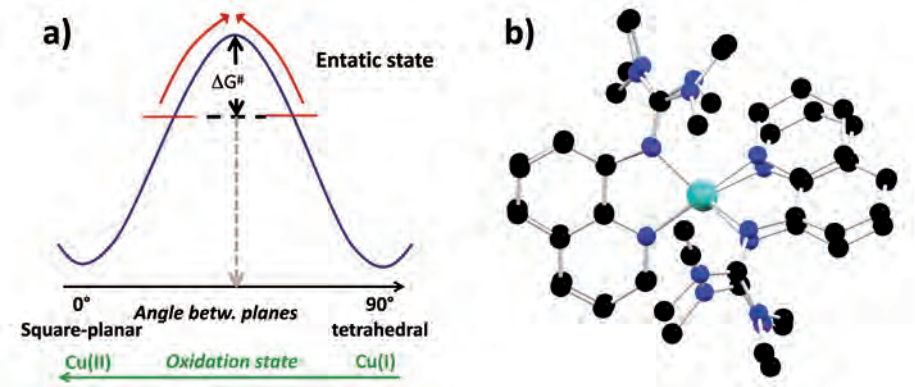
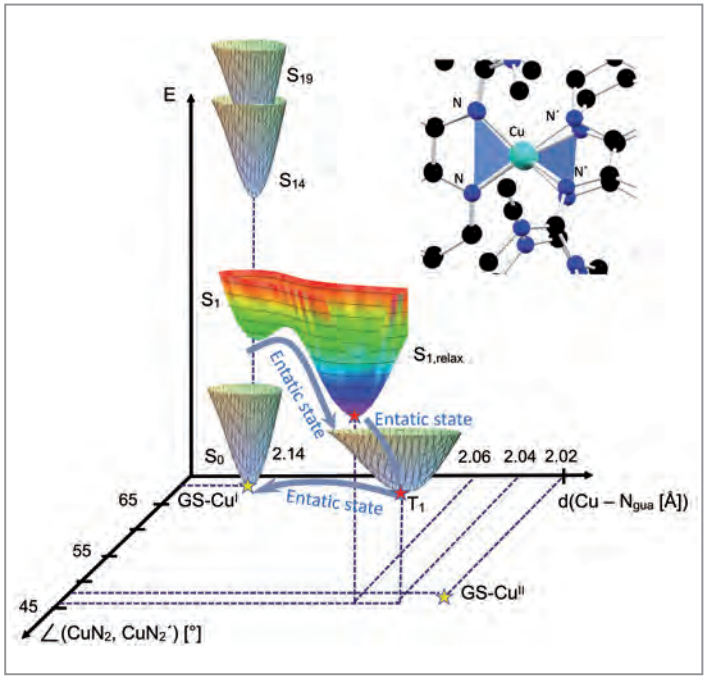


Figure 1

a) Illustration of the entatic state principle: Cu(II) has a clear electronic preference for square-planar coordination, whereas Cu(I) does not have an electronically favoured coordination mode (d^{10} configuration), but is sterically mostly driven to tetrahedral motifs. The entatic state principle denotes an energisation of both states (here: misfit of ligands to square-planar and tetrahedral coordination), which leads to a smaller activation barrier. b) Overlay of the molecular structures of $[Cu^{I}(TMGqu)_2]^+$ and $[Cu^{II}(TMGqu)_2]^{2+}$.

Figure 2

Photochemistry of $[Cu^{I}(TMGqu)_2]^+$: after initial excitation into S_{14} and higher Franck-Condon MLCT states, the complex falls back into the S_1 state which subsequently relaxes since the Cu centre feels being Cu(II) with a reduced ligand. The intersystem crossing from $S_{1,relax}$ to T_1 is then rather facile (by the structural similarity). Finally, the T_1 state decays to the ground state. It has been characterised by four different time-resolved techniques.



electronic intermediate states. Time-resolved IR spectroscopy characterizes these intermediates by probing the molecular vibrations in the ligand system. Finally, transient pump-probe X-ray absorption spectroscopy (XAS) performed at beamline P11 of the PETRA III synchrotron [3] focuses on the changes of the Cu oxidation state and its concomitant change on the coordination sphere in $[Cu^{I}(TMGqu)_2]^+$ following photoexcitation. The combination of these different experimental tools with extensive density functional theory (DFT) studies of the excited states and their spectroscopic features leads to a new comprehensive picture of the reaction dynamics involving excited singlet and – by intersystem crossing – triplet states.

The study shows in detail how the process proceeds (Fig. 2): from the initial state (S_0, copper in an oxidation state of +1) an electron is transferred from the copper to one of the ligands, by optical excitation into a higher singlet state (S_{14}). Within femtoseconds the excited state created decays into another, still excited state, known as the S_1 state. In this configuration, the geometry is slightly relaxed. Shortly afterwards, the electron undergoes a change in spin. Although one of the electrons has so far remained on the ligand, this electron and its corresponding partner on the copper were spin-coupled. The spin of the electron on the ligand now reverses, and this very rapid transition to the so-called triplet state, within just about two picoseconds, removes the spin coupling. This T_1 state exists for 120 picoseconds and drops back into the original state again after once again reversing its spin. This state reflects the photoexcited entatic state as has been shown by detailed comparison of the transient XAFS spectra. All the time constants are distinctly shorter compared with other copper complexes. A complete understanding of all the processes taking place has only become possible through the unique combination of different methods of study.

The detailed analysis of the reaction principle not only improves our understanding of natural processes. It can also help to customise new bio-inorganic complexes that imitate nature but whose range of reactions extend beyond those of natural molecules. These complexes could also accelerate or make possible chemical reactions associated with electron transfers in other areas.

Author contact: Sonja Herres-Pawlis, sonja.herres-pawlis@ac.rwth-aachen.de, Michael Rübhausen, mruebhau@physnet.uni-hamburg.de

References

1. J. Stanek, A. Hoffmann and S. Herres-Pawlis, 'Renaissance of the entatic state principle', Coord. Chem. Rev. 365, 103-121 (2018).
2. A. Hoffmann, S. Binder, A. Jesser, R. Haase, U. Flörke, M. Gnida, M. Salomone Stagni, W. Meyer-Klaucke, B. Lebsanft, L. E. Grünig, S. Schneider, M. Hashemi, A. Goos, A. Wetzel, M. Rübhausen and S. Herres-Pawlis, 'Catching an entatic state – a pair of copper complexes', Angew. Chem. 126, 305–310 (2014); Angew. Chem. Int. Ed. 53, 299–304 (2014).
3. D. Göries, B. Dicke, P. Roedig, N. Stübe, J. Meyer, A. Galler, W. Gawelda, A. Britz, P. Geßler, H. Sotoudi Namin, A. Beckmann, M. Schlie, M. Warmer, M. Naumova, C. Bressler, M. Rübhausen, E. Weckert and A. Meents, 'Time-resolved pump and probe X-ray absorption fine structure spectroscopy at beamline P11 at PETRA III', Rev. Sci. Instr. 87 (5), 053116 (2016).

Original publication

'Transferring the entatic state principle into copper photochemistry', Nature Chemistry 10, 355-362 (2018). DOI: 10.1038/nchem.2916

Benjamin Dicke[1,2], Alexander Hoffmann[3], Julia Stanek[3], Michael S. Rampp[4], Benjamin Grimm-Lebsanft[1,2], Florian Biebl[1,2], Dieter Rukser[1,2], Benjamin Maerz[4], Dennis Göries[5], Maria Naumova[1,6], Mykola Biednov[1,2], Gerd Neuber[1,2], Alina Wetzel[1,2], Stefan M. Hofmann[4], Philip Roedig[5], Alke Meents[5], Johan Bielecki[7], Jakob Andreasson[7,8,9], Kenneth Beyerlein[2], Henry N. Chapman[2,5], Christian Bressler[10,11,12], Wolfgang Zinth[4], Michael Rübhausen[1,2] and Sonja Herres-Pawlis[3]

1. Institute of Nanostructure and Solid State Physics, University of Hamburg, Hamburg, Germany
2. Center for Free-Electron Laser Science (CFEL), Hamburg, Germany
3. Institute for Inorganic Chemistry, RWTH Aachen University, Aachen, Germany
4. Institute for BioMolecular Optics and Center for Integrated Protein Science (CIPSM), Ludwig-Maximilians-Universität Munich, Munich, Germany
5. Deutsches Elektronen-Synchrotron DESY, Hamburg, Germany
6. Department of Chemistry, University of Paderborn, Paderborn, Germany
7. ELI Beamlines, Institute of Physics, Czech Academy of Science, Prague, Czech Republic
8. Laboratory of Molecular Biophysics, Department of Cell and Molecular Biology, Uppsala University, Uppsala, Sweden
9. Condensed Matter Physics, Department of Physics, Chalmers University of Technology, Göteborg, Sweden
10. European XFEL, Schenefeld, Germany
11. Department of Physics, Technical University of Denmark, Lyngby, Denmark
12. The Hamburg Center for Ultrafast Imaging, University of Hamburg, Hamburg, Germany

In situ coherent X-ray imaging reveals origin of voltage fade in batteries

X-ray nanovision improves battery design

Lithium-ion batteries are ubiquitous in a wide range of modern technologies, including mobile phones, electric vehicles, and sustainable energy systems. The battery performance is inherently connected to the calendar life of the capacity and voltage of a battery. Among the leading candidates for the next generation cathode material for energy storage are lithium-rich layered oxides, delivering 50 % excess capacity over commercially used compounds. Despite excellent prospects, voltage fade has prevented effective use of the excess capacity, and a major challenge has been the lack of understanding of the mechanisms underpinning the voltage fade. Here, using *operando* three-dimensional Bragg coherent diffractive imaging, we directly observe the nucleation of a mobile dislocation network in lithium-rich layered oxide nanoparticles. The dislocations form more readily in these oxides as compared with a classical layered oxide, suggesting a link between the defects and voltage fade. We show microscopically how the formation of partial dislocations contributes to the voltage fade. The insights allow us to design and demonstrate an effective method to recover the original high voltage functionality. Our findings reveal that the voltage fade in lithium-rich layered oxides is reversible and call for new paradigms for improved design of oxygen-redox active materials.

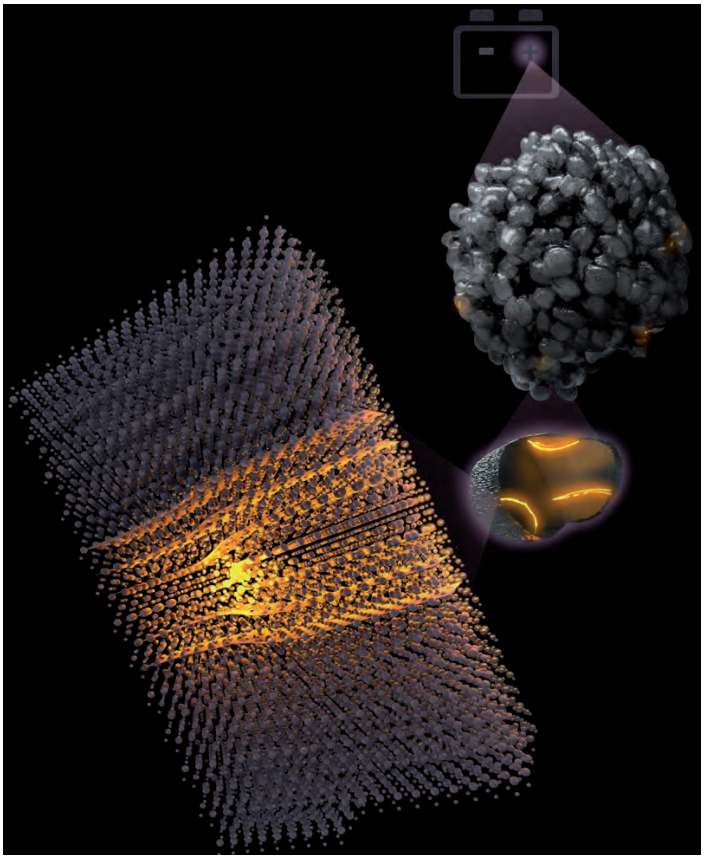


Figure 1

In a fully operational battery with the positive electrode consisting of agglomerates embedded in a multicomponent environment, we isolated single crystalline nanoparticles, in which we observe dislocation nucleation during charge.

(Image: Victor O. Leshyk)

Bragg coherent diffraction imaging (BCDI) allows studying the processes inside of the battery operando [1]: this method relies on interference produced by coherent X-rays and phase-retrieval algorithms to reconstruct the three-dimensional electron density and atomic displacement fields in nanocrystals [2]. By using *in-situ* Bragg coherent diffraction imaging on fully operational multi-component coin cells, we mapped the 3D displacement field inside primary lithium-rich layered oxides battery particles during battery operation (see Fig. 1). The experiments were performed at PETRA III beamline P10 and the Advanced Photon Source in Argonnne (U.S.). BCDI is particularly sensitive to dislocations, which are extra atomic layers that do not fit into the otherwise perfectly periodic crystal structure and give rise to singularities in the displacement field. While the pristine nanoparticle showed no such singularities in the present geometry, when charged, it contained two dislocations in the bulk of the nanoparticle, revealing the formation of dislocations in bulk during charge (see Fig. 2 a). The dislocation density increased upon subsequent charge, and a dislocation network emerged at higher voltages.

We connected the dislocation formation to the voltage fade by considering Pauling's third rule: in the energetically most favourable 'O3' structure, all lithium octahedral sites share edges with transition metal octahedral sites. In the O3 structure, the different oxygen layers (A, B and C) are ordered as ABCABC. The extra half-plane terminating at the dislocation line contains two oxygen layers; thus, the initial sequence ABCABC transforms to ABC BC ABC, which contains an

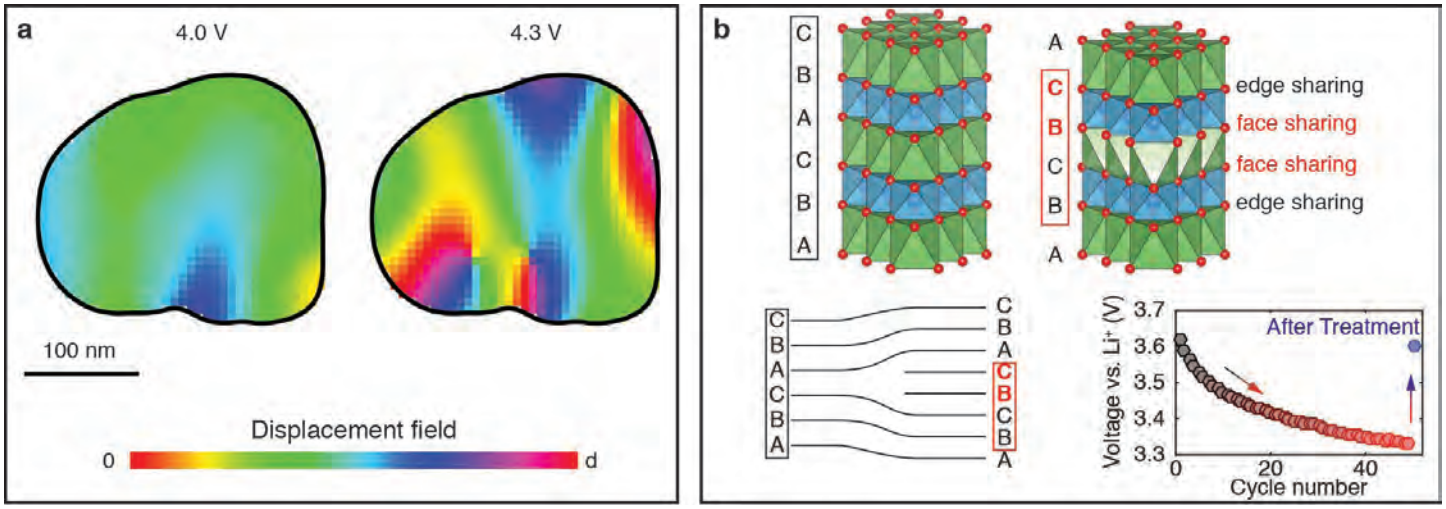


Figure 2

(a) A 2D slice through the 3D displacement field inside of a single cathode LRLO nanoparticle measured *operando* at various states of charge. While no dislocations are present in the beginning of the charge (4.0 V), two edge dislocations nucleate at 4.3 V during the charge. The dislocations are visible as singularities in the displacement field. (b) The dislocations result in unfavourable cation configuration (face sharing) leading to voltage fade. The voltage recovers after the heat treatment, which presumably restores the edge sharing configuration.

O1-like part BCBC (see Fig. 2b). The partial transition to O1 induces unfavourable face sharing between lithium and transition metal octahedral sites, thus, raising the Gibbs free energy of the system (see Fig. 2b). This energy penalty is greater at high lithium concentration simply because more face sharing sites are filled. We hypothesized that the difference in free energy induced by the presence of O1-like defects contributes to the voltage fade and confirmed our hypothesis by first-principles calculations. Based on the mechanistic description above, we designed a path to retrieve the voltage by high-temperature annealing (>150 °C). The voltage profile after treatment showed a recovery of the overall voltage (see Fig. 2b).

The experimental observation of significantly higher rate of dislocation formation in lithium-rich layered oxides as compared with classical material resonates with the excess capacity in this oxide. The current understanding of the activity of oxygen anions in lithium-rich layered oxides materials includes three processes: reversible oxidation of O^{2-} to O^{-}, further partially reversible oxidation to O, and irreversible release of O_2 gas from the bulk material to the surface. Step 2 and 3 require elevated oxygen mobility in the bulk of the oxide. While enhanced 'pipe' diffusion occurs along dislocations, recent theoretical works suggest a slower transport of oxygen along dislocations due to cation charge accumulation at the defect site. Whereas the oxygen mobility due to thermal fluctuations is predicted to be negligible at room temperature. However, an external electrical current leads to reversible accumulation or depletion of oxygen vacancies at dislocations in $SrTiO_3$. These dislocations play a major role in redox-based resistive switching in transition metal oxides used for electronic components, e.g. memristive applications. Moreover, we posit that during charge the lithium and electron extraction activates the emergent dislocation network in lithium-rich layered oxides for the transport of oxygen vacancies.

Author contact: Andrej Singer, asinger@cornell.edu

References

1. A. Ulvestad, A. Singer, J. N. Clark, H. M. Cho, J. W. Kim, R. Harder, J. Maser, Y. S. Meng and O. G. Shpyrko, 'Topological defect dynamics in operando battery nanoparticles', Science 348, 1344-1347, (2015).
2. I. K. Robinson, 'Nanoparticle Structure by Coherent X-ray Diffraction', J. Phys. Soc. Jpn. 82, 1-7, (2013).

Original publication

'Nucleation of dislocations and their dynamics in layered oxide cathode materials during battery charging', Nature Energy 3, 641–647 (2018). DOI: 10.1038/s41560-018-0184-2

Andrej Singer[1]*, Minghao Zhang[2], Shirley Meng[2], Oleg Shpyrko[1]

1. Department of Physics, University of California-San Diego, La Jolla, United States
2. Department of NanoEngineering, University of California-San Diego, La Jolla, United States

* present address: Department of Materials Science and Engineering, Cornell University, Ithaca, United States

Non-invasive virtual histology of the brain

Phase-contrast tomography reveals three-dimensional cytoarchitecture in human cerebellum

The cerebellum ('little brain') is a major part of the brain in vertebrates which plays an important role in the coordination of motion. Several types of cells are arranged in regular tightly folded layers, which persist throughout the cerebellum. The cerebellum is normally studied by histology, based on thin tissue sections which are investigated under a light microscope. We have used propagation-based phase-contrast tomography at PETRA III and a laboratory setup to reconstruct the neuronal cytoarchitecture in three dimensions in a non-destructive manner. The development of an automated cell segmentation workflow has enabled us to study the spatial distribution of millions of neurons and their spatial correlations.

In humans, the cerebellum contains approximately 80 % of all neurons within the brain despite its relatively small mass fraction of about 10 % of the total brain mass [1]. The main cell types within the cerebellum are the Purkinje cells with a flat dendritic tree, which are arranged in parallel, and the small granule cells, the most abundant cells in the cerebellum. Data on the precise locations of these neurons, however, was lacking, but is needed for example to model cerebellum function, or to observe small alterations in various diseases.

The cellular cytoarchitecture of such brain tissue is normally investigated via histology, a labour-intensive and invasive technique which is prone to artefacts due to the mechanical slicing procedure. While it provides excellent results on the individual 2D sections, 3D information can only be deduced by aligning successive slices, leading to a reconstructed volume with non-isotropic resolution. By X-ray phase-contrast tomography, we can study the neuronal cytoarchitecture in three dimensions without cutting the sample. The high penetration depth and small wavelength of hard X-rays allow for non-invasive imaging of the sample at sub-cellular resolution, enabling 3D histology, in which the sample can be virtually sliced in any arbitrary direction.

We have performed experiments on a 1 mm punch taken from such a paraffin-embedded human cerebellum both at the GINIX endstation [2] installed at the P10 beamline at PETRA III and at a home-built laboratory setup comprising a liquid-metal jet microfocus source [3]. Both setups revealed the underlying 3D cytoarchitecture due to the electron density contrast of cell nuclei compared to the surrounding tissue and allowed for the visualization of sub-cellular details as the

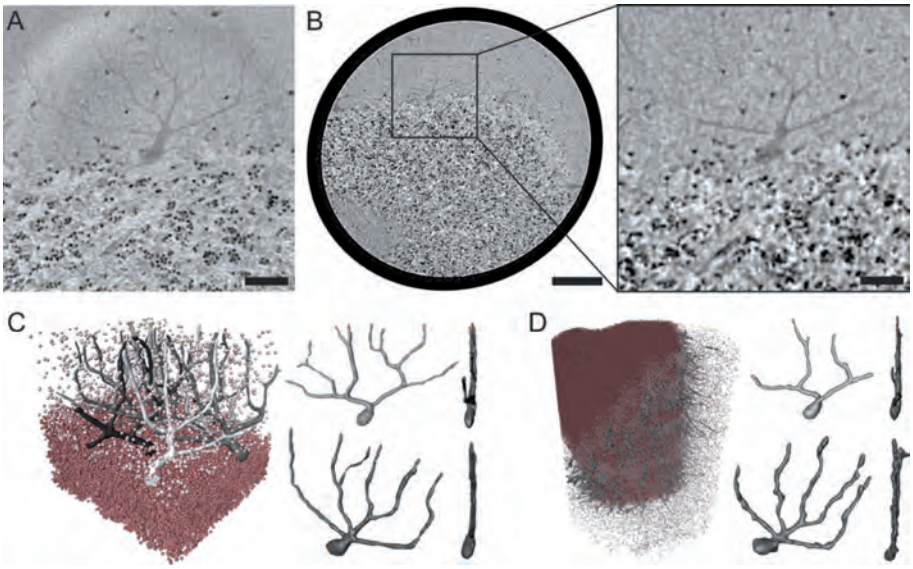


Figure 1

(a) Virtual slice through the reconstructed volume of the synchrotron data set, revealing the interface between the low-cell molecular (upper part) and cell-rich granular layer (lower part), including one cell of the mono-cellular Purkinje cell layer. (b) Corresponding slice through the laboratory data. (c) Automatic segmentation of the cells in the granular layer (dark red), the molecular layer (light red) and semi-automatic segmentation of the Purkinje cell layer (shades of gray) with two exemplary Purkinje cells shown separately, both from front and side view. (d) The same segmentation for the laboratory data set. Note that the individual Purkinje cells are the same as for the synchrotron data set and that the thick branches of the dendritic tree can already be resolved. Scale bars: 50 µm (a and b, right) and 200 µm (b, left).

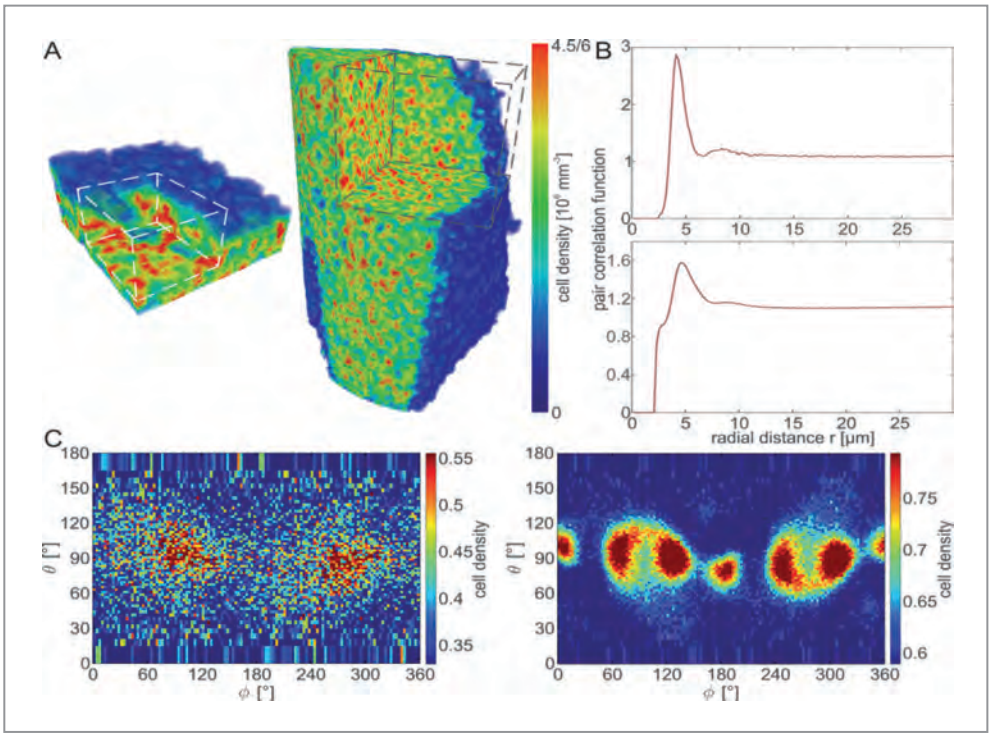


Figure 2

Analysis of cell distributions in the granular layer of human cerebellum. (a) Local cell density distribution within the granular layer of the cerebellum (left: synchrotron, right: laboratory). A clustering of cells within this layer can be clearly recognised. (b) Angular averaged pair correlation function of the cells in the granular layer (top: synchrotron, bottom: laboratory), revealing two distinct peaks at approximately once and twice the cell diameter, which indicates a local clustering of the cells. (c) Angular distribution of nearest neighbors in the granular layer (left: synchrotron, right: laboratory), showing an anisotropic distribution. Note that the data sets were aligned with respect to the Purkinje cell layer such that the dendritic tree lies approximately in the plane defined by $\theta = 90°$. Hence, the majority of nearest neighbors is distributed in parallel to the dendritic tree of the Purkinje cells.

dendritic tree of the Purkinje cells (Fig. 1a,b). To fully exploit the potential of 3D virtual histology, we have developed a workflow for the automatic segmentation of the small nuclei of the cells in the granular and molecular layer by image analysis based on the spherical Hough transform. While it led to the precise localisation of approximately 40000 cells in the data obtained at the GINIX setup, ~1.8 million cells could be found in the larger volume probed at the laboratory setup, though at slightly lower accuracy due to the lower data quality (Fig. 1c,d). Importantly, the GINIX data are used to validate the segmentation of the laboratory data.

This procedure has enabled the analysis of the spatial organization of cells within the molecular layer and, most importantly, also within the dense network of cells in the granular layer. An estimate of the local cell density distribution within the latter shows a clustering of cells (Fig. 2a), which persists throughout the granular layer, as can be recognised in the larger volume probed at the laboratory setup. This can be further quantified by the angular averaged pair correlation function, showing pronounced short range order visible as two peaks at approximately once and twice the cell diameter of 4 µm (Fig. 2b). As the exact positions of all cells within the granular layer are available, anisotropies in their arrangement can be determined as well. To this end, we have evaluated the angular distribution of connecting vectors between neighbouring cells in the granular layer. Since the large Purkinje cells define a natural coordinate system due to the almost two-dimensional shape of their dendritic tree and their parallel arrangement, we aligned the datasets accordingly. A strong anisotropy can be observed in the resulting plots in Fig. 2c, showing that the majority of nearest neighbours is distributed in parallel to the dendritic tree of the Purkinje cells, presumably enabling an optimized projection of the numerous granule cells to the Purkinje cell layer.

Our study demonstrates that phase-contrast tomography can be used to perform 3D virtual histology on paraffin-embedded human brain tissue both at a synchrotron facility and a home-built laboratory setup. This has enabled us to digitize 3D volumes with isotropic sub-cellular resolution and to automatically locate several ten thousand to over a million of cells. A subsequent analysis of cellular distributions in three dimensions showed a clustering within the granular layer as well as anisotropies governed by the natural coordinate system of the Purkinje cell layer, a result which would not have been accessible by standard 2D histology.

Author contact: Tim Salditt, tsaldit@gwdg.de

References

1. F. A. C. Azevedo, L. R. B. Carvalho, L. T. Grinberg, J. M. Farfel, R. E. L. Ferretti, R. E. P. Leite, W. J. Filho, R. Lent and S. Herculano-Houzel, 'Equal Numbers of Neuronal and Nonneuronal Cells Make the Human Brain an Isometrically Scaled-Up Primate Brain', J. Comp. Neurol., 513(5), 532 (2009).
2. T. Salditt, M. Osterhoff, M. Krenkel, R. N. Wilke, M. Priebe, M. Bartels, S. Kalbfleisch and M. Sprung, 'Compound focusing mirror and X-ray waveguide optics for coherent imaging and nano-diffraction', J. Synchrotron Rad. 22(4), 867 (2015).
3. M. Töpperwien, M. Krenkel, D. Vincenz, F. Stöber, A. M. Oelschlegel, J. Goldschmidt and T. Salditt, 'Three-dimensional mouse brain cytoarchitecture revealed by laboratory-based x-ray phase-contrast tomography', Sci. Rep. 7, 42847 (2017).

Original publication

'Three-dimensional virtual histology of human cerebellum by X-ray phase-contrast tomography', PNAS 115 (27), 6940-6945 (2018). DOI: 10.1073/pnas.1801678115

Mareike Töpperwien[1,2], Franziska van der Meer[3], Christine Stadelmann[3] and Tim Salditt[1,2]

1. Institute for X-Ray Physics, University of Göttingen, Göttingen, Germany
2. Center for Nanoscopy and Molecular Physiology of the Brain (CNMPB), Göttingen, Germany
3. Institute for Neuropathology, University Medical Center Göttingen, Göttingen, Germany

Coherent diffraction imaging of amyloid fibres

Graphene support allows imaging of (possibly) individual filaments at XFELs

Determination of a protein's structure at high-resolution without the need for crystallization would be a major advance for structural biology, and is one of the major aims of X-ray free-electron laser (XFEL) science. Biological filaments with one-dimensional order are of interest in many areas of research such as Alzheimer's disease, and lie between three-dimensional nanocrystals and single molecules. We have demonstrated a new approach to diffraction imaging of amyloid fibrils, combining a free-standing graphene support and single nanofocused X-ray pulses of femtosecond duration from an XFEL. Using a graphene support to provide both low background scattering and mutual alignment of filaments, we obtained diffraction from only a few tobacco mosaic virus (TMV) filaments and about fifty amyloid protofibrils to 2.7 Å and 2.4 Å resolution in single diffraction patterns, respectively.

All cells can assemble various proteins into slender filaments, also called fibres, that perform essential cellular functions including intracellular transport, cell movement and attachment, and cell division. We are particularly interested in amyloid fibres, which are related to the pathology of Alzheimer's, Parkinson's and other hereditary diseases, but that also execute functional roles such as in biofilm formation, storage of peptide hormones and the activation of an antiviral innate immune response. As all protein filaments, amyloid fibres are highly dynamic in nature and exist in different conformations and assembly states. This heterogeneity hampers their high-resolution structure determination by conventional means. Structural insights have been obtained from stable amyloid fibres – stable end products in fibre assembly processes – by solid-state nuclear magnetic resonance (NMR) and cryo-electron microscopy (cryo-EM). But there still remain major unanswered questions about the three-dimensional structures of the small assembly states arising at the start of the polymerization, and these are important for executing functional and toxic reactions. With femtosecond duration and highly brilliant pulses, XFELs provide new opportunities to study fibres and transient components away from equilibrium.

We exploited the single-pulse X-ray diffraction capabilities of XFELs to develop a novel approach to fibre diffraction. Fibre diffraction has not progressed significantly since the well diffracting structures of Tobacco Mosaic Virus or Bacteriophages were solved in the 1980s [1]. Acquisition of meaningful diffraction signals from only one-molecule-thick amyloids has been prevented by the necessity for millions of fibres to be exposed simultaneously to the X-ray beam in order to produce a sufficiently strong signal. In such a fibre specimen, every filament is randomly oriented about its fibre axis and slightly misaligned with its neighbouring filament. Both the misalignment and the cylindrical averaging result in signal broadening and loss of information. Another problem in fibre diffraction can be attributed to the solvent, which usually surrounds the fibre. This adds background diffraction, which obfuscates the weak coherent diffraction that contains information on the high-resolution features of the molecule. In our first experi-

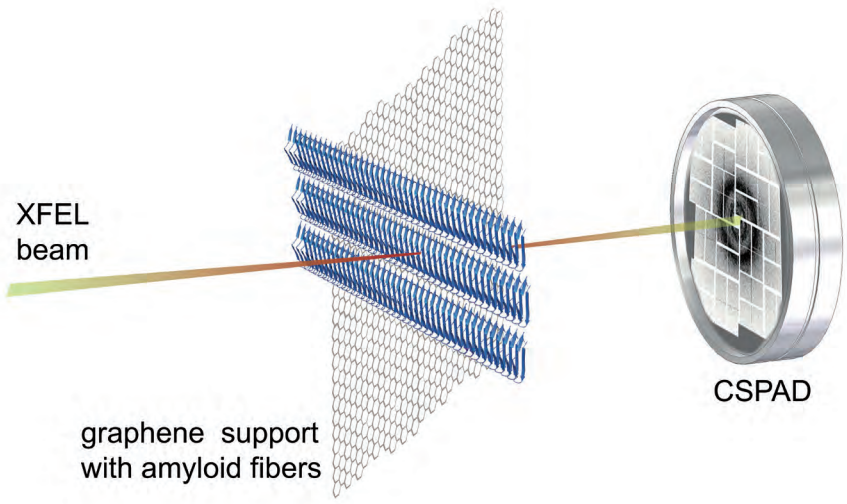


Figure 1

A schematic overview of the graphene based sample delivery. TMV filaments or amyloid protofibrils were aligned on a layer of graphene, mounted on a silicon window (not shown) and then scanned through the XFEL focus. Diffraction was recorded on the 2D Cornell-SLAC pixel array detector (CSPAD)-detector.

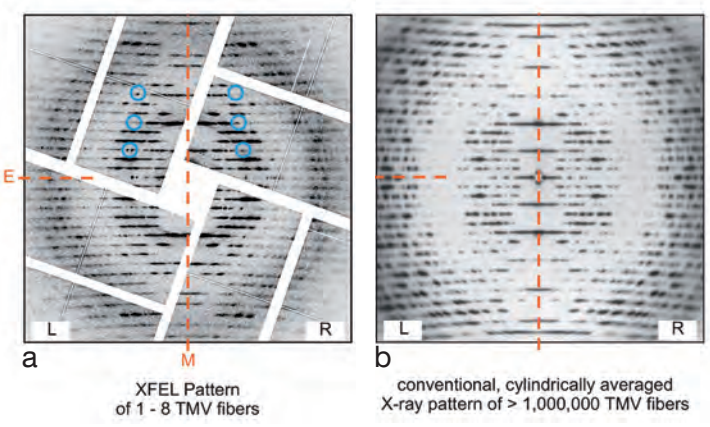


Figure 2

A classical X-ray fibre diffraction pattern from millions of mutually aligned TMV filaments (left) is compared to an XFEL diffraction pattern from TMV filaments aligned on a layer of graphene (right) (reprinted from original publication). The conventional pattern is symmetric about the equatorial and meridional axes E and M, respectively, as a result of the presence of many molecules with different rotations about their axis. The XFEL pattern exhibits asymmetry about the meridian, presumably as a result of the presence of a small number of molecules, with only one or a few rotations, and potentially contains more information than in the conventional case. Three positions that are not symmetric about the meridional axes are highlighted with circles.

ments at the Linac Coherent Light Source (LCLS) in 2013 and 2015, the XFEL in Stanford (U.S.), where we injected various amyloid fibres using a liquid jet into the X-ray beam, we observed major improvements in fibre diffraction data collection over the conventional approach [2]. While useful for crystalline fibres, the signal of one-molecule-thick amyloid filaments disappeared under the strong signal of the waterjet.

To increase the degree of alignment between amyloid fibres, and reduce background levels to a minimum, we developed a new experiment combining a free-standing graphene support with serial fibre diffraction at the XFEL. Graphene is essentially transparent to X-rays. Due to the unique honeycomb structure of the graphene surface, it also mutually aligns protein fibres along the graphene lattice forming a pseudo-2D-crystalline layer of fibres. Such mutual alignment increases the diffraction signal and simplifies data analysis.

Two samples were used in the study. We first used Tobacco Mosaic Virus (TMV) fibres as a well-known reference sample, as it has a large asymmetric unit whose 3D structure has been determined to high-resolution by fibre diffraction [1] and refined with cryo-EM. As native and biologically interesting fibres, we chose the functional hormone amyloid protofilaments prepared from bombesin and β-endorphin peptides [3]. We had characterized β-endorphin fibres by solid-state NMR and demonstrated that they exhibit a very low degree of conformational polymorphism [4] necessary for establishing novel methods [5]. Graphene supports with a layer of mutually aligned fibres were scanned through the XFEL focus, recording many diffraction frames from fibres in a serial manner. The high-dose exposure in an XFEL is essential to record the weak diffraction of one-molecule-thick amyloid fibrils, while outrunning radiation damage.

TMV and amyloid fibres diffract to 2.7 Å and 2.4 Å resolution in single diffraction patterns, respectively, when they are delivered on the free-standing graphene support to the XFEL nanofocus. Some of the TMV diffraction patterns exhibited asymmetry, indicating that only a few filaments are exposed to the bright XFEL pulse. Remarkably also, the diffraction signal from the graphene support, which was comparable to that from empty holes, was about two orders of magnitude lower than the signal from holes covered with both graphene and a layer of fibres. The approach holds promise to detect single fibres and other even smaller assemblies.

Our new approach to serial fibre diffraction combining highly brilliant XFEL beams and low background graphene substrates paves the way for structural investigations of protein filaments, non-crystalline biological assemblies and possibly single molecules. Having demonstrated that diffraction can be recorded from filaments, we anticipate our experiments to be a starting point for further investigations of biological assemblies and assembly processes in space – and in real time.

Author contact: Carolin Seuring, carolin.seuring@desy.de
Henry Chapman, henry.chapman@desy.de

References

1. K. Namba, R. Pattanayek and G. Stubbs, 'Visualization of protein-nucleic acid interactions in a virus. Refined structure of intact tobacco mosaic virus at 2.9 Å resolution by X-ray fiber diffraction,' J. Mol. Biol. 208, 307-325 (1989).
2. D. H. Wojtas, K. Ayyer, M. Liang, E. Mossou, F. Romoli, C. Seuring, K. R. Beyerlein, R. J. Bean, A. J. Morgan, D. Oberthuer, H. Fleckenstein, M. Heymann, C. Gati, O. Yefanov, M. Barthelmess, E. Ornithopoulou, L. Galli, P.L. Xavier, W. L. Ling , M. Frank et al., 'Analysis of XFEL serial diffraction data from individual crystalline fibrils', IUCrJ 4, 795-811 (2017).
3. S. K. Maji, M. H. Perrin, M. R. Sawaya, S. Jessberger, K. Vadodaria, R. A. Rissman, P. S. Singru, K. P. R. Nilsson, R. Simon, D. Schubert, D. Eisenberg, J. Rivier, P. Sawchenko, W. Vale and R. Riek, 'Functional Amyloids As Natural Storage of Peptide Hormones in Pituitary Secretory Granules', Science 325, 328-332 (2009).
4. C. Seuring, J. Verasdonck, P. Ringler, R. Cadalbert, H. Stahlberg, A. Bockmann, B. H. Meier and R. Riek, 'Amyloid Fibril Polymorphism: Almost Identical on the Atomic Level, Mesoscopically Very Different', J. Phys. Chem. B 121,1783/1792 (2017).
5. C. Seuring, J. Gath, J. Verasdonck, R. Cadalbert, J. Rivier, A. Bockmann, B. H. Meier and R. Riek, 'Solid-state NMR sequential assignment of the beta-endorphin peptide in its amyloid form', Biomol. NMR Assign. 10, 259-268 (2016).

Original publication

'Femtosecond X-ray coherent diffraction of aligned amyloid fibrils on low background graphene', Nature Communications 9, 1836 (2018).
DOI: 10.1038/s41467-018-04116-9

Carolin Seuring, Kartik Ayyer, Eleftheria Filippaki, Miriam Barthelmess, Jean-Nicolas Longchamp, Philippe Ringler, Tommaso Pardini, David H. Wojtas, Matthew A. Coleman, Katerina Dörner, Silje Fuglerud, Greger Hammarin, Birgit Habenstein, Annette E. Langkilde, Antoine Loquet, Alke Meents, Roland Riek, Henning Stahlberg, Sebastién Boutet, Mark Hunter, Jason Koglin, Mengning Liang, Helen M. Ginn, Rick P. Millane, Matthias Frank, Anton Barty, Henry N. Chapman

Affiliation details at
https://www.nature.com/articles/s41467-018-04116-9

Cells in a new light

When optical super-resolution microscopy meets X-ray holography and scanning SAXS in a correlative microscope

We have implemented a worldwide unique correlative microscope at the Göttingen Instrument for Nano-Imaging with X-rays at beamline P10 of the PETRA III storage ring. By combining X-ray and optical super-resolution fluorescence microscopy, complementary data can be recorded in a quasi-simultaneous manner, providing novel insights into biological cells. We have demonstrated this capability by imaging heart muscle cells. While the network of specifically labelled proteins was visualized by stimulated emission depletion (STED) microscopy, the entire distribution of electron density in the cell was imaged by X-ray holography. In addition, scanning of the cell through the X-ray focus led to a map of small-angle X-ray scattering (SAXS) data, which reflects the local molecular structure. In this way, high resolution images are not only obtained for the fraction of biomolecules, which emit fluorescence light, but for all molecular constituents. The information on the distribution of specific proteins provides important constraints for X-ray data analysis and interpretation, helping, for example, to rule out errors in the formulation of SAXS models.

Biological matter from single cells to tissue and organs is complex and heterogeneous, and therefore difficult to assess by diffraction methods alone, even if the diffraction volume is minimized by X-ray focusing optics. To unlock the full potential, additional information, such as the localization of specific proteins, is often required. This can be provided by fluorescence microscopy, and as introduced by Nobel prize winner Stefan Hell in Göttingen, controlled switching of the fluorescent dye between an on- and off-state by STED enables resolutions even below the Abbe limit for this technique. Conversely, X-ray imaging (in the present case holography and scanning SAXS) fills a major information deficit of fluorescence microscopy by providing contrast for both labelled and unlabelled cellular constituents.

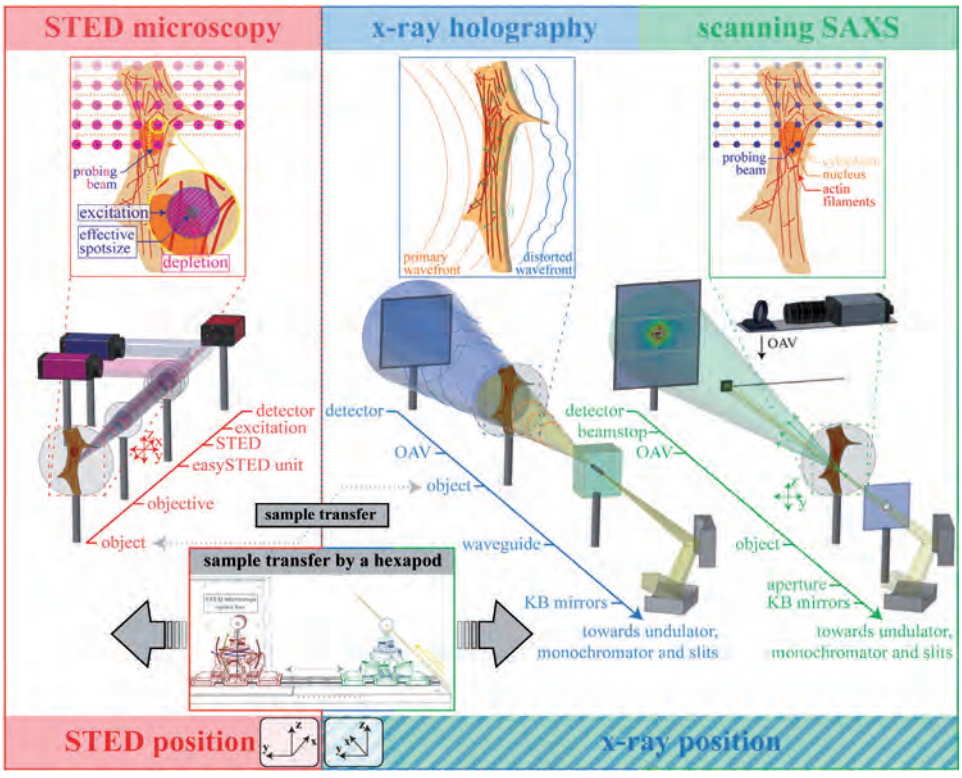


Figure 1

Sketch of the combined STED- and X-ray experiment, showing the setups for *in situ* STED microscopy, X-ray holography and scanning SAXS, from left to right. All modalities have been integrated into the GINIX instrument of beamline P10 at PETRA III. By stimulated emission of photons in STED microscopy (red box) fluorescent labels can be imaged below the Abbe limit. X-ray holography (blue box) provides phase- or electron density maps of the cell. Scanning SAXS (green box) yields a dark field map with a diffraction pattern for each pixel, which can be quantified in view of local (short range) order.

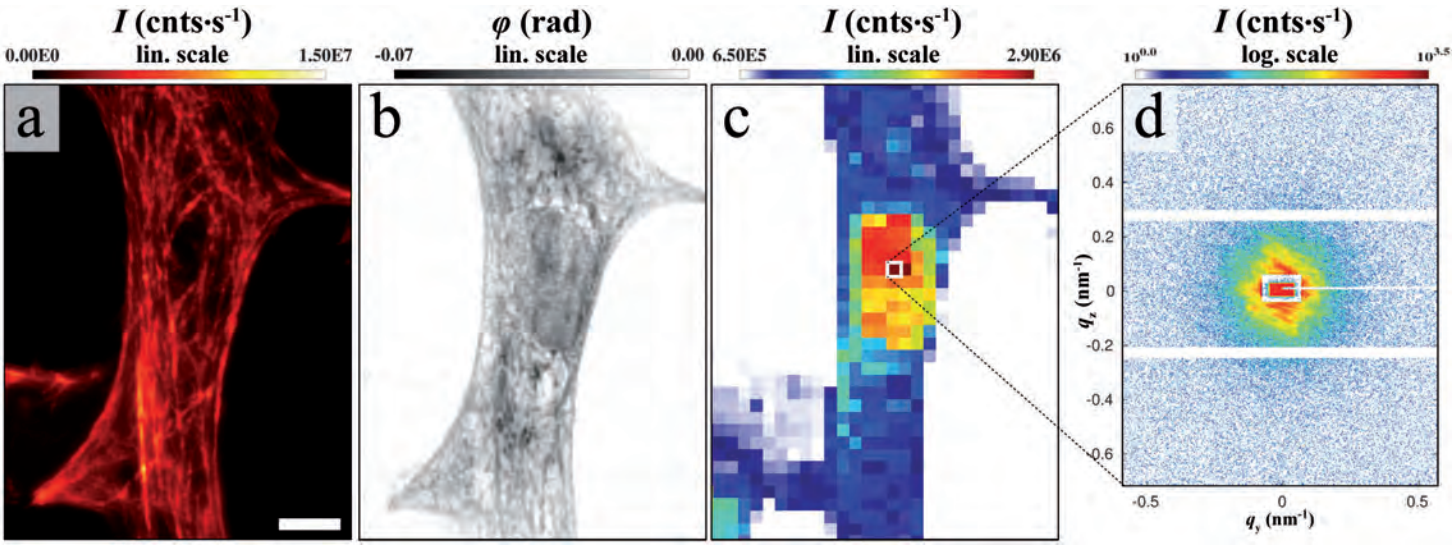


Figure 2

(a) STED micrograph of a cardiac tissue cell with labelled actin cytoskeleton. Scale bar: 5 µm. (b) Phase reconstruction of the same cellular area, as recorded by X-ray holography. (c) X-ray dark field as derived from scanning SAXS data showing the absolute photon counts of the scattering signal. (d) Single diffraction pattern of the nucleic area of the cell. Adapted from the original publication.

For the realization of this correlative approach we have designed a unique STED microscope, which can be installed *in situ* at the beamline and we have integrated it into the Göttingen Instrument for Nano-Imaging with X-rays (GINIX) at beamline P10. In this way, correlative recordings are now possible in close proximity and using the same sample environment and mounting.

Figure 1 shows a sketch of the combined setup with its main components. For STED microscopy (red box), a glass coverslip with freeze-dried heart tissue cells was raster-scanned by translation of the STED objective. Switching between the STED and X-ray recording positions was realised by a long-range sample translation stage. For X-ray holography (blue box), the synchrotron X-ray beam, focussed by a set of Kirkpatrick-Baez mirrors, was coupled into an X-ray waveguide. The sample was positioned in the divergent wavefront a few millimetres behind the waveguide. The resulting local phase shifts were made visible by self-interference with the primary, undistorted wave (inline holography). By phase retrieval algorithms applied to the holographic data, the object phase map can be reconstructed, showing the projected local electron density of all components in the cell. This provides highly complementary information to the fluorescently marked proteins as visualized on the STED micrographs. For scanning SAXS, the sample was raster-scanned in the KB focus, yielding an array of diffraction patterns.

Figure 2 shows the images of all three recording modes on the same cardiac tissue cell with a labelled actin cytoskeleton, including (a) the actin-STED micrograph, (b) the phase map obtained by phase retrieval and (c) the X-ray dark field map computed by integrating the photon counts for each local diffraction pattern. Figure 2d shows a single diffraction pattern recorded at a position within the nucleus of the cell.

As detailed in the original publication, filamentous actin, as being one of the three main cytoskeletal components, stands out to a certain degree in the holographic phase maps and the occurrence and direction of filament bundles can be derived by principal component analysis of the local diffraction data.

For the future, we plan to apply the approach of combined STED and X-ray microscopy to hydrated, and possibly living, cells in X-ray compatible chambers as well as to biological tissues with different labelled target structures. In addition, this approach will be used to monitor radiation damage. For all of these projects, the *in situ* configuration of the STED microscope at the beamline is essential!

Author contact: Tim Salditt, Sarah Köster, roentgenphysik@gwdg.de

Original publication

'Correlative microscopy approach for biology using X-ray holography, X-ray scanning diffraction and STED microscopy', Nature Communications 9, 3641 (2018).
DOI: 10.1038/s41467-018-05885-z

M. Bernhardt[1], J.-D. Nicolas[1], M. Osterhoff[1], H. Mittelstädt[2], M. Reuss[2], B. Harke[2], A. Wittmeier[1], M. Sprung[3], S. Köster[1] and T. Salditt[1]

1. Institute for X-Ray Physics, University of Göttingen, Göttingen, Germany
2. Abberior Instruments, Göttingen, Germany
3. Deutsches Elektronen-Synchrotron DESY, Hamburg, Germany

A new regulator of photosynthesis in cyanobacteria

The hexameric CBS-CP12 fusion protein

Cyanobacteria, also known as blue-green algae, are ancient organisms producing oxygen through photosynthesis. They inhabit a wide range of different environments, and are particularly known for the extensive and often toxic blooms in lakes during summer time. These blooms are not only ecologically unpleasant but have severe economic consequences, including contamination of drinking water and fish die-offs. Within their life cycle cyanobacteria use a number of proteins regulating their photosynthetic process. We have characterised a novel fusion protein 'CBS-CP12' composed of two individually functional photosynthetic regulators, cystathionine β-synthase and chloroplast protein. The fusion has led to an expansion of the regulatory function and may have contributed to the robust adaptation of the cyano-bacteria to different environments. Structural analysis of the novel protein revealed its unexpected hexameric assembly.

Plants, algae and cyanobacteria are oxygenic photosynthetic organisms capable of using sunlight to convert carbon dioxide into organic carbon (CO_2 fixation) while producing oxygen. Both pathways are regulated with the involvement of Trx (thioredoxin), the small, intrinsically disordered CP12 (Calvin cycle) and CBSX (cystathionine β-synthase) proteins [1]. Cyanobacteria are distinctive among photosynthetic organisms in containing genes encoding fusion proteins, CP12 and CBS [2]. These CBS-CP12 proteins often occur in the immediate vicinity of TrxA encoding genes frequently found in cyanobacteria exposed to harsh environmental conditions, such as *Microcystis aeruginosa* forming the most common toxic blooms in freshwater (Fig. 1). Neither structure nor function of any of these cyanobacterial CBS-CP12 proteins was known previously.



Figure 1

Cyanobacterial bloom in the freshwater lake Wannsee in the southwestern Berlin borough of Steglitz-Zehlendorf (Germany) in summer 2013. (Credit: E. Dittmann)

CP12 is an intrinsically disordered protein and its structural information is scarce and limited to only about 20 C-terminal residues [3]. By contrast, CBS domains from many organisms have been structurally characterised and, with one exception, they occur in pairs further assembling in homodimers, thus containing a total of four CBS domains [4]. Stand-alone CP12 proteins are major players in the regulation of CO_2 fixation in oxygenic photosynthetic organisms. They regulate two enzymes of the CO_2 fixation pathway, PRK (phosphoribulokinase) and GAPDH (glyceraldehyde-3-phosphate dehydrogenase) by forming a complex that inactivates both enzymes during the night, and thus the CO_2 fixation. This complex formation, in turn, is regulated by photosynthetic thioredoxins: triggered by sunlight and the consequential activation of photosynthetic electron transport, thioredoxins reduce a variety of different target proteins, including CP12. This causes the PRK-CP12-GAPDH complex to dissociate, activating the two enzymes and CO_2 fixation. In plants, the Trx-mediated regulation of photosynthesis is further stimulated by CBSX proteins bound to AMP (adenosine monophosphate), a molecule signalling the cellular energy status [1].

We crystallised CBS-CP12 and soaked an ytterbium complex into the crystals to solve the crystal structure. X-ray crystallographic data were collected at 100 K at the PETRA III beamline P13 (EMBL-Hamburg/DESY). The derivative structure was solved using the Crank2 pipeline (https://ccp4serv7.rc-harwell.ac.uk/ccp4online). All models in regions visible in the electron density were refined with Refmac [5] in the CCP4-suite [6] iterated with solvent adjustment as implemented in ARP/wARP (www.embl-hamburg.de/ARP).

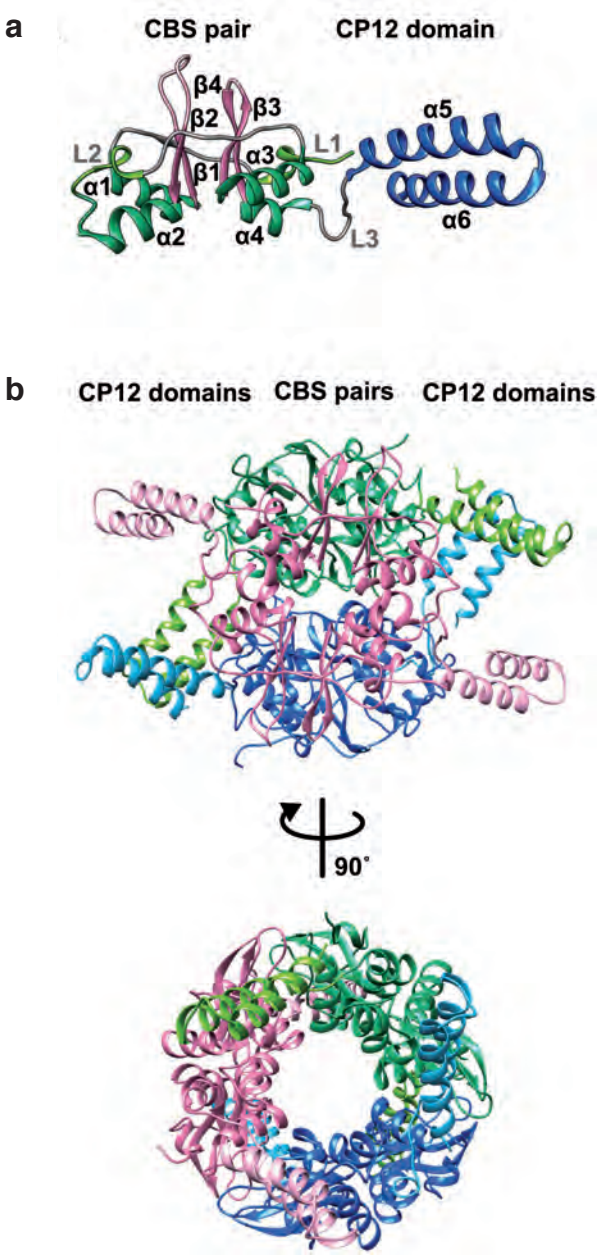


Figure 2

a) Cartoon representation of the monomeric CBS-CP12 subunit. The helices in the CBS domain are coloured yellow-green (linkers L1 and L2) and green, and the sheets are coloured pink. The helices in the CP12 domain are coloured blue. The secondary structural elements are sequentially labelled. b) Cartoon representation of hexameric CBS-CP12 in two different orientations related by a 90° rotation around a vertical axis. The canonical dimers are coloured pink, blue, and green, respectively. The respective CP12 domains are coloured light pink, light blue, and yellow-green, respectively.

The structural analysis of the CBS-CP12 fusion protein from *Microcystis aeruginosa* resulted in two important observations: the previously structurally uncharacterised N-terminal part of CP12 was ordered in CBS-CP12 (Fig. 2a) and the biological assembly of CBS-CP12 was a hexamer (Fig. 2b). The interface formed between the CBS pairs and the CP12 domains of adjacent subunits shows a prominent shape complementarity stabilising the CP12 domain (Fig. 2b). Moreover, the CP12 domain is essential for the hexamerisation and for the transfer of the AMP signal to the target proteins. Functional studies revealed that CBS-CP12 acts differently from its ancestral proteins.

Our results demonstrate that the novel domain architecture and the oligomeric state of the fusion protein CBS-CP12 expand its regulatory function in cyanobacteria beyond those of standalone CP12. The fusion protein acts as a redox- and AMP-dependent inhibitor and an antagonist of TrxA, counteracting the redox regulation of photosynthesis when the energy level of the cell is low.

The novel properties provide an additional layer in the regulation of photosynthesis in cyanobacteria that form densely populated communities with pronounced gradients of light, such as *Microcystis aeruginosa* blooms. We note that the CP12 domain is essential for hexamerisation as well as for the transfer of the AMP signal to the target proteins.

Author contact:
Claudia Hackenberg, hackenbergclaudia@gmail.com,
Elke Dittmann, editt@uni-potsdam.de,
Victor S. Lamzin, victor@embl-hamburg.de

References

1. K. S. Yoo, S. H. Ok, B.-C. Jeong, K. W. Jung, M. H. Cui, S. Hyoung, M.-R. Lee, H. K. Song and J. S. Shin, 'Single cystathionine β-synthase domain-containing proteins modulate development by regulating the thioredoxin system in Arabidopsis', Plant Cell 23, 3577–3594 (2011).
2. D. N. Stanley, C. A. Raines and C. A. Kerfeld, 'Comparative analysis of 126 cyanobacterial genomes reveals evidence of functional diversity among homologs of the redox-regulated CP12 protein', Plant Physiol. 161, 824–835 (2013).
3. H. Matsumura, A. Kai, T. Maeda, M. Tamoi, A. Satoh, H. Tamura, M. Hirose, T. Ozawa, N. Kizo, A. Wadano, T. Inoue and S. Shigoeka, 'Structure basis for the regulation of glyceraldehyde-3-phosphate dehydrogenase activity via the intrinsically disordered protein CP12', Structure 19, 1846–1854 (2011).
4. J. Ereño-Orbea, I. Oyenarte and L. A. Martínez-Cruz, 'CBS domains: Ligand binding sites and conformational variability', Arch. Biochem. Biophys. 540, 70–81 (2013).
5. G. N. Murshudov, A. A.Vagin and E. J. Dodson, 'Refinement of Macromolecular Structures by the Maximum-Likelihood method', Acta Cryst. D 53, 240–255 (1997).
6. M. D. Winn, C. C. Ballard, K. D. Cowtan, E. J. Dodson, P. Emsley, P. R. Evans, R. M. Keegan, E. B. Krissinel, A. G. Leslie, A. McCoy, S. J. McNicholas, G. N. Murshudov, N. S. Pannu, E. A. Potterton, H. R. Powell, R. J. Read, A.Vagin, K .S. Wilson, 'Overview of the CCP4 suite and current developments', Acta. Cryst. D 67, 235–242 (2011).

Original publication

'Structural and functional insights into the unique CBS-CP12 fusion protein family in cyanobacteria', Proc. Natl. Acad. Sci. U. S. A. 115, 7141-7146 (2018).
DOI: 10.1073/pnas.1806668115

Claudia Hackenberg[1], Johanna Hakanpää[1], Fei Cai[2], Svetlana Antonyuk[3], Caroline Eigner[1], Sven Meissner[4], Mikko Laitaoja[5], Janne Jänis[5], Cheryl A. Kerfeld[2,6,7], Elke Dittmann[4] and Victor S. Lamzin[1]

1. European Molecular Biology Laboratory (EMBL) at Deutsches Elektronen-Synchrotron (DESY), Hamburg, Germany
2. Molecular Biophysics and Integrated Bioimaging Division, Lawrence Berkeley National Laboratory, Berkeley, USA
3. Institute of Integrative Biology, Faculty of Health and Life Sciences, University of Liverpool, Liverpool, United Kingdom
4. Department of Microbiology, Institute for Biochemistry and Biology, University of Potsdam, Potsdam-Golm, Germany
5. Department of Chemistry, University of Eastern Finland, Joensuu, Finland
6. Michigan State University, Plant Research Laboratory, Michigan State University, East Lansing, Michigan, USA
7. Department of Biochemistry and Molecular Biology, Michigan State University, East Lansing, Michigan, USA

From water to plasma in femtoseconds

Extreme heating using X-rays

The conventional way of heating water, for example by boiling, is to transfer heat by adding kinetic energy to molecules, either by convection or excitation from thermal radiation. A different ultrafast pathway to heating, where the energy is deposited through ionisation, can be initiated by X-ray pulses from a free-electron laser. When tightly focused the intensity of such pulses is enough to cause severe ionisation, leading to exotic warm dense states of matter. We used single X-ray pulses as short as 25 fs and with fluences of 1.35 × 10^6 J/cm^2 to ionise a jet of water and bring it to a temperature above 100 000 K, thus achieving a heating rate above 10^{18} K/s. X-ray scattering from this ionic state of water shows a different structure compared to the neutral liquid state.

In Serial Femtosecond Crystallography (SFX) experiments, protein microcrystals are often transported to the X-ray free-electron laser (XFEL) pulse using a water jet. As a consequence, the diffraction signal from the crystals is always accompanied by a background scattering signal from water. The idea of the present project was born from the discussion if one could use this scattered water signal, that crystallographers normally struggle to get rid of, to measure the heating in the sample caused by the XFEL pulse. Since this signal is always present, it would be quite beneficial if it could tell us something about the dynamics in the sample during X-ray exposure. When exposed to the high intensity pulses from an XFEL, the difference between the dynamics in the water jet and the actual protein can be assumed to be small – meaning that if we could understand what happens in water on such short timescales, it would also tell us what happens in the protein.

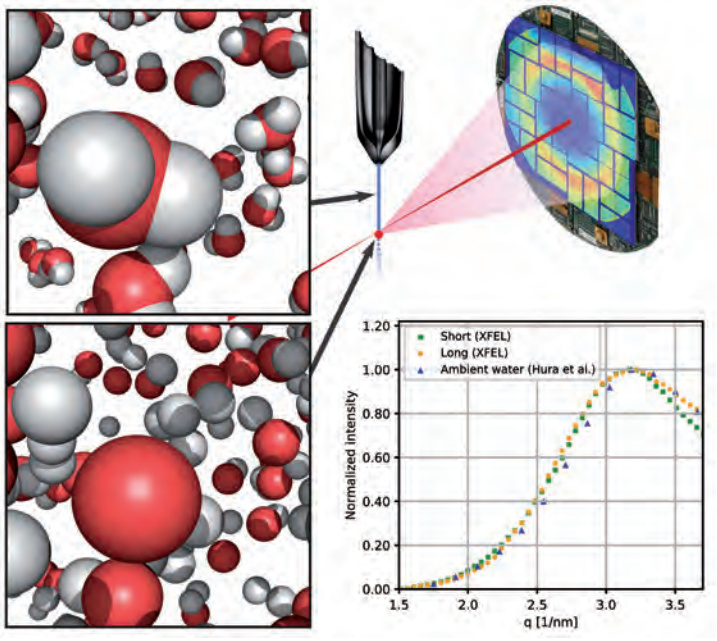


Figure 1

Schematic experimental setup. The water jet is intersected by X-ray pulses (red), which are scattered onto the detector as the characteristic 'water ring'. The graph shows the angularly integrated signal for the two different experiments, the 25 fs pulse duration (short) and the 75 fs pulse duration (long) compared to ambient water [4]. During XFEL exposure the oxygens in the water molecules will reach a charge state of +6, the temperature will be 160 000 K, and the oxygen-hydrogen bonds will break, illustrated in the bottom left panel.

To collect diffraction signal from a pure water jet, we used the SFX experimental setup shown in Fig. 1 and XFEL pulses from the Linac Coherent Light Source (LCLS in the U.S.) with a fluence of 1.35 × 10^6 J/cm^2 at two different pulse durations, 25 fs and 75 fs. The findings in the water data were quite astonishing. The scattered signal did not change the way one would naively expect, and we soon realised that using water as a simple 'thermometer' in SFX experiments to indicate the temperature of the sample is probably not feasible. To understand our observations we used a combination of two simulation tools to theoretically describe the dynamics in the water.

To simulate the interaction between the X-ray pulse and the sample, we used an approach well established in the high energy density community, namely non-local thermal equilibrium (NLTE) simulations [1]. We have shown in earlier studies that this code can describe the ionisation and heating during XFEL experiments [2]. However, to be able to compare the simulations to experimental data, i.e. the diffraction signal from the water jet, the structural dynamics of the individual atoms during interaction with the X-ray pulse need to be simulated explicitly. The NLTE approach itself cannot achieve

this, and we have therefore combined it with a molecular dynamics (MD) toolbox, as implemented in GROMACS [3]. The ionisation and heating rates from the NLTE simulations were then used as input for GROMACS MD simulations. This allowed us to calculate the expected diffraction signal as a function of time during the interaction of the X-ray pulse with the sample, as shown in Fig. 2, including the scattering from the new ionic state of water. Our simulated diffraction signal agreed quite well with the experimental data, indicating that our two step model was able to catch the ultrafast dynamics.

From the simulations one can learn several fascinating things about the transformation of liquid water into a plasma. In principle, two factors affect the water scattering signal: the ionisation (or loss of scattering power) of the scattering units and their structural dynamics. The NLTE simulations describe a phase transition from the liquid state to a plasma state, where the sample reaches an average ionisation of +6 per oxygen atom at the end of the X-ray exposure. It takes around 20-25 fs for the water structure to respond to the fast ionisation, as described by the temporal evolution of the radial distribution function in the sample, as shown in Fig. 2. For the exposure to the shorter X-ray pulse of 25 fs, most of the deviation in scattering intensity from a cold water sample is due to the ionisation, i.e. plasma formation. In the case of the longer 75 fs pulse, on the other hand, the system has more time to respond (although still ultrafast), and the change in the diffraction signal is caused both by the ionisation and by structural rearrangement.

This study shows that the scattering from water is varying when exposed to extreme intensities, even on time scales as short as 25 fs. This result is in itself important to highlight, as water is commonly present in SFX experiments at XFELs and is also routinely used for calibration measurements. Based on our simulations, we concluded that the observed changes in scattering intensity are attributed to non-thermal heating, and subsequent phase transition from the liquid to the plasma state. Substantial structural changes happen between 25 fs and 75 fs, which is a timescale commonly used in coherent X-ray diffractive imaging. This has implications for any structural determination experiment where water is used, and to any sample with similar density and ionisation cross section. On a fundamental level, this study shows that X-ray free-electron lasers can create and probe matter in conditions which are very difficult to find in the universe, even when heating samples as ubiquitous as water.

Author contact: Carl Caleman, carl.caleman@desy.de
Nicusor Timneanu, nicusor.timneanu@physics.uu.se
Olof Jönsson, olof.jonsson@biox.kth.se
Kenneth Beyerlein, kenneth.beyerlein@mpsd.mpg.de

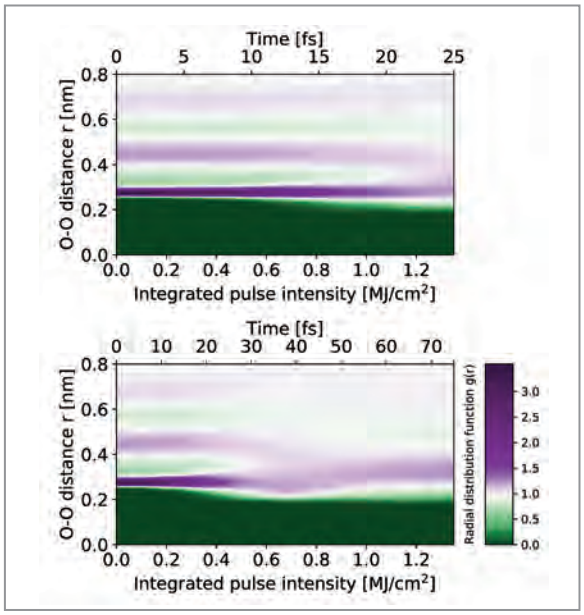


Figure 2

The simulated radial distribution function of oxygen pairs as a function of time in water undergoing ultrafast non-thermal heating. During the 25 fs pulse (top) the order is maintained almost throughout the pulse, whereas in the longer pulse with 75 fs duration (bottom) the ordering duration the ordering starts to disappear after around 20 fs, leading to significant changes in the radial distribution functions.

References

1. H. A. Scott, 'Cretin - a radiative transfer capability for laboratory plasma', J. Quant. Spectrosc. Radiat. Transf. 71, 687 (2001).
2. A. Barty et al., 'Self-termination diffraction gates femtosecond X-ray nanocrystallography measurements', Nat. Photon. 6, 35 (2012).
3. E. Lindahl, B. A. Hess and D. van der Spoel, 'GROMACS 3.0: A package for molecular simulation and trajectory analysis', J. Mol. Model. 7, 306 (2001).
4. G. Hura, J. M. Sorenson, R. M. Glaeser and T. Head-Gordon, 'A high-quality X-ray scattering experiment on liquid water at ambient conditions', J. Chem. Phys. 113, 9140 (2000)

Original publication

'Ultrafast nonthermal heating of water initiated by an X-ray Free-electron Laser', Proceedings of the National Academy of Science of the U. S. A. (2018).
DOI: 10.1073/pnas.1711220115

Kenneth R. Beyerlein[1], H. Olof Jönsson[2], Roberto Alonso-Mori[3], Andrew Aquila[3], Saša Bajt[4], Anton Barty[1], Richard Bean[1], Jason E. Koglin[3], Marc Messerschmidt[3], Davide Ragazzon[2], Dimosthenis Sokaras[3], Garth J. Williams[3], Stefan Hau-Riege[5], Sébastien Boutet[3], Henry N. Chapman[1,6,7], Nicuşor Tîmneanu[2,8] and Carl Caleman[1,2]

1. Center for Free-Electron Laser Science, Deutsches Elektronen-Synchrotron, Hamburg, Germany
2. Department of Physics and Astronomy, Uppsala University, Uppsala, Sweden
3. Linac Coherent Light Source, SLAC National Accelerator Laboratory, Menlo Park, USA
4. Deutsches Elektronen-Synchrotron DESY, Hamburg, Germany
5. Lawrence Livermore National Laboratory, Physics Division, Livermore, USA
6. Department of Physics, University of Hamburg, Hamburg, Germany
7. Centre for Ultrafast Imaging, University of Hamburg, Hamburg, Germany
8. Department of Cell and Molecular Biology, Uppsala University, Uppsala, Sweden

Superradiance of an ensemble of nuclei excited by a free-electron laser

Following the decay cascade of multiple excitations, photon by photon

In his seminal paper on 'Coherence in spontaneous radiation processes', Dicke laid the foundation for the concept of superradiance. One of his predictions was an accelerated initial decay of multiple excitations. Later work suggested that the emission of the total energy is also accelerated when the system approaches the inversion threshold. While this superradiant emission of the total energy is confirmed by numerous studies, the acceleration of the initial decay had not yet been observed. In our experiment we used a free-electron laser to excite the Mössbauer transition of ^{57}Fe nuclei, and followed the temporal decay of up to 68 simultaneous coherent excitations photon by photon. We observed the accelerated initial decay in agreement with Dicke's prediction. We further show that the results in the low excitation regime can be explained by using a simple statistical model.

Dicke's model [1] introduces superradiance as an accelerated initial decay of multiple atomic excitations, and provides exact predictions for the ensemble behaviour as a function of the number of atoms and the number of excitations in the system. It considers superradiant states emerging from incoherent excitation of a system of a size much smaller than the radiation wavelength, or created by coherent excitation of an extended system, and predicts an identical initial decay for both cases. More specifically, Dicke gave an explicit closed form expression for the accelerated decay of the first photon of the de-excitation cascade of a multiply excited system. The predicted behaviour of the initial decay differs qualitatively from the emission of the total energy, which exhibits a threshold [2]. In the low-excitation regime, the emission of the total energy follows a conventional single-photon decay. Approaching inversion conditions allows for an amplified spontaneous emission, and inverted systems can have an accelerated superradiant decay of the total energy.

In contrast, the accelerated initial decay appears without threshold and is even expected for a small number of excitations. The application of Dicke's formulation predicts a very large *N*-fold acceleration, even when the number of excitations is very small compared to the number of atoms in the system.

For our experiment we chose the Mössbauer isotope ^{57}Fe. The high transition energy of 14.41 keV and the long lifetime of 141 ns allowed us to follow the entire de-excitation cascade photon by photon. At the time of our experiment, the Japanese SPring-8 Angstrom Compact free-electron LAser (SACLA) was the only available source that could provide spatially and temporally coherent pulses to create multiple excitations at the high transition energy of the isotope ^{57}Fe. The decay of excited ^{57}Fe in a $FeBO_3$ crystal was detected in resonant diffraction from the pure nuclear (111) reflection [3] in order to be able to observe the coherent excitation of an extended

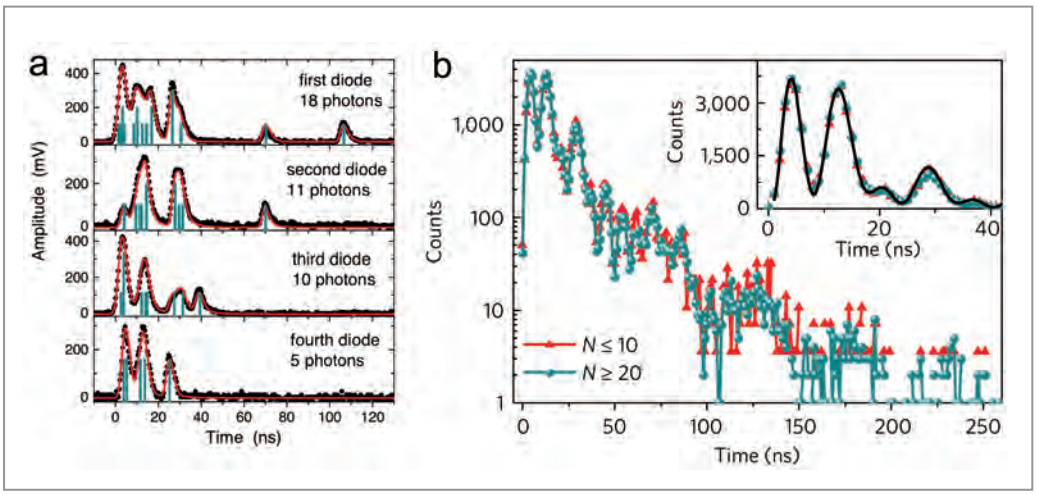


Figure 1

a) Timing the decay of a multi photon excitation with 44 events after a single X-ray pulse from a free-electron laser. The digitised response (black dots) from 4 avalanche photo diodes was fitted (red line) in order to de-convolute and time isolate (bars), multiple (close separated bars) and simultaneous (double and triple height bars) events. b) The decay of the total energy does not depend on the number of excitations. The spectra for $N \leq 10$ (red) and $N \geq 20$ (blue) are identical within statistics.

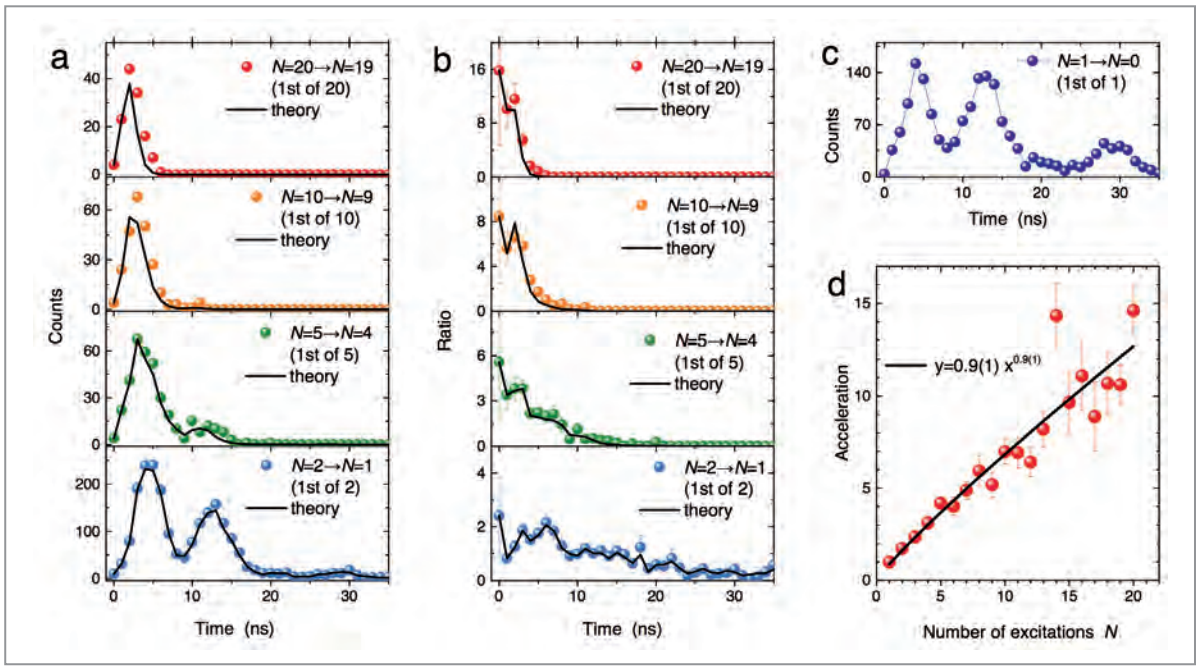


Figure 2

Accelerated initial decay: a) Decay of the first out of *N* excitations, b) decay of the first out of *N* excitations normalized by the single photon response, c) single photon response, d) acceleration of the initial decay as a function of the number of excitations.

system while supressing non resonant background on the detector. The diffracted beam was detected by a stack of 4 avalanche photodiode detectors with ~1 ns time resolution. The signal of the APDs was digitised with an oscilloscope and each trace was fitted iteratively with the instrumental function of the respective APD (Fig. 1 a). This allowed us to determine the time after excitation for each photon individually, sort the events according to the total excitation number, and to follow the de-excitation cascade photon by photon. A fit of the overall statistics of multi-photon events measured in the APDs confirms a coherent source with few modes.

Figure 1b shows a comparison of the decay of the total energy when only events with ≤ 10 or ≥ 20 photons are selected. The spectra are indistinguishable within the statistical accuracy. This shows that the decay of the total energy remains unaffected in our system far from inversion threshold. The complex modulations of the spectra are quantum beats resulting from interference of the decay from the nuclear levels split through magnetic hyperfine interactions. They can be fitted with great accuracy, as shown by the black line in the inset. Figure 2a shows the main result: if we construct spectra using only the first detected photon of the de-excitation cascade for different total excitation numbers *N*, the faster emission of this first photon becomes immediately apparent confirming the accelerated initial decay. For a quantitative evaluation in presence of quantum beats, Fig. 2b shows the same spectra normalised by the single photon response from Fig. 2c. The acceleration can then be evaluated from the intercept of the curves in Fig. 2b. In Fig. 2d this acceleration is plotted as a function of the number of excitations. A power law fit confirms the original prediction by Dicke within statistical accuracy: the *N*-fold acceleration for a total excitation number *N*.

We also considered the de-excitation cascade from the point of view of temporal sorting of sets of *N* statistically independent events: a calculation of the probability to detect the K^{th} out of *N* photons at time *t*, when *K*-1 photons were detected before, and *N-K* photons are detected later describes our data obtained in the low excitation regime equally well. This provides an alternative way to rationalize the data, and a simple necessary baseline to discuss further properties of superradiance within and beyond the low excitation regime.

Author contact: Cornelius Strohm, cornelius.strohm@desy.de
Aleksandr I. Chumakov, chumakov@esrf.fr
Alfred Q. R. Baron, baron@spring8.or.jp

References

1. R. H. Dicke, 'Coherence in spontaneous radiation processes', Phys. Rev 93, 99-110 (1954).
2. N. E. Rehler and J. H. Eberly, 'Superradiance', Phys. rev. A 3, 1735-1751 (1971).
3. G. V. Smirnov, V. V. Sklyarevskii, R. A. Voskanyan and A. M. Artem'ev, 'Nuclear diffraction of resonant γ-radiation by an antiferromagnetic crystal', JETP Lett. 9, 70-74 (1969).

Original publication

'Superradiance of an ensemble of nuclei excited by a free electron laser', Nature Physics 14, 261–264 (2018). DOI: 10.1038/s41567-017-0001-z

Alexandr I. Chumakov[1,2], Alfred Q. R. Baron[3], Ilya Sergueev[4], Cornelius Strohm[4], Olaf Leupold[4], Yuri Shvyd'ko[5], Gennadi V. Smirnov[2], Rudolf Rüffer[1], Yuichi Inubushi[6], Makina Yabashi[3], Kensuke Tono[6], Togo Kudo[3] and Tetsuya Ishikawa[3]

1. ESRF - The European Synchrotron, Grenoble, France
2. National Research Centre Kurchatov Institute, Moscow, Russia
3. RIKEN SPring-8 Center, Hyogo, Japan
4. Deutsches Elektronen-Synchrotron DESY, Hamburg, Germany
5. Advanced Photon Source, Argonne National Laboratory, Argonne, IL, USA
6. Japan Synchrotron Radiation Research Institute, Hyogo, Japan

Cool chemistry with spatially separated molecular species

From nuclear-spin-isomer-specific chemical reactivities to model peptides

Molecules are the entities defining the world around us, the building blocks of chemistry and biology. Everybody knows what a molecule is, but it's far from trivial to define exactly what is a 'molecule'. Partly this is related to the wide variety, for instance, of sizes from a small water molecule to a complex biomolecular machine such as the ribosome. One of the important details is that molecules undergo chemical reactions and that the same molecule reacts the same way. Here, we present an experimental demonstration of how even different forms of isolated water species exhibit distinct chemical reactivities and how these studies could be extended to complex biological macromolecules.

Unravelling, and eventually controlling, chemical reactivity and dynamics is at the heart of modern molecular sciences. One approach to this is to follow specific chemical reactions of isolated and well-defined reactants in real time through so-called molecular movies. However, while there has been tremendous success in the determination of atomic-resolution molecular structures through both, spectroscopic and imaging techniques, and the recording of molecular and chemical dynamics in real time, it remains elusive to watch molecular dynamics during a general bimolecular reaction with atomic resolution. Furthermore, the preparation of well-defined reactant samples with all species following the same reaction path is a challenge in itself.

Over the last decade, we have made significant progress in the preparation of well-defined samples of individual molecules through spatial separation of species using the electric deflector. Originally demonstrated for the separation of otherwise chemically inseparable structural isomers, so-called conformers [1], we have meanwhile extended this technique to the separation of individual quantum states of small molecules, the general applicability for the separation of structural isomers, and even the production of well-defined molecular aggregates, so-called clusters, of well-defined size and shape [2]. As demonstrated in the present contribution, this approach can even be combined with soft-vaporisation schemes for the production of spatially isolated samples of individual folding structures of complex biomolecules. In Fig. 1, the separation by the electric deflector is depicted for the model peptide Ac-Phe-Cys-NH_2.

In order to examine specific bimolecular chemical reactivities of individual molecules, we combined these controlled beams with ultracold trapped ion clouds in a collaboration of the Center for Free-Electron Laser Science (CFEL) with the University of Basel [3]. Molecular ions can be stored in electric-radiofrequency Paul traps and sympathetically cooled by laser-cooled co-trapped atomic ions. It yields relatively dense

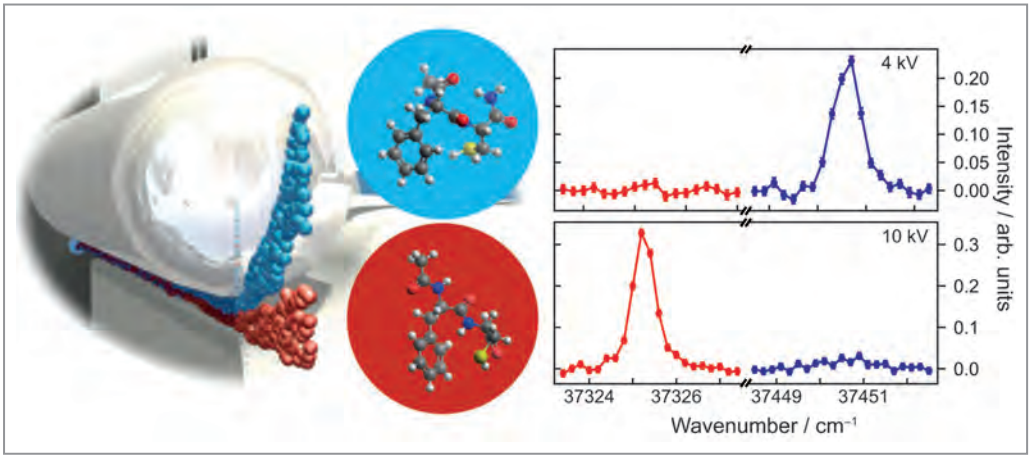


Figure 1

Separation of species by the electric deflector. Here, sketched for the spatial separation of the two conformational structural isomers of the model dipeptide Ac-Phe-Cys-NH_2, which are depicted by the ball-and-stick representations inside the large blue and red spheres. On the right electronic excitation spectra of the beams in the 'blue' and 'red' regions are shown, demonstrating the purity of the separated samples.

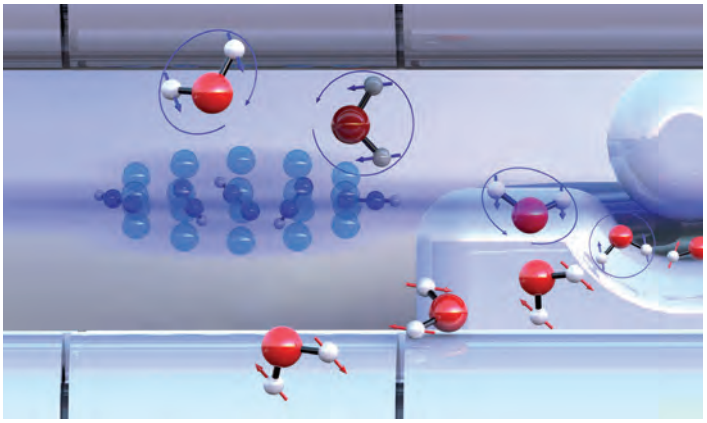


Figure 2

Artists rendering of the chemical-reaction arrangement. A species-selected beam of water emerges from the electric deflector on the right and the individual water isomers are directed at an ultracold cloud of NH_2^+ ions.

samples of ionic molecular reactants that can be essentially counted one by one based on the fluorescence from the co-trapped atomic ions and trap dynamics, enabling precision studies of even rare reaction events [3].

Here, we set out to investigate most intricate details of chemical reactions, namely the influence of nuclear spins on chemistry. We chose to investigate the astrochemically relevant proton transfer reaction from N_2H^+ ions to water molecules, forming H_3O^+ and nitrogen gas. N_2H^+ was produced inside the ion trap by ionising N_2 gas with a short-pulse laser and subsequent reaction with leaked-in hydrogen gas. The molecular ions were co-trapped with laser-cooled atomic Ca^+ ions, which slowed down the motion of the N_2H^+ ions via sympathetic cooling, to form an overall ion crystal, as depicted on the left side of Fig. 2. The second reactant, neutral water molecules, was provided in a cold molecular beam. We spatially separated water into its two forms [4], the two nuclear-spin isomers *para*- and *ortho*-water corresponding to distinct water molecules with overall nuclear spins of $I = 0$ and $I = 1$, respectively, which do not interconvert on any practically relevant timescales. Streams of these individual molecular species were then directed into the trapped ion cloud.

Carefully performing the reaction experiment and analysing the intricate details, we could unravel the differences in the reaction dynamics of the two water species and we observed that in the studied chemical reaction *para*-water reacts 25 % faster than *ortho*-water. This demonstrates that water (H_2O) is actually a mixture of two chemically distinct molecular species, *para*- and *ortho*-water — coming back to the original problem of a clear definition of the exact 'molecule' [2].

The reactivity results can be rationalised through the symmetrisation postulate of quantum mechanics, which dictates that the different nuclear-spin states correspond to distinct rovibronic states. Under the conditions of our very cold molecular beam, all molecules reside in the lowest rotational, vibrational, and electronic (vibronic) state. For *para*-water molecules this is the $J = 0$ rotational state of the vibronic ground state, whereas it is the $J = 1$ state for *ortho*-water. Now, when the water molecules in the beam approach an ion close enough to collide and react with, they are re-oriented in the electric field of the ion, resulting in a strong charge-dipole interaction, orientation of the water dipole moment toward the ion, and a correspondingly strong attraction between the two reaction partners. However, this re-orientation of water molecules is larger for *para*- than for *ortho*-water states. The quantitative agreement of a simple rotational-dynamics model employed in our original work provides a direct quantitative explanation, in terms of the generated pendular states and centrifugal barriers, of the underlying reaction process.

Based on the described experiments and the detailed analysis of species-specific reactivities for distinct water species and the demonstrated separation of folding structures of model peptides — combining the experimental approaches shown in Fig. 1 and Fig. 2 — the challenge of investigating the dependence of biological function on details of secondary structure seems to be experimentally feasible.

Author contact: Jochen Küpper, jochen.kuepper@cfel.de

References

1. F. Filsinger, U. Erlekam, G. von Helden, J. Küpper and G. Meijer, 'Selector for Structural Isomers of Neutral Molecules', Phys. Rev. Lett. 100, 133003 (2008).
2. Y.-P. Chang, D. A. Horke, S. Trippel and J. Küpper, 'Spatially-controlled complex molecules and their applications', Int. Rev. Phys. Chem. 34, 557–590 (2015).
3. S. Willitsch, 'Chemistry with Controlled Ions', Adv. Chem. Phys. 162, 307–340 (2017).
4. D. A. Horke, Y.-P. Chang, K. Długołęcki and J. Küpper, Angew. Chem. Int. Ed. 53, 11965–11968 (2014).

Original publications

'Observation of different reactivities of para and ortho-water towards trapped diazenylium ions', Nature Communications 9, 2096 (2018). DOI: 10.1038/s41467-018-044 83-3
'Spatially Separating the Conformers of a Dipeptide', Angew. Chem. Int. Ed. 4, 49 (2018). DOI: 10.1002/anie.201807646

Ardita Kilaj[1], Hong Gao[1], Daniel Rösch[1], Uxia Rivero[1], Stefan Willitsch[1], Nicole Teschmit[2,3,4], Daniel Horke[2,3] and Jochen Küpper[2,3,4,5]

1. Department of Chemistry, University of Basel, Basel, Switzerland
2. Center for Free-Electron Laser Science, DESY, Hamburg, Germany
3. Center for Ultrafast Imaging, Universität Hamburg, Hamburg, Germany
4. Department of Chemistry, Universität Hamburg, Hamburg, Germany
5. Department of Physics, Universität Hamburg, Hamburg, Germany

Visualising electron correlation

Imaging electronic wave functions of molecules in the gas phase

Photoelectron spectroscopy is an important tool to investigate the microscopic quantum properties of bound electronic states. In our present work we show in a proof-of-principle experiment that electronic wave functions of molecules in the gas phase are accessible by modern coincidence experiments and, furthermore, even many-body effects can be directly visualised.

Photoelectron emission is one of the most powerful tools to study the wave functions of bound electrons. For the condensed phase, i.e., when investigating solids, this concept is well established and band structure imaging by so-called ARPES (angle resolved photoelectron spectroscopy) has become an extensive field of fundamental research. The technique relies on the fact that the parallel component of bound electron momenta is conserved upon transmission through a flat surface, thus the photoelectric effect projects the momentum space wave function of the bound electron, devoid of distortions, into the continuum, where it can be measured. Such wave function imaging faces two major obstacles when single molecules in the gas phase are subject to investigations. Firstly, the molecules are randomly oriented in the laboratory frame. Only an averaged image integrated over all molecular orientations can be obtained, which does not provide meaningful information on the bound state. Secondly, the photoelectron is in most cases scattered by the non-isotropic potential of the molecule. While the effect of scattering is of interest in some experiments, it prohibits a direct access to the initial state wave function as well. A further challenge, which is common to gas and solid phases, is that the electronic wave function is often strongly correlated, i.e., the momentum distribution of one electron depends on the momenta of all the others. Thus if one measures the momentum distribution of only one electron while integrating over the others, many important effects are lost.

Recently, we employed a novel approach to overcome the obstacles mentioned above and to measure electron correlation directly. Almost for three decades, photoelectron angular emission patterns in the molecular frame have been accessible experimentally by measuring the emitted electron and the ionic fragments in coincidence. In cases, where the ionised molecule breaks up rapidly, the spatial orientation of the molecule can be deduced from the emission direction of the fragments [1]. For example, a simple diatomic molecule will always fragment along the initial molecular bond and thus the spatial orientation can be determined by measuring the fragments' emission direction. By additionally measuring the electron emission direction, the emission angle with respect to the molecular axis is obtained from the experimental data. The second hurdle, the scattering at the molecular potential, can be overcome by increasing the photoelectron kinetic

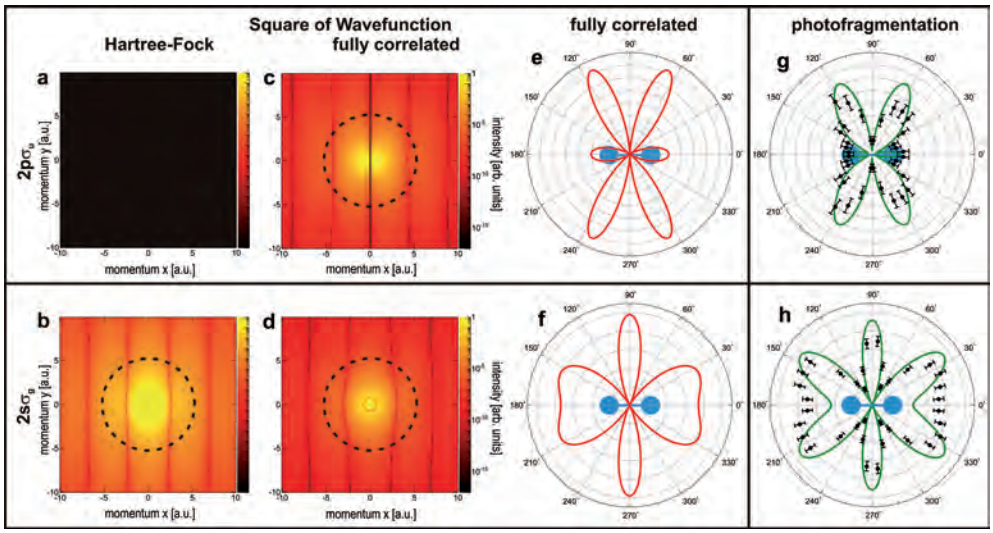
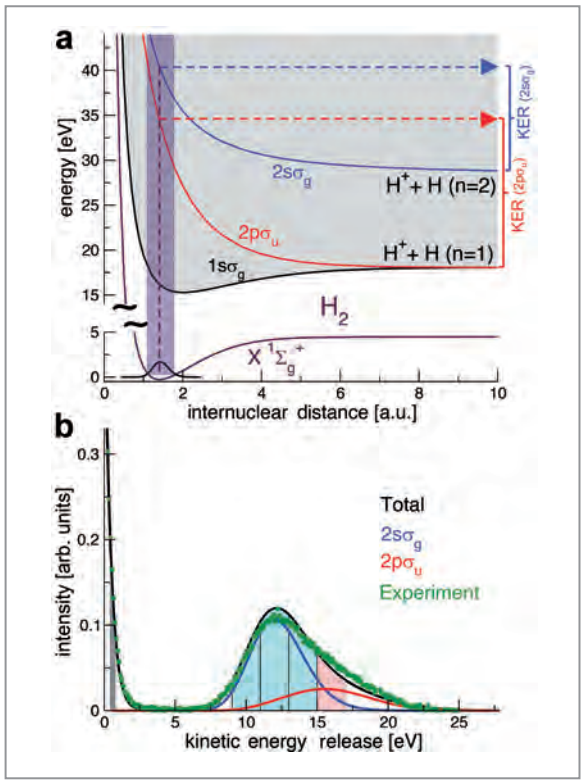


Figure 1

Correlation imaging of the H_2 two-electron wave function. (a)–(d) Momentum distributions of the emitted electron; (a), (b) uncorrelated Hartree-Fock wave function; (c), (d) fully correlated wave function. The different quantum states of the bound electron are $2p\sigma_u$ in the upper panel and $2s\sigma_g$ in the lower panel. Circular lines show $|\mathbf{k}|$ = 5.3 a.u. in (c) and $|\mathbf{k}|$ = 5.2 a.u. in (b) and (d), which correspond to ionisation by a photon of 400 eV energy. (e), (f) ground state wave function. (g), (h) Experimental and theoretical molecular frame photoelectron angular distributions.

Figure 2

Correlation diagram and kinetic energy distribution for dissociation of H_2^+. (a) Potential energy curves for the ground state of H_2 and the $1s\sigma_g$, $2s\sigma_g$, and $2p\sigma_u$ ionisation thresholds. (b) Distribution of the kinetic energy release obtained after single-photon ionisation of H_2 employing photons of 400 eV.



energy. At high kinetic energies, within the so-called Born regime, the emitted photoelectron is in good approximation described as a plane wave and it is indeed possible to observe the momentum distribution of the electron in the bound molecular state, as we have demonstrated as a proof-of-principle experiment in the present study. The experiment was carried out at beamline P04 of the PETRA III synchrotron light source by making use of the COLTRIMS (Cold Target Recoil Ion Momentum Spectroscopy) technique [2]. The sensitivity of this method is sufficiently high, so that the data directly show that the two electrons in hydrogen are not independent. The true hydrogen wave function entails correlations between the two electrons. This becomes directly visible as we image the electron momentum distribution of the emitted electron and simultaneously the quantum state of the second electron remaining bound inside the fragmenting molecule.

Figure 1 shows correlation imaging of the H_2 two-electron wave function. The theoretical predictions are shown as the square of the wave function of the emitted electron in momentum space (a,b) within the Hartree-Fock approximation (no correlation), (c,d) within the fully correlated approach, and (e,f) polar plots of the ground state wave function. While the lower row shows these distributions for the case of the second electron remaining in the ground state of the ionised molecule ($2s\sigma_g$), the upper row reveals the properties of the initially bound electron for cases where the second electron is in a distinct excited state as the molecule fragments ($2p\sigma_u$). Notable differences between both cases are the non-accessibility of the purely correlated $2p\sigma_u$ case in the Hartree-Fock approximation (empty black in Fig. 1a) and the interchange of the position of maxima and minima in the angular distributions which is due to the difference in parity of the state of the electron bound to the molecule. The theoretical work of the fully correlated wave functions was performed by Fernando Martín *et al.* (see also [3–5]). Good agreement between theory and experiment on the molecular frame photoelectron angular distributions in Fig. 1(g,h) has been achieved.

Figure 2 shows the correlation diagram and kinetic energy distribution. The upper panel illustrates the potential energy curves for the ground state of H_2 and the $1s\sigma_g$, $2s\sigma_g$, and $2p\sigma_u$ ionisation threshold corresponding to H_2^+. The violet shaded area represents the Franck-Condon region associated to the ground vibrational state of H_2. The lower panel shows the distribution of the kinetic energy release obtained after single-photon ionisation of H_2 employing photons of 400 eV. To identify the quantum state of the second electron, gates of the kinetic energy release can be used: the region of 9-15 eV mainly yields the $2s\sigma_g$ state, while the region of 15-17 eV mainly yields the $2p\sigma_u$ state.

While this experiment demonstrated a first use of this novel method, the next step will be to apply it to more complex molecules, like for example CO, N_2, or CF_4 or even to chiral molecules like methyloxirane.

Author contact: Florian Trinter, florian.trinter@desy.de
Till Jahnke, jahnke@atom.uni-frankfurt.de
Reinhard Dörner, doerner@atom.uni-frankfurt.de

References

1. M. Pitzer, M. Kunitski, A. S. Johnson, T. Jahnke, H. Sann, F. Sturm, L. Ph. H. Schmidt, H. Schmidt-Böcking, R. Dörner, J. Stohner, J. Kiedrowski, M. Reggelin, S. Marquardt, A. Schießer, R. Berger and M. S. Schöffler, 'Direct Determination of Absolute Molecular Stereochemistry in Gas Phase by Coulomb Explosion Imaging', Science 341, 1096–1100 (2013).
2. R. Dörner, V. Mergel, O. Jagutzki, L. Spielberger, J. Ullrich, R. Moshammer and H. Schmidt-Böcking, 'Cold Target Recoil Ion Momentum Spectroscopy: a 'momentum microscope' to view atomic collision dynamics', Phys. Rep. 330, 95–192 (2000).
3. F. Martín, 'Excitation of atomic hydrogen by protons and multicharged ions', J. Phys. B 32, 501–511 (1999).
4. A. Palacios, J. L. Sanz-Vicario and F. Martín, 'Theoretical methods for attosecond electron and nuclear dynamics: applications to the H_2 molecule', J. Phys. B 48, 242001 (2015).
5. F. Martín et al., 'Single photon-induced symmetry breaking of H_2 dissociation', Science 315, 629–633 (2007).

Original publication

'Imaging the square of the correlated two-electron wave function of a hydrogen molecule', Nature Communications 8, 2266 (2017). DOI: 10.1038/s41467-017-02437-9

Markus Waitz, Roger Y. Bello, Daniel Metz, Julian Lower, Florian Trinter, Carl Schober, Marco Keiling, Ute Lenz, Martin Pitzer, Karolin Mertens, Michael Martins, Jens Viefhaus, Stephan Klumpp, Thorsten Weber, Lothar Ph. H. Schmidt, Joshua B. Williams, Markus S. Schöffler, Vladislav V. Serov, Anatoli S. Kheifets, Luca Argenti, Alicia Palacios, Fernando Martín, Till Jahnke and Reinhard Dörner

Affiliation details at
https://www.nature.com/articles/s41467-017-02437-9

Molecule formation in the universe

Soft X-ray pump-probe experiment of the molecule formation dynamics in cold interstellar clouds

Photochemistry in molecular ices around grain particles in cold interstellar molecular clouds is a driving force for the formation of new, larger molecules. Soft X-ray pump-probe experiments open the door to reveal the dynamics behind reactions involved. In a first step photoreactions of water and methane are studied. The reactive formation of small cluster ions seems to be driven by collisions. The appearance of larger carbon cluster ions on a short timescale hints to the action of Coulombic forces both in the assembly and disassembly of these photoreaction products.

Interstellar molecular clouds are regions of active star formation in the universe and show a surprisingly rich chemistry with molecular species ranging from hydrogen to amino acids being formed. These cold clouds with temperatures in the range of 10 to 15 K typically appear as dark regions against background illumination, because visible and ultraviolet light cannot penetrate. This absorption, not caused by the high density of atoms and molecules, is due to the enormous size of the clouds which can extend up to several light years across. In fact, the density in the clouds—although several orders of magnitude higher than outside—is so low that the formation of the simplest molecule, H_2, cannot take place in the gas phase, because of the absence of three-body collisions that would enable the stabilization of the molecular product. Instead, current knowledge in astrochemistry suggests that new molecules are formed in or on top of molecular ice layers which form on small carbonaceous or silicate grain particles [1, 2]. Besides hydrogen, the most abundant small molecules are water, carbon monoxide, and carbon dioxide. Trace amounts of other simple molecules such as methanol, methane, ammonia, and many others contribute to the inventory of the interstellar medium.

The interaction of light with grains in cold clouds can only occur at the rim of a molecular cloud, in so-called photon dominated regions. The cloud can, however, be penetrated by cosmic rays which predominantly consist of protons. Their interaction with ice-covered grain particles occurs impact-like and thus bears a resemblance to irradiation with high-energy photons. Furthermore, the cosmic ray interaction with the cold gas creates VUV and XUV fluorescence within the cloud [3, 4], which in turn may induce photochemical reactions on the ice-covered grains. We have studied the photochemistry of ice driven by the interaction of mixed interstellar ice analogues with soft X-rays from FLASH.

We prepared mixed methane/deuterated water ices on a graphite substrate by calibrated dosing of the surface simultaneously with both gases. The coverages amount to about 6 and 11 monolayers, respectively. The irradiation with FLASH pulses ($h\nu$ = 40.8 eV) at an energy of 30 µJ (~35 mJ/cm^2) causes the desorption of fragment ions, ionic reaction products, and neutral molecules. The directly generated molecular ions were detected by a time-of-flight mass spectrometer.

Figure 1 shows the observed mass spectrum. Besides ionised hydrogen the mass spectrum is dominated by a series of peaks which are separated by approximately 12 mass units, denoted by red numbers. In addition, the two insets show with black numbers mass peaks associated with directly ionised small molecules and fragments. These small fragments

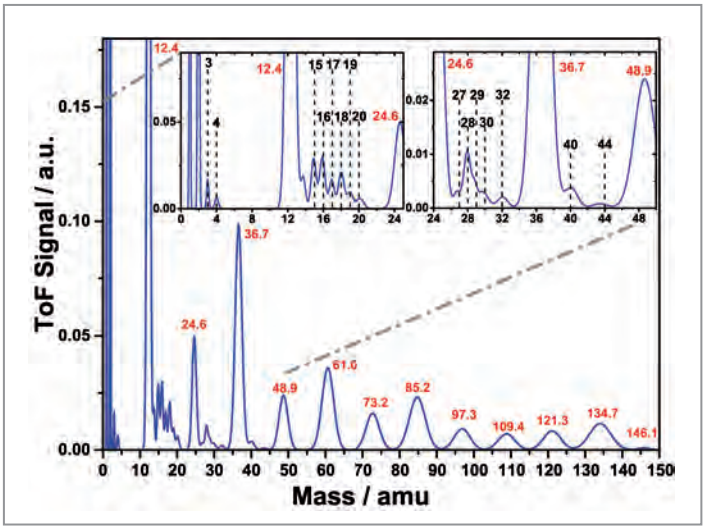


Figure 1

Time-of-flight mass spectrum of ionic species desorbing from a mixed CH_4:D_2O ice exposed to 40.8 eV photons. The peaks labelled with red masses correspond to C_n^+ cluster ions while those labelled in black correspond to ionic fragments from the parent species and new species formed in the ice as a result of photon irradiation.

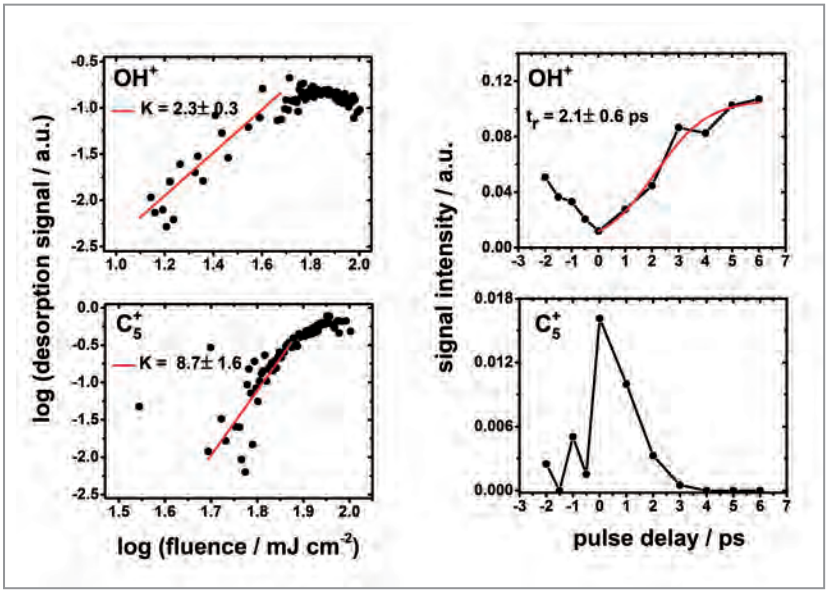


Figure 2

Power dependence (left) and two-pulse correlation signals (right) for XUV pump / XUV probe desorption of small and cluster ions from a mixed CH_4:D_2O ice irradiated with 40.8 eV photons. The strongly contrasting temporal dependencies of the desorption yield for carbon cluster ions and oxygen containing fragment ions is indicative of differing reaction dynamics.

originate in part directly from simple fragments of the ice constituents, representing CH_2^+, CH_3^+, and CH_4^+, and O^+, OD^+, and D_2O^+, respectively, for masses 14 to 20. The appearance of other small ions involves photochemical reactions within the icy layer, like HD^+, OH^+, and HDO^+. The group around mass 28 corresponds to photochemically produced ions of the C_2H_x family. Thus photo-induced reactions occur in these icy layers which lead to the build-up of larger molecules from simple products.

The most striking observation is the appearance of the group of mass peaks separated by about 12 amu, consistent with the desorption of carbon clusters, C_n^+, with n up to at least 12. The signal of these carbon ion clusters and the reactively formed products all show a non-linear dependence on the irradiation fluence, with a respective power exponent around K = 2 and 7 to 8 for small ions and clusters, as shown in Fig. 2. Such nonlinearity can be used for temporally correlated two-pulse desorption, in order to gain insight into the reaction mechanism [5].

Using the split-and-delay unit at FLASH1 we carried out such XUV pump-XUV probe measurements for delays between –2 ps and +6 ps for small ions and the family of carbon cluster ions. Figure 2 shows selected results which illustrate the contrasting dynamics. The reactively formed OH^+ shows a minimum when both pulses overlap in time, and increases to a plateau with a rise time of about 2.1 ps. This temporal behaviour is typical for all oxygen containing ions. The carbon cluster ions all show a peak at $\Delta t = 0$ which rapidly decreases within 1.2 ps (FWHM) to zero at times greater than 3 ps.

The analysis shows that the carbon cluster ions are formed by the instantaneous reaction of a large number of ionised methyl radicals, produced by the intense FEL pulse. Products involving D_2O required a longer reaction time, due to collisional interactions, in accordance with an earlier study using pure water ice [6]. A more extensive discussion which also illuminates the various reactive processes can be found in the original publication.

This study shows that photon-induced reactions in molecular ices on grain particles may play an important role for molecule formation in interstellar molecular clouds. That certainly holds for photon-dominated regions near the rim, but to some extent also inside the cloud. This experiment opens the way for a better understanding of the complex chemistry in cold molecular clouds.

Author contact: Helmut Zacharias, Zacharias@uni-muenster.de

References

1. E. Herbst and E. F. van Dishoeck, 'Complex Organic Interstellar Molecules', Ann. Rev. Astron. Astrophys. 47, 427–480 (2009).
2. E. F. van Dishoeck, E. Herbst and D. A. Neufeld, 'Interstellar water chemistry: from laboratory to observations', Chem. Rev. 113, 9043–9085 (2013).
3. S. S. Prasad and S. P. Tarafdar, 'UV radiation field inside dense clouds: its possible existence and chemical implications', Astrophys. J. 267, 603–609 (1983).
4. C. J. Shen, J. M. Greenberg, W. A. Schutte and E. F. van Dishoeck, 'Cosmic ray induced explosive desorption in dense clouds', Astron. Astrophys. 415, 203–215 (2004).
5. F. Budde, T. F. Heinz, M. M. T. Loy, J. A. Misewich, F. de Rougemont and H. Zacharias, 'Femtosecond time-resolved measurement of desorption', Phys. Rev. Lett. 66, 3024–3027 (1991).
6. B. Siemer, S. Roling, R. Frigge, T. Hoger, R. Mitzner and H. Zacharias, 'Free-electron laser induced processes in thin molecular ice', Faraday Discussions 168, 553–569 (2014).

Original publication

'XUV photodesorption of carbon cluster ions and ionic photofragments from a mixed methane-water ice', Phys. Chem. Chem. Phys. 20, 7457–7469 (2018).
DOI: 10.1039/c8cp00171e

Tushar Suhasaria[1], John D. Thrower[1], Robert Frigge[1], Sebastian Roling[1], Mathieu Bertin[2], Xavier Michaut[2], Jean-Hugue Fillion[2] and Helmut Zacharias[1,3]

1. Physikalisches Institut, Westfälische Wilhelms-Universität, Münster, Germany
2. Observatoire de Paris, Sorbonne Université, PSL Research University, Laboratoire d'Etudes du Rayonnement et de la Matière en Astrophysique et At mosphères, CNRS UMR 8112, Paris, France
3. Center for Soft Nanoscience, Westfälische Wilhelms-Universität, Münster, Germany

Quantum boiling and relativity

Ultra-intense hard X-rays boil atoms, revealing an interplay between relativistic and resonant effects on the atomic structure

Can you imagine boiling of atoms? Strong X-ray light can evaporate electrons from atoms in a process that is similar to the boiling of water. Quantum boiling of atoms by strong X-rays reveals in a new way the impact of Einstein's relativity on the quantum structure of atoms. Here we present a joint experimental and theoretical study of xenon atoms irradiated by unprecedentedly high-intensity hard X-rays. Our results show the importance of relativistic and resonant effects on multi-photon multiple ionisation of heavy atoms and demonstrate the predictive power of the theoretical model, which provides a basis for accurate modeling of radiation damage in X-ray free-electron laser experiments.

Quantum boiling evaporates electrons from an atom in a similar way conventional boiling evaporates water molecules (Fig. 1). The X-rays only knock out a small number of electrons directly, dislodging them from the inner shells. The holes left by the missing electrons quickly 'bubble up' towards the outer shells, transferring energy to other electrons, ultimately kicking them out of the atom, too. When boiling water, the collisions between molecules play a central role, and in analogy the collisions of electrons play the central role in quantum boiling of atoms. Producing the strongest ever X-ray flashes by an X-ray free-electron laser (XFEL) has made quantum boiling a reality, creating conditions corresponding to a temperature of a few hundred million degrees Celsius, higher than the temperature at the centre of the sun. Quantum boiling of atoms lays bare the atomic inner shells and, thus, makes the strong relativistic effects visible in a new way. The theory of quantum mechanics, together with the theory of special relativity, confirms the new experimental observation and explains the mechanism how to boil atoms.

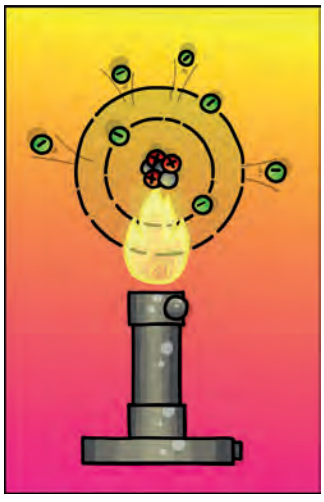


Figure 1
Quantum boiling evaporates electrons from an atom in a similar way conventional boiling evaporates water molecules. Illustration: Sherin Santra.

Technically, quantum boiling is referred to multi-photon multiple ionisation dynamics. We have developed a theoretical toolkit, XATOM [1, 2], that is able to describe such ionisation dynamics. Before, ionisation dynamics calculations were based on the non-relativistic electronic-structure theory. It is well-known, however, that the deep inner shell of heavy atoms is split due to relativistic spin-orbit coupling. In a previous experiment [3], it was speculated that the relativistic effects influence the ionisation dynamics of xenon in intense hard X-rays. In yet another previous experiment [4], it was shown that resonant excitations dramatically enhance X-ray multiple ionisation for xenon atoms exposed to intense X-ray pulses with broad energy bandwidths. However, the photon energies used in the latter were too low to ionise deep inner-shell electrons, so relativistic effects were marginal.

Recently, we extended the XATOM toolkit to include resonant transitions and relativistic energy corrections [5]. To simulate the multi-photon multiple ionisation dynamics, one needs to solve a set of coupled differential equations. For deep inner-shell ionisation dynamics of xenon atoms without any relativistic and resonant effects, the number of rate equations is about 20 million. When both effects are considered, the number approaches 10^{68}. This galactic number of coupled differential equations is dealt with using a Monte Carlo on-the-fly approach [3]. The computational task is extremely challenging and all the calculations for one xenon atom took several months on high-performance computers.

By using our computational tool, we are able to perform numerical experiments in various ways. We simply turn on and off resonant and relativistic effects in the calculations. We vary all X-ray parameters at will, such as photon energy and X-ray fluence. When the X-ray fluence is cranked up, striking effects emerge. Figure 2 shows calculated charge-

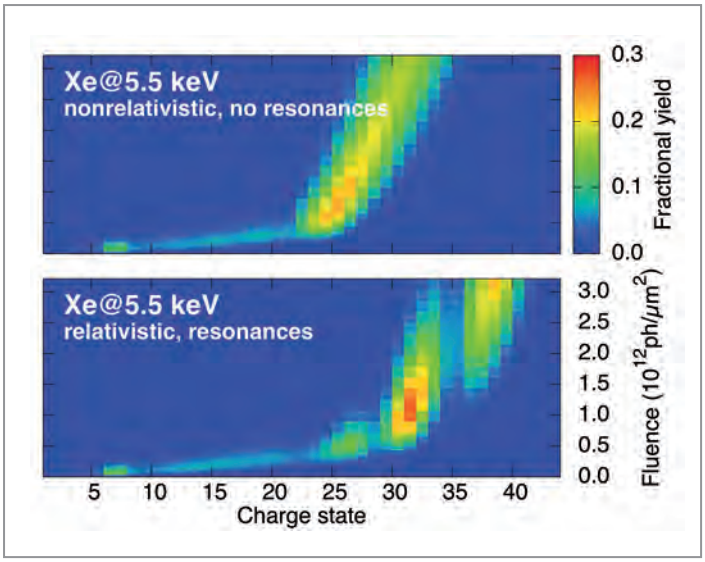


Figure 2

Calculated Xe charge state distribution at 5.5 keV as a function of X-ray fluence. The upper panel shows calculations without relativistic and resonant effects, while the lower panel shows calculations including both relativistic and resonant effects.

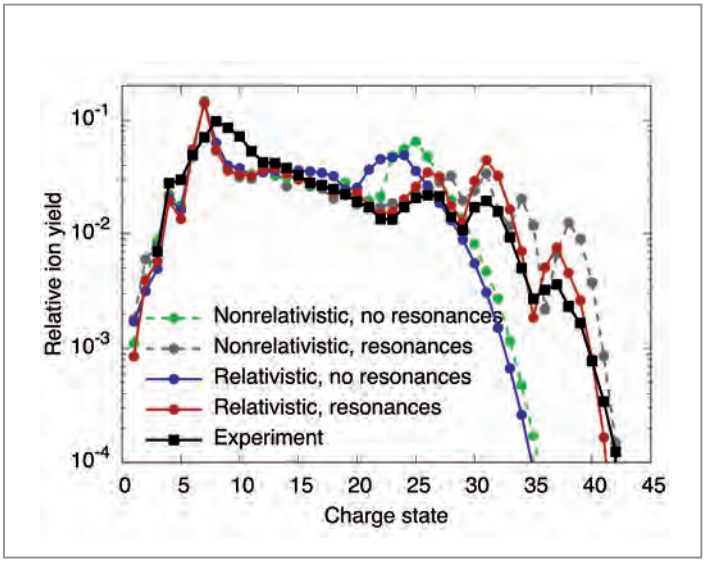


Figure 3

Experimental and calculated Xe charge state distributions at 5.5 keV. The calculations were carried out with and without consideration of relativistic effects and resonances. The calculation including relativistic effects and resonances (red) matches the experiment (black).

state distributions (CSDs) of Xe at 5.5 keV. The CSD is an output of the multiple ionisation dynamics, which is also measured in experiment. The upper panel exhibits CSD without resonant and relativistic effects. The bright yellow colour, indicating higher ion yields, rises up and moves towards higher charge states as the fluence increases. The bottom panel displays CSD with both resonant and relativistic effects. The CSD is not just shifted to the higher charge states, but also shows distinctive bumps in the charge states. Our calculations reveal that these bumps correspond to a relativistic splitting of the deep inner shell into certain distinct energy levels.

This unexpected appearance of structured CSDs was confirmed experimentally. In these studies, xenon atoms were exposed to ultra-intense XFEL pulses generated by LCLS at SLAC (U.S.). The X-ray peak intensity reached about 10^{20} W/cm^2, which is orders of magnitude higher than what was used in previous experiments. Figure 3 shows experimental (black) and theoretical CSDs taking into account all different fluence values present in the interaction volume. There are four different theoretical data sets, depending on whether resonant and relativistic effects are switched on or off in the simulation. Only one of them matches the experiment—when both resonant and relativistic effects are included (red). This fact clearly explains that the characteristic three bumps observed in experiment are signatures of the relativistic effects. This is the first observation of relativistic effects as fingerprints on the ion yield spectra.

Based on the good agreement, we are able to predict the degree of ionisation for heavy atoms after the interaction with intense hard X-rays for given X-ray parameters, which provides an important atomic benchmark in the formation of warm or hot dense matter and in the electronic radiation damage playing an important role in molecular imaging experiments. Therefore, not only do our results provide a successful description of quantum boiling and the accompanying manifestation of relativity, but they also demonstrate the predictive power of newly developed computational tools for future XFEL experiments.

Author contact: Sang-Kil Son, sangkil.son@cfel.de
Robin Santra, robin.santra@cfel.de

References

1. S.-K. Son, L. Young and R. Santra, 'Impact of hollow-atom formation on coherent x-ray scattering at high intensity', Phys. Rev. A 83, 033402 (2011).
2. Z. Jurek et al., 'XMDYN and XATOM: versatile simulation tools for quantitative modeling of X-ray free-electron laser induced dynamics of matter', J. Appl. Cryst. 49, 1048–1056 (2016).
3. H. Fukuzawa et al., 'Deep inner-shell multiphoton ionization by intense X-ray free-electron laser pulses', Phys. Rev. Lett. 110, 173005 (2013).
4. B. Rudek et al., 'Ultra-efficient ionization of heavy atoms by intense X-ray free-electron laser pulses', Nat. Photonics 6, 858–865 (2012).
5. K. Toyota, S.-K. Son and R. Santra, 'Interplay between relativistic energy corrections and resonant excitations in X-ray multiphoton ionization dynamics of Xe atoms', Phys. Rev. A 95, 043412 (2017).

Original publication

'Relativistic and resonant effects in the ionization of heavy atoms by ultra-intense hard X-rays', Nature Communications 9, 4200 (2018). DOI: 10.1038/s41467-018-06745-6

Benedikt Rudek, Koudai Toyota, Lutz Foucar, Benjamin Erk, Rebecca Boll, Cédric Bomme, Jonathan Correa, Sebastian Carron, Sébastien Boutet, Garth J. Williams, Ken R. Ferguson, Roberto Alonso-Mori, Jason E. Koglin, Tais Gorkhover, Maximilian Bucher, Carl Stefan Lehmann, Bertold Krässig, Stephen H. Southworth, Linda Young, Christoph Bostedt, Kiyoshi Ueda, Tatiana Marchenko, Marc Simon, Zoltan Jurek, Robin Santra, Artem Rudenko, Sang-Kil Son and Daniel Rolles

Affiliation details at
https://www.nature.com/articles/s41467-018-06745-6

A new window to probe electron-electron interactions

Direct double ionisation of F^- by a single photon

The common photo-effect involves removal of a single electron from an atom by a photon. With reduced probability, two or more electrons may also be simultaneously released by a single photon. This is due to the electron-electron interaction, commonly termed electron correlation that also provides the additional electron binding force in negative ions. Photo-multiple-ionisation experiments with negative ions permit electron correlation to be investigated at an unprecedented level of sensitivity. Similar experiments with singly or multiply charged positive ions along sequences of ions having the same number of electrons but different nuclear charge enable the relative strengths of electron-electron and electron-nucleus interactions to be 'tuned'. Such systematic studies open a new window to probe electron correlation in atoms and their interactions.

Direct multiple ionisation of atoms and atomic ions by a single photon is a fundamental many-body process. Distinct from inner-shell excitation or ionisation with subsequent relaxation by the release of so-called Auger electrons, direct photo-double-ionisation involves the absorption of a photon by an atom and the simultaneous release of two electrons. A theoretical mechanism to describe this process involves ejection of a photoelectron that, as it leaves, knocks off a second electron [1]. This is a direct manifestation of electron-electron interaction, providing a sensitive probe of electron correlation in atoms. This sensitivity is quadratically enhanced in photo-double-ionisation of negative ions, in which electron correlation also provides the binding force for the extra electron.

Photo-multiple-ionisation is of interest because of the fundamental importance and applications of this many-body process. International symposia on this topic have been held biennially for nearly four decades. The prototypical system for studying photo-double-ionisation is the helium atom, for which countless experimental and theoretical investigations have been performed [2]. Theoretical investigations have been extended to helium-like ions to study the competition between the Coulomb attraction of electrons to the nucleus and the interactions between electrons as the charge of the nucleus increases [3]. The importance of relativistic effects also increases with nuclear charge [4]. Although numerous theoretical calculations of direct multiple photo-ionisation of ions await experimental verification, previous measurements have been largely restricted to neutral atoms and molecules for technical reasons. Only a few indications of two-electron ejection from ions by one photon have been reported in lim-ited photon-energy ranges.

Using the PIPE facility at P04 at PETRA III, absolute cross sections $\sigma_{-1,1}$ for double and $\sigma_{-1,2}$ for triple ionisation of negatively charged fluorine ions were measured in the photon-energy range 660-1000 eV. The cross section is a measure of the likelihood for a process, representing an effective target area for the photon in units of megabarns: 1 Mb = 10^{-18} cm^2. Measured cross sections $\sigma_{-1,2}$ are displayed in Fig. 1, exhibiting two energy thresholds, the first near 681 eV marking the onset of direct single 1s (referred to as *K*-shell) ionisation with subsequent Auger emission of 2 electrons. The second threshold near 700 eV corresponds to direct simultaneous ionisation of a 1s and a 2p electron followed by single Auger-electron decay.

The cross section $\sigma_{-1,1}$ (not shown) is associated with direct single *K*-shell ionisation producing an intermediate $F(1s\,2s^2\,2p^6)$ atom which then decays to $F^+(1s^2\,2s^2\,2p^4)$ by a single-Auger decay. The maximum of $\sigma_{-1,1}$ is reached at the *K*-shell ionisation threshold energy with a magnitude of approximately 0.4 Mb. Since the cross section $\sigma_{-1,2}$ for triple ionisation has a contribution arising from single *K*-shell ionisation with subsequent double-Auger processes, the ratio $\sigma_{-1,2}$ / $\sigma_{-1,1}$ is expected to be constant at energies below the second threshold at 700 eV. The measured value of 0.153 is interpreted as the ratio of probabilities for double- versus single-Auger decay of the intermediate $F(1s\,2s^2\,2p^6)$ atom. Accordingly, the cross section $\sigma_{-1,1}$ scaled by a factor 0.153 is

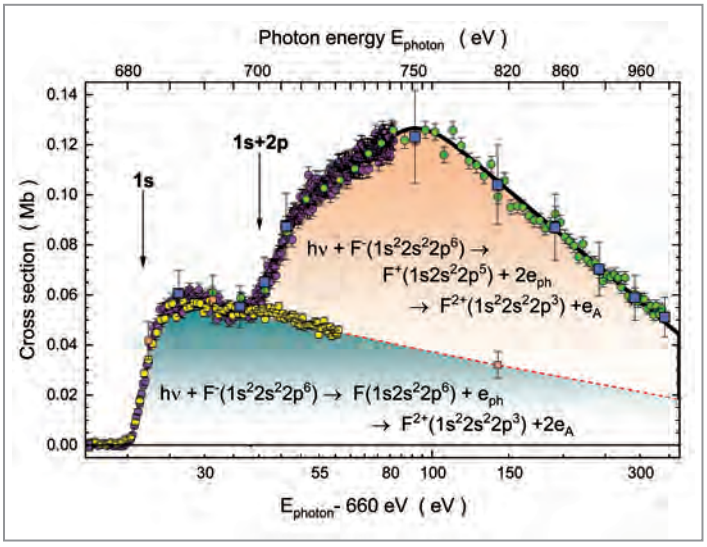


Figure 1

Measured cross sections for triple-ionisation (symbols with dark shading) of $F^-(1s^22s^22p^6)$ ions by a single photon. The arrows indicate the thresholds for 1s-shell ionisation and for the simultaneous removal of a 1s and a 2p electron from F^-. Also shown is the experimental double-ionisation cross section (light-shaded symbols and dashed red line) scaled by a factor 0.153 to match the triple-ionisation cross section below ~698 eV. Electrons released in the different steps of net-triple-ionisation processes are identified as Auger-electrons, e_A, and photo-electrons, e_{ph}. The solid black line is a smooth curve representing the total triple-ionisation cross section.

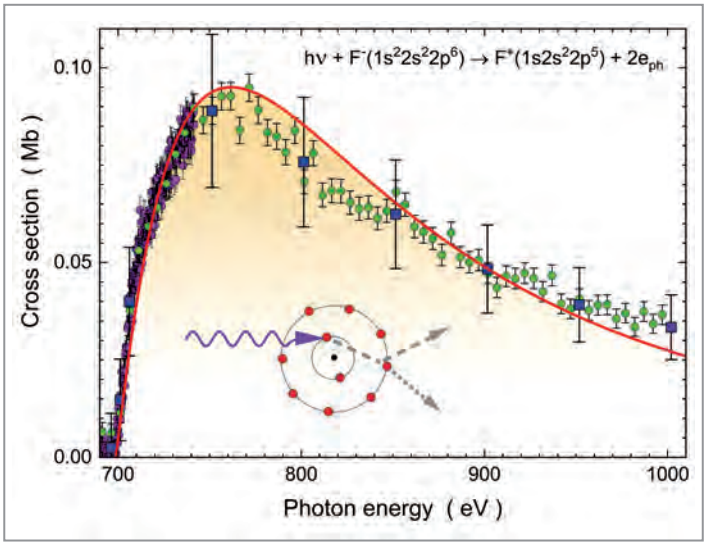


Figure 2

The difference $\Delta\sigma/0.95$ (see text) of the measured triple-ionisation cross section and the dashed line shown in Fig. 1, representing the cross section for direct photo-double-ionisation of the F^- ion, simultaneously removing a pair of electrons, one from the 1s shell and one from the 2p sub-shell. The solid (red) line models the photo-double-ionisation cross section on the basis of a scaling rule [5]. The inset shows a cartoon of the photo-double-ionisation process.

represented by the dashed red line and the light-shaded symbols in Fig. 1, separating the 1s (single) and 1s+2p (double) ionisation contributions to $\sigma_{-1,2}$.

The difference $\Delta\sigma = \sigma_{-1,2} - 0.153\ \sigma_{-1,1}$ is interpreted to be the cross section for 1s+2p photo-double-ionisation multiplied by the branching ratio B for single-Auger decay of the intermediate $F^+(1s\ 2s^2\ 2p^5)$ ion. With B = 0.95, the cross section for 1s+2p photo-double-ionisation of the $F^-(1s^2\ 2s^2\ 2p^6)$ ion can be inferred, as shown in Fig. 2. This interpretation is supported by its compliance with a theoretical scaling relationship for the photo-double ionisation cross section [5]. The dominance of the photo-double-ionisation contribution to the total triple-ionisation cross section is attributed to the small binding energy of the outermost 2p electron in the F^- parent ion. The ability of PIPE experiments to differentiate between the charge states of photoions produced by a single photon provided a clear signature of a process with a minuscule cross section. The subtlest of effects are often the most revealing about nature.

These measurements on the F^- anion clearly demonstrate for the first time the photo-double-ionisation of an ion by a single photon, opening a new dimension in photo-double-ionisation studies. Varying the electrical charge on the target atom directly probes the relative strengths of electron-electron and electron-nucleus interactions, thereby refining our understanding of many-body phenomena.

Author contact: Alfred Müller, Alfred.Mueller@physik.jlug.de

References

1. T. Schneider, P. L. Chocian, and J.-M. Rost, 'Separation and identification of dominant mechanisms in double photoionization', Phys. Rev. Lett. 89, 073002 (2002).
2. M. S. Schöffler, C. Stuck, M. Waitz, F. Trinter, T. Jahnke, U. Lenz, M. Jones, A. Belkacem, A. L. Landers, M. S. Pindzola, C. L. Cocke, J. Colgan, A. Kheifets, I. Bray, H. Schmidt-Böcking, R. Dörner and T. Weber, 'Ejection of quasi-free-electron pairs from the helium-atom ground state by single-photon absorption', Phys. Rev. Lett. 111, 013003 (2013).
3. M. W. McIntyre, A. J. Kinnen and M. P. Scott, 'Photo-double-ionization of the He and Be isoelectronic sequences within an intermediate-energy R-matrix framework', Phys. Rev. A 88, 053413 (2013).
4. V. A. Yerokhin and A. Surzhykov, 'Relativistic theory of the double photoionization of heliumlike atoms', Phys. Rev. A 84, 032703 (2011)
5. T. Pattard, 'A shape function for single-photon multiple ionization cross sections', J. Phys. B 35, L207-L213 (2002).

Original publication

'Near-*K*-Edge Double and Triple Detachment of the F^- Negative Ion: Observation of Direct Two-Electron Ejection by a Single Photon', Physical Review Letters 120, 133202 (2018).
DOI: 10.1103/PhysRevLett.120.133202

Alfred Müller[1], Alexander Borovik Jr.[2], Sadia Bari[3], Ticia Buhr[2], Kristof Holste[2], Michael Martins[4], Alexander Perry-Saßmannshausen[2], Ronald Arthur Phaneuf[5], Simon Reinwardt[4], Sandor Ricz[6], Kaja Schubert[3] and Stefan Schippers[2]

1. Institut für Atom-und Molekülphysik, Justus-Liebig-Universität Gießen, Gießen, Germany
2. I. Physikalisches Institut, Justus-Liebig-Universität Gießen, Gießen, Germany
3. Deutsches Elektronen-Synchrotron DESY, Hamburg, Germany
4. Institut für Experimentalphysik, Universität Hamburg, Hamburg, Germany
5. Department of Physics, University of Nevada, Reno, Nevada, USA
6. Institute for Nuclear Research, Hungarian Academy of Sciences, Debrecen, Hungary

How to keep up with X-ray FEL pulse trains

Sample delivery for serial crystallography at megahertz rates

Femtosecond-duration pulses from free-electron lasers out-run the damaging effects of X-rays to allow exposures of macromolecular crystals that are thousands of times stronger than using conventional methods. Since the sample is vaporised by the X-ray flash, building up a complete dataset requires thousands of microcrystals, delivered one crystal at a time. This is the disruptive new technique of serial crystallography. The European XFEL delivers pulses at rates up to 4.5 MHz, requiring a new crystal every 220 ns. We demonstrated that samples could be delivered at the necessary speeds, and that it will thus be possible to record diffraction patterns 30 times more frequently than before, reducing the acquisition time of full datasets to minutes or seconds.

The recent development of serial femtosecond crystallography has allowed the analysis of crystals too small or radiation sensitive for conventional means, all without the need to cryogenically cool the sample. The method is also ideal for following reactions in real time. The recently opened European XFEL (EuXFEL) now offers a vastly increased number of pulses per second compared to all other hard X-ray FEL facilities. The EuXFEL delivers pulses in trains, with pulses spaced by as little as 220 ns. The high rate gives the promise of rapid and efficient measurements of both macromolecular structure and dynamics, but also presents challenges in sample delivery.

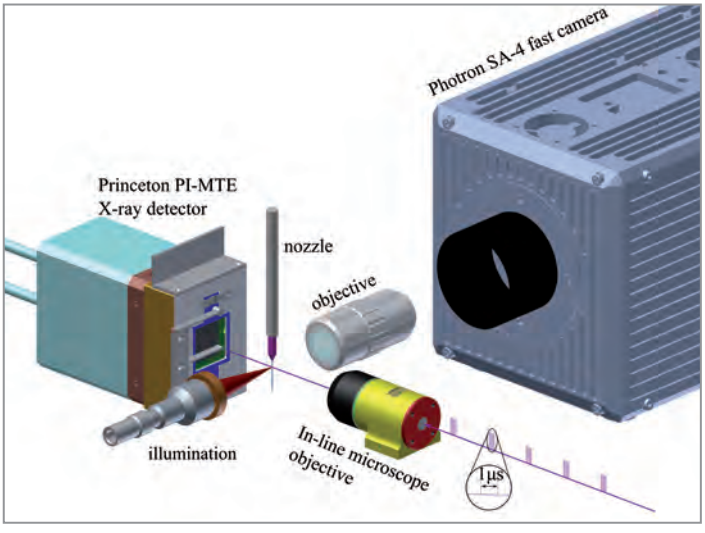


Figure 1

Schematic of the experimental setup at FLASH. The X-ray-pulse trains pass through the in-line microscope into the interaction region. The nozzle is positioned so that the emerging jet intercepts the X-rays. The effects of the interaction between the X-ray pulses and the jet are monitored with a bright-field microscope setup.

The speed of the liquid jet used to deliver a protein crystal must be proportional to the X-ray pulse rate, but also to the distance that must be traversed between pulses. Since all material intersecting the focused X-ray pulse is vaporised, this creates a gap in the jet much larger than the focus itself. This gap must flow by the interaction region for the jet to recover in time for the next pulse. A prior study of the dynamics of X-ray-induced explosions of jets made at the LCLS (U.S.) [1] observed gaps in excess of 150 µm and recovery times of 10 µs, much too long for the pulse rates of the EuXFEL. In addition, a pressure wave propagated along the jet, that could potentially harm the unexposed crystals that are flowing towards the measurement point. It was imperative to address these issues before first experiments could be conducted at the EuXFEL.

Liquid microjets are created by flow-focusing a liquid by a high-speed gas. By examining the physics of the formation of such jets and utilising the design freedom afforded by a high-precision 3D printer, we found that faster jets can be made by reducing the flow rate of the liquid medium containing the sample. This allows greater acceleration of the liquid. Such faster jets are therefore thinner, and this reduction of liquid volume in the X-ray focus reduces the explosion and the size of the gap. Both effects—faster and thinner—act to reduce the recovery time of the jet.

To test our approach for megahertz pulse rates we performed an experiment at the FLASH facility at DESY; the only megahertz FEL facility at the time. We used soft X-ray pulse trains to drive the jet explosion, which we recorded by flash photography at specific times after the X-ray pulse (see Fig. 1). With diameters less than 3 µm and jet speeds in excess of

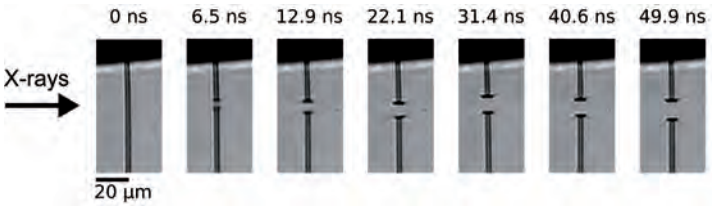


Figure 2

Sideview images of a water jet at various delays after interception by a FLASH FEL pulse, showing the propagation of the jet explosion. The water jet was flowing at a rate of 6.7 µl/min resulting in a jet diameter of 3.1 µm and velocity of 60 m/s. The dose deposited into the jet was approximately 30 MGy.

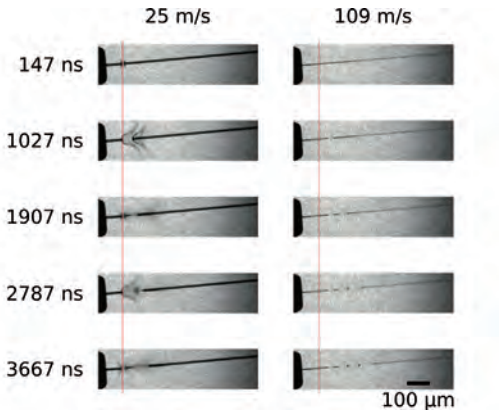


Figure 3

Evolution of the jet as it is exposed to the X-ray pulse train at EuXFEL with pulses arriving at a rate of 1.1 MHz, i.e., with a separation of 880 ns. The position of the X-ray beam is indicated by the red line. The jet shown on the left side is too slow to recover from the explosion induced by the first pulse before the second pulse arrives and only the third can intercept a fresh part of the jet again. The fast jet depicted on the right side recovers in time before the subsequent pulse interacts with the jet.

80 m/s, we found that liquid jets could indeed recover, as seen in Fig. 2. The dynamics match the theoretical predictions [1] and validate our design approach. By using a photon energy of 288 eV, just above the absorption edge of carbon, the full X-ray pulse energy was deposited into liquids such as alcohol, which have a high carbon content. The dose to the liquid of 1.4 GGy exceeds that expected in hard X-ray experiments. In addition to pulse trains with up to 250 pulses at 1 µs spacing, the FLASH facility also generated pulse pairs with a spacing of only 220 ns, thus matching the expected final parameters of EuXFEL. This was achieved with a novel operating mode of the FEL where double laser pulses were used to generate pairs of electron bunches from the FLASH photocathode. No pressure waves could be observed in these thin jets, another advantage of our design.

Our new jet technology was subsequently used to carry out serial crystallography at megahertz rates at the EuXFEL, where we performed further tests of the jet explosions. Fig. 3 shows the evolution of the explosion of jets that were too slow (25 m/s) and fast enough (~110 m/s) for the experiment. As reported in the article 'Megahertz serial crystallography' in this issue, the measurements yielded structures of lysozyme and of a medically relevant beta-lactamase enzyme bound to an inhibitor molecule, with excellent refinement metrics [2]. This method will allow the acquisition of full datasets for protein structure determination in minutes or less, providing a platform for high-throughput studies of the dynamics of proteins.

Author contact: Max O. Wiedorn, max.wiedorn@desy.de
Henry N. Chapman, henry.chapman@desy.de

References

1. C. A. Stan et al., 'Liquid explosions induced by X-ray laser pulses', Nature Physics 12, 966–971 (2016).
2. M. O. Wiedorn et al., 'Megahertz serial crystallography', Nat. Commun. 9, 4025 (2018)

Original publication

'Rapid sample delivery for megahertz serial crystallography at X-ray FELs', IUCrJ 5, 574–584 (2018). DOI: 10.1107/S2052252518008369

Max O. Wiedorn[1,2,3], Salah Awel[1,3], Andrew J. Morgan[1], Kartik Ayyer[1], Yaroslav Gevorkov[1,4], Holger Fleckenstein[1], Nils Roth[1,2], Luigi Adriano[5], Richard Bean[6], Kenneth R. Beyerlein[1], Joe Chen[7], Jesse Coe[7], Francisco Cruz-Mazo[8], Tomas Ekeberg[1], Rita Graceffa[6], Michael Heymann[1,9], Daniel A. Horke[1,3], Juraj Knoška[1,2], Valerio Mariani[1], Reza Nazari[7], Dominik Oberthür[1], Amit K. Samanta[1], Raymond G. Sierra[10], Claudiu A. Stan[11,12], Oleksandr Yefanov[1], Dimitrios Rompotis[13], Jonathan Correa[1,5], Benjamin Erk[13], Rolf Treusch[13], Joachim Schulz[6], Brenda G. Hogue[14], Alfonso M. Gañán-Calvo[8], Petra Fromme[7,14], Jochen Küpper[1,2,3], Andrei V. Rode[15], Saša Bajt[5], Richard A. Kirian[7] and Henry N. Chapman[1,2,3]

1. Center for Free-Electron Laser Science, Deutsches Elektronen-Synchrotron DESY, Hamburg, Germany
2. Department of Physics, Universität Hamburg, Hamburg, Germany
3. The Hamburg Center for Ultrafast Imaging, Universität Hamburg, Hamburg, Germany
4. Institute of Vision Systems, Hamburg University of Technology, Hamburg, Germany
5. Deutsches Elektronen-Synchrotron DESY, Hamburg, Germany
6. European XFEL GmbH, Schenefeld, Germany
7. Arizona State University, Tempe, AZ, USA
8. Universidad de Sevilla, Department of Aerospace Engineering and Fluid Mechanics, Sevilla, Spain
9. Max Planck Institute of Biochemistry, Department of Cellular and Molecular Biophysics, Martinsried, Germany
10. LCLS, SLAC National Accelerator Laboratory, Menlo Park, CA, USA
11. Department of Physics, Rutgers University Newark, Newark, NJ, USA
12. Stanford PULSE Institute, SLAC National Accelerator Laboratory, Menlo Park, CA, USA
13. Deutsches Elektronen-Synchrotron DESY, Hamburg, Germany
14. Biodesign Institute, School of Life Sciences, Arizona State University, Tempe, AZ, USA
15. Laser Physics Centre, Research School of Physics and Engineering, Australian National University, Canberra, ACT, Australia

Megahertz serial crystallography

First results from user experiments at the European XFEL

Barely two weeks after the European XFEL opened its doors to users, the first user experiment was performed by a DESY-led international team of over 120 researchers. The European XFEL is the first hard X-ray FEL in the world capable of producing femtosecond pulses at a megahertz repetition rate. The key question was: can one take advantage of this increased repetition rate for protein structure determination by serial crystallography? The experiment was a success, showing that measurement of high quality structural data is possible and determining a new protein structure to 1.7 Å resolution. Thanks to this combined effort it is now possible to measure enough data for a protein structure in minutes instead of hours, opening the door to a range of studies that had previously not been feasible.

To date serial femtosecond crystallography (SFX) measurements have been limited by available pulse repetition rates to measuring data at 120 frames per second. The European XFEL (EuXFEL) is the first hard X-ray free-electron laser to produce bursts of X-ray pulses with an intra-bunch repetition rate of 1.1 MHz, nearly four orders of magnitude faster than previously available. The decreased time between X-ray pulses enables the EuXFEL to deliver more pulses per second at the same X-ray peak power. But the same increase in repetition rate poses several challenges for the serial crystallography approach. To probe crystals at full speed, exposed sample must clear the X-ray interaction

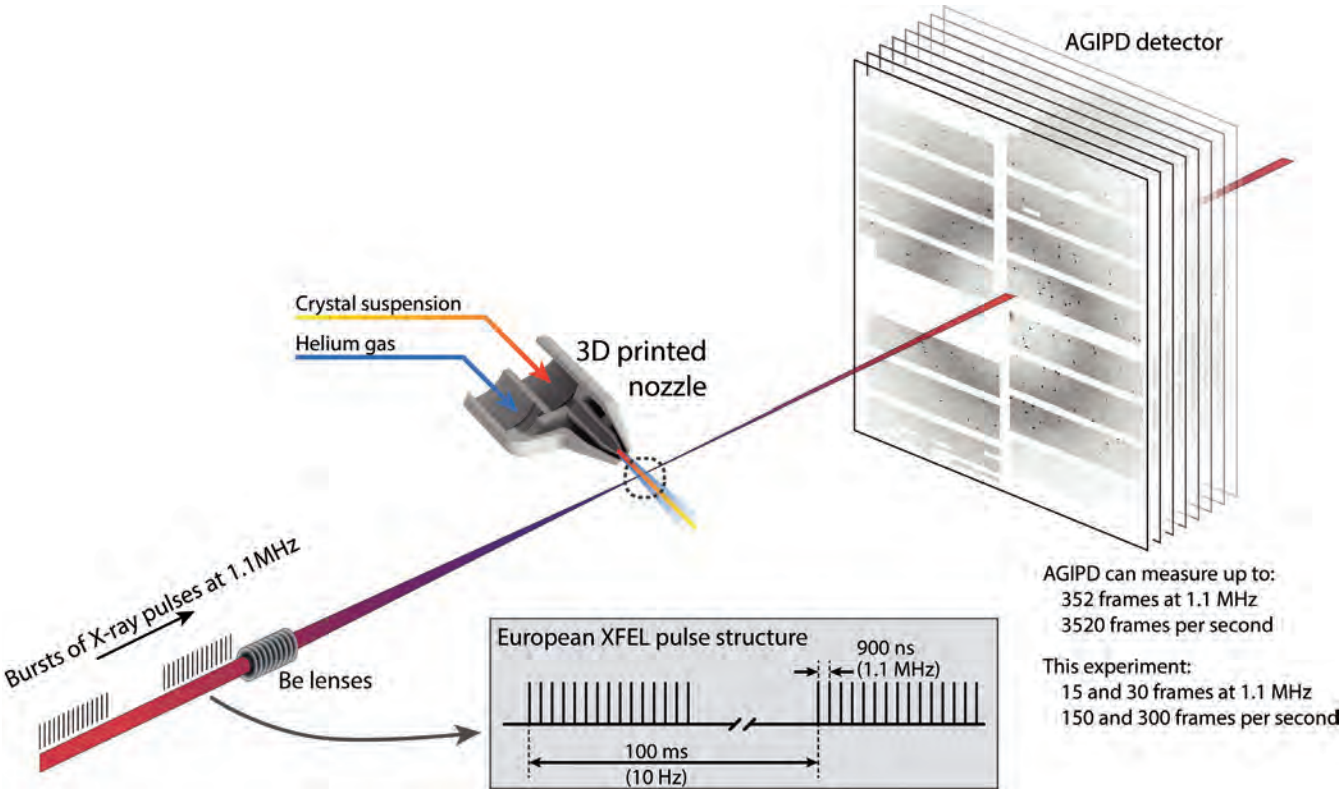


Figure 1

Schematic of the megahertz serial crystallography setup at the SFX/SPB instrument of the European XFEL. Protein crystals were introduced into the focussed XFEL beam using a liquid jet of 1.8 µm diameter moving at speeds of 50-100 m/s and diffraction measured using an AGIPD detector. Figure reproduced from original publication.

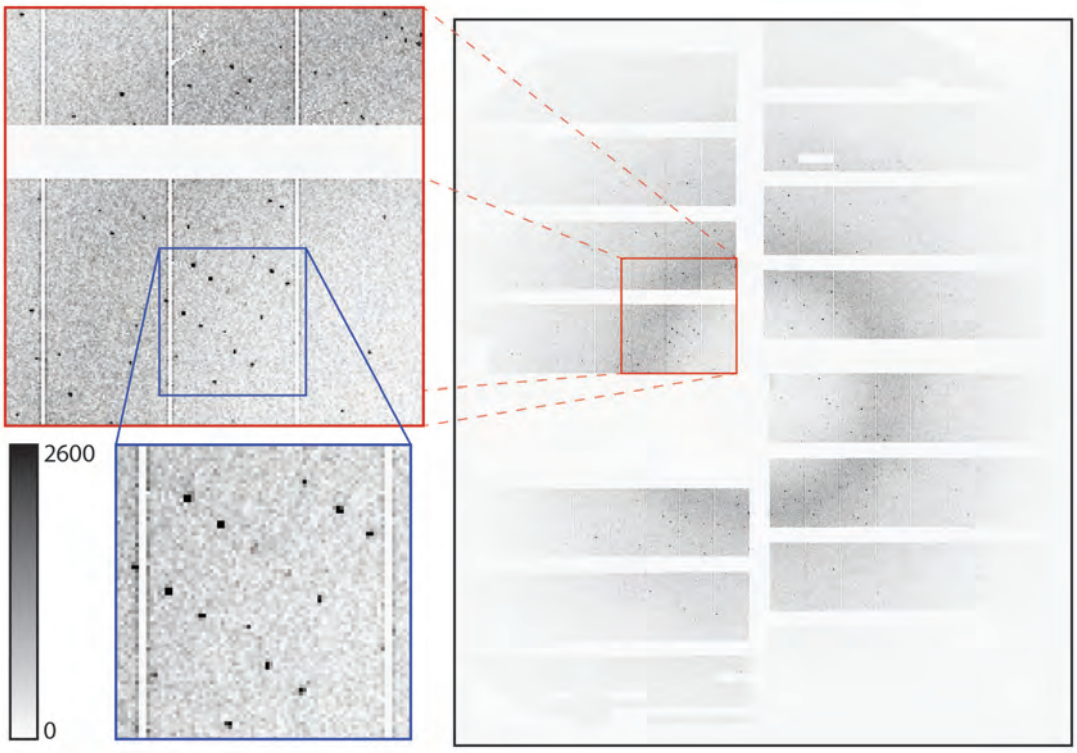


Figure 2

Diffraction pattern from a single crystal of enzyme lysozyme from hen egg-white (HEWL) measured using X-rays at 9.3 keV photon energy and 40 fs duration at MHz repetition rate. Dynamic gain switching of the AGIPD detector enables simultaneous low noise and high dynamic range: full dynamic range of brightest spots in this image extend to 109000 counts, but the image has been clipped at 2600 counts to show content. Figure reproduced from original publication.

point in less than one microsecond before the arrival of the next X-ray pulse, while the high dose deposited by a single FEL pulse can vaporise the jet creating a void which must also clear the interaction point before the next X-ray pulse arrives [1]. Detecting full-frame diffraction patterns with megahertz pulse repetition rates also requires a totally new class of detectors with new data acquisition and control systems. Before we started this experiment, EuXFEL was brand new and all components had not yet been used together to perform user experiments.

The experiment took place at the SPB/SFX instrument of the European XFEL, one of the first two instruments available for user operation (Fig. 1). A newly developed X-ray detector, the 'Adaptive Gain Integrating Pixel Detector' (AGIPD) developed specifically for EuXFEL by a DESY-led international consortium, can measure diffraction patterns at megahertz repetition rates. It furthermore not only records images as fast as the X-ray pulses arrive, but also automatically adjusts the sensitivity of every pixel. For sample delivery, a team at DESY's CFEL developed new liquid jet injection techniques capable of delivering sample at a speed of over 100 metres per second, as detailed in the article 'How to keep up with X-ray FEL pulse trains' in this issue [2]. The team also had to solve the challenge of managing and visualising data at the high data rates of the EuXFEL.

The team first determined the structure of a very well-known sample, the enzyme lysozyme from hen egg-white (HEWL), to verify the systems worked as expected. Microcrystals of 6-8 µm size were introduced into the X-ray interaction region in a 1.8 µm diameter liquid jet by a gas dynamic virtual nozzle at speeds of between 50 and 100 m/s.

Analysis of measured X-ray diffraction images from the sample showed that the adaptive gain switching of individual pixels worked well at MHz repetition rates, enabling both high dynamic range and low noise at the same time (Fig. 2). Indeed, the structure determined from indexing and integrating 25000 similar such diffraction patterns perfectly matches the known lysozyme structure to 1.8 Å. Not only did the liquid jets recover in time for the next pulse, but good quality diffraction could be recorded from any pulse in the EuXFEL pulse train for structure

determination. This confirmed the stroboscopic imaging results that showed that the developed new liquid jets are indeed fast enough for the megahertz repetition rates of the EuXFEL. It furthermore indicated that the induced pressure wave from the explosion of the water jet does not produce measureable damage in nanocrystals further up the liquid column. This in itself was an important milestone for structural biology experiments at EuXFEL.

The team then turned their attention to determining the structure of a bacterial enzyme that plays an important role in antibiotics resistance, the structure of which was previously unknown. The molecule designated CTX-M-14 β-lactamase was isolated from the bacterium *Klebsiella pneumoniae* whose multidrug-resistant strains are a grave concern in hospitals worldwide. The particular complex of CTX-M-14 β-lactamase studied was from the non-resistant, 'wild type' of the bacterium with avibactam bound to the enzyme's active centre, a structure that has not been analysed before. Crystals of CTX-M-14 were mixed with avibactam just prior to injection. Good diffraction was observed with the new structure determined to 1.7 Å resolution (PDB 6GTH) from only 12500 indexed diffraction patterns (Fig. 3).

These first measurements show that it is possible to record high quality structural information under the exposure conditions available at the European XFEL, which is the first step towards recording snapshots of the biochemical reaction between enzymes and their substrates at different stages. The key advance is in exploiting sub-microsecond inter-pulse spacing. Subsequent experiments have already reported results from 600 pulses per second [3], and at the time of writing experiments are performed using 1200 pulses per second at 1.1 MHz pulse rates. Indeed it would be possible to measure each of the structures presented here in 15 minutes or less once European XFEL achieves its full pulse rate operation of 4.5 MHz in the near future. This is pointing the way towards rapid measurement of structures at many time points as required when going from static structures to molecular movies of proteins in action.

This experiment was open to all scientists from the community to participate, contribute, learn, and gain experience in how to carry out such measurements at this facility – an example of early open science in action and which has helped all later experiments at the SPB/SFX instrument.

Author contact: Anton Barty, anton.barty@desy.de
Christian Betzel, christian.betzel@uni-hamburg.de

References

1. C. A. Stan et al., 'Liquid explosions induced by X-ray laser pulses', Nature Physics 12, 966–971 (2016).
2. M. O. Wiedorn et al., 'Rapid sample delivery for megahertz serial crystallography at X-ray FELs', IUCrJ 5, 1-11 (2018).
3. M. L. Grünbein et al., 'Megahertz data collection from protein microcrystals at an X-ray free-electron laser', Nature Comms. 9, 1–23 (2018).

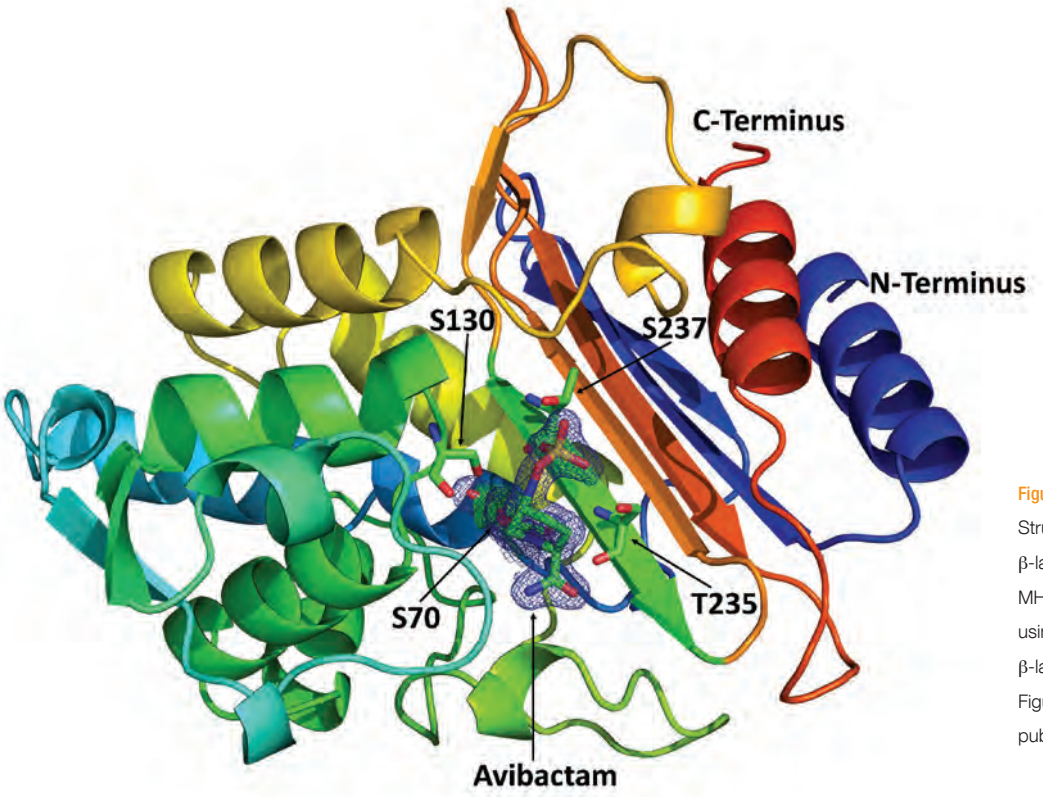


Figure 3
Structure of avibactam bound to β-lactamase determined using MHz SFX at European XFEL, solved using a solvent-free version of β-lactamase as the starting model. Figure reproduced from original publication



Figure 4

The international collaboration that conducted the first user experiment at European XFEL.

Original publication

'Megahertz serial crystallography', Nature Commun. 9, 4025 (2018).
DOI: 10.1038/s41467-018-06156-7

Max O. Wiedorn[1,2,3], Dominik Oberthür[1], Richard Bean[4], Robin Schubert[5,3,6], Nadine Werner[5], Brian Abbey[7], Martin Aepfelbacher[5], Luigi Adriano[8], Aschkan Allahgholi[8], Nasser Al-Qudami[4], Jakob Andreasson[9,10,11], Steve Aplin[1], Salah Awel[1,3], Kartik Ayyer[1], Saša Bajt[8], Imrich Barák[12], Sadia Bari[8], Johan Bielecki[4], Sabine Botha[5,3], Djelloul Boukhelef[4], Wolfgang Brehm[1], Sandor Brockhauser[4,13], Igor Cheviakov[8], Matthew A. Coleman[14], Francisco Cruz-Mazo[15], Cyril Danilevski[4], Connie Darmanin[7], R. Bruce Doak[16], Martin Domaracky[1], Katerina Dörner[4], Yang Du[1], Hans Fangohr[4], Holger Fleckenstein[1], Matthias Frank[14], Petra Fromme[17], Alfonso M. Gañán-Calvo[15], Yaroslav Gevorkov[1,18], Klaus Giewekemeyer[4], Helen Mary Ginn[19,20], Heinz Graafsma[8,21], Rita Graceffa[4], Dominic Greiffenberg[22], Lars Gumprecht[1], Peter Göttlicher[8], Janos Hajdu[9,10], Steffen Hauf[4], Michael Heymann[23], Susannah Holmes[7], Daniel Horke[1,3], Mark S. Hunter[24], Siegfried Imlau[1], Alexander Kaukher[4], Yoonhee Kim[4], Alexander Klyuev[8], Juraj Knoška[1,2], Bostjan Kobe[25], Manuela Kuhn[8], Christopher Kupitz[26], Jochen Küpper[1,2,27,3], Janine Mia Lahey-Rudolph[28,1], Torsten Laurus[8], Karoline Le Cong[5], Romain Letrun[4], P. Lourdu Xavier[1,29], Luis Maia[4], Filipe R. N. C. Maia[9,30], Valerio Mariani[1], Marc Messerschmidt[4], Markus Metz[1], Davide Mezza[22], Thomas Michelat[4], Grant Mills[4], Diana C. F. Monteiro[3], Andrew Morgan[1], Kerstin Muhlig[9], Anna Munke[9], Astrid Münnich[4], Julia Nette[3], Keith A. Nugent[7], Theresa Nuguid[5], Allen M. Orville[20], Suraj Pandey[26], Gisel Pena[1], Pablo Villanueva-Perez[1], Jennifer Poehlsen[8], Gianpietro Previtali[4], Lars Redecke[28,8], Winnie Maria Riekehr[28], Holger Rohde[5], Adam Round[4], Tatiana Safenreiter[1], Iosifina Sarrou[1], Tokushi Sato[1,4], Marius Schmidt[26], Bernd Schmitt[22], Robert Schönherr[28], Joachim Schulz[4], Jonas A. Sellberg[31], M. Marvin Seibert[9], Carolin Seuring[1,3], Megan L. Shelby[14], Robert L. Shoeman[16], Marcin Sikorski[4], Alessandro Silenzi[4], Claudiu A. Stan[32], Xintian Shi[22], Stephan Stern[1,4], Jola Sztuk-Dambietz[4], Janusz Szuba[4], Aleksandra Tolstikova[1], Martin Trebbin[3,33,34], Ulrich Trunk[8], Patrick Vagovic[1,4], Thomas Ve[35], Britta Weinhausen[4], Thomas A. White[1], Krzysztof Wrona[4], Chen Xu[4], Oleksandr Yefanov[1], Nadia Zatsepin[36], Jiaguo Zhang[22], Markus Perbandt[5,3], Adrian P. Mancuso[4], Christian Betzel[5,3,6], Henry Chapman[1,2,3], Anton Barty[1]

1. Center for Free Electron Laser Science CFEL, Deutsches Elektronen-Synchrotron DESY, Hamburg, Germany
2. University of Hamburg, Department of Physics, Hamburg, Germany
3. Center for Ultrafast Imaging, University of Hamburg, Hamburg, Germany
4. European XFEL GmbH, Schenefeld, Germany
5. Institute for Biochemistry and Molecular Biology, Laboratory for Structural Biology of Infection and Inflammation c/o DESY, University of Hamburg, Hamburg, Germany
6. Integrated Biology Infrastructure Life-Science Facility at the European XFEL (XBI), Schenefeld, Germany
7. Australian Research Council (ARC) Centre of Excellence in Advanced Molecular Imaging, Department of Chemistry and Physics, La Trobe Institute for Molecular Sciences, La Trobe University, Bundoora, Australia
8. Deutsches Elektronen-Synchrotron DESY, Hamburg, Germany
9. Laboratory of Molecular Biophysics, Department of Cell and Molecular Biology, Uppsala University, Uppsala, Sweden
10. ELI Beamlines, Institute of Physics of the Czech Academy of Sciences, Prague, Czech Republic
11. Condensed Matter Physics, Department of Physics, Chalmers University of Technology, Gothenburg, Sweden
12. Institute of Molecular Biology, SAS, Bratislava, Slovakia
13. Biological Research Centre (BRC), Hungarian Academy of Sciences, Szeged, Hungary
14. Lawrence Livermore National Laboratory, Livermore, USA
15. Depart. Ingeniería Aeroespacial y Mecánica de Fluidos ETSI, Universidad de Sevilla, Sevilla, Spain
16. Max Planck Institute for Medical Research, Heidelberg, Germany
17. School of Molecular Sciences and Biodesign Center for Applied Structural Discovery, Arizona State University, Tempe, USA
18. Hamburg University of Technology, Vision Systems E-2, Hamburg, Germany
19. Division of Structural Biology, Headington, Oxford, United Kingdom
20. Diamond Light Source, Research Complex at Harwell, and University of Oxford, Diamond House, Harwell Science and Innovation Campus, Didcot, Oxfordshire, United Kingdom
21. Mid Sweden University, Sundsvall, Sweden
22. Paul Scherrer Institut, Villigen, Switzerland
23. Department of Cellular and Molecular Biophysics, Max Planck Institute of Biochemistry, Martinsried, Germany
24. Linac Coherent Light Source, SLAC National Accelerator Laboratory, Menlo Park, USA
25. School of Chemistry and Molecular Biosciences, Institute for Molecular Bioscience and Australian Infectious Diseases Research Centre, University of Queensland, Brisbane, Australia.
26. Physics Department, University of Wisconsin-Milwaukee, Milwaukee, USA
27. Department of Chemistry, University of Hamburg, Hamburg, Germany
28. Institute of Biochemistry, University of Lübeck, Lübeck, Germany
29. Max-Planck Institute for the Structure and Dynamics of Matter, Hamburg, Germany
30. NERSC, Lawrence Berkeley National Laboratory, Berkeley, USA
31. Biomedical and X-Ray Physics, Department of Applied Physics, AlbaNova University Center, KTH Royal Institute of Technology, Stockholm, Sweden
32. Physics Department, Rutgers University Newark, Newark, USA
33. Department of Chemistry, University at Buffalo, Buffalo, USA
34. Institute of Nanostructure and Solid State Physics, Department of Physics, University of Hamburg, Hamburg, Germany
35. Institute for Glycomics, Griffith University, Southport, Australia
36. Department of Physics, Arizona State University, Tempe, USA

Generation of nanoscale liquid sheets

A new tool for the study of liquid solutions

The physics and chemistry of liquid solutions play a central role in science and in our understanding of life on Earth. Unfortunately, key tools for interrogating aqueous systems, such as infrared and soft X-ray spectroscopy, cannot readily be applied because of strong absorption in water. We recently demonstrated the use of gas-dynamic forces to generate free-flowing, sub-micron, liquid sheets which are two orders of magnitude thinner than anything previously reported. These sheets are tuneable in thickness from thicker than 1 µm down to less than 20 nm, which corresponds to fewer than 100 water molecules. Our experiments at the FLASH free-electron laser demonstrate that these aqueous sheets can readily transmit and reflect photons from a large spectral range, leading to new understanding of the behaviour of water, solvents and solutions. These first studies measured the properties of water in extreme conditions as found in the atmosphere of Jupiter-like giants.

We recently demonstrated generation of free-flowing liquid sheets, with thickness tuneable down to tens of nm, using a microfluidic nozzle operating in the 150 µL/min flow range. The device used for generating ultra-thin liquid sheets is a gas dynamic nozzle [1] consisting of three microfluidic channels in a borosilicate chip. Figure 1a shows a microscope image of the microfluidic chip housing the sheet nozzle, and Figure 1b shows a higher magnification image of the nozzle exit geometry, where two 50 µm diameter channels intersect a central 20 µm channel at angles of ±40° before exiting the chip. To form a liquid sheet, liquid is sent through the central channel, and gas is sent through the outer channels. The colliding gas jets create a radial force, spreading the liquid into a thin sheet with thick rims.

Figure 2 shows a reflection image of a water sheet running in air at a flow rate of 250 µL/min. Thin-film interference fringes can clearly be seen from the sheet, demonstrating the surface quality and integrity of the sheet. These fringes can also be used to estimate the thickness of the sheet. In the thin-film interference regime, a film of liquid has a spectral reflectance curve that depends strongly on thickness. The rapidly varying reflectance spectra along the length of the sheet leads to interference fringes of distinct colours, which can be captured by a camera as seen in Fig. 2. Above the image is a colour bar where we plot the simulated thickness-dependent colour variation for a water film, calculated using the measured index of refraction of water and assuming a 3000 K blackbody illuminating spectrum. The sheet in Fig. 2 goes from about 1 µm near the nozzle to about 100 nm close to the re-convergence point. We note that this is not the thinnest sheet possible, but one in the thickness range to best illustrate the thin-film interference. Thinner sheets were measured with a special microscope, and the thickness was estimated to be as low as 17 nm.

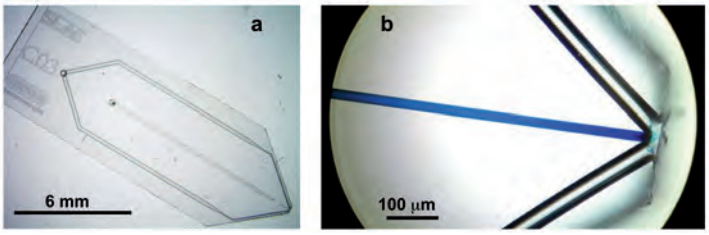


Figure 1

Microfluidic gas-dynamic nozzle. The microfluidic device for generating free-flowing liquid sheets is shown in (a). The gas and liquid ports are on the underside of the chip on the left. Microfluidic channels for gas (outer), and liquid (central) can be traced to the output of the nozzle on the right side of the chip. The chip dimensions are 6 × 19 mm. A close-up of the nozzle output is shown in (b), where a blue dye has been introduced into the liquid channel.

Ultra-thin liquid sheets have the potential to be used in a wide variety of X-ray measurements, most notably in the soft X-ray regime, where sub-micron penetration depths have severely limited measurements on liquids. The ultra-thin sheets presented here not only allow for transmission of soft X-rays, but also offer a superior geometry compared with sub-micron round jets. Since the typical X-ray focus at a synchrotron or free-electron laser (FEL) is larger than 1 µm, a round jet thin enough for transmission will necessarily capture only a small fraction of the beam. This not only reduces the signal of interest, but also causes scattering from the edge of the jet, which can be a significant source of background.

In our experiment at BL3 at FLASH, an ultra-thin sheet was used to study the electronic and thermal properties of isochorically heated water. The 225 eV photon pulses from FLASH were used to excite the water sheet, and the subsequent time-evolution was monitored by transmission and reflection of visible light pulses from a femtosecond

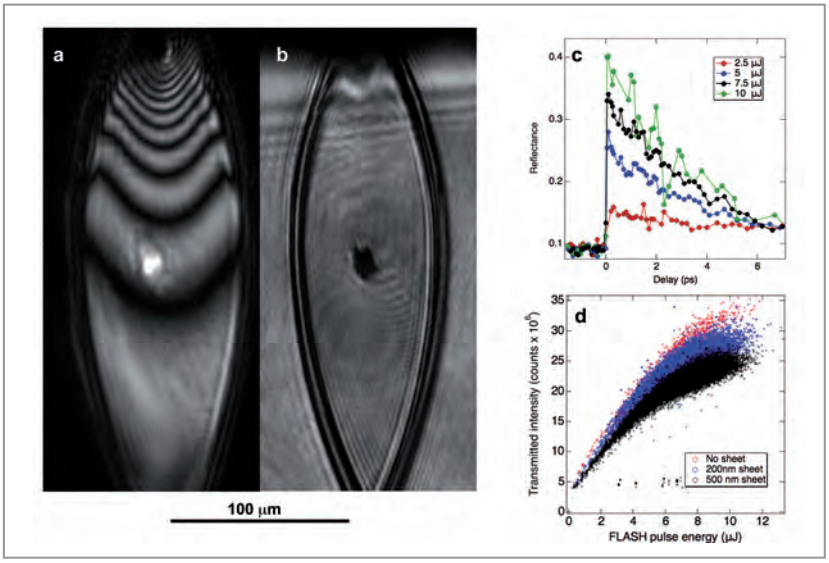


Figure 3

Soft X-ray measurements of liquid water sheets. Measurements from the FLASH free-electron laser are shown as described in the text. Shown are optical reflection (a) and transmission (b) images taken *in situ*. The entire sheet was illuminated by a pulsed optical laser (500 nm), which was used as a probe of the dynamics induced by the soft X-ray pulses. The X-ray spot can be seen as a bright spot in reflection and a dark spot in transmission, induced by the X-ray pump. c) The reflectivity of the X-ray pumped region of the water sheet, as a function of time delay between the X-ray pump and optical probe, for a series of different pump fluences. d) The intensity of soft X-rays transmitted through the water sheet, as a function of FLASH pulse energy, for different sheet thicknesses.

laser. A flowing water sheet was necessary in order to present a flat water surface for reflection and transmission measurements, which would not be possible with a cylindrical jet. Figure 3 shows optical reflection and transmission images taken during the experiment. Thin-film interference from the laser illumination can be seen in the reflection image (Fig. 3a) and was used to monitor the stability and thickness of the sheet. In this case, interpretation of the thin-film interference fringes is simplified by illumination with a monochromatic source, giving accurate measurement of sheet thickness *in situ*. The FLASH pulse excites free charge carriers near the critical density of the 500 nm probe. The high electron density leads to transient metal-like behaviour, resulting in increased reflection and simultaneously reduced transmission. Hence, the X-ray spot can be seen as a bright spot in the reflection image (Fig. 3a) and a dark spot in the transmission image (Fig. 3b), both taken within picoseconds following excitation. The dynamics are extracted by monitoring the change in reflectivity (within the bright spot) as a function of time delay between the X-ray pump and optical probe as plotted in Fig. 3c for several different pump intensities. We use the measured reflection and transmission data to find the complex index of refraction of the FEL-heated water. Assuming the charge carrier's behaviour in the excited water can be described by a Drude model, we estimate the charge carrier density of 2–4 × 10^{21} cm^{-3}, which indicates ~10 % ionisation of water. This number is significantly higher than the direct photo-ionised electron density by direct FEL light absorption of a single electron (the absorbed FEL photon density is ~1–2 × 10^{20} cm^{-3}), and thus indicating the importance of secondary collisional processes. We also monitored the intensity of FLASH photons transmitted through the water sheet as a function of incident pulse energy which is plotted in Fig. 3d.

This work, demonstrating the use of ultra-thin liquid sheets at FLASH, paves the way for soft X-ray spectroscopy and imaging in free-flowing liquid samples. Further details of the FLASH experiment will be presented in an upcoming publication on novel measurements of the conductivity of water in extreme conditions.

Author contact: Jake Koralek, koralek@slac.stanford.edu

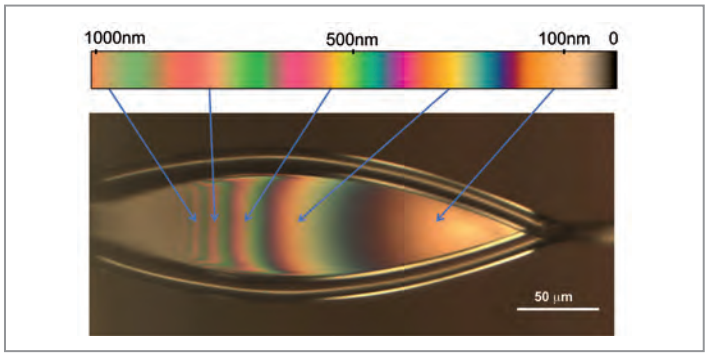


Figure 2

Optical reflection image of a water sheet running in air, at a flow rate of 250 µL/min, taken with a CCD camera through ×10 long working distance objective and fibre-coupled tungsten light source. The colour bar above the image is a simulation of the observed reflected colour for water films, as a function of thickness. Arrows indicate the corresponding fringes on the liquid sheet, in agreement with the spectral reflectance measurements from our publication.

Reference

1. D. P. DePonte, U. Weierstall, K. Schmidt, J. Warner, D. Starodub, J. C. H. Spence and R. B. Doak. 'Gas dynamic virtual nozzle for generation of microscopic droplet streams' J. Phys. D Appl. Phys. 41, 19 (2008).

Original publication

'Generation and characterization of ultrathin free-flowing liquid sheets', Nature Communications, 9, 1353 (2018). DOI: 10.1038/s41467-018-03696-w

Jake D. Koralek[1], Jongjin B. Kim[1], Petr Brůža[2,3], Chandra Curry[1,4], Zhijiang Chen[1], Hans A. Bechtel[5], Amy A. Cordones[1], Philipp Sperling[1,6], Sven Toleikis[7], Jan F. Kern[1], Stefan P. Moeller[1], Siegfried H. Glenzer[1], Daniel P. DePonte[1]

1. SLAC National Accelerator Laboratory, Menlo Park, CA, USA
2. ELI Beamlines, Institute of Physics of the ASCR v.v.i, Prague, Czech Republic
3. Thayer School of Engineering, Dartmouth College, Hanover, NH, USA
4. Department of Electrical and Computer Engineering, University of Alberta, Edmonton, Alberta, Canada
5. Advanced Light Source, Lawrence Berkeley National Laboratory, Berkeley, CA, USA
6. European X-Ray Free-Electron Laser Facility GmbH, Schenefeld, Germany
7. Deutsches Elektronen-Synchrotron DESY, Hamburg, Germany

STEAM - Segmented terahertz electron accelerator and manipulator

A terahertz-driven electron accelerator and manipulator

Terahertz-based accelerators are prominent candidates for driving next-generation compact light sources, promising high-brightness, ultrashort X-ray and electron pulses. Here, we present a segmented terahertz electron accelerator and manipulator capable of performing multiple high-field operations on key properties of ultrashort electron bunches. With this single device, powered by few-µJ, single-cycle, 0.3 THz pulses, we demonstrate record THz-acceleration of bunches with >30 keV, their temporal characterisation with <10 fs resolution, focusing with >2 kT/m strength and compression down to ~100 fs as well as real-time switching between these modes of operation. The STEAM device demonstrates the feasibility of THz-based electron accelerators, manipulators and diagnostic tools enabling science beyond current resolution frontiers with transformative impact.

Ultrafast electron beams are the basis for free-electron lasers, ultrafast streak cameras, and femtosecond electron diffractometers. Microwave technology at gigahertz frequencies has been the conventional choice for powering accelerators, which provide these beams due to its high degree of technical maturity. However, it requires costly infrastructure and suffers from inherent difficulties in laser-electron synchronisation that limit its further development fur pursuing even higher temporal and spatial resolution. Strong motivation thus exists for exploring alternative technologies of diminishing their size and cost adapted for pushing the resolution frontier especially where lower levels of bunch charge in the pC range is sufficient. Among such alternative sources, terahertz (THz) driven accelerators are currently under intense investigation as a potential alternative approach with the promise to overcome both the limitations of radio-frequency acceleration and the challenges in other compact accelerators, such as critical tolerances in dielectric laser accelerators (DLAs) [1] and instabilities and difficulties in controlling electron injection in laser-plasma accelerators [2].

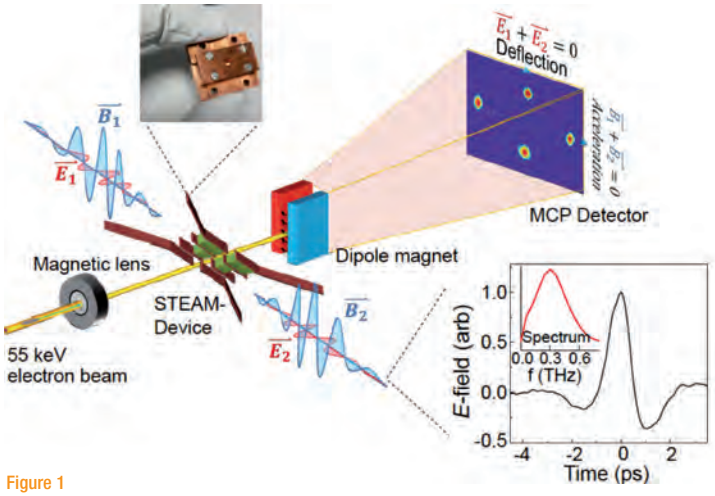


Figure 1

Acceleration and manipulation of an electron bunch from a 55 keV DC electron gun using a STEAM device. The two counter-propagating THz beams (E_1, E_2) interact with the 55 keV electron beam inside the STEAM device. Subsequently, the electron beam is detected by the camera. The Figure was adapted from the original publication.

Here, we demonstrate a segmented THz waveguide device (STEAM device) whose structure is designed to optimise the interaction of THz radiation and electrons over long (multi-millimetre) interaction lengths. The use of two-sided, transverse pumping allows the timing of the two THz drivers and the electrons to be used to select between multiple high-field modes of operation on the 6D-phase-space (position and momentum distribution) of ultrashort electron bunches.

The experimental setup (Fig. 1) consisted of a 55 keV photo-triggered DC electron gun, a THz-powered STEAM device for electron manipulation and a diagnostic section. Ultraviolet pulses for photoelectron emission were generated by two successive stages of second harmonic generation (SHG), while single-cycle THz pulses were generated by difference frequency generation using a non-collinear phase-matching technique (i.e., pulse-front tilting) [3]. According to the Lorentz force law, the electrons experience both the electric and magnetic fields of the THz pulses during interaction inside the STEAM device. The electric field is responsible for acceleration and deceleration, while the magnetic field induces transverse deflections.

Efficient interaction of the electrons with the fields was accomplished by means of segmentation [4] in which the interaction volume was sub-divided into multiple layers of varying thickness (Fig. 1). Each layer was isolated from the

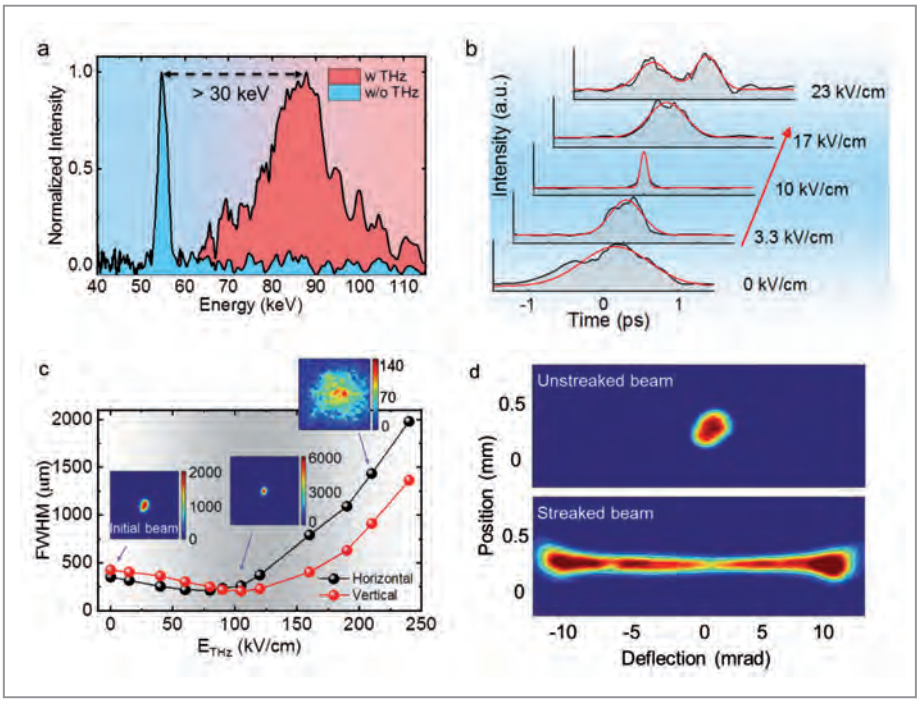


Figure 2

Functions of the STEAM device. (a) Electron energy spectra for input beam (blue curve) and accelerated beam (red curve) demonstrating electron acceleration. (b) Temporal compression of the electron pulses as a function of the THz field in the rebunching mode. (c) Transverse electron beam focusing as a function of the THz field in the focusing mode. (d) Images of the electron beam on the detector with and without the THz deflection field in the streaking mode. The Figure was adapted from the original publication.

others by thin metal sheets so they could act as waveguides channelling THz energy to the interaction regions despite sub-wavelength dimensions. Dielectric slabs of varying length were inserted into each layer to delay the arrival time of the THz waveform to coincide with the arrival of the electrons. The use of two counter-propagating drive pulses enabled two key modes of operation: an 'electric' mode, used for acceleration, compression (rebunching) and focusing, and a 'magnetic' mode, used for deflection and streaking.

In the electric mode, maximum acceleration and deceleration occurred when electrons were injected at the peak of the electric fields of the counter-propagating THz pulses (Fig. 2a). In this configuration, the deflection was minimized due to the cancellation of the magnetic fields. At the zero-crossing of the electric field, the temporal field gradient is maximized resulting in a time-varying electric field and thus a velocity gradient that induces either compression or stretching of the electron bunch as it moves forward (Fig. 2b). The temporal electric-field gradient at the zero-crossing is intrinsically coupled to a transverse spatial gradient in the magnetic fields, which results in focusing or defocusing of the electron beam (Fig. 2c).

In the magnetic mode, the relative timing of the THz fields is different from that of the electric mode by a half period, resulting in reinforcement of the magnetic and cancellation of the electric fields. When electrons are on the crest of the magnetic field, the deflection is maximized and the acceleration (or deceleration) is minimized. Electrons arriving at the zero-crossing of the THz magnetic field experience a deflection that is a steep function of time, effectively streaking the bunch and projecting the temporal electron charge profile onto the spatial dimension of the microchannel plate detector with high temporal resolution (Fig. 2d).

In summary, we have demonstrated a novel segmented THz electron accelerator and manipulator setting new records in THz acceleration, streaking and focusing with a very compact device. The segmented structure makes it possible to phase match the electron–THz interaction for non-relativistic beams, making it ideal for use as a high-gradient photogun. The independent control over the counter-propagating THz pulse timing gives the STEAM device the ability to switch dynamically between different modes. The results presented here are an important step in demonstrating a practical, compact THz-driven electron or light source capable of probing material structure and function well beyond current limits of temporal resolution.

Author contact: Dongfang Zhang, dongfang.zhang@desy.de

References

1. J. Breuer and P. Hommelhoff, 'Laser-Based Acceleration of Nonrelativistic Electrons at a Dielectric Structure', Phys. Rev. Lett. 111, 134803 (2013).
2. V. Malka, J. Faure, Y.A. Gauduel, E. Lefebvre, A. Rousse and K. T. Phuoc, 'Principles and applications of compact laser–plasma accelerators', Nature Physics 4, 447–453 (2008).
3. J. Hebling, G. Almasi, I. Z. Kozma and J. Kuhl, 'Velocity matching by pulse front tilting for large area THz-pulse generation', Opt. Express 10, 1161–1166 (2002).
4. A. Fallahi, M. Fakhari, A. Yahaghi, M. Arrieta and F. X. Kärtner, 'Short Electron Bunch Generation Using Single-Cycle Ultrafast Electron Guns', Phys. Rev. Accel. Beams 19, 081302 (2016).

Original publication

'Segmented Terahertz Electron Accelerator and Manipulator (STEAM)', Nature Photonics 12, 336–342 (2018). DOI: 10.1038/s41566-018-0138-z

Dongfang Zhang[1,2], Arya Fallahi[1], Michael Hemmer[1], Xiaojun Wu[1], Moein Fakhari[1,2], Yi Hua[1], Huseyin Cankaya[1], Anne-Laure Calendron[1,2], Luis E. Zapata[1], Nicholas H. Matlis[1] and Franz X. Kärtner[1,2,3]

1. Center for Free-Electron Laser Science, DESY, Hamburg, Germany
2. Department of Physics and The Hamburg Centre for Ultrafast Imaging, University of Hamburg, Hamburg, Germany
3. Research Laboratory of Electronics, MIT, Cambridge, Massachusetts, USA

Novel X-ray lenses for nanometre imaging

Efficient focusing with high numerical aperture multilayer Laue lenses

High-resolution X-ray imaging and spectroscopy techniques are rapidly increasing our understanding of the structure, function and mechanisms of materials on the nanometre scale. X-rays are ideally suited for such analysis because of their short wavelength, penetrating power, and elemental and structural sensitivity. One very promising way to achieve a nanometre resolution X-ray microscope is with multilayer-based volume zone plates. Here we report the development of multilayer Laue lenses (MLL), 3D nanostructures prepared from novel materials that focused X-rays well below 10 nm and which were used to form images of samples with high efficiency and high resolution. The lenses focus light through diffraction from thousands of layers that make up the structure. These layers vary in thickness from below 3 nm to 30 nm. This variation in layer thickness causes a disparity in material properties, which makes multilayer preparation very challenging. A material phase transition, which previously hindered our progress in the MLL development, was eliminated by introducing a novel material pair, silicon carbide and tungsten carbide, and opened up a way to X-ray imaging with nanometre resolution.

Multilayer Laue lenses are diffraction-based zone plates based on depth-graded multilayers. The layers in such structures are deposited layer by layer with sub-nanometre precision using magnetron sputtering. As compared to the standard zone plates, used to focus soft X-rays and prepared using a lithography process, large aspect ratios can be easily obtained by slicing a piece of the multilayer to the desired thickness. The large aspect ratio of the layers is required to get reasonable diffraction efficiency for hard X-rays. The layer thickness in these lenses has to be precisely controlled throughout the lens. To ensure that X-rays are always reflected to a common focal point each layer also has to be properly wedged to satisfy Bragg's law at each point in the lens for a collimated incident beam, for example. We developed a novel method to obtain the correct curvature of each layer [1]. A straight-edge mask placed above the substrate during the deposition creates a shadow of the depositing material. The penumbra of this shadow gives a thickness gradient, which can be controlled easily by the mask to substrate distance. The final MLL is cut out of the deposited film using a focused ion beam at the position of the desired gradient profile.

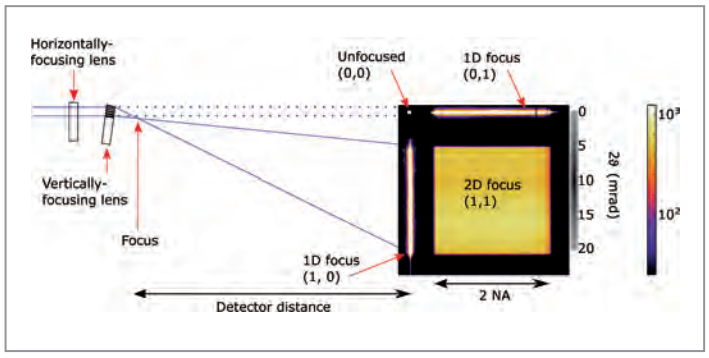


Figure 1

Typical experimental setup with an example of the X-ray lens efficiency measurement performed at the P11 beamline of PETRA III, with recorded intensities shown on a logarithmic color scale. A collimated monochromatic beam diffracts from one MLL focusing X-rays in horizontal and from the orthogonal MLL in vertical direction. The intensity was measured in the far field (~1.4 m from the focus) with a LAMBDA detector with 55 µm pixels.

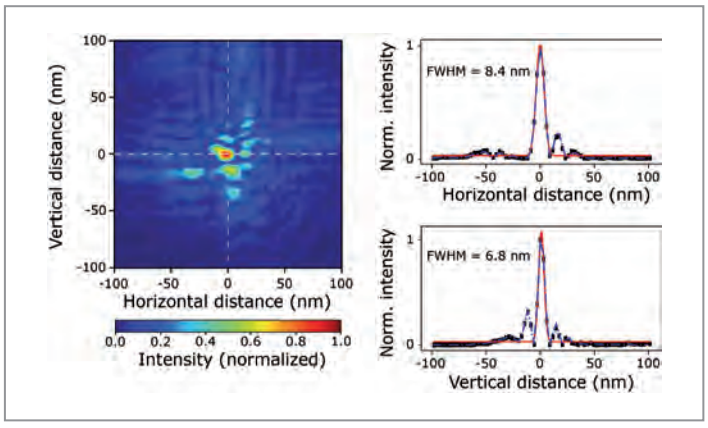


Figure 2

Using ptychography it was possible to reconstruct the intensity distribution of the beam in the MLL focus. Lineouts in horizontal (top right) and vertical directions (bottom right) of the in-focus intensities (black dots) were fitted with Gaussian functions (red lines) with width of 8.4 and 6.8 nm, respectively. The color bar indicates the normalized intensity in the 2D distribution. The measurements were performed at the hard X-ray nanoprobe (HXN) beamline at NSLS II, Brookhaven National Laboratory in Upton, U.S.

Fabricating lenses is still technologically very challenging. A lens that focuses in both transverse dimensions can be created, in principle, by depositing layers onto a wire. We find it easier to deposit layers on flat surfaces, creating a lens that only focuses in one direction, akin to a cylindrical lens. Two of these placed in orthogonal directions to one another can form a 2D focus (similar to Kirkpatrick-Baez mirrors, or two crossed cylindrical lenses). Because any orthogonal misalignment of the two MLL or any error in their relative separation leads to separate astigmatism aberrations, each MLL is mounted on a separate goniometer for optimal alignment (Fig. 1). This requires that both MLL are optimized for the same wavelength λ but have a slightly different focal length. Each MLL is therefore fabricated in a separate deposition run. We prepared MLL, which consisted of as many as 10200 layers with periods varying from 3 nm to 23 nm. MLL were deposited on a flat and very smooth silicon wafer. The deposition process started with the thinnest layers to reduce accumulated roughness, thickness and positioning errors.

The resolution of an MLL is determined by its smallest zone height, similarly to standard zone plates, and in principle multilayers with a period thickness of less than 1 nm can be deposited with state-of-the-art deposition systems. The numerical aperture (NA) of a lens describes the range of angles over which the optic focuses X-rays of a certain wavelength λ. The achievable resolution, or focal spot size, is equal to λ/NA. Here, the NA of the MLL was 0.008, providing a nominal resolution of 6 nm in both transverse directions at a photon energy of 16 keV.

The lenses were made of novel materials, tungsten carbide (WC) and silicon carbide (SiC). This enabled focusing of hard X-rays to 8.4 × 6.8 nm^2 (Fig. 2) with very high efficiency, and also opened a path towards even higher resolution and high-efficiency lenses. The new material pair was critical to overcome a phase error observed in the wavefront of the focused beam of previous lens we made from layers of tungsten (W) and silicon carbide (SiC) [2]. Although we demonstrated 8 nm focus in 1D (at 22 keV) in that case, a phase transition in the microstructure of the W layers at a 3 nm thickness caused an abrupt density and thickness change, splitting the beam into two foci. Replacing W with WC led to a multilayer structure where both SiC and WC remain amorphous throughout the whole range of deposited layer thicknesses. The WC/SiC multilayer structure has further beneficial properties, among others also very high thermal stability [3].

Such lenses can be used in different geometries and imaging modes. As one example, a projection image of a plankton organism, called a diatom, is shown in Fig. 3. The magnification was limited by the pixel size of the detector. Diatoms are unicellular algae with shells that consist of silica with superior material properties — their strength is 10 times that of construction steel, even though they are produced under low temperature and pressure conditions. The structure of these highly complex stable lightweight constructions could so far only be inferred from surface images obtained with a scanning electron microscope or from thin slices studied by high-resolution transmission electron microscopy. Knowing the 3D structure of diatoms may enable us to model and understand the high mechanical performance of these shells and help develop new, environmentally friendly and high performance materials.



Figure 3

Silica shell of a plankton organism called a diatom (*Actinoptychus senarius*), measuring only 0.1 mm across, is revealed in fine detail in the X-ray hologram recorded at a magnification of 5000 times. By placing the diatom just behind the focus in the highly divergent beam and thus fully illuminating it we formed the hologram shown here. A diatom was provided by Christian Hamm (AWI, Bremenhaven) and the measurements were performed at PETRA III (P11 beamline).

Author contact: Saša Bajt, sasa.bajt@desy.de

References

1. M. Prasciolu, A. F. G. Leontowich, J. Krzywinski, A. Andrejczuk, H. N. Chapman and S. Bajt, 'Fabrication of wedged multilayer Laue lenses', Opt. Mater. Express 5, 748-755 (2015).
2. A. J. Morgan, M. Prasciolu, A. Andrejczuk, J. Krzywinski, A. Meents, D. Pennicard, H. Graafsma, A. Barty, R. J. Bean, M. Barthelmess, D. Oberthuer, O. Yefanov, A. Aquila, H. N. Chapman and S. Bajt, 'High numerical aperture multilayer Laue lenses', Sci. Rep. 5, 09892 (2015).
3. M. Prasciolu and S. Bajt, 'On the properties of WC/SiC multilayers', Appl. Sci. 8, 571 (2018).

Original publication

'X-ray focusing with efficient high-NA multilayer Laue lenses', Light: Science and Applications 7, e17162 (2018). DOI: 10.1038/10.1038/lsa.2017.162

Saša Bajt[1], Mauro Prasciolu[1], Holger Fleckenstein[2], Martin Domaracký[2], Henry N. Chapman[2,3,4], Andrew J. Morgan[2], Oleksandr Yefanov[2], Marc Messerschmidt[5], Yang Du[2], Kevin T. Murray[1], Valerio Mariani[2], Manuela Kuhn[1], Steven Aplin[2], Kanupriya Pande[2], Pablo Villanueva-Perez[2], Karolina Stachnik[1], Joe P.J. Chen[6], Andrzej Andrejczuk[7], Alke Meents[2], Anja Burkhardt[1], David Pennicard[1], Xiaojing Huang[8], Hanfei Yan[8], Evgeny Nazaretski[8], Yong S. Chu[8] and Christian E. Hamm[9]

1. Deutsches Elektronen-Synchrotron DESY, Hamburg, Germany
2. Center for Free-Electron Laser Science, DESY, Hamburg, Germany
3. Department of Physics, University of Hamburg, Hamburg, Germany
4. Centre for Ultrafast Imaging, Hamburg, Germany
5. National Science Foundation BioXFEL Science and Technology Center, Buffalo, NY, USA
6. Department of Physics, Arizona State University, Tempe, USA
7. Faculty of Physics, University of Bialystok, Bialystok, Poland
8. National Synchrotron Light Source II, Brookhaven National Laboratory, Upton, NY, USA
9. Alfred-Wegener Institute, Helmholtz Center for Polar and Marine Research, Bremerhaven, Germany

Splitting hard X-ray FEL pulses enables measuring ultrafast dynamics

Nanosecond X-ray photon correlation spectroscopy at free-electron lasers

Understanding ultrafast, atomic-scale fluctuations that determine dynamic processes in equilibrium and non-equilibrium materials is one of the most important challenges in condensed matter science. An important step towards reaching that goal was the first split-pulse X-ray correlation spectroscopy measurement carried out at a hard X-ray free-electron laser (FEL). A state-of-the-art crystal-based split-and-delay system, allowed to split individual FEL pulses and delay them by nanoseconds to capture the dynamics of ultra-small gold nanoparticles on timescales of a few nanoseconds. The experiment paves the way to more complex dynamics experiments of materials on atomic length and even shorter femtosecond timescales.

X-ray photon correlation spectroscopy (XPCS) is a very powerful tool especially for studying slow dynamics of colloids in solution, polymers, capillary wave fluctuations and various magnetic systems. In conventional XPCS measurements, a disordered sample, for instance a colloidal suspension, is illuminated coherently by an X-ray beam and the resulting grainy interference pattern is observed in the far field. This speckle pattern is related to the spatial arrangements of scatterers in the sample. If structural arrangements in the sample change with time, the corresponding speckle pattern will evolve accordingly. Thus, the dynamics of the sample can be traced by measuring temporal intensity fluctuations in the patterns at a fixed length-scale (or wave-vector transfer q) at time τ. Here, τ is the lag time between successive speckle patterns, which in case of conventional XPCS [1] is given by the frame rate of the detector. However, the limited spatial and temporal coherence properties of synchrotron radiation and 2D detector technologies have limited XPCS studies to milliseconds.

Hard X-ray free-electron lasers such as LCLS in Stanford (U.S.), SACLA at SPring-8 (Japan) and the European XFEL in Schenefeld have changed the accessible range fundamentally. Ultra-bright and extremely short (< 100 fs) and fully transverse coherent FEL pulses enabled to capture ultrafast motions of molecules and nanoparticles. The intrinsic time-structure of the FEL sources is still not optimum for studying high-speed dynamical processes via XPCS. Current FELs generate discrete bursts of X-ray radiation at repetition rates ranging typically between 60 to 120 Hz. In the future 4.5 MHz will be routinely accessible (see Fig. 1). Applying such pulse structures results in measuring moderately fast dynamics i.e., not faster than 8.3 ms at LCLS [2], 16.6 ms at SACLA [3] or 220 ns at European XFEL [4].

The split-and-delay technique enables ultrafast XPCS experiments without the need for ultrafast detectors (see Fig. 1) [5].

Here a single FEL pulse is split into two equal parts with femtosecond to nanosecond time delay before impinging on the sample. The coherent scattering from the two pulses is collected during the same exposure of an area detector. If the dynamics in the sample are sufficiently slow compared to the time delay between the two pulses, the contrast – a measure of intensity fluctuations in the speckle pattern – will be equivalent to that of the static sample β_0. However, when the characteristic timescale is comparable or shorter than the time delay, the speckle contrast will decrease in a known manner (see Fig. 1). Thus, the sample dynamics can be directly measured by monitoring the reduction in the speckle contrast as a function of the time delay between two probing pulses.

To demonstrate the feasibility of the split-pulse XPCS approach we have developed a state-of-art split-and-delay

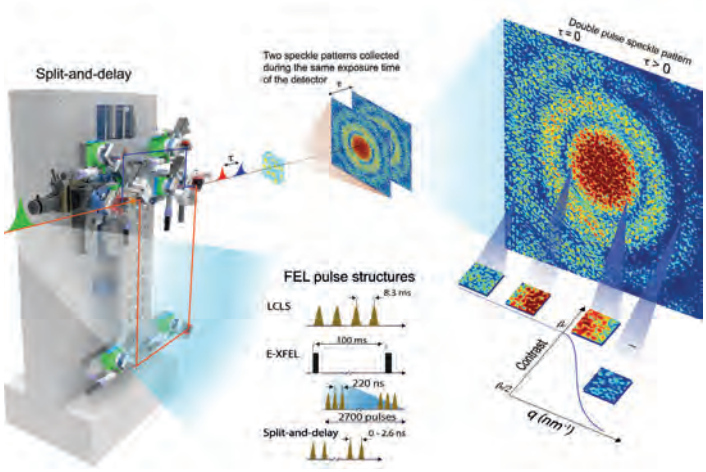


Figure 1

Schematic representation of the split pulse X-ray photon correlation technique (XPCS) at free-electron lasers. The pulse structure of a FEL source is modified via a split-and-delay device which delivers double pulses to the sample over timescales ranging from femtoseconds to nanoseconds.q-dependent sample dynamics is measured from the resulting double pulse speckle pattern via speckle contrast analysis.

system [6,7] and employed it to investigate nanoseconds dynamics of 1-nm-radius spherical gold particles in hexane. The experiment was performed at the XCS instrument using 7.9 keV femtosecond-short FEL pulses from LCLS. Individual pulses were split into two parts and delayed by 1.3 ns and generated double-pulse speckle patterns, which were collected by the pnCCD detector. The challenge in this work was the extraction of speckle contrast from extremely low intensity speckle patterns of about 0.003 photons per pixel. This means that the photon statistics of a typical double-pulse speckle pattern was mostly dominated by a signal of zero photons accompanied by few single and very few double photon events (see Fig. 2).

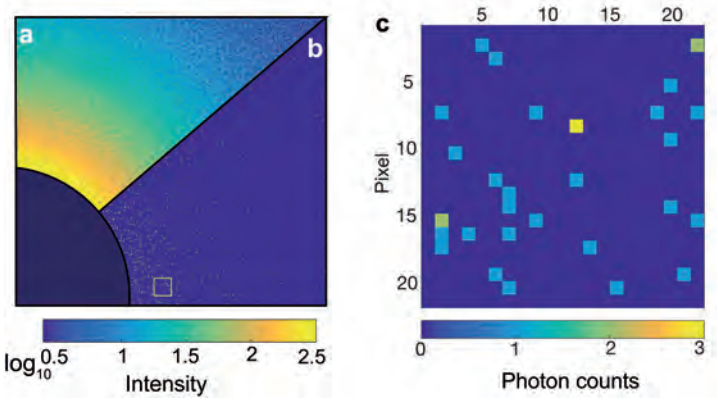


Figure 2

a) Sum of 2.5 x 10^3 scattering patterns. b) Single split-pulse scattering pattern. c) Selected region of interest (shown by the yellow square in b).

We have developed a new statistical analysis of very weak double-pulse speckle patterns via a maximum likelihood fitting approach to simultaneously fit thousands of speckle patterns. The speckle contrast was extracted from the measured split-pulse speckle patterns as a function of scattering vector *q*. Figure 3 shows the measured contrast values of about 0.25 at low *q* values that decrease to about 0.15 at larger values, as expected from the underlying sample diffusive dynamics. Figure 3 shows a fit (solid line) of the diffusion coefficient to the data yielding the free diffusion coefficient $D_0 = (6.1 \pm 2.2) \times 10^{-10}$ m^2 s^{-1} which is in excellent agreement with the calculated self-diffusion coefficient of 1-nm-radius gold nanoparticles in hexane.

The results show that the development of a coherence-preserving split-and-delay instrumentation for hard X-rays in combination with new statistical analysis of double-pulse speckle patterns pave the way for routine split-pulse XPCS studies at FEL sources on more complex systems. This capability is very essential step towards an experimental understanding of equilibrium and non-equilibrium dynamics in a wide variety of materials. Moreover the tracking of atomic scale fluctuations in liquid metals, multi-scale dynamics in water, fluctuations in the undercooled state, heterogeneous dynamic of glass transitions, and atomic scale surface fluctuations is within reach. The successful demonstration of the split-pulse XPCS technique is in particular interesting for future European XFEL experiments.

Author contact: Wojciech Roseker, wojciech.roseker@desy.de

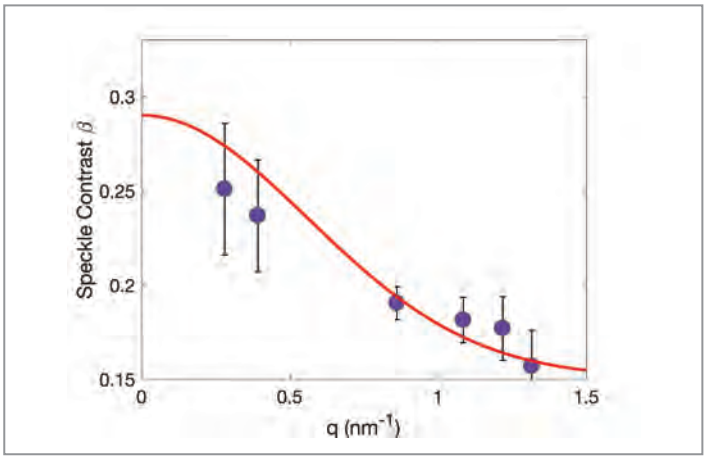


Figure 3

Speckle contrast revealing nanosecond dynamics. Scattering vector dependent contrast decay caused by diffusing gold nanoparticles and measured via the split-pulse XPCS method with two X-ray pulses separated by 1.3 ns. The red line corresponds to the model and yields the free particle diffusion coefficient $D_0 = (6.1 \pm 2.2)\ 10^{-10}$ m^2 s^{-1}.

References

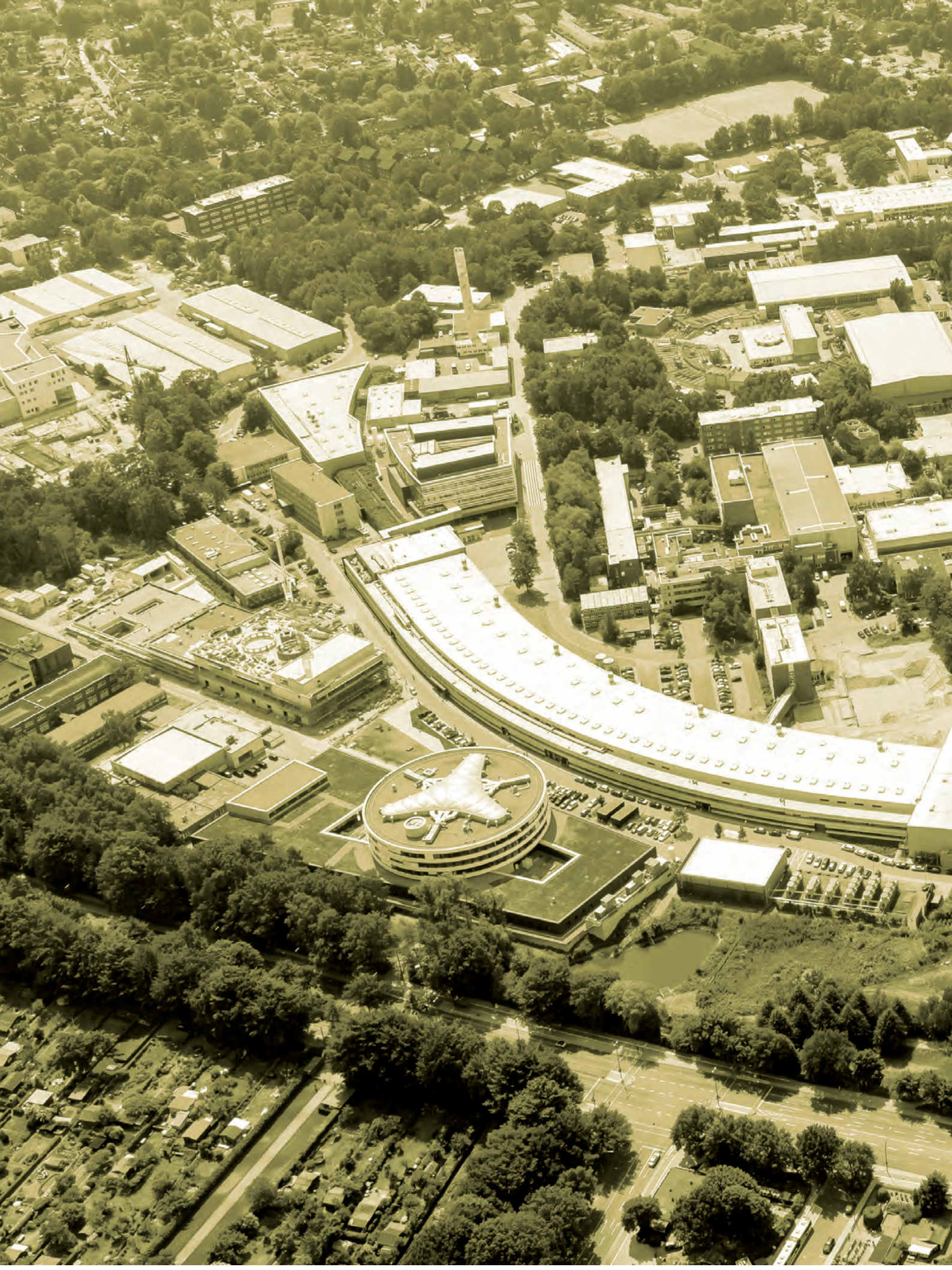
1. G. Grübel and F. Zontone, 'Correlation spectroscopy with coherent X-rays', J. Alloy Compd. 362, 3 (2004).
2. J. Carnis et al., 'Demonstration of Feasibility of X-Ray Free Electron Laser Studies of Dynamics of Nanoparticles in Entangled Polymer Melts', Sci. Rep. 4, 6014 (2014).
3. F. Lehmkühler et al., 'Sequential Single Shot X-ray Photon Correlation Spectroscopy at the SACLA Free Electron Laser', Sci. Rep. 5, 17193 (2015).
4. T. Tschentscher et al., 'Photon Beam Transport and Scientific Instruments at the European XFEL', Appl. Sci. 7, 592 (2017).
5. G. Grübel, et al., 'XPCS at the European X-ray free electron laser facility', Nucl. Instr. and Meth. B 262, 357 (2007).
6. W. Roseker et al., 'Performance of a picosecond x-ray delay line unit at 8.39 keV', Opt. Lett. 34, 1768 (2009).
7. W. Roseker et al., 'Development of a hard X-ray delay line for X-ray photon correlation spectroscopy and jitter-free pump–probe experiments at X-ray free-electron laser sources', J. Synchr. Rad. 18, 481 (2011)

Original publication

'Towards ultrafast dynamics with split-pulse X-ray photon correlation spectroscopy at free electron laser sources', Nature Communications 9 1704 (2018), DOI: 10.1038/s41467-018-04178-9

Wojciech Roseker[1], Stephan Hruszkewycz[2], Felix Lehmkühler[1,3], Michael Walther[1], Horst Schulte-Schrepping[1], Sooleyhoong Lee[4,5], Taito Osaka[6], Lothar Strüder[7], Robert Hartmann[6], Marcin Sikorski[8,11], Sanghoon Song[8], Aymeric Robert[8], Paul H. Fuoss[2,12], Mark Sutton[9], G. Brian Stephenson[2] and Gerhard Grübel[1,3]

1. Deutsches Elektronen-Synchrotron DESY, Hamburg, Germany
2. Materials Science Division, Argonne National Laboratory, Argonne, USA
3. The Hamburg Centre for Ultrafast Imaging, Hamburg, Germany
4. Frontier in Extreme Physics, Frontier in Extreme Physics, KRISS, Daejeon, Korea
5. Department of Nanoscience, University of Science and Technology, Daejeon , Korea.
6. Department of Precision Science and Technology, Osaka University, Suita, Osaka, Japan
7. PNSensor GmbH, München, Germany
8. Linac Coherent Light Source, SLAC National Accelerator Laboratory, Menlo Park, USA
9. Department of Physics, McGill University, Montreal, Canada
10. Present address: RIKEN SPring-8 Center, Sayo-gun, Japan
11. Present address: European XFEL, Schenefeld, Germany
12. Present address: SLAC National Accelerator Laboratory, Menlo Park, USA





Light Sources

> FLASH 90

> PETRA III 94

FLASH

Right in time – better synchronisation and other upgrades in 2018

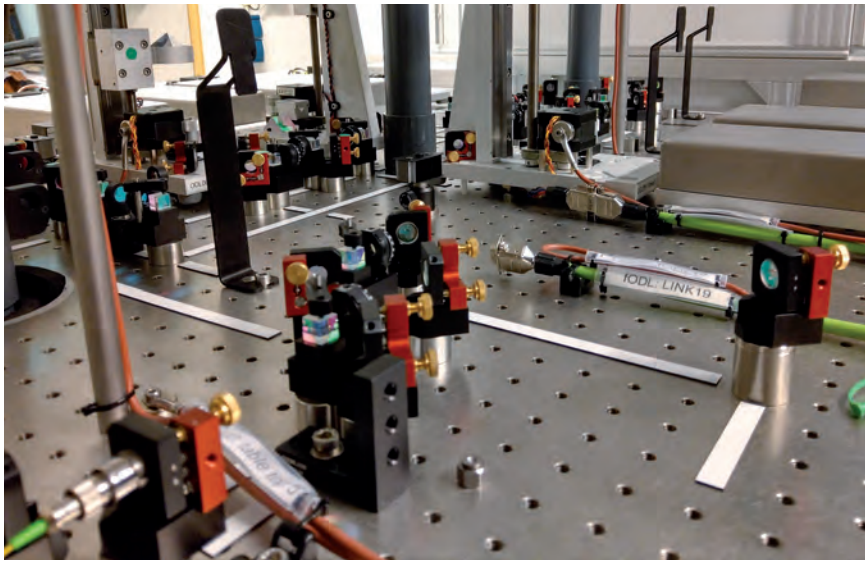




Figure 1

(left) Main optical table in the synchronisation hutch with new free-space laser distribution optics, optical delay lines and link stabilising units (LSUs, the grey boxes at the right outer edge of the laser table). (right) New BAM units as they are installed at FLASH and the European XFEL (this photo) – four 40 GHz pickups (one of them pointing towards the camera here) in a vacuum-tight body, along with recesses in between the pickups for survey fiducials.

2018 was a very busy and productive year at FLASH, seeing many new facility features, a large variety of innovative user experiments and a high number of publications. Roughly one third of already 25 publications until the beginning of December stems from the permanent endstation CAMP, where the experiments are in full swing meanwhile.

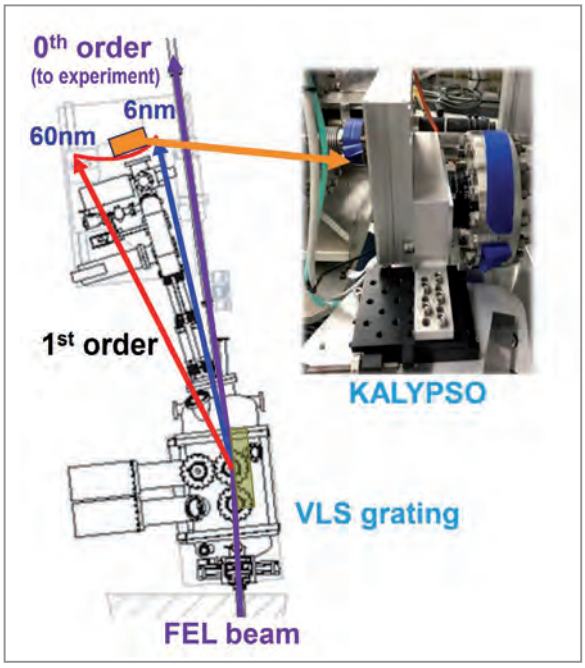
At FLASH, the beamtime for users in 2018 was allocated in two user periods and six beamtime blocks. The 11th user period took place from January to June and the 12th from July to December. FLASH delivered in 2018 in total 4188 hours (FLASH1) and 2268 hours (FLASH2) for user operation – including time for setup, tuning and contingency – with an uptime of 97 % into the two experimental halls 'Albert Einstein' (FLASH1) and 'Kai Siegbahn' (FLASH2). Since FLASH2 started operation for users in April 2016, 60-70 FLASH proposals per year are submitted regularly. FLASH has two annual calls for proposals which are typically due on 1 April and 1 October.

In course of the last year, many updates and new features were added to the FLASH user facility: On the machine side, the laser-based synchronisation systems as well as the electron beam arrival monitors (BAMs) were upgraded. The optical pump-probe laser in the FLASH1 hall is now also available at the Raman spectrometer endstation at beamline PG1 enabling time-resolved RIXS investigations. Furthermore, KALYPSO, a fast pixelated line detector has been successfully applied as an online monitoring device to record the individual spectra of all free-electron laser (FEL) pulses in a train and to optimise the accelerator settings based on these data. Moreover, an experiment at the reaction microscope (ReMi) endstation at beamline FL26 was the first to use the laser pulses from the new FLASH2 pump-probe laser.

Upgrade of optical synchronisation and bunch arrival time measurement systems

FLASH is equipped with a laser-based synchronisation system [1] based on the distribution of an optical pulse train using actively length-stabilised optical fibres to provide a femtosecond-precise time reference across the accelerator facility. This optical reference is used for electron bunch arrival time measurements at different locations and the synchronisation of external laser systems, such as the electron gun photocathode lasers and the pump-probe lasers for user experiments.

In summer 2018, the optical synchronisation system has been upgraded significantly, beginning with the synchronisation laser laboratory infrastructure (Fig.1, left) and adapting the state-of-the-art computing architecture for controls, the implementation of a new fibre link stabilisation scheme for



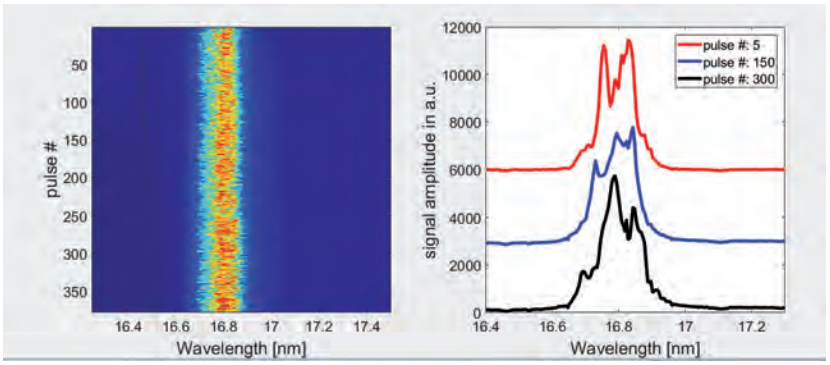


Figure 2

(left) Sketch of the VLS Online Spectrometer, reflecting most of the FEL intensity in 0th order towards the experiment while using some 1-10 % of the intensity to measure spectra online in 1st order, e.g. with the KALYPSO detector. (right) Series of spectra of a full pulse train of – in this case – 380 bunches from the KALYPSO detector. The three individual spectra at right have been offset vertically for better distincition.

improved performance and reliability, as well as the preparation for future accelerator module radio-frequency stabilisation. For soft X-ray/optical pump-probe user experiments both pump-probe laser systems at FLASH1 and FLASH2 were equipped with new optical cross-correlators for a femtosecond-level lock to the reference pulse train. Furthermore, laser systems for temporal photon pulse diagnostics, as well as those for accelerator seeding studies were connected to the system with new fibre links and optical cross-correlators.

In addition to these upgrades of the synchronisation system itself, the existing electron bunch arrival monitors have been upgraded to new versions which are also installed at the European XFEL (Fig. 1, right). Their enhanced electro-optical front-end and the usage of the new computing architecture will improve the temporal resolution for very low electron bunch charges which are required for short-pulse operation, as well as the overall reliability. These improvements are particularly important when coping with the often quite different parameters of the electron bunch trains, which are delivered to the FLASH1 and FLASH2 undulator beamlines. In addition, the modifications will enable an upgrade of the fast, intra-train arrival time feedback in order to stabilise both electron bunch trains delivered to FLASH1 and FLASH2 individually and also simultaneously. Moreover, the upgraded BAM hardware will allow for a nanosecond-range, sub-picosecond resolution monitoring of the timing, what complements the existing streak camera-based measurement for establishing coarse temporal overlap and compensating slow timing drifts.

In summary, the combination of high-resolution electron bunch arrival time measurements, longitudinal acceleration stabilisation loops and highly precise laser synchronisation will routinely improve the timing jitter to the few-ten femtosecond level with minimum temporal drift for user experiments.

KALYPSO: a fast line detector for MHz readout of FEL single pulse spectra

A novel line detector named KALYPSO (KArlsruhe Linear arraY detector for MHz rePetition-rate SpectrOscopy) in version 2.1 [2] was implemented at the variable line spacing (VLS) online spectrometer [3] at FLASH (Fig. 2, left) for sampling all the spectra of individual pulses in a train. The KALYPSO detector has been developed in a collaboration between the Karlsruhe Institute of Technology (KIT), the Paul-Scherrer-Institute (PSI) in Switzerland and DESY. Data transfer of the KALYPSO detector is handled via direct memory access (DMA), based on novel field-programmable gate array (FPGA) readout cards in MTCA.4 crate standard for electronic modules. In the front-end, the detector at FLASH uses Si strip detectors from PSI with 256 pixels of 50 µm width and

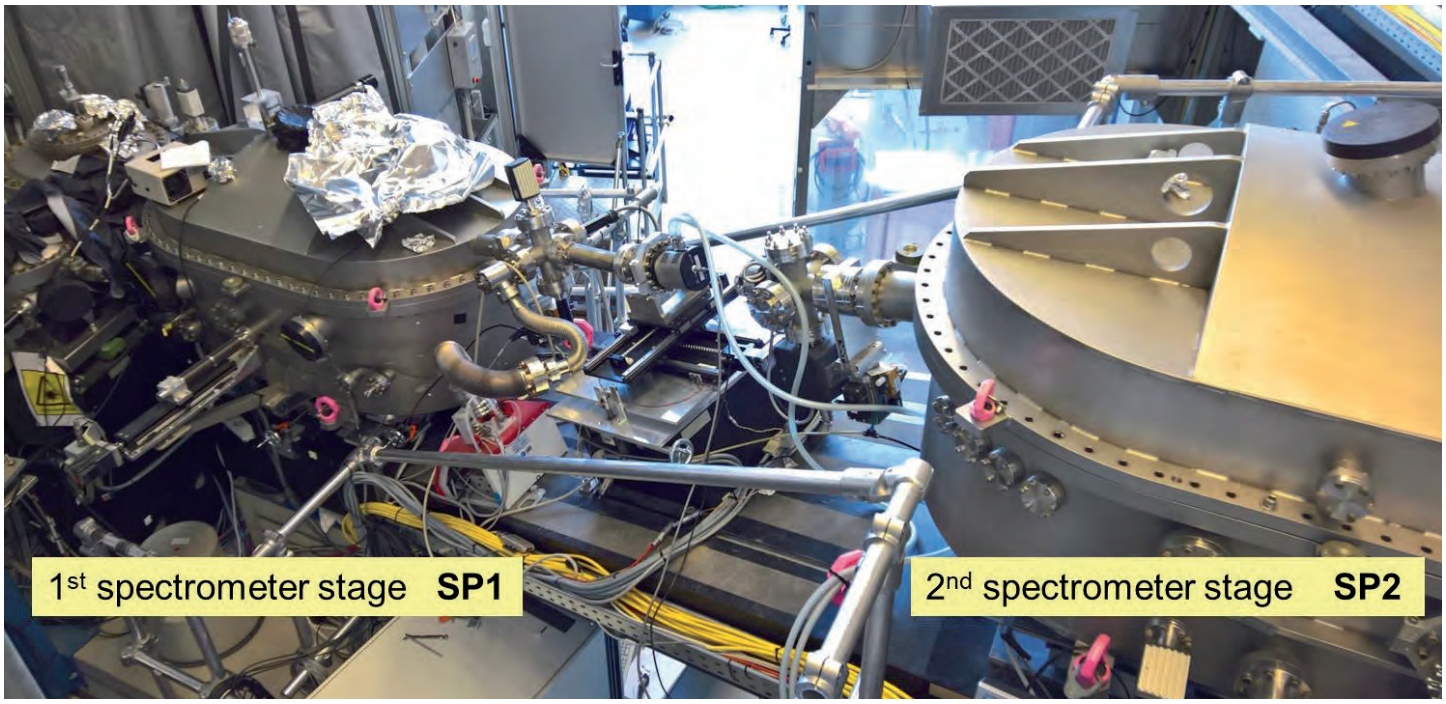


Figure 3

RIXS spectrometer with two grating spectrometer stages at FLASH1 beamline PG1.

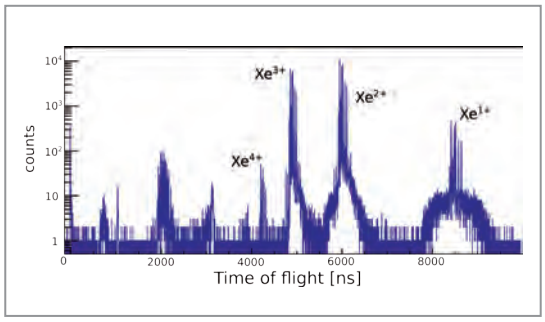
10 mm height, which are sensitive in a wavelength range from 200 nm to 1050 nm, and the GOTTHARD [4] ASIC chip, also from PSI, for readout. The KALYPSO detector was integrated into the data acquisition (DAQ) system at FLASH and is triggered by a MTCA trigger signal, such that it allows to record the spectra of several hundred FEL pulses in a pulse train at 1 MHz readout rate for a full line/spectrum. The image of a sequence of spectra, one below the other (Fig. 2, right) is available on demand in the FLASH control room. It can be used as a very efficient tool for the FLASH operators during machine tuning to keep all individual FEL pulses within a narrow wavelength band close to the inherent ~1 % bandwidth of an individual pulse. The information about the spectral shape of individual pulses can also be used in user experiments to improve the spectral resolution [5].

Time-resolved RIXS at beamline PG1

In mid of 2018, the transport line for the FLASH1 optical pump-probe laser was installed at the XUV double stage Raman spectrometer endstation of the PG1 monochromator beamline branch. This upgrade will soon enable time-resolved resonant inelastic X-ray scattering (RIXS) experiments at the transition metal M-edges (20 - 200 eV) with an energy resolution of < 20 meV (using both spectrometer stages) and a time resolution of < 250 fs (FWHM). With such a resolution, the double stage Raman spectrometer will provide information about dynamic properties of solid matter approaching the Heisenberg limit. The FLASH1 pump-probe laser has a fundamental wavelength of 800 nm. By non-linear optical frequency conversion, further wavelengths of 400 nm and 267 nm for optical pump – XUV probe measurements can be generated close to the experiment. The first monochromator stage (SP1) with an energy resolution < 60 meV (FWHM) is already operational and will have been used for first experiments at the end of 2018. After some further experiments in 2019, implementation of the second monochromator stage (SP2) is planned for the winter shutdown 2019/2020.

FLASH2 pump-probe laser now available at the reaction microscope at beamline FL26

In mid September 2018, the very first reaction microscope (ReMi) test experiment with the new FLASH2 pump-probe laser was successfully performed. The goal was to overlap the foci of the pump-probe laser and the FEL in space and time within the gas-jet target of the reaction microscope and to monitor the production of high charge states in Xenon. After multi-photon ionisation of Xe by the FEL, a subsequent IR laser pulse with sufficiently high intensity leads to a yield enhancement of high charge states in contrast to the opposite case, where the IR-pulse is followed by the FEL pulse. In the experiment, the yields of Xe^{2+} and Xe^{3+} ions and, in particular, the ratio between both as a function of the FEL-probe laser delay were monitored. This first commissioning experiment allowed to test the overall functionality of the setup and in addition to get a rough estimate for the temporal resolution. For the latter, the data analysis including the beam arrival (BAM) data from the



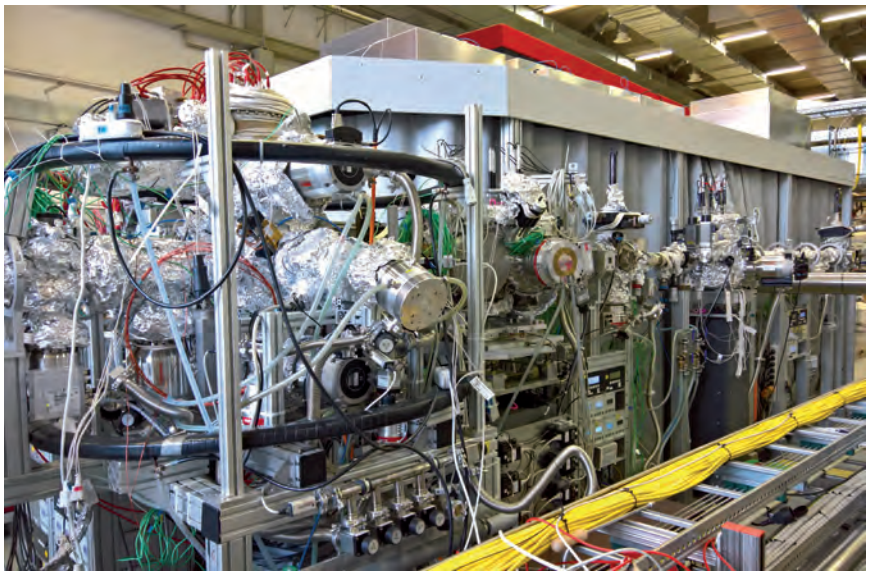


Figure 4

(left) Mass spectrum of Xenon ions after multiphoton ionisation by the FEL and the pump-probe laser. (right) ReMi part of beamline FL26 with differential pumping at right, the Reaction Microscope at left and the tent for the optical laser behind both.

FLASH accelerator is currently well underway. During the experiment, it could be shown that the achieved probe-laser intensity alone was sufficiently high to create up to Xe^{2+} ions, which means that an IR laser intensity of about 10^{14} W/cm^2 has been reached. The IR pulse-duration was measured to be 21 fs (FWHM) or better, this is at the limit of the detector resolution. It is also mentionable that a spatial and temporal overlap stability over more than 12 hours has been achieved. This is another proof that the optical laser and its transport into the ReMi experiment were well prepared for the first user experiment in November 2018.

The long term future 'FLASH2020+'

Within the overall DESY strategy process for the next decade 'DESY2030' several long-term goals for the future of FLASH have been defined. They are strongly based on users' demands for a high repetition rate XUV and soft X-ray FEL facility formulated at the FLASH user workshop in September 2017.

The FLASH strategy 'FLASH2020+' is based on an envisioned development programme of the two FEL lines and the accelerator which includes

- the operation of two independent FEL lines (FLASH1 and FLASH2) with variable magnet structures (undulators) for new lasing concepts and 'seeding' with a high repetition rate
- the extension of the wavelength range of the fundamental from carbon across nitrogen to the oxygen K-edge, in order to reach these elements important for energy research and to cover the whole water window for biology related reseach
- flexible pump-probe schemes for time-resolved experiments
- variable polarisation for the investigation of, e.g., the light-induced switching of magnetic storage media
- shortest pulses up to the attosecond range.

Currently the FLASH team is preparing a conceptual design report (CDR) for 'FLASH2020+'. The concepts and the performance goals will be discussed with the users in a satellite workshop at the DESY Photon Science Users' Meeting 2019.

Contact: Rolf Treusch, rolf.treusch@desy.de

References

1. S. Schulz et al., 'Femtosecond all-optical synchronization of an X-ray free-electron laser', Nature Communications 6, 5938 (2015); http://dx.doi.org/10.1038/ncomms6938
2. L. Rota et al., 'KALYPSO: linear array detector for high-repetition rate and real-time beam diagnostics', Nucl. Instr. and Meth. A, in press ; https://doi.org/10.1016/j.nima.2018.10.093
3. G. Brenner et al., 'First results from the online variable line spacing grating spectrometer at FLASH', Nucl. Instr. and Meth. A 635, 99–103 (2011); http://dx.doi.org/10.1016/j.nima.2010.09.134
4. A. Mozzanica et al., 'The GOTTHARD charge integrating readout detector: design and characterization', JINST 7, C01019 (2012); https://doi.org/10.1088/1748-0221/7/01/C01019
5. S. Palutke et al., 'Spectrometer for shot-to-shot photon energy characterization in the multi-bunch mode of the free-electron laser at Hamburg', Rev. Sci. Instrum. 86, 113107(2015); http://dx.doi.org/10.1063/1.4936293

PETRA III

New high-energy beamlines for PETRA III



Figure 1

The 4 m long in-vacuum undulator PU21 installed at the Swedish Materials Science beamline P21 in the experimental hall 'Ada Yonath' (left). View into the vacuum vessel showing the magnet structure (right).

The year 2018 was a very busy one. Five beamlines of the PETRA III extension are now in user operation: the HAXPEX beamline P22, the nano-diffraction beamline P23, the chemical crystallography beamline P24 and beamlines P64 and P65 for absorption spectroscopy applications. Commissioning of the Swedish Materials Science beamline P21 has started in September 2018, it will be available for users in 2019.

In 2018, PETRA III beamlines hosted nearly 2600 individual users. In total, 20 beamlines are now available for user proposals. The PETRA III operation was split in two periods in 2018, one from end of March until mid of July and a second from beginning of September until end of December. Overall, 3380 hours were available for proposals of users at beamlines P01-P14, P24, P64 and P65. Beamlines P22 and P23 went into user operation only after the summer shutdown. For all these beamlines, a record number of 1062 proposals were submitted in 2018. In addition, 211 proposals have been collected for the EMBL beamlines P12-P14.

Machine operation and beamline frontends

Compared to last year the availability of the PETRA III storage ring was lower (96.5 %) with a mean time between failures of 47 hours (as of 10 December 2018). After the last winter shutdown the operation for users was successfully resumed with very short commissioning. Although the storage ring was running well for most of the time with weekly availabilities reaching 98 – 100 %, three uncorrelated incidents unfortunately led to a significant reduction of the overall availability: the repair of a leaking ring current monitor, a major fault of a central power station, the failure of a synthesizer of the storage ring. These problems are now solved.

As in the previous years, different bunch filling modes in the PETRA III storage ring were offered: a 'time resolved' mode with 40 bunches and 'continuous' mode with 480 bunches, both with approximately the same share. This bunch mode distribution has proven to be optimal for providing a maximum number of timing mode shifts while minimising the radioactive activation of ring components as well as radiation damage of undulators. As an exception, an 80 bunch mode was operated for 10 days in October to enable experiments with a new time-of-flight spectrometer at beamline P22.

In the shutdown period at the beginning at 2018, the first *in-vacuum* undulator at PETRA III was installed at the

Swedish Materials Science beamline P21 (Fig. 1). The new device with a period length of 21 mm and a total length of 4 m is optimised for generating bright high energy X-rays in the range 40 – 150 keV.

The P21 side station has a shorter canted standard undulator. The storage ring operation has been optimised with respect to optimal conditions at both insertion devices while keeping the beam position stable at all other beamlines during undulator movements.

The winter shutdown began on 21 December 2018 for a period of 12 weeks to install another *in-vacuum* undulator of the same type at the HZG materials science beamline P07 and to prepare the frontends of beamlines P62 and P63 in the PETRA III experimental hall 'Paul P. Ewald'.

Beamlines and experiments

In the PETRA III experimental hall 'Max von Laue', first experiments were performed at the new liquid jet instrument at beamline P04 (Fig. 2) which has been installed in cooperation with the Fritz-Haber-Institut der Max-Planck-Gesellschaft (Berlin) to investigate chiral molecules in liquids with photoelectron circular dichroism. The newly commissioned additional beamline branch allows installing new instruments while experiments are ongoing at the other branch. Furthermore, using both branches allows splitting of beamtimes into day and night shifts to alternately run different experiments efficiently during the same beamtime period. This is especially attractive in cases where time consuming sample preparation is required.

In the experimental hall 'Ada Yonath', significant progress has been made at the Swedish Materials Science beamline (P21) which is the longest beamline at PETRA III with a total length of 165 m from the undulator source to the SAXS detector at the end of the diffraction hutch. The beamline optics, media infrastructure, radiation safety and instrumentation were completed until the summer shutdown 2018 and the first beam was available in the main branch and the side station at the beginning of September. The diffraction station of the main beamline branch specifically benefits from the performance of the high-energy *in-vacuum* undulator. One field of application is tomography for 3D characterisation of bulk materials. Here, the undulator beam profile should cover the whole sample and a homogeneous intensity distribution is advantageous. This can be achieved by tuning the undulator gap setting to even harmonics, in particular of low order, which yields a relative wide and flat intensity profile. It then may be of interest to 'zoom-in' to points of interest by diffraction with a focused beam. For this case the highest on-axis brightness is produced by odd harmonics (Fig. 3). The change-over between the two settings can be as fast as a few seconds and is therefore also suited for *in situ* experiments.

Using the experimental configuration shown in Fig. 4 (top), a first diffraction pattern (bottom) was recorded on a reference sample with the cryo-cooled double Laue monochromator

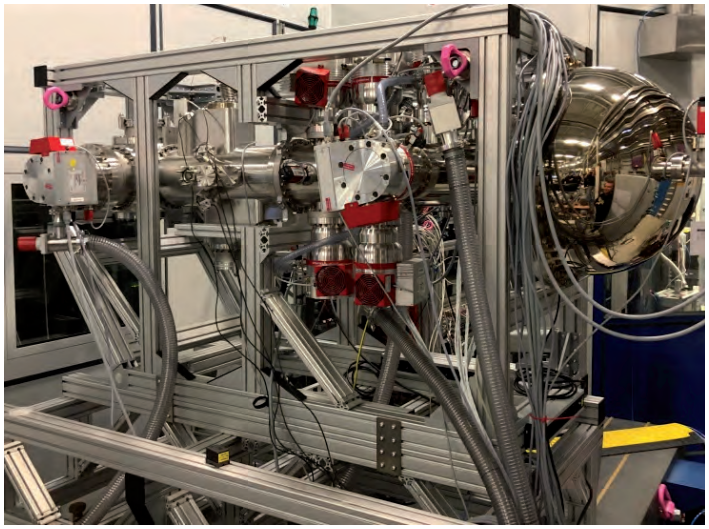


Figure 2

Photoelectron dichroism setup for liquid jets at branch 1 of the variable polarisation XUV beamline P04 at PETRA III.

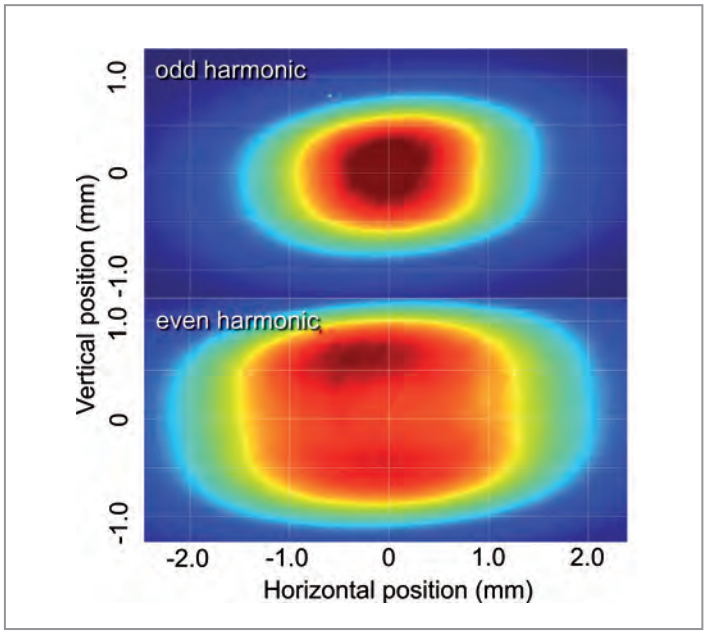
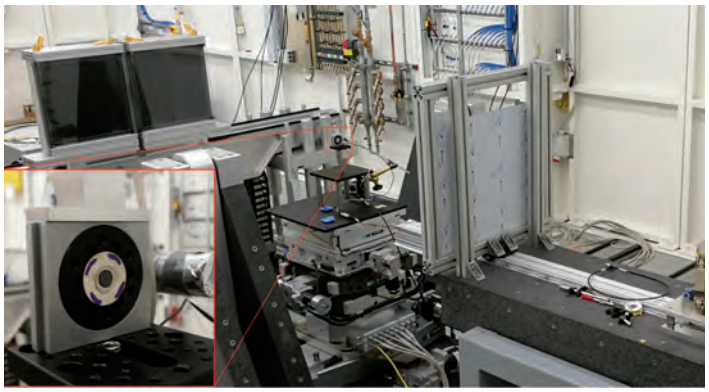
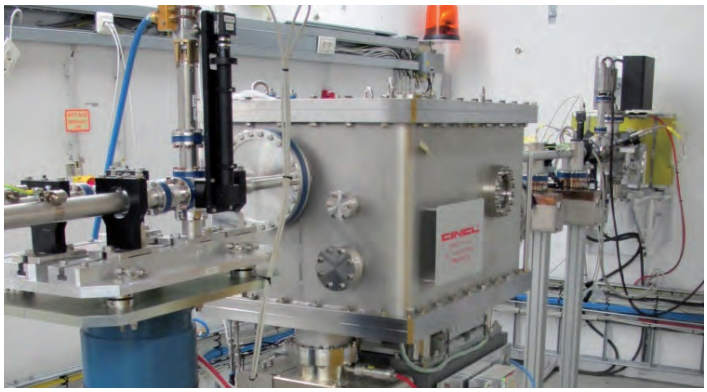
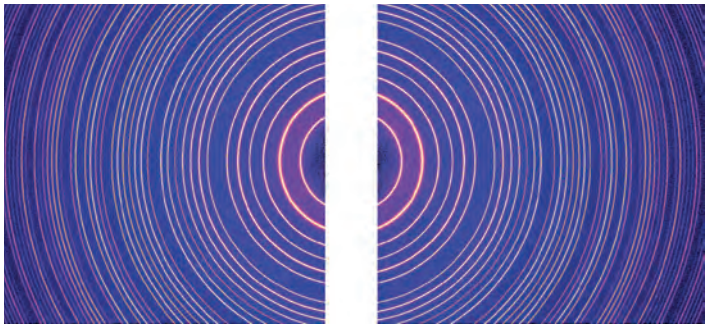


Figure 3

Measured spatial intensity profile (67.4 keV) of the *in-vacuum* undulator of beamline P21.2 at 102 m from the source: 7th harmonic at 8.82 mm gap (top) and 8th harmonic at 7.93 mm gap (bottom).







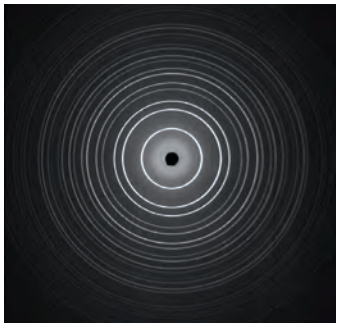


Figure 4

(Top) Setup at beamline P21.2 to record the first diffraction pattern from a sample located 150 m downstream from the *in-vacuum* undulator. The gap between the two area detectors enables simultaneous SAXS measurements. (Bottom) Diffraction pattern of a 0.9 mm thick NIST SRM660b standard LaB_6 powder at 88 keV with two detectors placed 2 m away from the specimen (beam size 1 mm^2). The outermost diffraction ring corresponds to a d-spacing of 0.6 Å.

Figure 5

(Top) Single-bounce Laue monochromator at the PETRA III beamline P21 (side station). (Bottom) Diffraction pattern of Si powder taken at 100 keV using a 2D Si-detector (sample to detector distance 1 m).

tuned to a photon energy of 88 keV. Since then the beamline main branch and the side station (Fig. 5) are in the commissioning phase. First users from Sweden will have performed initial test experiments with surface diffraction before the winter shutdown.

The new hard X-ray photoelectron spectroscopy (HAXPES) PETRA III beamline P22 is in user operation since September 2018. The instruments formerly operated in hutch 3 of beamline P09 have been relocated to P22. In addition to the established HAXPES spectroscopy and energy filtered HAXPEEM instruments (implemented in collaboration with Universität Würzburg and Forschungszentrum Jülich), two new setups were commissioned and operated for user experiments in 2018: (1) the ambient-pressure instrument POLARIS (developed and built by Stockholm University) is dedicated to HAXPES investigations of catalytic processes on surfaces and interfaces under realistic conditions, i.e. pressures > 1 bar and temperatures up to 450 °C during the measurement. (2) a momentum microscope working in the HAXPES regime (designed and built by Johannes Gutenberg-Universität Mainz), which is capable of detecting photoelectrons with kinetic energies > 6 keV and high angular resolution < 0.1°. Its large k-space acceptance allows for simultaneous full-field imaging of many Brillouin zones. This is combined with time-of-flight electron energy recording, yielding maximum parallelization of data acquisition. First experiments at P22 (Fig. 6) have shown that tomographic k-space mapping previously demonstrated in the soft X-ray regime works equally well in the hard X-ray range (Fig. 7). The combination of the PETRA III timing modes and the high X-ray brilliance of P22 allow full 3D bulk Brillouin zone mapping in just a few hours.

At the *in situ* and nano diffraction beamline P23 user experiments also began in September 2018. Some further commissioning will be required to fine tune the optical parameters in order to reach full specifications. Sub-micron focusing in the vertical direction has already been accomplished using compact refractive Be lenses. The beamline capabilities have been presented and discussed at a user workshop in January 2018. A setup with a user supplied *in-operando* cell for surface X-ray diffraction studies, mounted on the diffractometer, is shown in Fig. 8. It has been used for investigation of electrochemical parameters and reciprocal space mapping during catalytic processes. The diffractometer in the heavy load configuration can accommodate bulky sample environments with a weight of up to 150 kg.

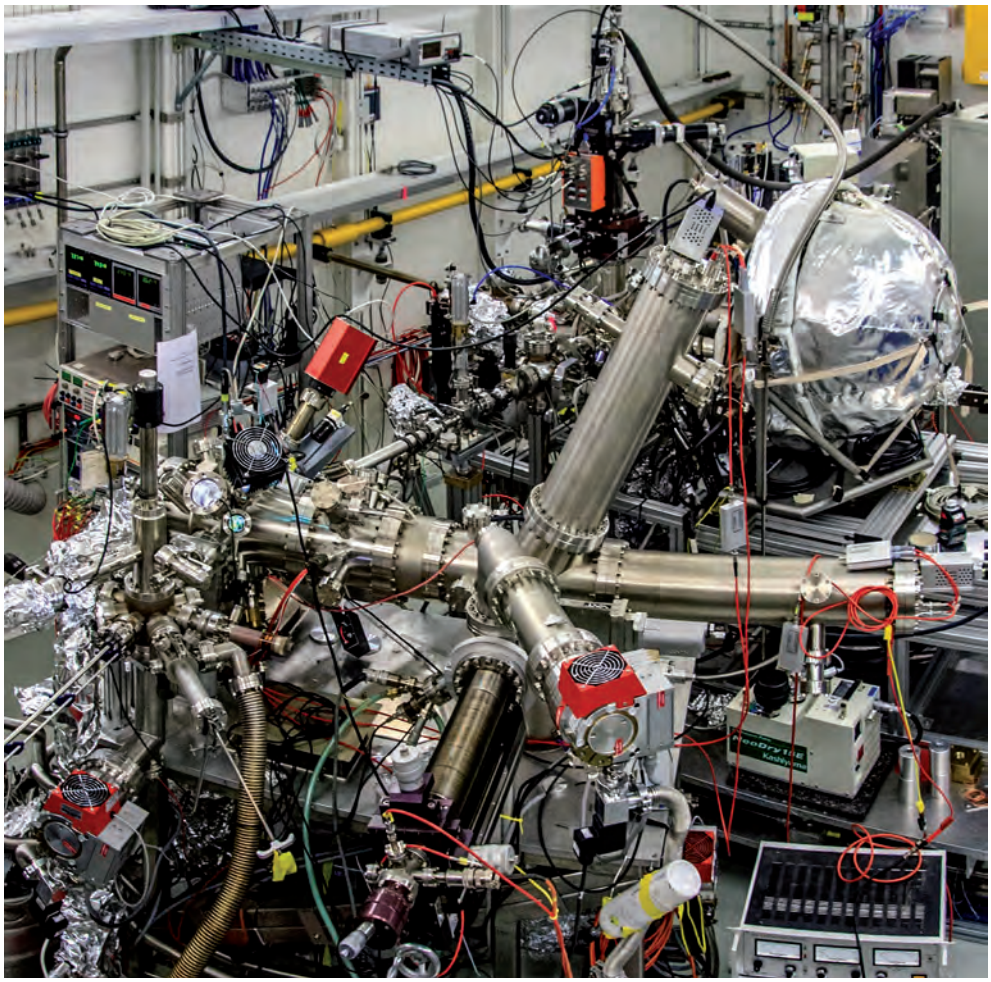


Figure 6

New HAXPES k-space microscope at PETRA III beamline P22 using time-of-flight electron energy discrimination.

Regular operation for users at the newly commissioned chemical crystallography PETRA III beamline P24 began in April 2018 as planned. The beamtime applications are distributed more or less evenly between the two instruments, the heavy load Kappa diffractometer in the first hutch for X-ray diffraction studies in complex sample environments, and the 4-circle diffractometer for small molecule crystallography in the second hutch.

Further new beamlines are currently being constructed in the PETRA III experimental hall 'Paul P. Ewald'. The beamline frontend and the optics and experiment hutches have been built at the high-energy wiggler beamline P61 which is shared between HZG (EH1) and DESY (EH2) (Fig. 9). The hutches are made of up to 50 cm thick heavy concrete for radiation shielding of the powerful white beam. The beam will be filtered at low energies (< 30 keV) to manage the heat

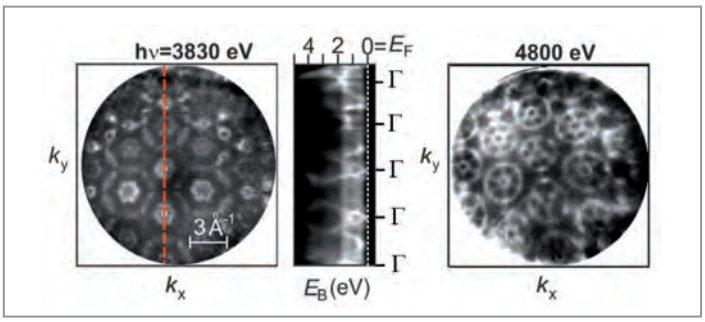


Figure 7

Measured at beamline P22: Large-area k-space map for the d-bands of Re (hν = 3830 eV, 4800 eV) at low temperatures (20K) imaging multiple Brillouin zones (BZ). The E_B(k) band dispersion for 3830 eV (centre) is obtained from a k_x cut along the dashed line (left) and reflects the repeated BZ structure.

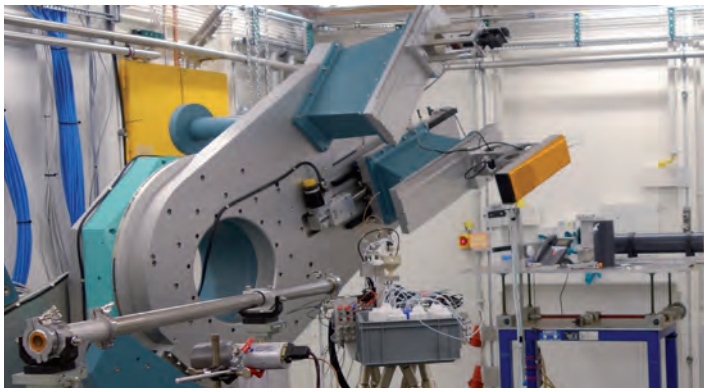


Figure 8

Setup for electrochemistry experiments at the *in situ* and nano diffraction PETRA III beamline P23.



Figure 9

View into the PETRA III experimental hall 'Paul P. Ewald' showing the newly installed hutches of the high-energy wiggler beamline P61. The installation of the anomalous SAXS (ASAXS) beamline P62 will start in January 2019.

load, and will have significant flux up to even 200 keV. It is ideal for energy-dispersive X-ray diffraction experiments in materials and earth science research, which will in particular be carried out in the downstream hutch (EH2) on materials under extreme conditions of high pressures and temperatures using the 6 ram large volume press (LVP) operated by DESY, in collaboration with the Bavarian Research Institute of Experimental Geochemistry and Geophysics (BGI). The LVP has already been in use for off-line materials synthesis. It will get a major upgrade in 2019 to operate three modes: isostatic compression (current mode), anisotropic compression (in vertical direction) on cubic assemblies and uniaxial compression using only vertical rams. The remaining beamline optics and instrumentation is currently being constructed, first beam is expected in summer 2019.

In the still open sector 2 (Fig. 9) a new PETRA III beamline P62 for small-angle X-ray scattering (SAXS) will be constructed. The science case along with suitable design parameters were discussed with the user community during a workshop at DESY in April 2018. The beamline will provide a variety of SAXS techniques, including anomalous SAXS (ASAXS). The energy range will be 3.5 – 35 keV covering the K and L_3 absorption edges of elements $Z \geq 18$. The technical



Figure 10

Experimental hutch of the VUV Beamline P66 located on top of the PETRA III ring tunnel, adjacent to the experimental hall 'Max von Laue'.

design has been reviewed by international experts in September 2018. The beamline frontend and the optics and experiment hutches of P62 will be installed at the beginning of 2019, first beam for commissioning is expected in spring 2020.

Progress has also been made for PETRA III beamline P66 (the former 'Superlumi' at DORIS III) for time-resolved vacuum ultraviolet (VUV) spectroscopy. The bending magnet source of this beamline lies in a storage ring section outside

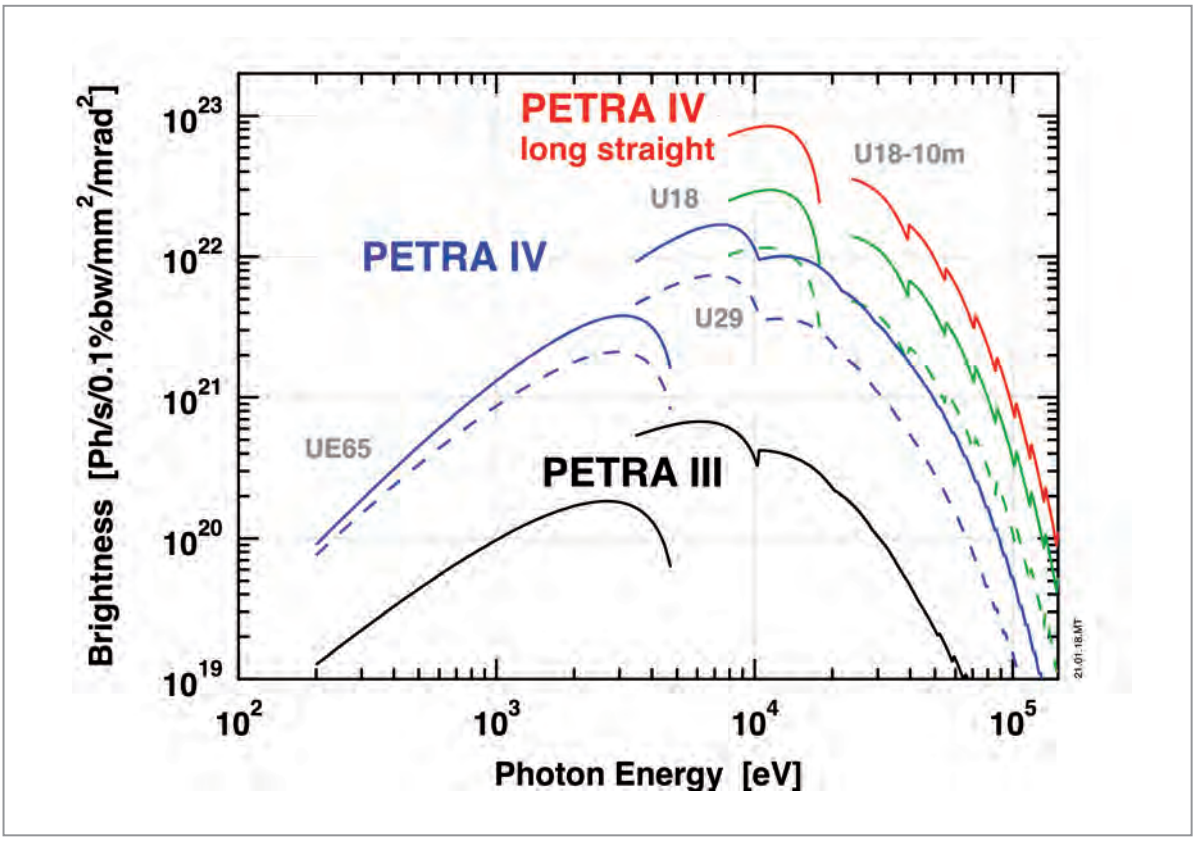


Figure 11

Spectral brightness of PETRA IV (blue, green and red) compared to PETRA III (black). With optimised insertion devices, PETRA IV will exceed the PETRA III brightness by about a factor of 200 at 10 keV and by more than a factor of 400 at energies above 60 keV.

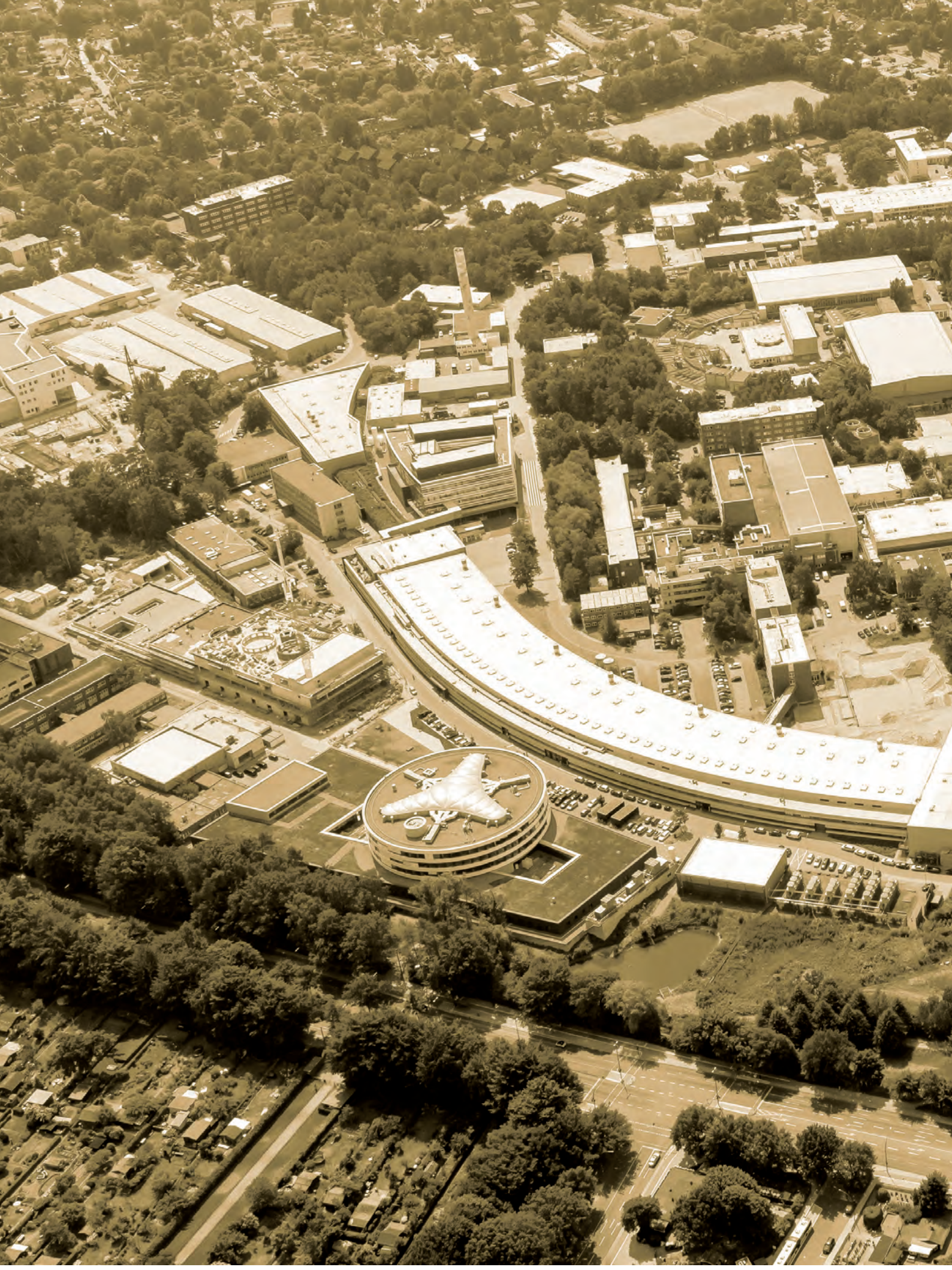
the PETRA III experimental halls, and a separate experimental hutch has been constructed on top of the ring tunnel (Fig. 10). The construction of the beamline frontend components will begin next year, instrumentation for the end station is already being assembled.

The next big step: PETRA IV

Currently, most medium and high-energy synchrotron radiation facilities worldwide undergo an upgrade process to achieve a significant reduction of the horizontal emittance and thus an increase in spectral brightness. As the emittance decreases with increasing storage ring size, the particularly large PETRA III circumference of 2304 m offers the unique opportunity to push the generation of hard X-ray synchrotron radiation to its physical limits. Therefore, DESY plans a major upgrade of PETRA III towards the ultralow-emittance source PETRA IV. With a horizontal emittance in the range of 10 – 30 pm rad and a vertical emittance smaller than 10 pm rad, PETRA IV would reach the diffraction limit for X-rays of up to 10 keV in both directions, providing extremely high values for the spectral brightness (Fig. 11). The outstanding coherence of these beams will allow to efficiently focus nearly the full undulator beams to nanometre dimensions, providing a corresponding spatial resolution for all X-ray analytical techniques and pushing the sensitivity and resolution in coherent X-ray diffraction imaging techniques to the atomic level. The PETRA IV project at DESY is currently in its conceptual design phase. This involves the development of a detailed scientific case and a conceptual design of the storage ring with an additional experimental hall in the west of the PETRA ring. Right after completion of the conceptual design report (CDR) in spring 2019, a detailed technical design report (TDR) for PETRA IV will be compiled by the end of 2021. Based on the TDR, all components of PETRA IV are to be fabricated until the middle of the next decade. PETRA III is then planned to be shut down in 2025, and PETRA IV shall go into operation after a shutdown period of about two years.

PETRA IV will accommodate 26 insertion device sections of approximately 5 m length and four longer straight sections at the beginning of each experimental hall. In total 30 independent undulator stations with world-leading brightness can be realised. The PETRA IV project will pave the way to a future generation of synchrotron radiation sources.

Contact: Oliver Seeck, oliver.seeck@desy.de
Wolfgang Drube, wolfgang.drube@desy.de





Campus and Collaborations

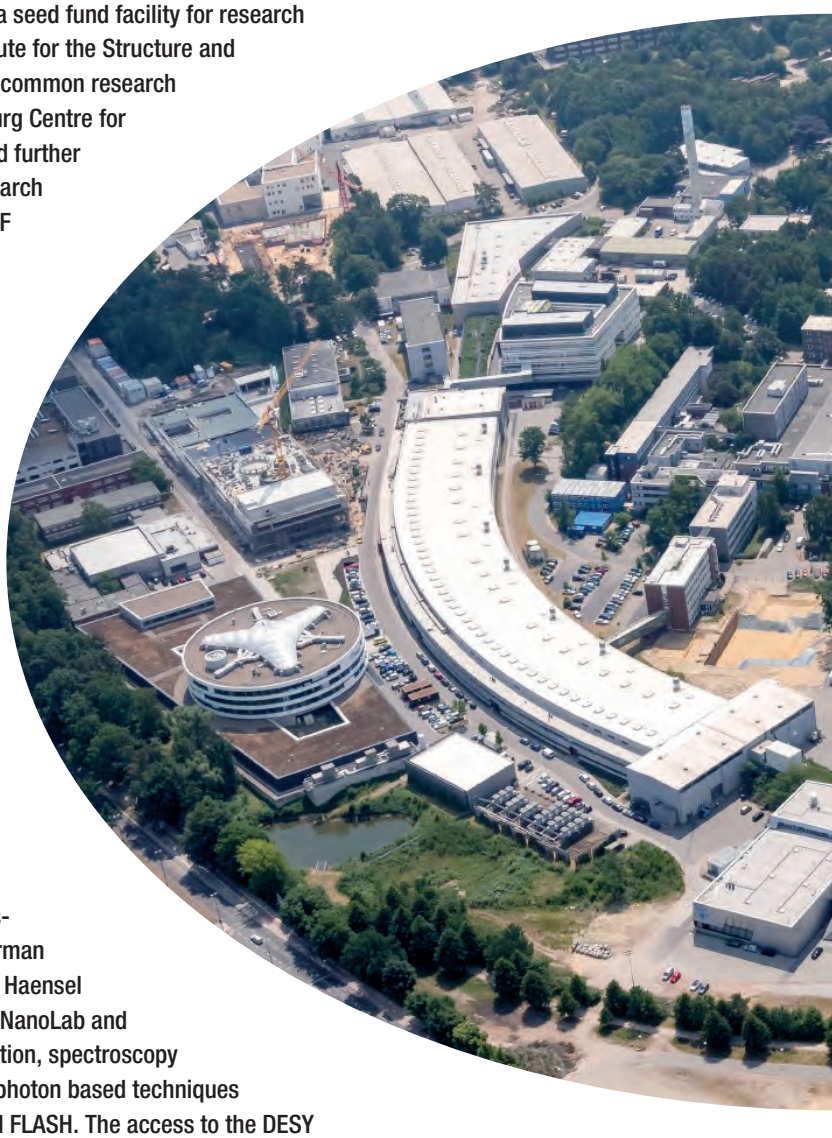
- Campus and Collaborations – Overview 102
- Cooperation for research and education 104
- Center for Free-Electron Laser Science CFEL 106
- DESY NanoLab at the Center for X-ray and Nanoscience (CXNS) 107
- Centre for Structural Systems Biology CSSB 108
- European Molecular Biology Laboratory Hamburg Unit 110
- The GEMS branch at DESY 112
- DESY Photon Science at the European XFEL 114
- DESY Innovation and Technology Transfer 116
- Outlook on campus and collaborations 117

Campus and Collaborations – Overview

DESY Photon Science is part of a worldwide collaborative network. Cooperation creates new scientific and technological opportunities at DESY's facilities, increases the pool of talents and is also indispensable to further coordinate research roadmaps and agendas. The collaboration landscape at DESY Photon Science is diversified and involves local as well as national and international partners.

Universities

A strong connection to the Universität Hamburg (UHH) is established through the 'Partnership for Innovation, Education and Research' (PIER). This structural cooperation has provided the ground for a joint graduate school (PIER Helmholtz Graduate School, PHGS), joint professorships and a seed fund facility for research projects. Together with colleagues from the Max Planck Institute for the Structure and Dynamics of Matter (MPSD) and European XFEL, DESY and UHH run common research projects in the DFG funded Cluster of Excellence CUI ('The Hamburg Centre for Ultrafast Imaging'). DESY is expanding collaborations with UHH and further German universities through joint professorships, common research projects, collaborative research centres (SFBs) and BMBF Collaborative Research at PETRA III and FLASH. With some of the universities joint laboratories and outstations on the DESY campus are being formed. Examples of current partnerships are the Technische Universität Hamburg, and the Universities of Göttigen, Kiel and Erlangen-Nürnberg.



Centre for Structural Systems Biology (CSSB)

Within the CSSB – a cooperation of ten partner institutions – scientists use a novel approach which combines integrative structural biology with systems biology to advance our understanding of the molecular mechanisms of some of the world's most widespread infections.

Center for X-ray and Nano Science (CXNS)

The 'Center for X-ray and Nano Science' is built in cooperation with Helmholtz-Zentrum Geesthacht (HZG) and Christian-Albrechts-Universität zu Kiel (CAU) and will house the outstation of the German Engineering Materials Science Centre of HZG and the Ruprecht Haensel Laboratory of CAU and DESY. CNXS encompasses also the DESY NanoLab and further DESY groups. DESY NanoLab provides nano-characterisation, spectroscopy and nano-structuring methods, which are complementary to the photon based techniques available for users at the DESY X-ray facilities PETRA III and FLASH. The access to the DESY NanoLab is granted for external users via regular PETRA III or FLASH proposals (through DOOR) or via proposals from the European transnational user platform Nanoscience Foundries Fine Analysis (NFFA Europe).

Center for Free-Electron Laser Science (CFEL)

The Center for Free-Electron Laser Science as a joint enterprise of DESY, the Max Planck Institute for the Structure and Dynamics of Matter (MPSD) and the Universität Hamburg is designed to advance science with next generation light sources and lasers.The three partners join forces to explore structural changes of atoms, molecules, condensed, biological, or warm dense matter on femtosecond time scales. CFEL envisions uncovering the 'dynamics of matter' by uniting expertise from various disciplines and research institutions into a new interdisciplinary and synergistic effort.

DESY within User Consortia at the European XFEL

Besides being responsible for the construction and the operation of the European XFEL linear accelerator, DESY plays an important role as user of the European XFEL. DESY is partner in several user consortia, which have been formed to prepare the facility's user operation in an optimal way. These user consortia are:

- the Serial Femtosecond Crystallography (SFX) user consortium,
- the Helmholtz International Beamline for Extreme Fields (HIBEF),
- the Heisenberg Resonant Inelastic X-ray Scattering (hRIXS) user consortium,
- the DataXpress consortium for data analysis
- the consortium on state-, size-, and isomer-selected samples of polar molecules and clusters at the European XFEL (COMO).

Moreover, DESY scientists develop lasers and detectors for usage at the European XFEL.



European Molecular Biology Laboratory (EMBL) Hamburg

At EMBL Hamburg, scientists investigate the structure of challenging molecules that impact human health. The Hamburg site's service teams develop methods and software to support scientists from around the world in every step of biological structure determination. EMBL runs three beamlines at PETRA III: one for Small Angle X-ray Scattering experiments and two for Macromolecular Crystallography.

Helmholtz-Zentrum Geesthacht (HZG)

The German Engineering Materials Science Centre (GEMS) is a user platform of HZG for the complementary research with photons and neutrons with an outstation at DESY. GEMS research groups work in X-ray diffraction and imaging on the DESY campus. HZG operates several beamlines and end stations at PETRA III focusing on research in the field of engineering materials science.

DESY Innovation and Technology Transfer

With support of the DESY department for Innovation and Technology Transfer (ITT) scientists from DESY Photon Science contribute to the DESY innovation strategy including the transfer of knowledge and technology from the laboratory to industry.

International cooperation

DESY is engaged in international cooperation and user consortia, for example to leverage new resources and contributions to DESY facilities and installations. Significant examples for DESY Photon Science in that respect are the international contributions to PETRA III by Sweden in connection to the Röntgen-Angström-Cluster (RAC), by Russia through the Ioffe-Röntgen-Institute (IRI) and by India via the India@DESY collaboration.

Cooperation for research and education

News from the partner universities



Figure 1

The picture shows the happy faces of the spokespersons of AIM after the results of the cluster evaluation were made public (from left): Horst Weller, Klaus Sengstock (both Universität Hamburg), and Henry Chapman (DESY, Universität Hamburg) Photo: Claudia Höhne.

Universität Hamburg (UHH)

The first highlight in the 'Photon Science' year 2018 at the university was the presentation of the Mildred Dresselhaus Award at the New Year's Reception of the Hamburg Centre for Ultrafast imaging (CUI) in January. The award was given to Anna Krylov, 'Gabilan Distinguished Professor of Science and Engineering' at the University of Southern California, Los Angeles and Tanya Zevelinsky, Associate Professor for Atomic, Molecular, and Optical Physics at the Columbia University in New York. Both award winners will spend time at the Universität Hamburg and collaborate with groups from CUI.

Also in January, the foundation stone for the new building 'Light & Schools' was laid close to the side entrance of the Campus Bahrenfeld at Luruper Chaussee. The new university building will host advanced laboratory courses for physics students and the 'Light & Schools' activities of the Center for Optical Quantum Technologies for pupils.

The month of April has seen the next round of the very successful outreach activity 'Wissen vom Fass – Science on Tap', during which researchers from the Universität Hamburg and DESY presented their science to the public in local pubs in Hamburg. The event was initiated four years ago by Jan Louis from the Physics Department, who is now Vice President for Research at the Universität Hamburg. He imported the idea from Tel Aviv in Israel. Year by year the event has attracted more and more interest from the public. A record number of 45 pubs and researchers have participated in the event in 2018.

On 6 November the topping out ceremony for the new research building 'Hamburg Advanced Research Centre for Bioorganic Chemistry (HARBOR)' of Universität Hamburg took place at the Campus Bahrenfeld. This centre will provide new infrastructure for experiments with ultra-short time resolution on molecular biological systems.

The highlight of the 'Photon Science' year at the Universität was of course the success of the Excellence Cluster 'AIM-Advanced Imaging of Matter' in the Federal Excellence Initiative. On 27 September, when the results of the Federal Excellence Initiative were presented in a press conference, the Universität Hamburg had every reason to celebrate, since all four Hamburg applications for excellence clusters were successful and will be funded, among them are AIM (Fig. 1) and the cluster 'Understanding Written Artefacts', which involve a DESY Photon Science contribution.

AIM, which is a collaboration of the Universität Hamburg, DESY, MPSD, and European XFEL will exploit the expertise gained in CUI to open new avenues in 'observing, understanding, and controlling' matter with the help of advanced imaging techniques. In the new cluster, 160 scientists from the four institutions will be working together. The research project will be funded for a period of seven years starting 1 January 2019. AIM relies on the enormous expertise in photon and nanoscience gathered on Campus Bahrenfeld over the last decade and the outstanding infrastructure for photon science in Hamburg. In a multidisciplinary effort the scientists will focus on imaging chemical reactions in action and the creation of new reaction pathways, manipulating the functionality of materials such as driving initially non-conducting material into a superconducting state, and mapping the atomic details and motions of proteins.

The overall goal of AIM is to be able to contribute to solving the grand societal challenges like how to efficiently capture and store energy from the sun, inhibit infectious agents in our cells, or carry out computations at lower energy cost, with an in-depth understanding of nature's functioning principles.

Christian-Albrechts-Universität zu Kiel (CAU)

The established cooperation between the Christian-Albrechts-Universität zu Kiel (CAU) and DESY continues to flourish in particular through the Ruprecht Haensel Laboratory. Scientists at both institutions continue to work

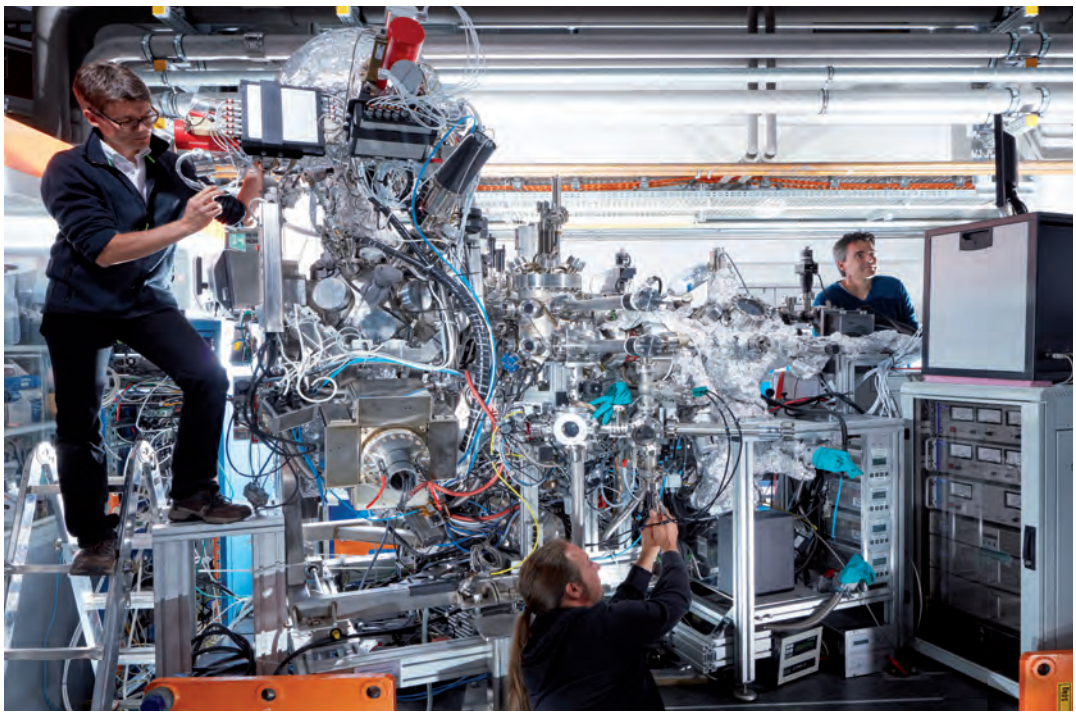


Figure 2
Kiel university scientists Matthias Kalläne, Jens Buck and Kai Rossnagel (CAU / DESY) working at ASPHERE III in the PETRA III experimental hall.
Photo: DESY, Heiner Müller-Elsner

towards a common goal of excellent science in a range of fields from understanding behaviour at liquid interfaces to the spectroscopy of molecular processes. BMBF collaborative funding ('Verbundforschung') provides continued opportunity for new science and instrumentation at PETRA III, including the study of biodegradable magnesium at P05 and ultra-fast investigation of water and liquid metals at the LISA X-ray diffractometer dedicated to liquid interfaces at P08. Together with DESY, CAU continues to support the joint CAU/Helmholtz-Zentrum Geesthacht Nanofocus Endstation at P03 for materials science. Developments also continue at the spin and momentum resolved photoemission experimental station (ASPHERE III) at the soft X-ray beamline P04, (shown in Fig. 2) with particular focus on quantum materials.

Georg-August-Universität Göttingen (GAU)
In 2018, Universität Göttingen and DESY have continued to strengthen their collaborations in research and education of students. After a testing phase, web-based teaching has now become routine simultaneously on both campus sites in Göttingen und at DESY. Furthermore, the GAU endstations for X-ray spectroscopy and X-ray imaging at DESY photon sources have been intensively used within the energy-research-related Collaborative Research Center SFB1073 and the nano-imaging-related Collaborative Research Center SFB755. Both instruments, the setup for resonant inelastic scattering 'ChemRIXS/TiRIXS' at PETRA III and FLASH as well as the 'GINIX' setup for nano-imaging with X-rays at the PETRA III beamline P10, are also included and supported by the newly funded 'Göttingen Campus Laboratory' (https://www.uni-goettingen.de/en/532762.html) as one of the laboratories essential for the Göttingen Excellence Cluster in Medicine.

Technische Universität Hamburg (TUHH)
There are several joint research projects of scientist at DESY Photon Science and TUHH. Within the joint project '*In situ* XANES and EXAFS of titanium silicalites during the epoxidation of propylene to propylene oxide' as part of the 'Landesforschungsförderung' the method of XANES (X-ray absorption near edge structure) imaging was implemented at PETRA III, imaging the chemical state of a catalyst under working conditions. In parallel, an optimised chemical reactor for the epoxidation reaction was developed at TUHH that is compatible with experiments at PETRA III. In a next step, this reactor will be used to study the epoxidation reaction and image the chemical state of the catalyst under working conditions.

The materials science departments of the TUHH continue the fruitful cooperation with the DESY NanoLab within the SFB 986 'Tailor-made Multi-scale Material Systems', funded by the German Science Foundation (DFG). Currently, two subprojects are funded. In the first one the interaction of organic acids with oxide surfaces is investigated, whereas in the second subproject conducting polymers in confinement are in the focus. Both projects aim at a better understanding of structure–functionality relations in bottom-up fabricated materials. The SFB986 serves as an incubator for the Hamburg wide initiative for material science, called CIMMS – Center for Integrated Multiscale Materials Systems.

Contact: Wilfried Wurth, UHH and DESY, wilfried.wurth@uni-hamburg.de
Bridget Murphy, CAU, murphy@physik.uni-kiel.de
Simone Techert, GAU and DESY, simone.techert@desy.de
Christian G. Schroer, UHH and DESY, christian.schroer@desy.de
Andreas Stierle, UHH and DESY, andreas.stierle@desy.de

Center for Free-Electron Laser Science CFEL

Three institutions working successfully together

Along with internal research projects between the three CFEL partners (DESY, the Max Planck Institute for the Structure and Dynamics of Matter MPSD, and Universität Hamburg UHH), collaborations with other institutions have led to significant scientific success and excellent publications.

'Quantum boiling' reveals relativity in atoms
In a way of 'quantum boiling' with intense X-ray flashes, scientists have stripped xenon atoms of most of their electrons. The experiments reveal the impact of Albert Einstein's theory of Special Relativity on the quantum structure of atoms. The international team around Sang-Kil Son and Robin Santra from CFEL, DESY and Daniel Rolles and Artem Rudenko from Kansas State University report their study in Nature Communications.

In the experiment, xenon atoms were exposed to intense X-ray pulses generated by the X-ray free-electron laser LCLS at the U.S. National Accelerator Laboratory SLAC in California. This created xenon ions with high electric charges, depending on the number of electrons that were knocked out of the atoms. When counting how many atoms had lost how many electrons, the scientists noted three distinctive bumps at telltale charge states. The theory of quantum mechanics, together with the theory of special relativity, confirmed the experimental observation and explains the mechanism how to lose electrons. Details can be found in the highlight section of this report.

Scientists decipher key principle behind reaction of metalloenzymes
An interdisciplinary team of researchers has worked out the details of how important bioinorganic electron transfer systems operate. The group headed by Sonja Herres-Pawlis from the RWTH Aachen University, Michael Rübhausen from the UHH at CFEL and Wolfgang Zinth from Munich's Ludwig-Maximilians-Universität was supported by colleagues from DESY, Paderborn University, Uppsala University, European XFEL, Czech Academy of Science, Chalmers University of Technology Göteborg and Technical University of Denmark. Using a combination of very different, time-resolved measurement methods at PETRA III and other facilities, the scientists were able to show that so-called pre-distorted states can speed up photochemical reactions or make them possible in the first place [1].

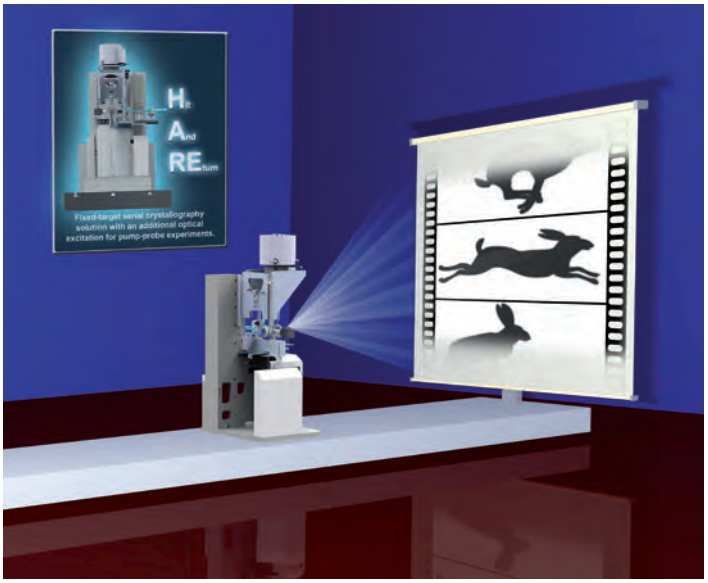


Figure 1
The 'hit and return' (HARE) method simplifies taking snap-shot movies of biomolecules at work. Image: Jörg Harms / MPSD

Atomic view of nature's amazing molecular machines at work
Researchers around Eike Schulz, Pedram Mehrabi and Henrike Müller-Werkmeister from the MPSD's Department of Atomically Resolved Dynamics at CFEL, the Centre for Ultrafast Imaging (CUI), and scientists from the University of Toronto in Canada and the ETH in Zurich, Switzerland, have developed a new method to watch biomolecules at work. This method not only simplifies the experiment but accelerates it so much that many snapshots can now be recorded in a single experimental session. These can then be assembled into a time-lapse sequence that shows the molecular foundations of biology [2].

Contact: Ralf Köhn, ralf.koehn@cfel.de

References

1. B. Dicke et al., Nat. Chem. 10, 355-362 (2018).
2. E.C. Schulz et al., Nat. Methods 15, 901-904 (2018).

DESY NanoLab at the Center for X-ray and Nanoscience (CXNS)

Shaping up for the nano future

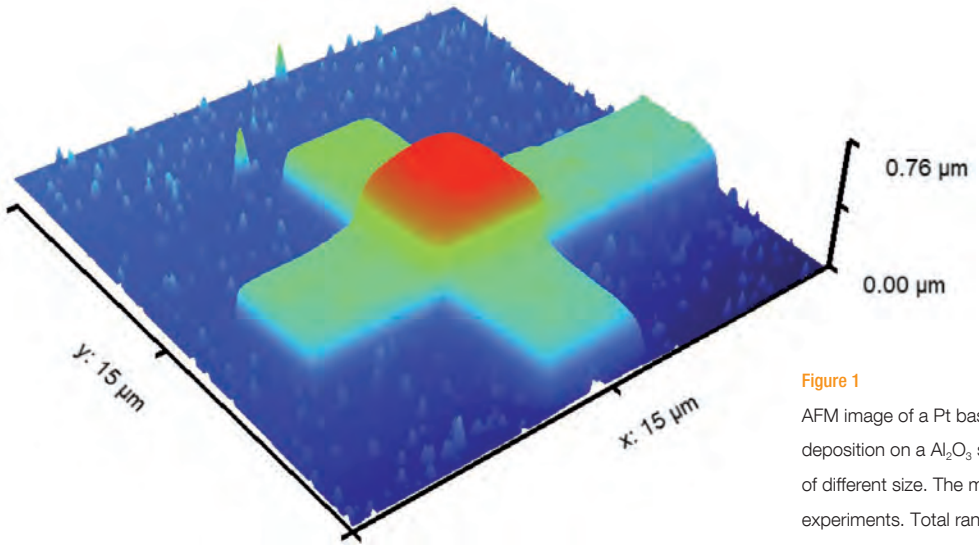


Figure 1

AFM image of a Pt based marker deposited by ion beam assisted deposition on a Al_2O_3 substrate surrounded by PtRh nanoparticles of different size. The marker serves as guide during nano focus X-ray experiments. Total range: 15 µm × 15 µm, maximum height: 760 nm.

The DESY NanoLab provides nano-characterisation, spectroscopy and nano-structuring methods, which are complementary to the photon based techniques available for users at the DESY X-ray facilities PETRA III and FLASH. The access to the DESY NanoLab is granted for external users via regular PETRA III or FLASH proposals or via proposals from the European transnational user access platform Nanoscience Foundries and Fine Analysis (NFFA Europe). Further on, DESY NanoLab is involved in cooperative projects with various German universities (Universität Hamburg, Technische Universität Hamburg, Friedrich-Alexander Universität Erlangen, Justus-Liebig Universität Gießen). In addition, it supports Photon Science research in the DESY competence team 'Nano- and Materials science' and in DESY-wide related research projects. Industrial users have access via DESY ITT (Innovation & Technology Transfer).

The future location of the DESY NanoLab from 2020 on will be in the Center for X-ray and Nanoscience (CXNS, building 94), which is built in cooperation with Helmholtz-Zentrum Geesthacht (HZG) and Christian-Albrechts-Universität zu Kiel (CAU). CXNS is currently under construction in close vicinity to the PETRA III experimental hall 'Max-von-Laue'. Some parts of the DESY NanoLab, such as the X-ray diffraction laboratory, will not be located in the CXNS building, but in close vicinity: In 2018, the new X-ray laboratory was planned and its construction work in the former DORIS hall (building 25) was nearly completed. It consists of three independent hutches and will host a grazing incidence six circle diffractometer, a reflectometer and as a new instrument a horizontal six circle instrument with a 2D detector. The latter allows for grazing incidence small angle X-ray scattering measurements. Further on, a dedicated electrochemistry lab was planned together with the CAU to serve future needs for the preparation of X-ray experiments in the field of electrochemistry, -catalysis and corrosion, related to the envisioned Centre for Molecular Water Science (CMWS).

In 2018 the high resolution fast atomic force microscope for routine investigations was commissioned. It shows the expected performance as demonstrated by the Pt nanomarker image in Fig. 1. A further upgrade of the scanning electron microscope comprises a system for electron backscatter diffraction (EBSD) for a local determination of nanoparticle and grain orientation prior to nano focus X-ray experiments. The focussed ion beam (FIB) setup was upgraded by software for nano tomography, allowing a FIB nano-slicing of 3D objects for comparison with 3D X-ray imaging at PETRA III. To complement instruments for magnetic investigations, a Kerr microscope was purchased, which will be available for users in 2019.

Contact: Andreas Stierle, andreas.stierle@desy.de

Centre for Structural Systems Biology CSSB

We investigate how pathogens infect humans



Figure 1
CSSB Building in 2018.
Photo: Tina Mavric

With all but two research groups now residing in the CSSB Building (Fig. 1), 2018 has been dedicated to fostering communication between research groups and building a common sense of purpose among all CSSB staff. Events such as a bi-weekly internal seminar series and the first CSSB staff meeting have provided opportunities for conversation and networking. Everyday routines and internal procedures have been established, thus creating a solid foundation that will enable scientific collaboration to flourish.

The CSSB lecture hall serves as a local meeting place and has hosted symposia, seminars, and courses organized by several partner institutions. The below list provides examples of the activities that have taken place at CSSB:

- MALDI-TOF[1] operational training
- Video-Rate AFM[2] Workshop
- Sino-German Summer School 'Structural Biology in Infection' (partly at CSSB)
- EMBO[3] Practical Course: Membrane Protein Expression, Purification and Characterisation
- HPI overarching day 'Structure and Dynamics of Viral Morphogenesis'
- Helmholtz Training Course on Integrative Structural Biology

Collaborative research highlights

CSSB's interdisciplinary and collaborative nature is illustrated below with a few examples of research highlights from the last year.

A study lead by CSSB Group Leader Christian Löw and Dmitri Svergun (both EMBL Hamburg) revealed an unexpected conformation for scaffolding protein PDZK1. The protein is comprised of four so-called PDZ domains, three linkers and a C-terminal tail. While bioinformatics tools had suggested that PDZK1's PDZ domains and linkers would behave like beads on a string, moving around in a highly flexible manner, the X-ray experiments performed at PETRA III beamline P12 showed that PDZK1 has a relatively defined L-shaped conformation (Fig. 2) with only moderate flexibility [1].

An international team of researchers, including CSSB scientist Jörg Labahn, developed a way to make membrane proteins

[1] MALDI-TOF = Matrix-assisted laser desorption/ionisation – time-of-flight

[2] AFM = Atomic Force Microscopy

[3] EMBO = European Molecular Biology Organization



Figure 2

Artistic shape interpretation of PDZK1 [1].

Photo: Manon Boschard

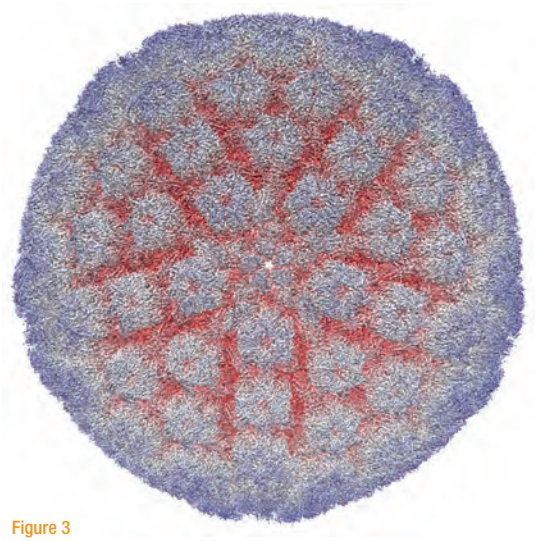


Figure 3

Rendering of the cryo-EM electric potential map of the herpes simplex virus 1 capsid with associated tegument protein complexes (EMD-7472; Dai & Zhou, Science 2018).

Photo: Martin Hällberg (Karolinska Instituet)

water-soluble by swapping some of their hydrophobic amino acids for hydrophilic ones. This advance could make it easier to perform structural studies on membrane proteins thus enabling researchers to learn more about protein structures and functions [2].

The funding of three internal seed projects will serve as catalyst for collaboration among group leaders from different CSSB partner institutions. The seed projects aim to promote the development of young scientists and to support the adaptation of innovative methods and approaches that have a wider impact on the research performed within CSSB.

Strategic Partnerships

CSSB and the Swedish Research Council have agreed upon the establishment of a strategic partnership with a focus on the CSSB Research Hotel. In June 2018, Martin Hällberg (Karolinska Institutet) and Kay Grünewald (HPI and UHH) were awarded a 1 million Euro research project grant from the Röntgen-Ångström Cluster, a Swedish-German research collaboration. The grant supports the 'Integrative Structural Biology of Herpesvirus Replication' project which will investigate the molecular basis of the herpesvirus family's replication mechanisms (Fig. 3). Hällberg and Grünewald are confident that the insights gained over the course of this project will contribute to the development of new antiviral therapies for herpesvirus infections. Martin Hällberg will once again join the CSSB Research Hotel.

CSSB scientist Christian Löw (EMBL) is also part of a project that was awarded a grant from the Röntgen-Ångström Cluster. Together with Henry Chapman (DESY, UHH) and Susanna Törnroth-Horsefield (Lund University), the Löw group will further develop a new method for diffractive imaging of macromolecules in disordered crystals.

Infrastructure investments

CSSB will be investing 600k Euro to upgrade the S3** laboratory to a full S3 laboratory. One room in the new laboratory will host a cryo-electron microscope. Once the construction work begins, the new S3 laboratory should be operational within approximately 12-14 months.

Governance

In January of this year, CSSB welcomed Chris Meier (UHH) as its new Scientific Director. Chris Meier, along with deputy directors Thomas Marlovits (UKE) and Dietmar Manstein (MHH), will serve a two year term.

Contact: Ina Plettner, ina.plettner@desy.de
Chris Meier, chris.meier@cssb-hamburg.de

References

1. N. Hajizadeh et al., Structure, S0969-2126(18)30262-4 (2018).
2. Shuguang Zhang et al., PNAS, 115 (37) E8652-E8659 (2018).

CSSB Partner Institutions

- Bernhard Nocht Institute for Tropical Medicine (BNITM)
- Deutsches Elektronen-Synchrotron (DESY)
- European Molecular Biology Laboratory (EMBL)
- Forschungszentrum Jülich (FZJ)
- Hannover Medical School (MHH)
- Heinrich Pette Institute (HPI), Leibniz Institute for Experimental Virology
- Helmholtz Centre for Infection Research (HZI)
- Universität Hamburg (UHH)
- University Medical Center Hamburg-Eppendorf (UKE)
- Research Center Borstel (FZB) (associated partner)

CSSB Investors

- Federal Republic of Germany
- Free and Hanseatic City of Hamburg
- Federal State of Lower Saxony
- Federal State of Schleswig-Holstein

European Molecular Biology Laboratory Hamburg Unit

Structural biology research and service provision

The European Molecular Biology Laboratory (EMBL) operates from six sites across Europe. The focus of the Hamburg Unit is to provide state-of-the art research services for applications in structural biology to the external research community. This is complemented by in-house research activities, which are focused on the development of new approaches in structural biology and infection biology.

Provision of research services in structural biology

Beamlines for structural biology

The EMBL Hamburg Unit operates three beamlines for structural biology applications at the PETRA III storage ring; one for Small Angle X-ray Scattering (SAXS) experiments (P12) and two for Macromolecular Crystallography (P13, P14).

Key developments in 2018 were:

At the SAXS beamline P12 pilot experiments were conducted on protein solutions using the multilayer monochromator and EIGER 4M detector (DECTRIS) with an exposure time of 100 μsec. A new sample changing robot with extended features (ARINAX, France) was taken into operation in April. A PILATUS 6M detector (DECTRIS) was installed at P12, allowing for SAXS data recording in a broad resolution range from 200 to 1 nm, without the need to change either the sample-detector distance or wavelength. The in-line size-exclusion chromatography (SEC-SAXS) data collection was used increasingly, with numerous user groups requesting to conduct both, batch and SEC-SAXS measurements. To ensure a more convenient access for these users, a special valve was introduced to rapidly change between the two modes of operation. For data interpretation, a new approach was developed to directly analyse the SAXS data off systems, for which only the scattering from the initial and final states of the process are known. The method was implemented in a computer program *DAMMIX* that directly reconstructs the low-resolution shape of transient components together with volume fractions from multiple scattering patterns recorded by time-resolved SAXS experiments [1].

On the MX beamline P14, a second experimental station, P14.EH2, dedicated to time-resolved pump-probe serial crystallography experiments has been installed (Fig. 1). The project is funded by the Verbundforschungsprogramme of the Federal Ministry of Education and Research (BMBF) as a collaboration between the groups of Arwen Pearson at the University of Hamburg and EMBL-Hamburg. All principal components – experimental table, transfocator, beam-shaping device, and the IT infrastructure – were delivered and assembled during 2018. First successful time-resolved diffraction data collections were performed in October. The physical separation of the new endstation and the standard endstation of P14 in separate sequential experimental hutches allows to optimise pump-probe setups without disturbing the standard user operation on the beamline.

In spring 2018, a high-performance data storage system with a capacity of 1 Petabyte was installed at the EMBL beamlines. The system is embedded into an InfiniBand network infrastructure and capable of simultaneously accepting multi-Gigabyte/sec data streams from all detectors on the EMBL beamlines while at the same time serving the data to multiple compute servers for processing.

Serial data collection approaches have been implemented as a standard data collection protocol into the MXCuBE beamline user interface. Users can now run serial helical scan data collections in a convenient and transparent way. Data quality diagnostics are provided in real-time; data processing can be completed on a time-scale of hours using the local computing capacity and custom data processing programs.

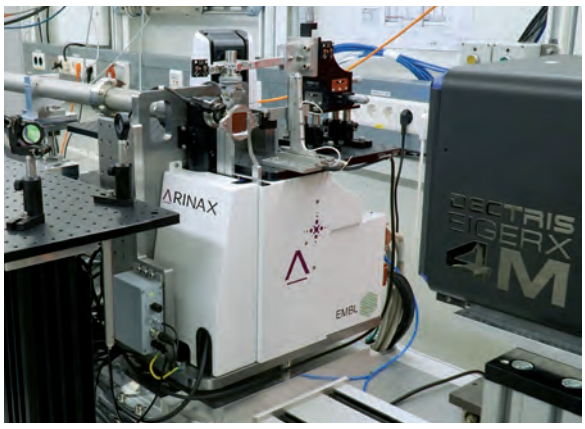


Figure 1

P14.EH2 endstation: Beam-shaping unit with a chip-presentation stage in the centre; platform for coupling in pump lasers on the left; EIGER 4M detector (DECTRIS) for diffraction data collection on the right.
Photo: Michael Agthe, UHH/CFEL

Sample preparation and characterisation (SPC) facilities
Within the framework of the establishment of the core facilities at the Centre for Structural Systems Biology (CSSB), part of the EMBL facilities, namely the protein characterisation platform is now housed within the CSSB building.
Maria Garcia Alai became the new head of this platform in March.

EMBL is also a major contributor to the biological sample preparation infrastructure at European XFEL facility. The 'XFEL Biology Infrastructure (XBI)' is a user consortium focused on providing state-of-the-art preparation facilities for biological samples. Since its official opening in September 2017, the XBI laboratory has hosted 70 users working in the laboratory preparing and characterising samples for experiments. Nearly all of the planned equipment was installed and is available for the users.

Research at the EMBL Hamburg Unit

Structural biology is presently undergoing tremendous transitions due to the rapid emergence of new technologies, instruments and infrastructures. In order to brainstorm and discuss the present state-of-the-art in structural biology and to provide the base for subsequent strategic planning with respect to new applications and challenges in the molecular and cellular life sciences, a 'Life Science Summit' workshop was organised. It brought together thirty internationally leading experts in structural biology and was convened on behalf of DESY, the European XFEL and EMBL. Reflecting the importance of Integrative Structural Biology, a number of new challenges in imaging, dynamic and integrative experiments to understand the molecular basis of biological function on the organelle, cellular, tissue and organism levels were discussed.

Research highlights from this year include the work done by Claudia Hackenberg from the Lamzin group about the structural and functional insights into the unique CBS-CP12 fusion protein family in cyanobacteria. This work describes a crystallographic structure determination and functional study of a novel fusion protein of cystathionine beta-synthase and an intrinsically disordered chloroplast protein in photosynthetic cyanobacteria. For more details, please see the highlights section of this report.



Figure 2

The Israeli students enjoying the visit.

News and Events

The year 2018 has been an exciting time for EMBL and a year of transition to prepare for a major leadership change. After successfully leading EMBL for thirteen years, Iain Mattaj is leaving the position of Director General of EMBL and will as of January 2019 be succeeded by Edith Heard, who is an internationally leading scientist with a focus in developmental biology. A joint meeting by both Iain Mattaj and Edith Heard with the Chair of the DESY Directorate Helmut Dosch and DESY Photon Science Director Edgar Weckert took place at the EMBL Headquarters in Heidelberg in September 2018.

EMBL has run several external training courses and an extensive seminar programme throughout the year. The first time, a group of young students from Tel Aviv University in the age of 15-17 years visited the EMBL Hamburg Unit (Fig. 2). These students were selected within the exchange programme Odyssey to promote Israel's next generation of trailblazing scientists and inventors. The students explored the experimental EMBL facilities for structural biology applications, attended lectures and completed experimental hands-on training.

Dmitri Svergun, the Head of the Small Angle X-ray Scattering group at the EMBL Hamburg Unit, has been awarded with this year's Guinier Prize by the International Union of Crystallography (IUCr).

Contact: Matthias Wilmanns, matthias.wilmanns@embl-hamburg.de

References

1. P. V. Konarev and D. I. Svergun. IUCrJ 5, 402-409 (2018).
2. C. Hackenberg et al., Proc. Natl. Acad. Sci. USA 115 (27), 7141-7146 (2018).

The GEMS branch at DESY

Helmholtz-Zentrum Geesthacht operates the German Engineering Materials Science Centre

All the experimental stations of the German Engineering Materials Science Centre (GEMS) continue to be highly requested by engineering materials science users from institutions in Germany and all over Europe. Their studies result in very interesting publications (a selection is presented below) and drive the instrumental developments at the beamlines. In particular, *in situ* techniques and specifically additive manufacturing are in the focus.

Diffraction

The new hutches of beamline P61A in the PETRA III experimental hall 'Paul P. Ewald' are finished and installation work is going on. P61 will be the only white-beam beamline at PETRA III, and P61A will be focused on materials research such as depth-resolved residual stress analysis.

The new large melting zone furnace for directional solidification experiments (FlexiDS) is a unique sample environment that was successfully tested and has already been used for two beamtimes at P07. FlexiDS is a BMBF-funded collaborative research project of Karlsruhe Institute of Technology (KIT) (M. Heilmeier) and University of Magdeburg (M. Krüger, now at FZ Jülich) that allows melting of 12 mm thick samples; the sample size is crucial because not all processes relevant for the microstructure formation do scale with size. First experiments with an *in situ* selective laser melting (SLM) chamber of the TU Berlin groups of W. Reimers and E. Uhlmann took successfully place at P07.

At P07, an investigation of peritectic titanium alloys for 3D printing has been carried out [1]. Today, metal additive manufacturing (AM) techniques mostly have to work with conventional alloys that often lead to mediocre properties of the resulting microstructures as the alloys are not optimised for the high cooling rates and thermal gradients occurring in AM techniques. They result in strong textures and corresponding anisotropic mechanical properties. A team from German Aerospace Center (DLR) (G. Requena *et al.*) studied a promising new solidification and cooling path that leads to more equiaxed microstructures and could open a path to next generation Ti alloys for AM. The improvement was achieved with a Ti-2 wt% La alloy. The crystallographic phases α and β and the way they form from the liquid (L_1) determine the mechanical properties of the material. During cooling, α grains nucleate in the $L_1 + \beta$ field via peritectic $L_1 + \beta \rightarrow \alpha$ reaction and subsequently transform from β ($\beta \rightarrow \alpha$). The resulting α phase is not always related to the orientation of the parent β phase and therefore, significant texture reductions as well as equiaxed microstructures can be achieved (Fig. 1). The samples were produced with the

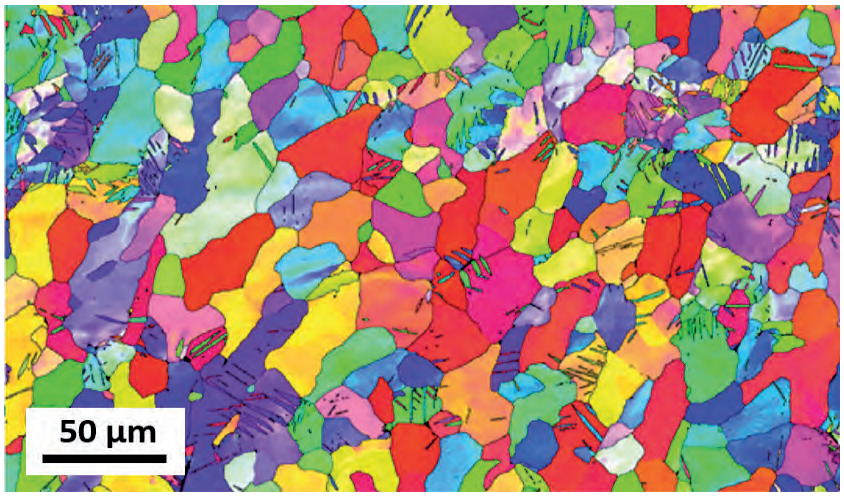


Figure 1

Globular microstructure in a Ti-2 wt% La alloy after post-SLM thermal treatment at 950 °C and cooling with 20 K/min [1].

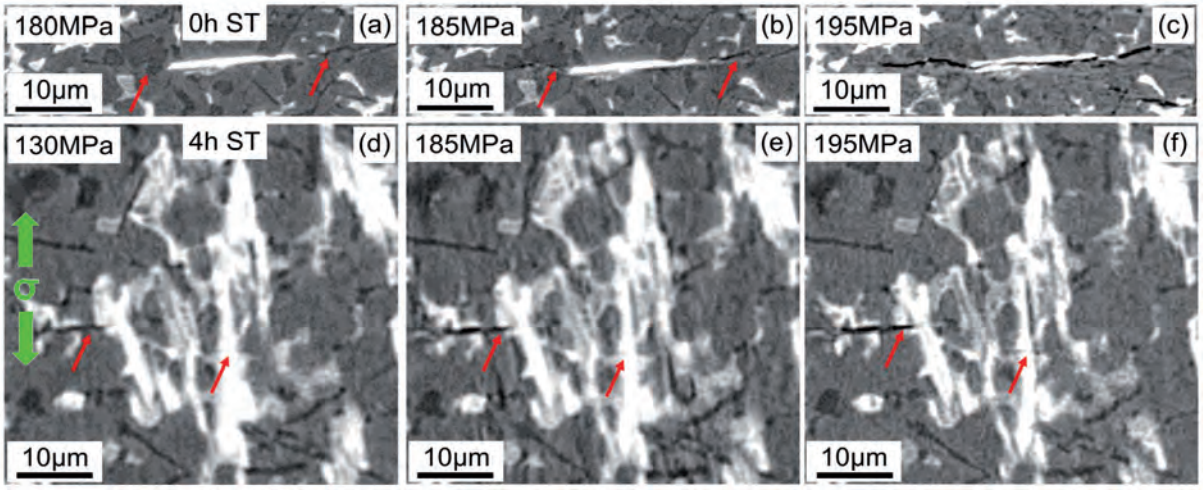


Figure 2
Microcracks through Si particles and aluminides at several load steps of the alloy in (a-c) 4 h / 500 °C and (d-f) 5 h / 230 °C + 100 h / 300 °C. Load direction is indicated by the green arrows. [2]

selective laser melting (SLM) technique. The experiment was carried out with the P07 dilatometer, allowing for various precise cooling rates. Diffraction patterns were collected during cooling. Details can be found in the highlight section of this report.

Imaging

At the P05 micro tomography end station the high beam quality and stability of the double multilayer monochromator combined with the exceptionally large beam were used to extensively speed up the measuring process while maintaining an extraordinarily high scan quality. Owing to the collaboratively developed 20 megapixel CMOS detector (developed with KIT), now operated at its full framerate of 30 Hz, it is possible to generate high quality tomograms in under 30 seconds. Improvements in scan and reconstruction software have led to a significant reduction of ring artefacts before the application of filtering as well as to enhancements in the setup's flexibility of scan operation.

Thanks to the high flexibility of the micro tomography setup at beamline P05, complex *in situ* sample environments can be combined with high-resolution imaging. The microstructural evolution of cracks was investigated using micro CT during tensile deformation of a near-eutectic Al-Si alloy ($AlSi_{12}Cu_4Ni_2$), commonly used for pistons in high performance combustion engines. The alloy contains an interconnected 3D hybrid network formed by Si and intermetallic phases embedded in a soft alpha-Al matrix, whose load carrying capability is affected by heat-induced changes. It was found that damage during tensile deformation begins as crack formation preferably through primary Si particles and as debonding at the interface between Si particles and alpha-Al, both for solution treated material (4h at 500 °C) and for material which has only been aged (5h at 230 °C and 100h at 300 °C). As shown in Fig. 2, these cracks are oriented perpendicular to the load direction and tend to accumulate at Si clusters [2].

At the P05 nano tomography station a nice example of how material science can drive instrumental development has been demonstrated and published [3] showing the potential of nano-porous gold becoming a test structure for hard X-ray microscopy techniques. Thanks to this 3D test structure the overall stability of the instrument was improved significantly, allowing for high quality nano-CT scans in well below one hour. Fast tomograms with reasonable quality can now be performed within 3 minutes scan time, taking 681 projections. In addition, Zernike Phase contrast has successfully been implemented and first user experiments have been performed with this technique.

At the nanofocus endstation of the P03 beamline, spatially resolved scanning wide-angle X-ray scattering (WAXS) experiments were performed to study damage tolerance of Ti-Al-N coatings, one of the best-established supersaturated material system in the field of hard protective coatings. From data recorded at selected positions it was found that the formation of even tiny fractions of hcp structured (ZnS-wurtzite type) Al-N during decomposition of supersaturated fcc structured (NaCl-type) Ti-Al-N gives rise to high in-plane compressive stresses which impede the formation and propagation of cracks, leading to enhanced damage tolerance of annealed Ti-Al-N [4].

The coming year will bring new developments, improvements and challenges with a new undulator at P07, the upgrade of the monochromator at P05 and the construction of the new Beamline P61A, from which our users will benefit in the future.

Contact: Christina Krywka, christina.krywka@hzg.de
Peter Staron, peter.staron@hzg.de
Martin Müller, martin.mueller@hzg.de

References

1. P. Barriobero-Vila et al., Nature Communications 9 1–9 (2018).
2. K. Bugelnig et al., Mat. Sci. Eng. A 709 193–202 (2018).
3. E. Larsson et al., J. Synchr. Rad, in press (2018).
4. M. Bartosik et al., Vacuum 155 153–157 (2018).

DESY Photon Science at the European XFEL

User consortia and detector development

SFX

The SFX Consortium is developing methodologies and instrumentation for conducting serial femtosecond crystallography at the 'Single Particles, Clusters, and Biomolecules and Serial Femtosecond Crystallography' (SPB/SFX) instrument of the European XFEL. As described in the highlights section of this report, serial crystallographic measurements have successfully been carried out at megahertz rates to obtain high-quality structures of macromolecules [1]. This validates the approaches developed in the consortium to be able to deliver fresh microcrystals to the focused X-ray beam in less than 1 µs, without suffering from any deleterious effects due to their high speed or due to the strong interaction of the previous X-ray pulse. It is particularly satisfying that molecular structures are refined to a greater precision than is usually obtained in serial crystallography experiments for the same number of patterns collected—which is attributed to the high dynamic range of the AGIPD detector as well as the stability of the X-ray beam delivered to the experiment. Nevertheless, learning from these experiments is being used to make improvements to the design of the detector electronics that will be used in the 4-million-pixel AGIPD detector that the consortium will field next year for the second end station at the SPB/SFX beamline. The design, construction, and integration is led by the SPB/SFX project leader, Adrian Mancuso, with contributions from over 15 consortium-funded scientists and engineers and many in-kind contributions from the consortium partners, comprising members of the scientific communities in Germany, United Kingdom, Sweden, Slovakia, Switzerland, United States, and Australia.

HIBEF

DESY is part of HiBEF, an international consortium led by the Helmholtz-Zentrum Dresden-Rossendorf (HZDR), which is dedicated to the exploration of extreme states of matter. These can only be generated transiently, and the study of these states requires the time structure, peak brilliance, energy range, and coherence of the European XFEL. HiBEF provides drivers for the generation of extreme conditions along with necessary instrumentation at the High Energy Density (HED) instrument of European XFEL to detect and explore new states of matter.

This year, the 'Pulsed High Magnetic Field' project held a fruitful satellite workshop with broad international attendance on the scientific scope during the users' meeting. HZDR reports successful tests of a first conical bore prototype coil reaching close to 60 T, while details of the capacitor bench location and the diffractometer are currently discussed.

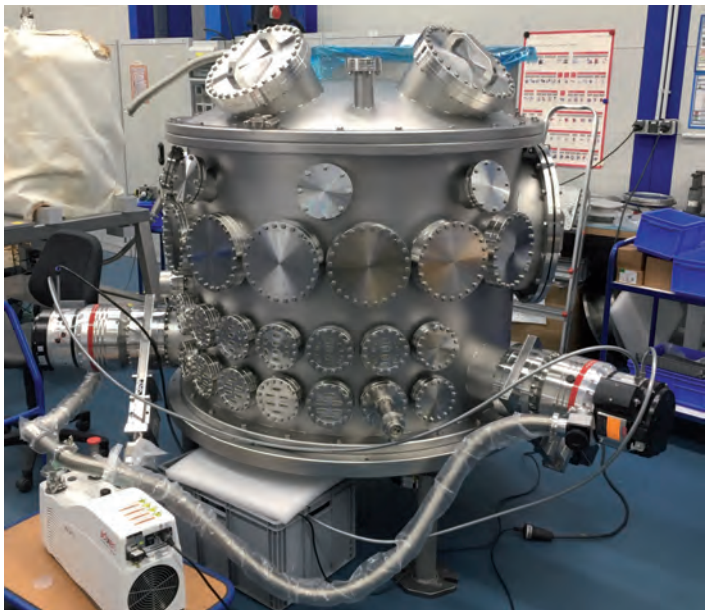


Figure 1

Interaction chamber 2 for the HiBEF user consortium approaching final assembly. Factory acceptance, delivery, and site acceptance test are scheduled for December 2018.

Production and assembly of the second interaction chamber (Fig.1, at the company Pfeiffer) is nearing completion with factory and site acceptance tests scheduled still this year. Details of the diamond anvil cell setup are currently being finalized and a conceptual design for the laser shock compression- and nanofocusing-setups were presented. Parts of the HiBEF AGIPD 1M Detector have gone into production, and the integration is making progress. In particular, the detector bench was cleared for manufacturing. The 'High Intensity' laser manufactured by Amplitude Technologies France is currently being installed in the clean room on top of the HED hutch, and the site acceptance test is scheduled for February 2019. The 'High Energy' laser provided by HiBEF UK 'DiPOLE-100X' is being manufactured at the moment, and installation at HED is foreseen for starting summer 2019.

hRIXS

The Heisenberg RIXS consortium will bring resonant inelastic soft X-ray scattering (RIXS) to the transform limit in energy and time at the European XFEL. Unique insights to chemical dynamics, driven phases as well as fundamental X-ray matter interaction open up new science directions. The optical design of the spectrometer is based on spherical variable line-spacing gratings with the ability to achieve resolving powers

≥ 20.000 over an energy range of 250-1600 eV. hRIXS will be the world leading instrument to detect static properties and transient excitations in structure, charge, spin and orbital polarization for chemical processes as well as a wide range of energy- and bio-relevant materials. To enable this vast range of experiments, the hRIXS spectrometer will be operated with two complementary, exchangeable endstations optimised for measurements on solid-state and liquid/gas phase targets.

The spectrometer (Fig. 2) and associated endstations are currently under construction at the Company Bestec. The installation and commissioning at the Spectroscopy and Coherent Scattering (SCS) instrument at XFEL is scheduled for the second half of 2019.

Funding is provided by the Helmholtz Association via strategic investment in the Helmholtz-International Users consortium hRIXS. The project is partially supported by the ERC Advanced Grant 'EDAX' at Potsdam University. The hRIXS consortium includes partners from Germany, Switzerland, Finland, France, Sweden, Italy, and the UK. The project is coordinated by Potsdam University in close collaboration with DESY and European XFEL.

DataXpress

Experiments at the European XFEL are already capable of recording up to 1700 full detector frames per second, or over 6 million images per hour. Processing this flood of data in order to make decisions during an experiment and efficiently arrive at a publication afterwards is a major challenge for users. The DataXpress consortium led by scientists from CFEL/DESY has developed software for both offline data analysis and real time experiment feedback for experiments at the SFX/SPB instrument at European XFEL, primarily for serial crystallography and single particle diffraction. The DataXpress team has been involved in numerous experiments at European XFEL and enabled the first experimental results from European XFEL [1]. Software developed through DataXpress is available for use by all users and is installed centrally on the Maxwell cluster. This has enabled European XFEL users to focus immediately on scientific output without having to handle the data processing and reduction challenges in each group individually. The consortium includes partners from Germany, Sweden, and the U.S.

COMO

The enduser consortium 'State-, size-, and isomer-selected samples of polar molecules and clusters at the European XFEL' (COMO) will provide molecular-beam-injector setups for European XFEL instruments. In 2018, COMO has made significant steps toward implementation and use at the European XFEL. The development of improved deflectors as well as knife-edges included in the molecular-beam setup have significantly increased the purity of the delivered samples [2, 3] and this was confirmed in experiments at PETRA III [4], FLASH, and LCLS. A full design including these advances over the original proposal was finished and the setup is currently being setup and commissioned. Furthermore, a user-community proposal for commissioning and exploiting the COMO setup at the Small Quantum Systems (SQS) endstation was handed in.

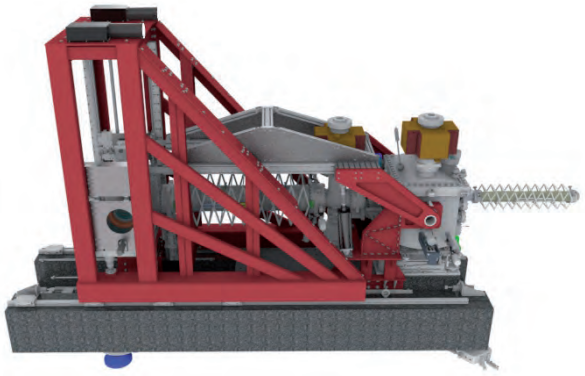


Figure 2

Final layout of the hRIXS spectrometer. The instrument has a height of 3 m and total length of 5 m. Image: hRIXS consortium

Detector development for user consortia and instruments at European XFEL

After the successful installation and first user operation of the Adaptive Gain Integrating Pixel Detector (AGIPD) at the SPB/SFX beamline the end of 2017, the DESY Photon Science Detector group provided operational support during the user experiments, and gradually upgraded and improved the system. The detector has been used in the vast majority of the experiments at SPB/SFX in the past year. In parallel, the DESY group completed a second identical system for the Materials Imaging and Dynamics (MID) station at the European XFEL. This second system was handed over to the European XFEL in July for integration into the DAQ and control system. It was successfully installed on the experimental station in the beginning of November, ready to accept first beam still in 2018. In addition to these two systems, the DESY Photon Science Detector group is in an advanced stage of development of a 4-Million pixel AGIPD for the SFX user consortium, as well as a high-energy version for the HiBEF user consortium. Both systems are foreseen to be delivered in 2019.

Contact:
SFX: Henry Chapman, CFEL/DESY and Univ. Hamburg, henry.chapman@desy.de
HIBEF: Thomas Cowan, HZDR, t.cowan@hzdr.de
hRIXS: Alexander Föhlisch, Potsdam University and HZB, alexander.foehlisch@helmholtz-berlin.de
DataXpress: Anton Barty, CFEL/DESY, anton.barty@desy.de
COMO: Jochen Küpper, CFEL/DESY and Univ. Hamburg, jochen.kuepper@desy.de
Detector development: Heinz Graafsma, DESY, heinz.graafsma@desy.de

References

1. M. Wiedorn, et al., Nat Comms 9, 4025 (2018).
2. S. Trippel, et al., Rev. Sci. Instrum. 89, 096110 (2018).
3. J. S. Kienitz, et al., J. Chem. Phys. 147, 024304 (2017).
4. T. Kierspel, et al., Phys. Chem. Chem. Phys. 20, 20205 (2018).

DESY Innovation and Technology Transfer

Linking industry and science



Figure 1
DESY CTO Arik Willner (right) represents the team Innovation and Technology Transfer at the Hannover Messe 2018, here in conversation with Katharina Fegebank (second from the right), Second Mayor of the City of Hamburg and Senator for the Ministry of Science, Research and Equality (BWFG) and the DESY Industrial Liaison Officer Eva Crosas (left).

Innovation and Technology Transfer is – not only within DESY, but in society, science, industry and politics – gaining more and more importance. This is reflected by the DESY Innovation Strategy. Moreover the DESY Chief Technolgy Officer (CTO), Arik Willner, has been appointed as the Delegate of the Directorate for Innovation. Main goals of the strategy are to strengthen DESY's image as a partner for industry with respect to cooperation, to enhance industry services as well as to develop networks of innovation, transfer and business development agencies on a regional, national and international level.

Major activities in the field of Innovation and Technology Transfer relevant for Photon Science at DESY include developing a better access for industrial companies to beamtime at DESY. An Industry Services Manager is exclusively handling these requests and supports the communication with the scientists, thus facilitating the whole process. In this respect, the Manager serves as a key contact for industry reducing the workload for involved beamline scientists.

Furthermore, an Industrial Liaison Officer has been introduced, who enables a professional and fast handling of industrial requests for beamtime by servicing these requests at the beamline itself. The team Innovation and Technology Transfer (ITT) aims to recruit further Industry Liaison Officers working at the interface between ITT team, the scientific group and the industry.

Another aim is to intensify a strong and reliable network with other partners located at the Bahrenfeld Campus in order to handle requests by industry more flexibly and efficiently. This includes a close collaboration with the Industrial Liaison Offices of the Helmholtz-Zentrum Geesthacht (HZG) and the European Molecular Biology Laboratory (EMBL) Hamburg Unit who are both operating beamlines at PETRA III.

In addition, the team ITT works closely with Photon Science in the frame of the upgrade project PETRA IV, specifying the Industrial Case in the Conceptual Design Report. Here, industrial needs and fields of application for PETRA IV are developed and addressed as well as supported by partners from industry. This includes industrial research in a multitude of fields such as energy storage in new battery systems, catalytic reactions for the design of more efficient processes and an in-depth understanding of processes in microchips.

Contact: Arik Willner, arik.willner@desy.de

Outlook on campus and collaborations

Interdisciplinary research platforms

The cooperation between the research fields, links to other divisions at DESY and joint projects with external partners are of decisive importance for the interdisciplinary research at DESY Photon Science. Connections are for example established in joint centres via common thematic focus points as part of the 'DESY 2030' strategy (Fig. 1). Besides the existing Center for Free-Electron Laser Science (CFEL), the Centre for Systems and Structural Biology (CSSB) and its envisioned extensions, DESY is planning to establish new centres together with partner institutions to foster cooperation and to extend the research possibilities on the Bahrenfeld research campus.

Center for X-ray and Nano Science
The building of the Center for X-ray and Nano Science (CXNS) will be constructed in cooperation with the Helmholtz-Zentrum Geesthacht (HZG) and the Christians-Albrechts-Universität zu Kiel (CAU). Construction has started in autumn 2018 and the new research building CXNS is scheduled for completion in 2020. In addition to several DESY research groups, the building will also house the DESY NanoLab (details can be found in the previous part of this section). The idea of this new centre is to establish a new home for already existing activities, now spread all over the campus.

Centre for Molecular Water Science
In the envisioned Centre for Molecular Water Science (CMWS), experts from DESY and several cooperation partners will come together to work on the following topics: Fundamental properties of water, geo- and astrophysical processes, nanoscience and nanotechnologies, chemical dynamics, biochemical and biological reactions as well as theory and simulations. The research objectives are closely linked to current developments of the photon sources in Hamburg. In 2018, two CMWS workshops took place at DESY to define a first draft of the research programme. The plan of an interdisciplinary centre focusing on the molecular properties of water has found wide-spread interest in the international science community: DESY received more than 30 Letters of Intent of potential partners. The start of the early science programme in the form of a virtual laboratory is planned for 2019.

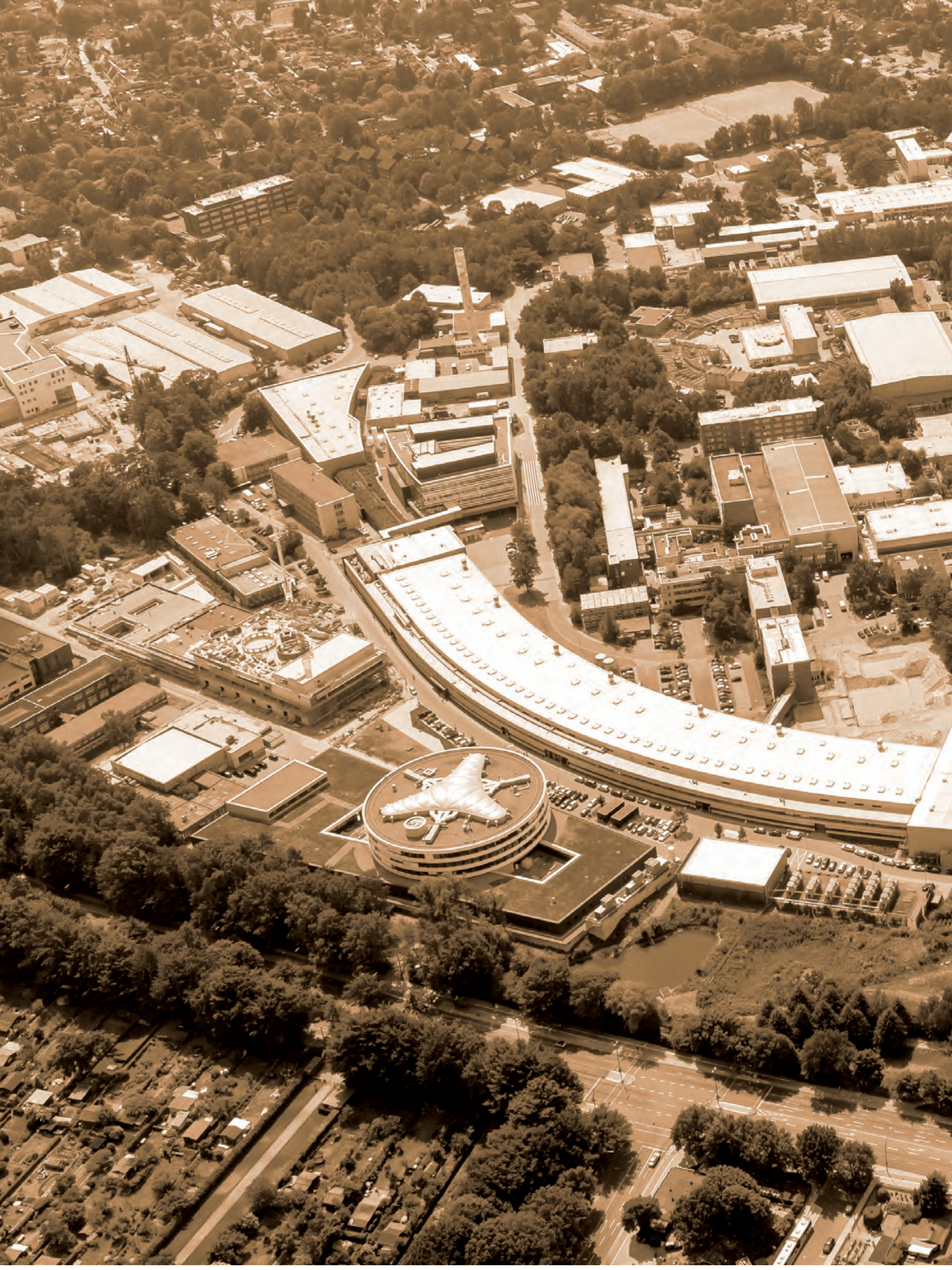
Wolfgang-Pauli-Centre
The Wolfgang-Pauli-Centre (WPC) for theoretical physics is an important measure to facilitate scientific exchange between the DESY divisions, scientists of the Universität Hamburg (UHH) and other partners. WPC pursues and promotes interdisciplinary research to address the fundamental challenges in the understanding of matter, materials and the universe under one organisational roof. Profiting from its unique embedding in a large-scale research centre, the WPC fosters international cooperation as well as a vivid dialogue between theory and experiment. Within WPC, scientists of DESY Photon Science contribute in the field of non-equilibrium physics as well as simulation and numerical techniques. The latter research field forms a natural bridge to the Center for Data and Computing Science described in the following.

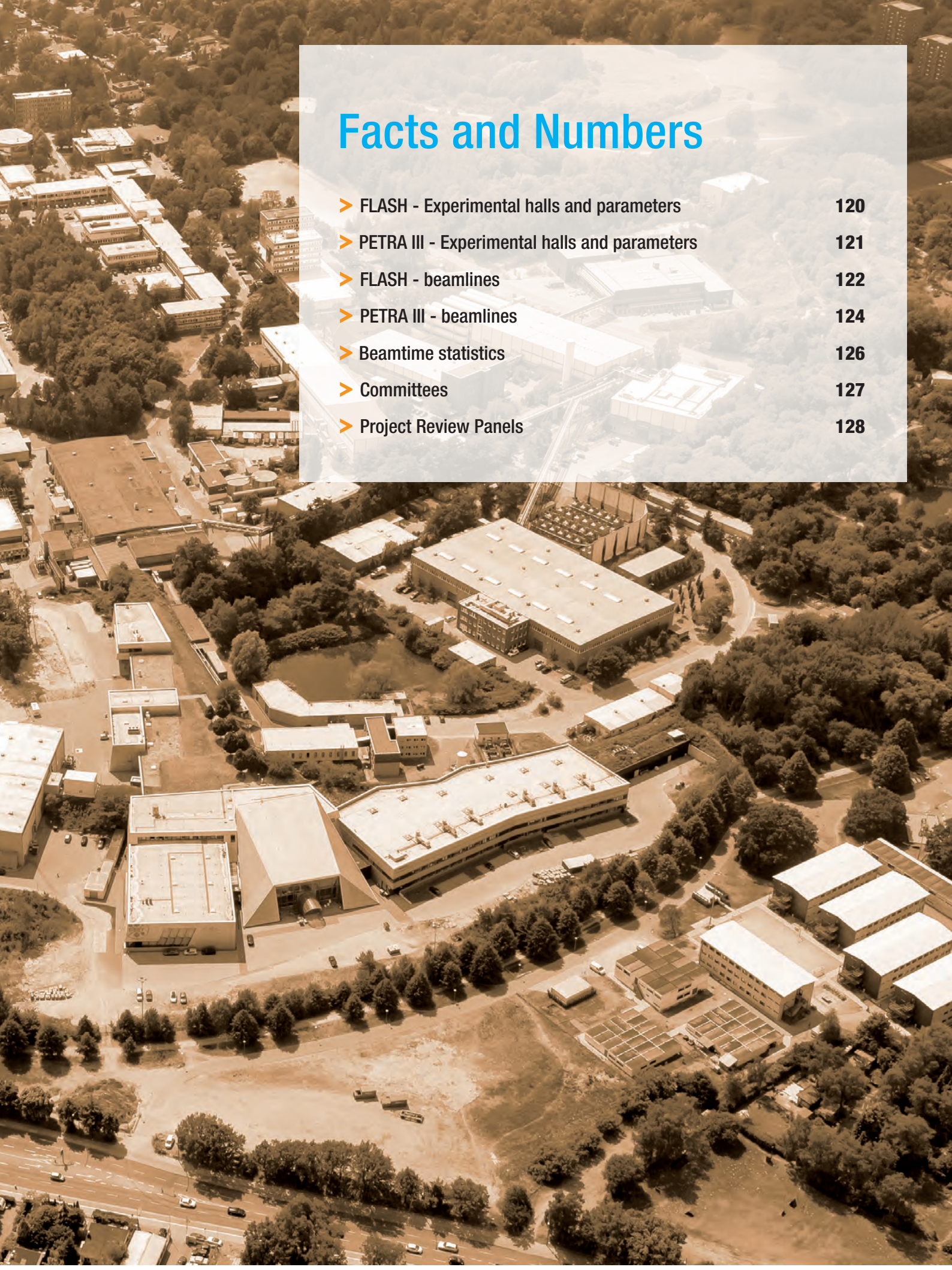
Center for Data and Computing Science
At the photon sources as well as in the research fields of photon science, a special need for action was identified in the area of scientific computing and data analysis. At DESY several measures are taken to meet this increased need: A DESY-wide Center for Data and Computing Science (CDCS) has been proposed. It should bundle competences from the various divisions at DESY and includes UHH, TUHH, and European XFEL as well as other universities and research centres. Within this framework the approved graduate school DASHH (Data Science in Hamburg – Helmholtz Graduate School for the Structure of Matter) is to be emphasised. DESY is founding the Graduate School together with the UHH and other partners. The first students are expected in mid-2019. These DESY activities align with strategies on the level of the Helmholtz Association (Helmholtz Incubator within the strategic initiative for Information & Data Science) and on the European level (IT working group within The League of European Accelerator-based Photon Sources, LEAPS).

Contact:
CXNS: Andreas Stierle, andreas.stierle@desy.de
CMWS: Gerhard Grübel, Gerhard.gruebel@desy.de
WPC: Robin Santra, robin.santra@desy.de
CDCS: Nina Rohringer, nina.rohringer@desy.de



Figure 1
As part of the 'DESY2030' strategy external partners are involved via joint research platforms, which connect the research competence teams at DESY Photon Science.



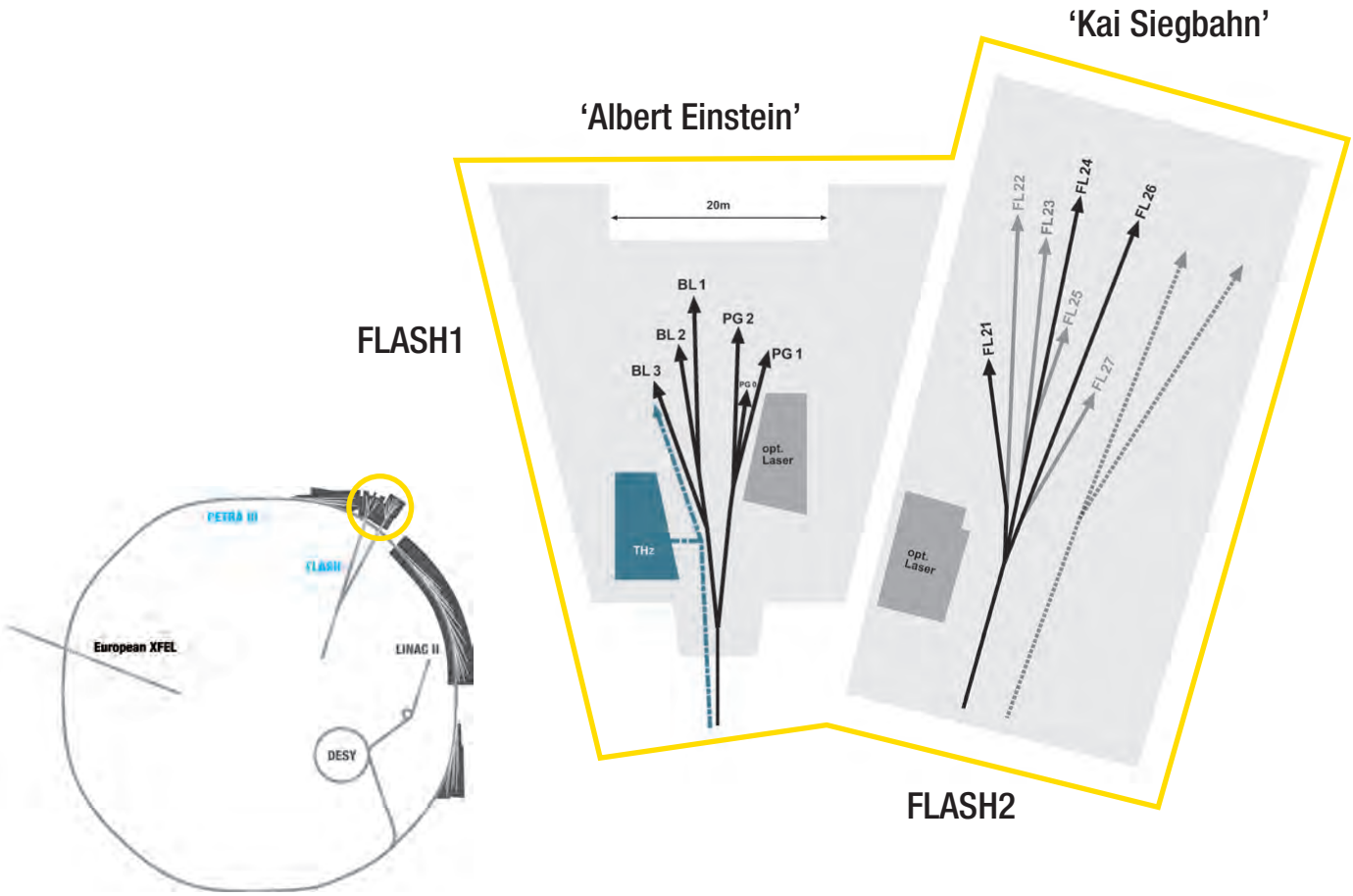


Facts and Numbers

- FLASH - Experimental halls and parameters 120
- PETRA III - Experimental halls and parameters 121
- FLASH - beamlines 122
- PETRA III - beamlines 124
- Beamtime statistics 126
- Committees 127
- Project Review Panels 128

FLASH

Experimental halls and parameters



FLASH - machine parameters

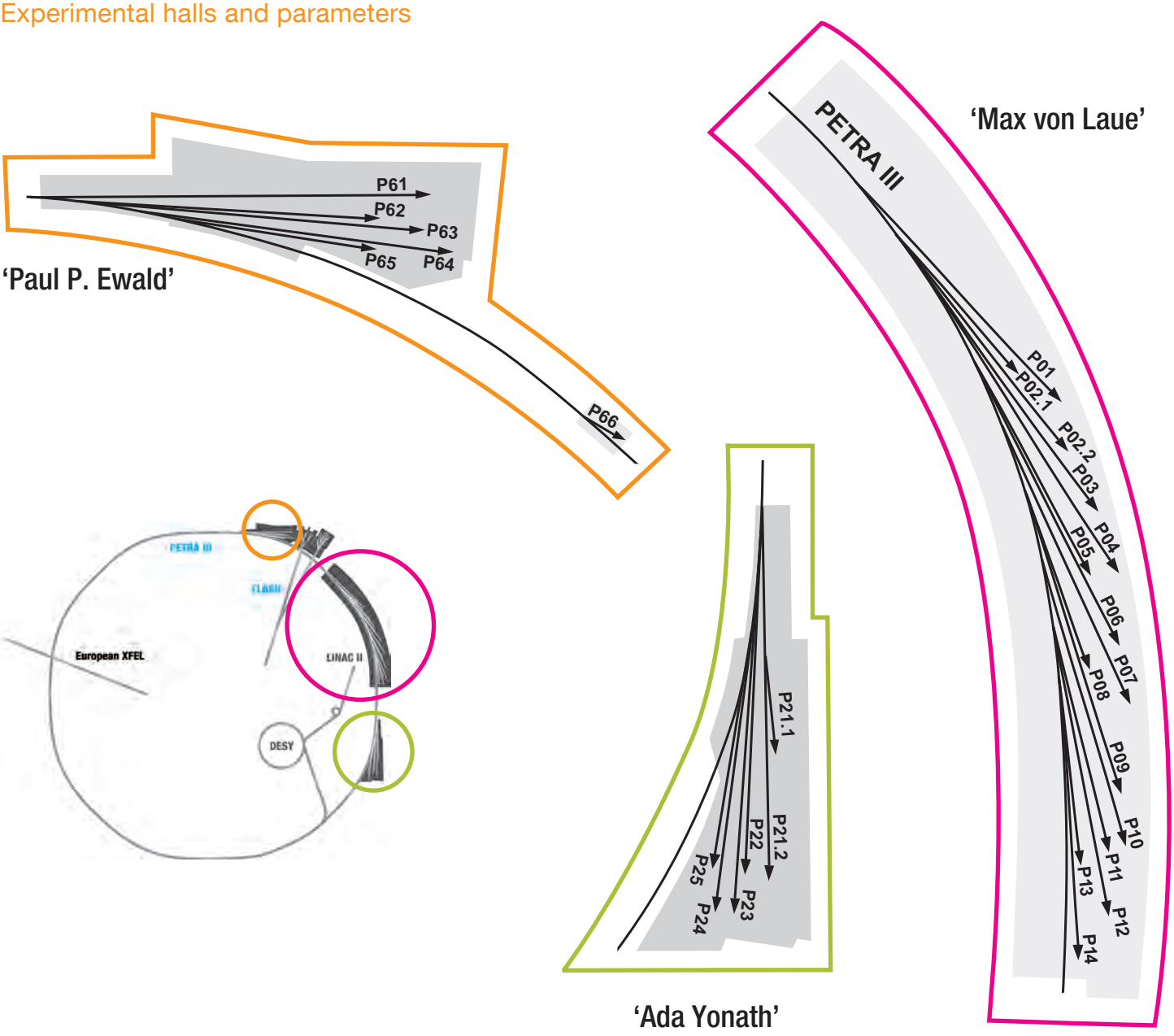
	FLASH1	FLASH2
Electron energy range	0.35 – 1.25 GeV	0.4 – 1.25 GeV
Normalised emittance at 1 nC (rms)	1.4 mm mrad	1.4 mm mrad
Energy spread	200 keV	500 keV
Electron bunch charge	0.02 – 1.2 nC	0.02 – 1 nC
Peak current	1 – 2.5 kA	1 – 2.5 kA
Electron bunches per second (to be shared between FL1 and FL2)	5000	5000

FLASH - lasing parameters

	FLASH1	FLASH2
Photon energy fundamental	24 – 295 eV	14 – 310 eV
Wavelength fundamental	51 – 4.2 nm	90 – 4 nm
Photon pulse duration (FWHM)	30 – 200 fs	10 – 200 fs (estimated)
Peak power	1 – 5 GW	1 – 5 GW
Single photon pulse energy (average)	1 – 500 µJ	1 – 1000 µJ
Spectral width (FWHM)	0.7 – 2 %	0.5 – 2 %
Photons per bunch	10^{11} – 10^{14}	10^{11} – 10^{14}
Peak brilliance photons/sec/mm^2/mrad^2/0.1%	10^{28} – 10^{31}	10^{28} – 10^{31}

PETRA III

Experimental halls and parameters



PETRA III - machine parameters

Electron energy	6.08 GeV
Circumference of the storage ring	2304 m
Number of bunches	960, 480, 80, 60, and 40
Bunch separation	8 ns, 16 ns, 96 ns, 128 ns, and 192 ns
Electron beam current	100 mA (top-up)
Horizontal electron beam emittance	1.2 nmrad
Vertical electron beam emittance	0.01 nmrad
Electron beam energy spread (rms)	0.1%
Horizontal x vertical beam size (rms) at 5 m undulator (high β section) and 10 keV photon energy	141 µm x 5.2 µm
Horizontal x vertical beam size (rms) at 5 m undulator (low β section) and 10 keV photon energy	36 µm x 5.7 µm

FLASH

Beamlines

FLASH1

BL1	non-monochromatic FEL photons Kirkpatrick-Baez (KB) focusing optics, FEL focal spot of ~7 µm × 8 µm (FWHM)	
	split-and-delay unit for XUV pump – XUV probe experiments (mirrors for 13.57 nm, - 30 ps to + 650 ps delay)	*TU Berlin**
	optional pump – probe experiments using FLASH1 optical laser system	
	4-mirror polarizer for variable FEL polarization from 30 – 70 eV	*TU Berlin**
	permanent end station: multipurpose CAMP chamber with pnCCD detectors, electron and ion spectrometers and collinear incoupling optics for optical laser	
BL2	non-monochromatic FEL photons focused to ~20 µm(>4.5 nm) / unfocussed beam size ~5 – 10 mm (FWHM, depending on wavelength)	
	XUV beam splitter with variable time delay (-3 ps to 15 ps) for photon diagnostics and XUV pump – XUV probe experiments	
	optional pump-probe experiments using FLASH1 optical laser system	
	4-mirror polarizer for variable FEL polarization from 30 – 70 eV	*TU Berlin**
	about 3 × 4 m platform for user-provided end station	
BL3	non-monochromatic FEL photons, spectral range: >4.5 nm (carbon coated optics) focused to ~20 µm / unfocussed beam size ~5 – 10 mm (FWHM, depending on wavelength)	
	optional pump – probe experiments using FLASH1 optical laser system	
	4-mirror polarizer for variable FEL polarization from 30 – 70 eV	*TU Berlin**
	optional pump – probe experiments using **THz radiation**: - tunable: 10 – 230 µm; up to 150 µJ/pulse; ~10 % bandwidth - broadband at 200 µm; up to 10 µJ/pulse; ~100 % bandwidth - synchronized and phase stable to X-ray pulses (down to 5 fs) - delivered to the experiment via vacuum beamline as: (i) ultra-high vacuum (~10^{-8} mbar), shorter delay between THz and X-ray (~4 m path difference), can accommodate up to 0.3 m wide setup (ii) high vacuum (~10^{-6} mbar), longer delay between THz and X-ray (~7 m path difference); can accommodate up to 2 m wide setup - available UHV chamber with mounts for refocusing XUV optics to compensate for XUV/THz path delay	
	about 3 × 4 m platform for user-provided end station	
PG1	high resolution plane grating XUV monochromator (SX 700 type, < 10^{-4} bandwidth, carbon coated optics): - variable combination of photon flux and resolution (from high flux to high resolution) - controlled temporal-spectral properties at moderate resolution for pump – probe experiments - high photon flux with harmonic filtering Kirkpatrick-Baez (KB) refocusing optics, FEL focal spot of 5 µm (vertically)	
	permanent end station: in commissioning - two-stage VUV-Raman spectrometer for high-resolution RIXS measurements close to Rayleigh line (energy resolution < 60 meV FWHM) - optional pump-probe experiments using FLASH1 optical laser system (time resolution ~300 fs)	
PG2	uses the same monochromator as PG1 50 µm focus	
	XUV beam splitter with variable time delay (±6 ps) for time resolved studies	
	optional pump – probe experiments using FLASH1 optical laser system	
	about 3 × 4 m platform for user-provided end station	

FLASH1 optical / NIR laser system for pump – probe experiments

10 Hz single pulse	a) compressed pulse transported over beamline 810 nm, 1.5 mJ, 60 fs FWHM pulse duration, 25 nm FWHM spectral bandwidth synchronization to FEL better than 60 fs rms b) stretched pulse (chirped) transported over beamline pulse compressor must be included in experimental set-up 810 nm, 15 mJ, 200 ps FWHM uncompressed, 25 nm FWHM bandwidth 810 nm, 10 mJ, 60 fs FWHM with external pulse compressor, 25 nm FWHM bandwidth SHG 407 nm, 600 µJ, 5 nm FWHM spectral bandwidth THG 270 nm, 200 µJ, 2.5 nm FWHM spectral bandwidth synchronization to FEL better than 60 fs rms, corrected for drifts
burst-mode	up to 400 pulses / burst 805 nm, 20 µJ per single pulse, 120 fs FWHM pulse duration synchronization to FEL better than 60 fs rms
All laser options are available at Beamlines BL1-3, burst mode laser options are available at PG1-2.	

FLASH2

FL24	non-monochromatic FEL photons wavelength range: 4 – 90 nm fundamental Kirkpatrick-Baez (KB) focusing optics with variable foci down to < 10 µm (FWHM) / unfocussed beam size ~5 – 10 mm (FWHM, depending on wavelength)	
	optional pump – probe experiments using FLASH2 optical laser system	
	grazing incidence split-and-delay unit with ± 12 ps time delay (to be installed 2019)	*Univ. Münster**
	about 3 × 4 m platform for user-provided end station	
FL26	non-monochromatic FEL photons wavelength range: 6 – 90 nm fundamental	
	optional pump – probe experiments using FLASH2 optical laser system	
	permanent end station: - reaction microscope (REMI) for time-resolved AMO spectroscopy - grazing incidence delay-line and refocusing optics: FEL focal spot < 10µm × 10µm (FWHM, depending on wavelength) - ± 2.7 ps time delay range, 1 fs precision	*MPI-K Heidelberg**

FLASH2 optical / NIR laser system for pump – probe experiments
available for the FLASH2 beamlines FL24 (from February 2019 onwards) and FL26

central wavelength	700 to 900 nm (fast tuneable)
spectral bandwidth	30 to 100 nm (pre-set for experiment)
intra-burst-repetition rate	50 kHz
number of pulses per burst	1 – 40
pulse duration	15 – 30 fs FWHM (compressed to 1.1 × bandwidth limit), 500 fs FWHM (uncompressed)
timing jitter to FEL	< 75 fs rms
pulse energy	0 – 250 µJ (before coupling to chamber), 0 – 150 µJ (at interaction region)
polarization	flexible
focus size (1/e² diameter)	FL24: < 100 µm, FL26: < 50 µm
peak intensity	> 10^{14} W/cm²
time delay to FEL	- 4 ns to + 4 ns, 10 fs resolution, larger delays optional
energy instability	< 10 % pulse-to-pulse peak (3 % rms)

400 nm and 266 nm will be available on a best effort basis with expected conversion efficiencies of > 30 % SHG, > 5 % THG

All FLASH beamlines provide online photon diagnostics for intensity, wavelength, and beam position; fast shutter, aperture and filter sets.

PETRA III

Beamlines

PETRA III experimental hall 'Max von Laue'

Beamline and instruments		Operated by
P01	High resolution dynamics 10 m U32 | 2.5 – 80 keV	DESY
	Nuclear resonant scattering	DESY
	Resonant inelastic scattering	DESY / MPG
	X-ray Raman scattering	DESY / MPG
P02.1	High resolution powder diffraction 2 m U23 | 60 keV	DESY
	Standard & time resolved powder diffraction	DESY
	High resolution powder diffraction	DESY
P02.2	Extreme conditions 2 m U23 | 10 – 60 keV	DESY
	Laser heated diamond anvil cells	DESY
	General purpose high pressure	DESY
P03	Micro- and Nano-SAXS / WAXS 2 m U29 | 8 – 23 keV	DESY
	Micro-beam small and wide angle scattering	DESY
	Nano-beam scattering and diffraction	DESY
P04	Variable polarization soft X-rays 5 m UE65 | 200 – 3000 eV	DESY
	UHV diffractometer	DESY
	Photon-ion spectrometer (PIPE)	DESY
	Ultra-high resolution photoelectron spectroscopy (ASPHERE)	DESY
	Soft X-ray absorption spectrometer	DESY
	Nano focus apparatus for spatial and time resolving spectroscopy	DESY
P05	Micro- and nanoimaging 2 m U29 | 8 – 50 keV	HZG
	Micro-tomography	HZG
	Nano-tomography	HZG
P06	Hard X-ray micro-/nanoprobe 2 m U32 | 5 – 100 keV	DESY
	Microprobe	DESY
	Nanoprobe	DESY
P07	High energy X-ray materials science 2 m U29 (planned: 4 m IVU19) | 50 – 200 keV	HZG
	Multi-purpose triple-axis diffractometer	DESY
	Heavy load diffractometer	HZG
	Grain mapper	HZG
	High energy tomography	HZG
P08	High resolution diffraction 2 m U29 | 5.4 – 29.4 keV	DESY
	High resolution diffractometer	DESY
	Liquid surface diffractometer	DESY
	Langmuir trough in-plane diffractometer	DESY
P09	Resonant scattering and diffraction 2 m U32 | 2.7 – 50 keV	DESY
	High precision psi-diffractometer	DESY
	Heavy load diffractometer	DESY
P10	Coherence 5 m U29 | 4 – 20 keV	DESY
	X-ray photon correlation spectroscopy (4 – 20 keV)	DESY
	Coherent imaging (8 – 15 keV)	DESY
	Multi-purpose diffractometer (8 – 20 keV)	DESY
P11	Bio-imaging and diffraction 2 m U32 | 2.4 – 30 keV	DESY
	Imaging of biological samples (2.4 – 10 keV)	DESY (in commissioning)
	Macromolecular crystallography (5.5 – 30 keV)	DESY / MPG / HZI

Beamline and instruments		Operated by
P12	Bio SAXS 2 m U29 | 4 – 20 keV	EMBL
	Small-angle X-ray scattering	EMBL
P13	Macromolecular crystallography I 2 m U29 | 4.5 – 17.5 keV	EMBL
	Macromolecular crystallography	EMBL
P14	Macromolecular crystallography II 2 m U29 | 6 – 20 keV	EMBL
	Macromolecular crystallography	EMBL

PETRA III experimental hall 'Ada Yonath'

Beamline and instruments		Operated by
P21	Swedish materials science (SMS) beamline 4 m IVU21 | 40 – 150 keV side branch: 2 m U29 | 50, 80, 100 keV	Swedish institution / DESY
	Diffraction and imaging Broad band diffraction	Swedish institution / DESY in commissioning; user operation starting fall 2019
P22	Hard X-ray photoelectron spectroscopy 2 m U33 | 2.4 – 15 keV	DESY
	HAXPES, ambient and high pressure, HAXPEEM	DESY
P23	*In situ* and nano-diffraction beamline 2 m U32 | 5 – 35 keV	DESY
	Nano-XRD, *in situ* and complex environments	DESY
	2nd hutch instrument t.b.d.	not yet funded
P24	Chemical crystallography 2 m U29 | 8, 15 – 45 keV	DESY
	Single crystal diffraction in complex sample environments	DESY
	Small molecule crystallography	DESY
P25	t.b.d.	not yet funded

PETRA III experimental hall 'Paul P. Ewald'

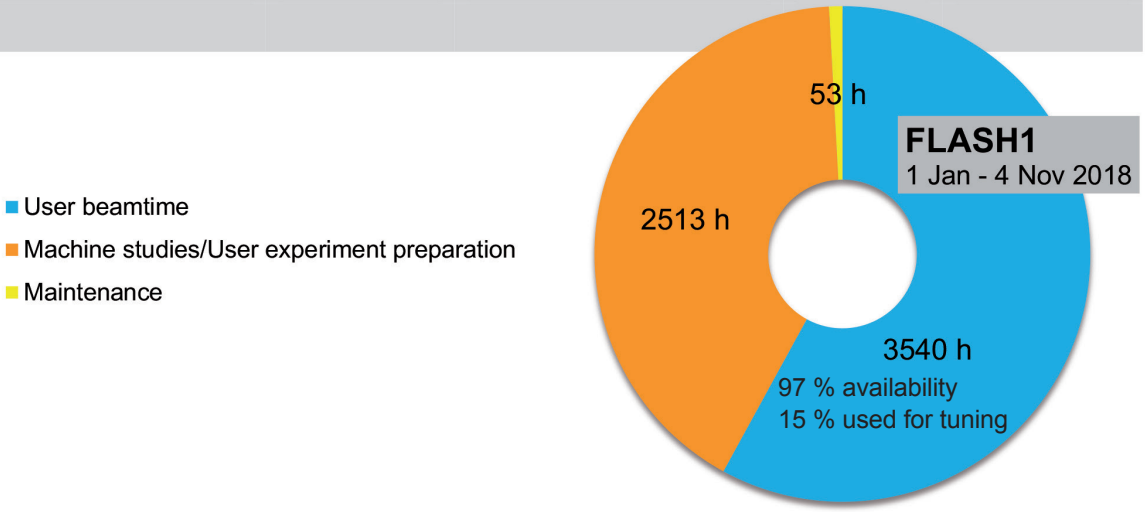
Beamline and instruments		Operated by
P61	High-energy wiggler beamline 40 m damping wiggler | 50 – 200 keV / pink beam	DESY
	High-energy engineering materials science	HZG
	Large volume press - Extreme conditions (LVP-EC)	DESY (commissioning 2019)
P62	Anomalous small-angle X-ray scattering 2 m U32 | 4 – 44 keV	DESY
		(operation planned 2020)
P63	t.b.d.	not yet funded
P64	Advanced X-ray absorption spectroscopy 2 m U32 | 4 – 44 keV	DESY
	Time-resolved *in situ* XAFS, QEXAFS, bioXAFS	DESY
P65	Applied X-ray absorption spectroscopy 36 cm U32 | 4 – 44 keV	DESY
	Ex situ and *in situ* XAFS of bulk samples	DESY
P66	Superlumi Bending magnet | 4 – 40 eV	DESY
	Time-resolved luminescence spectroscopy *(separate building)*	DESY (commissioning 2019)

We would like to acknowledge all contributions to beamline & instrument development and operation provided within the framework of BMBF-Verbundforschung, the Röntgen-Ångström-Cluster (RAC), the Ioffe-Röntgen-Institute (IRI), the Department of Science & Technology (Government of India) within the India@DESY collaboration, the Ruprecht-Haensel-Laboratory (University of Kiel), Max Planck Society, Forschungszentrum Jülich, University of Stockholm.

Beamtime statistics 2018

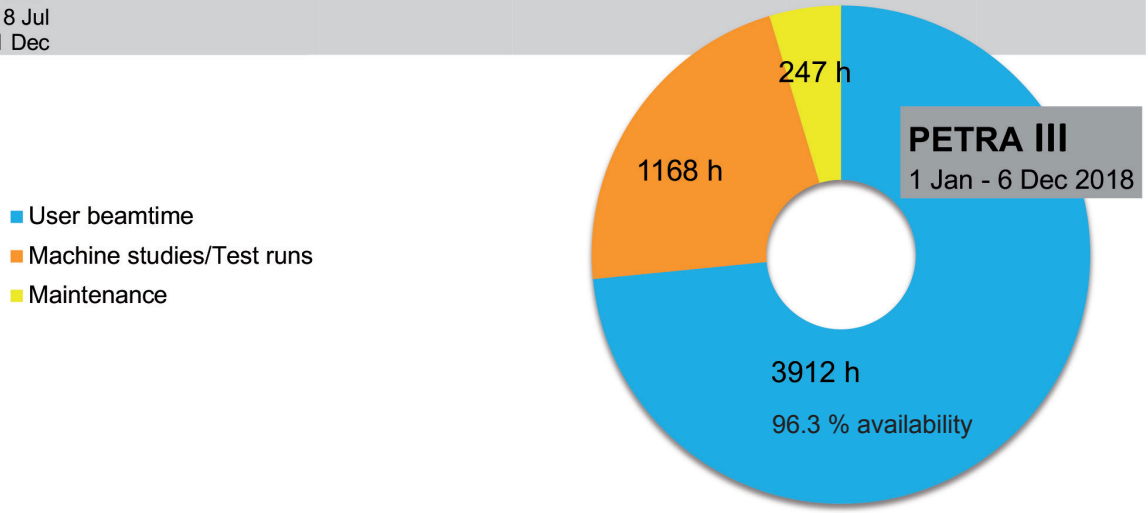
FLASH
Operation period 2018

	User beamtime	Machine studies and user experiment preparation	Maintenance	Shutdown and commissioning
FLASH1				
1 Jan – 4 Nov	3540 h	2513 h	53 h	1293 h
planned for 5 Nov – 31 Dec	648 h	402 h	6 h	305 h
FLASH2				
1 Jan – 4 Nov	1920 h	4029 h	54 h	1396 h
planned for 5 Nov – 31 Dec	348 h	534 h	6 h	473 h



PETRA III
Operation period 2018

	User beamtime	Machine studies and test runs	Maintenance	Shutdown
1 Jan – 6 Dec	3912 h	1168 h	247 h	
planned for 7 Dec – 31 Dec	332 h	12 h	12 h	
				3077 h
run periods:				
26 Mar – 18 Jul				
3 Sep – 21 Dec				



Committees 2018

Photon Science Committee PSC — advises the DESY Photon Science management

Christian David (chair)	PSI, Villigen, CH
Melissa A. Denecke (vice chair)	University of Manchester, UK
Stefan Eisebitt	MBI and Technische Universität Berlin, DE
Gwyndaf Evans	Diamond Light Source Ltd., Didcot, UK
Jan-Dierk Grunwaldt	KIT, Karlsruhe, DE
Simo Huotari	University of Helsinki, FI
Maya Kiskinova	Elettra-Sincrotrone, Trieste, IT
Edvin Lundgren	Lund University, DK
Arwen Pearson	CUI, Universität Hamburg, DE
Thomas Pfeifer	MPI for Nuclear Physics, Heidelberg, DE
Harald Reichert	ESRF, Grenoble, FR
Daniela Rupp	MBI and Technische Universität Berlin, DE
Bernd Schmitt	PSI, Villigen, CH
Thomas Schröder	HU Berlin and IKZ, Berlin, DE
Andrea Somogyi	Synchrotron SOLEIL, Saint-Aubin, FR
Stefan Vogt	Argonne National Laboratory, Lemont, US
Nele Müller (PSC secretary)	DESY, Hamburg, DE

Laser Advisory Committee LAC — advises DESY and European XFEL

Jonathan Zuegel (chair)	LLE, Rochester, US
Giulio Cerullo	Politecnico di Milano, IT
Miltcho Danailov	Elettra-Sincrotrone, Trieste, IT
Thomas Dekorsy	DLR, Stuttgart, DE
Patrick Georges	CNRS, FR
Uwe Morgner	Leibniz University and Laser Zentrum Hannover, DE
Robert W. Schoenlein	LBNL, Berkeley, US
William E. White	SLAC, Menlo Park, US
Andreas Galler (LAC secretary)	European XFEL, Schenefeld, DE
Oliver D. Mücke (LAC secretary)	CFEL-DESY, Hamburg, DE

DESY Photon Science User Committee DPS-UC — represents the user community

Peter Müller-Buschbaum (chair)	Technische Universität München, DE
Markus Mezger	MPI für Polymerforschung, Mainz, DE
Daniela Rupp	Technische Universität Berlin, DE
Chrystèle Sanloup	Institut des Sciences de la Terre de Paris, FR
Gregor Witte	Ludwig-Maximilians-Universität München, DE

Komitee Forschung mit Synchrotronstrahlung KFS
representative body of the German SR and FEL user community

Bridget Murphy (chair)	Christian-Albrechts-Universität zu Kiel, DE
Jan-Dierk Grunwaldt (vice chair)	KIT, Karlsruhe, DE
Peter Albers	Evonik Technology & Infrastructure GmbH, DE
Stefan Eisebitt	MBI and Technische Universität Berlin, DE
Ronald Frahm	Universität Wuppertal, DE
Christian Gutt	Universität Siegen, DE
Birgit Kanngießer	Technische Universität Berlin, DE
Sarah Köster	Georg-August-Universität Göttingen, DE
Kai Rossnagel	Christian-Albrechts-Universität zu Kiel, DE
Hermann Schindelin	Universität Würzburg, DE

Project Review Panels 2018

PRP VUV- and Soft X-ray	
Lucia Aballe	CELLS-ALBA Barcelona, ES
Yves Acremann	ETH Zürich, CH
Arno Ehresmann	Universität Kassel, DE
Stephan Fritzsche	Helmholtz Institut Jena, DE
Marc Golden	University of Amsterdam, NL
Emma Sokell	University College Dublin, IE
Jan-Erik Rubensson	Uppsala University, SE
Moritz Hoesch (PRP Secretary)	DESY, Hamburg, DE

PRP X-ray Spectroscopy	
Iztok Arčon	University of Nova Gorica, SL
Matthias Bauer	Universität Paderborn, DE
Ralph Claessen	Julius-Maximilians-Universität Würzburg, DE
Jörg Evers	MPI für Kernphysik, Heidelberg, DE
Greg Hughes	Dublin City University, IE
Catherine McCammon	Bayerisches Geoinstitut, Bayreuth, DE
Marco Moretti	ESRF, Grenoble, FR
Martina Müller	Forschungszentrum Jülich, DE
Maarten Nachtegaal	PSI, Villigen, CH
Christian Papp	FAU Erlangen-Nürnberg, DE
Håkan Rensmo	Uppsala University, SE
Claudia Schnohr	Friedrich-Schiller-Universität Jena, D
Svetoslav Stankov	Karlsruher Institut für Technologie KIT, DE
Vladimir N. Strocov	PSI, Villigen, CH
Max Wilke	Universität Potsdam, DE
Wolfgang Drube (PRP secretary)	DESY, Hamburg, DE

PRP High Pressure and Extreme Conditions	
Leonid Dubrovinsky	Bayerisches Geoinstitut, Bayreuth, DE
Diego Gatta	University of Milan, IT
Ulrich Haussermann	Stockholm University, SE
Malcolm McMahon	University of Edinburgh, UK
Sébastien Merkel	Lille University, FR
Clemens Prescher	Universität Köln, DE
Carmen Sanchez-Valle	Universität Münster, DE
Andreas Zerr	Université Paris Nord, Villetaneuse, FR
Hanns-Peter Liermann (PRP Secretary)	DESY, Hamburg, DE

PRP Engineering Materials Science	
Jens Gibmeier	Karlsruher Institut für Technologie KIT, DE
Astrid Haibel	Beuth Hochschule für Technik Berlin, DE
Patrick Huber	Technische Universität Hamburg-Harburg, DE
Rolf Kaufmann	Comet Group, Flamatt, CH
Jozef Keckes	Montanuniversität Leoben, AT
Svea Mayer	Montanuniversität Leoben, AT
Thomas Niendorf	Universität Kassel, DE
Wolfgang Pantleon	Technical University of Denmark, DK
Walter Reimers	Technische Universität Berlin, DE
Carsten Siemers	Technische Universität Braunschweig, DE
Dieter Lott (PRP secretary)	HZG, Geesthacht, DE
Ulrich Lienert (DESY representative)	DESY, Hamburg, DE

PRP Soft Condensed Matter – Bulk	
Christian Gutt	Universität Siegen, DE
Thomas Hellweg	Universität Bielefeld, DE
Fredrik Lundell	KTH, Stockholm, SE
Daniel Söderberg	KTH, Stockholm, SE
Rainer Gehrke (PRP secretary)	DESY, Hamburg, DE

PRP Soft Condensed Matter – Surfaces and Interfaces	
Tiberio A. Ezquerra	CSIC, Madrid, ES
Alexander Gerlach	Universität Tübingen, DE
Markus Mezger	MPI für Polymerforschung, Mainz, DE
Guiseppe Portale	University of Groningen, NL
Tobias Unruh	Technische Universität München, Garching, DE
Andreas Zumbühl	University of Fribourg, CH
Oliver Seeck (PRP Secretary)	DESY, Hamburg, DE

PRP Imaging (full-field, scanning, coherent)	
Martin Bech	Lund University, SE
Oliver Bunk	PSI, Villigen, CH
Manfred Burghammer	ESRF, Grenoble, FR
Frank Friedrich	Universität Hamburg, DE
Julia Herzen	Technische Universität München, DE
Koen Janssens	University of Antwerp, BE
Stephan Peth	Universität Kassel, DE
Sebastian Schoeder	Synchrotron SOLEIL, Saint-Aubin, FR
Katarina Vogel-Mikuš	University of Ljubljana, SL
Florian Meirer	Utrecht University, NL
Jürgen Thieme	Brookhaven National Laboratory, Upton NY, US
Gerald Falkenberg (PRP secretary)	DESY, Hamburg, DE
Felix Beckmann (HZG representative)	HZG, Geesthacht, DE

PRP Methods and Instrumentation	
Yngve Cerenius	MAX IV Laboratory, Lund University, SE
Cameron Kewish	Australian Synchrotron, Melbourne, AU
Raymond Barrett	ESRF, Grenoble, FR
Horst Schulte-Schrepping (PRP secretary)	DESY, Hamburg, DE

PRP Hard Condensed Matter – Surface and Coherent Scattering	
Ralf Busch	Universität des Saarlandes, DE
Johan Gustafson	Lund University, SE
Václav Holý	Charles University, Prague, CZ
Alexander Komarek	MPI CPfS, Dresden, DE
Guido Meier	MPI MPSD, Hamburg, DE
Bogdan Sepiol	Universität Wien, AT
Julian Stangl	Johannes Kepler Universität Linz, AT
Jesper Wallentin	University Lund, SE
Peter Wochner	MPI für Festkörperforschung, Stuttgart, DE
Michael Sprung (PRP Secretary)	DESY, Hamburg, DE

PRP Hard Condensed Matter – Bulk (diffraction and scattering)	
Emil Bozin	Brookhaven National Laboratory, Upton NY, US
Johan Chang	University of Zurich, CH
Robert Dinnebier	MPI für Festkörperforschung, Stuttgart, DE
Markus Huecker	Weizmann Institute of Science, Rehovot, IL
Mads Ry Vogel Jørgensen	Aarhus University, DK
Simon Pauly	IFW Dresden, DE
Helen Walker	ISIS, Didcot, GB
Xiaodong Zou	Stockholm University, SE
Ann-Christin Dippel (PRP secretary)	DESY, Hamburg, DE

PRP Soft X-Ray – FEL Experiments (FLASH)	
Katharina Al-Shamery	Universität Oldenburg, DE
Michael Bonitz	Universität Kiel, DE
Christoph Bostedt	EPFL, Lausanne and PSI Villigen, CH
Hermann Dürr	SLAC Nat. Accelerator Laboratory, Menlo Park, US
Marion Harmand	Sorbonne Université, Paris, FR
Chris Jacobsen	APS, Argonne, US
Claudio Masciovecchio	Elettra Sincrotrone Trieste, IT
Ronald Redmer	Universität Rostock, DE
Robert W. Schoenlein	SLAC Nat. Accelerator Laboratory, Menlo Park, US
Marc Simon	Sorbonne Université, Paris, FR
Kiyoshi Ueda	Tohoku University, Sendai, JP
Marc Vrakking	MBI, Berlin, DE
Martin Weinelt	FU Berlin, DE
Elke Plönjes-Palm, Rolf Treusch (PRP secretary)	DESY, Hamburg, DE

PEC: EMBL Life Science beamlines P12-P14 / PRP Bio-crystallography at P11	
Savvas Savvides (chair)	Ghent University, BE
Pau Bernadó	CBS/CNRS, Montpellier, FR
Kristina Djinovic-Carugo	Universität Wien, AT
Gwyndaf Evans	Diamond Light Source, Didcot, GB
Robert Fischetti	Argonne National Laboratory, US
Mariusz Jaskolski	Adam Mickiewicz University of Poznan, PL
Javier Pérez	Synchrotron SOLEIL, Saint-Aubin, FR
Zehra Sayers	Sabanci University, Istanbul, TR
Joel Sussman	Weizmann Institute of Sciences, Rehovot, IL
Maria Vanoni	University of Milan, IT
Bente Vestergaard	University of Copenhagen, DK
Gregor Witte	Ludwig-Maximilians-Universität München, DE
Christian Schroer (DESY observer)	DESY, Hamburg, DE

Photographs and Graphics:

Manon Boschard, Hamburg
DESY
EMBL
European XFEL
Claudia Höhne, Hamburg
HZG
LEAPS
Victor O. Leshyk, U.S.
Lucid Berlin
Tina Mavric, DESY
Marta Mayer, DESY
MPG
Heiner Müller-Elsner, Hamburg
Reimo Schaaf, Hamburg
SPIE 2018
Universität Hamburg

Figures of the Research Highlights were reproduced by permission from authors or journals.

Acknowledgement

We would like to thank all the authors and all those who have contributed to the realisation of this Annual Report.

Imprint

Publishing and Contact:
Deutsches Elektronen-Synchrotron DESY
A Research Centre of the Helmholtz Association

Hamburg location:
Notkestr. 85, 22607 Hamburg, Germany
Tel.: +49 40 8998-0, Fax: +49 40 8998-3282
desyinfo@desy.de

Zeuthen location:
Platanenallee 6, 15738 Zeuthen, Germany
Tel.: +49 33762 7-70, Fax: +49 33762 7-7413
desyinfo.zeuthen@desy.de

Photon Science at DESY
Tel.: +49 40 8998-2304, Fax: +49 40 8998-4475
photon-science@desy.de
photon-science.desy.de

www.desy.de

ISBN 978-3-945931-23-3

Online version:
photon-science.desy.de/annual_report

Realisation:
Wiebke Laasch, Daniela Unger

Editing:
Sadia Bari, Martin Beye, Lars Bocklage, Rainer Gehrke, Daniel Horke, Thomas Keller, Tim Laarmann, Wiebke Laasch, Wolfgang Morgenroth, Nele Müller, Sang-Kil Son, Daniela Unger, Hans-Christian Wille

Layout: Sabine Kuhls-Dawideit, Büro für Grafik und Design, Halstenbek

Printing and image processing: EHS Druck GmbH, Schenefeld

Copy deadline: December 2018

Reproduction including extracts is permitted subject to crediting the source.

HELMHOLTZ
RESEARCH FOR GRAND CHALLENGES

Deutsches Elektronen-Synchrotron
A Research Centre of the Helmholtz Association

The Helmholtz Association is a community of 18 scientific-technical and biological-medical research centres. These centres have been commissioned with pursuing long-term research goals on behalf of the state and society. The Association strives to gain insights and knowledge so that it can help to preserve and improve the foundations of human life. It does this by identifying and working on the grand challenges faced by society, science and industry. Helmholtz Centres perform top-class research in strategic programmes in six core fields: Energy, Earth & Environment, Health, Aeronautics, Space and Transport, Matter, and Key Technologies.

www.helmholtz.de